

NOVEL METHODS AND APPLICATION OF OPTOGENETICS FOR
DETERMINING THE FUNCTIONS OF KERATIN FILAMENTS IN EARLY
EMBRYOGENESIS

by

RUCHA SHAH

A dissertation submitted to the Graduate School-Newark

Rutgers, The State University of New Jersey

In partial fulfillment of the requirements

For the degree of

Doctor of Philosophy

Graduate Program in Biological sciences

Written under the direction of

Gregory Weber, Ph.D.

And approved by

Newark, New Jersey

October 2019

©2019

Rucha Shah

All rights reserved

ABSTRACT OF THE DISSERTATION

NOVEL METHODS AND APPLICATION OF OPTOGENETICS FOR DETERMINING THE FUNCTIONS OF KERATIN FILAMENTS IN EARLY EMBRYOGENESIS

By RUCHA SHAH

Dissertation Director:

Gregory Weber, Ph.D.

To study the functional role of keratin filaments during early embryological development I developed a novel biomolecular tool for specifically disrupting keratin filaments in living cells. Conventional genetic approaches such as, knockdown, knockout and transgenic overexpression have attempted to study the role of keratin IFs but fall short of identifying the functional significance of keratin filamentous network during early development. The utility of small molecular inhibitors withaferin A and acrylamide to experimentally interfere with keratin network organization were also evaluated in this study. The comparative analysis done here emphasizes that the effect of these inhibitors is dependent on many factors, such as cell type, cell density, dose of the drug and time of exposure. Furthermore, correlative evidence suggests that the keratin network in the vicinity of the cell-cell contacts was resistant to both the small molecular inhibitors. It was also observed that both keratin filaments and keratin precursor particles have spatially defined subcellular

localization in tissues, such as presumptive ectoderm and mesendoderm. In order to specifically study the functional role of keratin filamentous network, a genetically encoded PhotoActivatable disruptor of keratin filaments was developed, taking advantage of *Xenopus* keratin 8 mimetic peptide and a light sensitive LOV domain of the *Avena sativa* phototropin. The inhibitory effects of this peptide were validated in multiple cell lines and tissues. Upon photoactivation, PA-2B2 induces localized rapid subcellular disruption of the keratin filaments and thus destabilization of the network leading to cell shape changes. Specific disruption of keratin filaments by light-based activation of PA-2B2 leads to a dramatic disruption of early embryological development in *Xenopus*. Additionally, disruption of keratin filaments leads to failure of fibronectin assembly along the blastocoel roof. Collectively, the data shows the critical importance of keratin filaments in morphogenetically active tissues and early embryogenesis. The optogenetic novel tools developed here to disrupt keratin filaments with spatiotemporal precision are a powerful means to probe keratin filament function within living cells and direct future investigations.

Acknowledgments

Foremost, I would like to express my sincere gratitude to my advisor Dr. Gregory Weber for his continuous support throughout my thesis research. As my teacher and mentor, he has provided extensive personal and professional guidance and taught me a lot about scientific research and life in general. He has shown me, by his example, what a good scientist (and person) should be. His continuous motivation, enthusiasm, patience and guidance has helped me throughout my research and writing of the thesis. Thank you so much for your endless support.

I would like to thank each of my thesis committee members-Dr. Haesun Kim, Dr. Edward Bonder, Dr. Daniel Conway, for their great support and valuable feedback. Additionally, I would like to thank both Dr. Wilma Friedman and Dr Jonakait for accepting me as a rotation student and for the training. I am also very thankful to Dr. Rodriguez for the training and mentorship during the time I was in his lab. I additionally thank all the faculty members of the cell and molecular biology track at Rutgers, Newark, for their valued suggestions during colloquium and cell bio talks.

Special mention to my dear lab mates, Shalaka Paranjpe, Richard Mariani, Huri Mucahit, Abid Haque and Charmi Rana. You guys have been simply amazing! Shalaka for being a great friend, who speaks straight from her heart. She was a great technician and have assisted me in numerous ways. Richard for being such a great lab partner, it was fun to

have scientific and non-scientific discussions with you. And troubleshoot problems that we would encounter during our experiments almost at the same time. Huri for being such an easygoing and a great lab member, and also for helping me around in the Rodriguez lab. Abid for bringing fun ideas, models and slime molds to lab meetings. Charmi, thanks for working with me for a while, it was fun teaching you the basic lab techniques.

Throughout my PhD training, I have had the pleasure of having some great colleagues and friends. Thanks to all the previous and present members of the cell and molecular biology program who have been great friends. Especially, Shalaka, Chaitali, Kavya, Soumya, Connie, Ishwarya, Lissette and Ming for your constant love and support. And having most memorable conversations, exchange of ideas, sharing sorrows, joys and lunches. I would also like to thank my friends from the chemistry department, Aparna, Evrim, Elena and Jiyeu for being such good companions and friends.

On a more personal note, I would like to express my deepest gratitude to my family. Most importantly, I would like to thank my husband, Sapan and my kids, Riva and Riaan. This dissertation would not have been possible without their warm love, utmost patience and endless support. A very special thanks to my sister and her family and my brother, for their unconditional love, unfailing emotional support and for constantly believing in me. Finally, I would also like to dedicate this thesis to my loving parents. Thank you for being extremely supportive, encouraging and for always being there for me I am thankful to my in-laws for their continuous support. I love you all!

Table of Contents

Abstract.....	ii
Acknowledgements	iv
Table of contents	vi
List of tables.....	xi
List of figures.....	xii
Chapter 1: Review of literature	1
1.1 Intermediate Filaments: An Overview	2
1.2 Intermediate filaments and the establishment of a cellular architectural framework .	13
1.3 Intermediate filaments and modulation of signal transduction pathways.....	23
1.4 Role for intermediate filaments in mechanotransduction	28
1.5 Intermediate filaments as determinants of migration.....	32
1.6 Functional roles for intermediate filaments during development	38
1.7 <i>Xenopus laevis</i> : model organism	43
Chapter 2: Introduction	51
Introduction to the thesis project.....	52
Significance of the study.....	58

Chapter 3: Materials and methods.....	59
3.1 Cell culture and transfection	60
3.2 Small molecule inhibitor treatments	65
3.3 <i>Xenopus laevis</i> embryo culture and microinjections	65
3.4 Biochemistry	70
3.5 Molecular biology	73
3.6 Direct Immunofluorescence.....	77
3.7 Microscopy	78
3.8 Experimental analyses	81
 Chapter 4: Keratin filaments maintain a specific subcellular localization in migratory cells.....	 85
Abstract	86
Introduction.....	87
Results.....	91
4.1 Gastrulation movements and modes of migration of the <i>Xenopus laevis</i> explants.....	91
4.2 Keratin precursors are predominant in the lamellipodia, while keratin filaments are excluded from the lamellipodia of migrating mesendodermal cells	92
4.3 Keratin precursors are predominant in the lamellipodia, while keratin filaments are excluded from the lamellipodia of ectodermal (animal cap) cells	92
4.4 Subcellular localization of keratin filaments is dependent on cell context in both <i>Xenopus</i> and MDCK cells.....	93

4.5 Keratin filament organization is dependent on microtubule network in <i>Xenopus</i> mesendoderm cells.....	94
Discussion	106

Chapter 5: Withaferin A and Acrylamide Alter Keratin Intermediate Filament

Network Organization in MDCK and <i>Xenopus</i> cells.....	110
Abstract	111
Introduction.....	112
Results.....	121
5.1 Small molecule inhibitor WFA alters keratin filament organization dependent on time and cell-cell contacts	121
5.2 Small molecule inhibitor acrylamide alters keratin filament organization dependent on time and cell-cell contacts.....	122
5.3 WFA induces disruption of keratin network in MDCK single cells.....	122
5.4 WFA induces disruption of keratin network in MDCK cells pairs	123
5.5 Acrylamide induces keratin network alterations in MDCK single cells.....	124
5.6 Acrylamide induces keratin network alterations in MDCK cell pairs	124
5.7 Withaferin A Treatment Alters Keratin Filament Organization and Cell Morphology of <i>Xenopus</i> mesendoderm cells.....	125
5.8 WFA treatment induces alterations of the microtubule filament organization in <i>Xenopus</i> mesendoderm cells	126
Discussion	155

Chapter 6: Rational Design and Development of Photoactivatable Inhibitory

Peptides to Specifically Disrupt Keratin Filaments	160
Abstract	161
Introduction	162
Results	167
6.1 Identifying peptides to generate photoswitchable disruptor of keratin filaments	167
6.2 Keratin 8 mimetic peptides 2B2 and 1A readily promotes keratin network disruption	168
6.3 In silico analyses and molecular modeling to design PA-2B2 and PA-1A	169
6.4 Design of 2B2 and 1A peptide photoswitches	170
6.5 Hypothesized mechanism for keratin network disruption	173
6.6 Constitutively active open-2B2 disrupts keratin filaments in cultured MDCK cells	173
6.7 Constitutively active open-2B2 disrupts keratin filaments in HEK293T cells	175
6.8 Expression of open-2B2 binds to and disrupts keratin filaments in embryonic <i>Xenopus</i> cells	175
6.9 Keratin 8 2B2 mimetic peptide is a specific inhibitor of keratin filaments	178
Discussion	213

Chapter 7: Targeted Disruption of Keratin Filaments in the Progenitor Ectodermal

Tissue Alters Keratin Network Organization and Induces Major Defects During

<i>Xenopus</i> Early Development	217
Abstract	218
Introduction	219

Results	222
7.1 Photoactivation of PA-2B2 induces disruption of endogenous keratin filaments	222
7.2 Localized activation of PA-2B2 induces rapid disruption of keratin filaments.....	223
7.3 Keratin filaments are necessary for normal <i>Xenopus</i> embryo development.....	225
7.4 Disruption of keratin filamentous network affects fibronectin fibrillar organization.	228
Discussion	252
 Chapter 8: Discussion and Future Studies	257
Discussion	258
Future Directions	268
 Bibliography	300

List of tables

Table 1.1: General Classification of Intermediate Filament Proteins.....	4
Table 1.2: Post-translational modifications of cytoplasmic intermediate filaments.....	12
Table 1.3: Comparison of the mechanical properties of cytoskeletal elements.....	15
Table 5.1: Summary of Withaferin A targets.....	113
Table 5.2: Summary of acrylamide targets	116
Table 5.3: Effect of Withaferin A on MDCK single cells	147
Table 5.4: Effect of DMSO on MDCK single cells.....	148
Table 5.5: Effect of Withaferin A on MDCK cell pairs	149
Table 5.6: Effect of DMSO on cell pairs	150
Table 5.7: Effect of withaferin A on MDCK cell clusters	151
Table 5.8: Effect of DMSO on MDCK cell clusters	151
Table 5.9: Effect of acrylamide on MDCK single cells	152
Table 5.10: Control MDCK single cells	152
Table 5.11: Effect of acrylamide on MDCK cell pairs	153
Table 5.12: Control MDCK cell pairs	153
Table 5.13: Effect of acrylamide on MDCK clusters	154
Table 5.14: Control MDCK clusters	154
Table 6.1: Protein Sequences for keratin 8 2B2 mimetic analogues	209
Table 6.2: Protein Sequences for keratin 8 1A mimetic analogues	211
Table 8.1: List of mutations that improve caging of LOV-J α domain	288

List of figures

Figure 1.1: Interdependent network model of cytoplasmic intermediate filaments as a centerpiece between mechanical stimuli and directional cell migration	47
Figure 1.2: Intermediate filaments and the establishment of cellular subdomains to drive directional migration	49
Figure 3.1: Varying cell-cell interaction conditions	64
Figure 3.2: Equipment for validation and application of PA-2B2 photoswitch	84
Figure 4.1: Gastrulation movements and modes of migration of the <i>Xenopus laevis</i>	95
Figure 4.2: Keratin precursors are predominant in the lamellipodia, while keratin filaments are excluded from the lamellipodia of mesendodermal cells.....	98
Figure 4.3: Keratin precursors are predominant in the lamellipodia, while keratin filaments are excluded from the lamellipodia of progenitor ectodermal cells	100
Figure 4.4: Subcellular localization of keratin filaments is dependent on cell context in both <i>Xenopus</i> and MDCK cells.....	102
Figure 4.5: Keratin filament organization is dependent on microtubule network in <i>Xenopus</i> mesendoderm cells.....	104
Figure 5.1: Chemical structure of small molecular inhibitors	120
Figure 5.2: Small molecule inhibitors withaferin A and acrylamide alter keratin filament organization dependent on cell-cell contacts within 1hr.....	128

Figure 5.3: Small molecule inhibitors WFA and acrylamide alter keratin filament organization dependent on cell-cell contacts within 3hrs	131
Figure 5.4: Small molecule inhibitors WFA and acrylamide alter keratin filament organization dependent on cell-cell contacts within 6hr.....	133
Figure 5.5: WFA induces disruption of keratin network in MDCK single cells	135
Figure 5.6: WFA induces disruption of keratin network in MDCK cell pairs	137
Figure 5.7: Acrylamide induces disruption of keratin network in MDCK single cells ...	139
Figure 5.8: Acrylamide induces disruption of keratin network in MDCK cells pairs.....	141
Figure 5.9: Withaferin A treatment alters keratin filament organization and cell morphology of <i>Xenopus</i> mesendoderm cells.....	143
Figure 5.10: WFA treatment induces alterations of the microtubule filament organization in <i>Xenopus</i> mesendoderm cells	145
Figure 6.1: Identification of peptides to generate photoactivatable disruptor of keratin filaments.....	179
Figure 6.2: Keratin 8 mimetic peptide 2B2 readily promotes keratin network disruption	182
Figure 6.3: Conserved amphipathic pattern in J α -helix facilitates interactions between 2B2 and J α -helix	184
Figure 6.4: Conserved amphipathic pattern in J α -helix facilitates interactions between 1A and J α -helix.....	186

Figure 6.5: Secondary structure shows continuous α -helical domain	188
Figure 6.6: Design of 2B2 and 1A peptide photoswitches	190
Figure 6.7: Structural modelling shows a nearly contiguous α -helical domain.....	192
Figure 6.8: Strategy for mechanism of action.....	194
Figure 6.9: Constitutively active open-2B2 disrupts keratin filaments in MDCK cells..	196
Figure 6.10: Constitutively active open-2B2 disrupts keratin filaments in HEK293T cells	199
Figure 6.11: Constitutively active open-2B2 disrupts keratin filaments in <i>Xenopus</i> ectodermal cells	201
Figure 6.12: Constitutively active open-2B2 disrupts keratin 19 filaments in <i>Xenopus</i> ectodermal cells	203
Figure 6.13: Keratin 8 2B2 mimetic peptide target keratin 18 to induce disruption of filaments.....	205
Figure 6.14: Keratin 8 2B2 mimetic peptides are specific inhibitors to keratin filaments	207
Figure 7.1: Photoactivation of PA-2B2 induces disruption of endogenous keratin filaments	230
Figure 7.2: Localized activation of mCherry PA-2B2 induces rapid disruption of keratin filaments.....	233
Figure 7.3: Localized photostimulation of mCherry PA-2B2 induces rapid disruption of keratin filaments.....	237

Figure 7.4: Keratin filaments are necessary for normal <i>Xenopus</i> embryo development	239
Figure 7.5: Light induced disruption of keratin filaments elicits abnormal <i>Xenopus</i> development	242
Figure 7.6: mCherry fluorescence is present in dorsal most tissues in embryos expressing PA-2B2	245
Figure 7.7: Light induced disruption of keratin filaments perturbs internal morphology of embryos	247
Figure 7.8: Keratin filamentous network is required for fibronectin assembly	249
Figure 8: Role for keratin filaments in fibronectin fibrillogenesis during early embryogenesis	265
Figure 8.1: Localization of pSer71-Rac1 is influenced by cell-cell contacts	275
Figure 8.2: Acute disruption of keratin filaments alters pSer71-Rac1 localization at cell-cell contacts	278
Figure 8.3: Specific disruption of keratin filaments reduces pSer71-Rac1 localization at cell-cell contacts	282
Figure 8.4: Constitutively active open-2B2 induces lamin disruption in cultured MDCK cells	292
Figure 8.5: Constitutively active open-2B2 induces lamin disruption in cultured HEK293T cells	297

Chapter 1

Review of the literature

Information included in this chapter is adapted from and are published in

Sanghvi-Shah, R., and Weber, G. F. (2017). Intermediated filaments at the junction of mechanotransduction, migration, and development. *Front. Cell Dev. Biol.* 5, 81. doi: 10.3389/fcell.2017.0081

1.1 Intermediate Filaments: An Overview

Cytoplasmic intermediate filaments belong to a superfamily of highly conserved proteins (~65 genes) (Hesse et al., 2001) unique to metazoan species (Herrmann and Strelkov, 2011). These members of the intermediate filament family likely originated through the divergence of the more ubiquitously expressed, yet highly conserved, nuclear intermediate filaments- the lamins (Dodemont and Riemer, 1990; Döring and Stick, 1990; Hering et al., 2016; Peter and Stick, 2015). The expression and assembly of these 10-12 nm filament forming cytoplasmic proteins is developmentally regulated in a cell-, tissue- and context-dependent manner. Based upon their expression pattern, structure and sequence identity, cytoplasmic intermediate filament proteins are classified into five different gene families (**Table 1**), with a sixth intermediate filament family comprised of lamins which reside in the nucleus (Type V). Type I and II consist of the keratins, which are intermediate filaments highly expressed by epithelia. Notably keratins are also expressed by several non-epithelial cell types and, of particular relevance to this review, are the earliest expressed intermediate filament types during embryogenesis (Franz et al., 1983; Lehtonen et al., 1983). In humans, keratins are encoded by 28 genes for Type I members and 26 genes for Type II members on only two loci (Hesse et al., 2001). While mice have a similar number of keratin genes, the number of keratin genes varies with species, with organisms lower on the phylogenic tree exhibiting fewer keratin genes. For instance, at the other end of the spectrum a single Type I-Type II keratin pair of genes exists in the sea squirt *Ciona intestinalis*, a difference indicative of the evolutionary expansion of keratins through gene duplication (Hesse et al., 2001; Karabinos et al., 2004). Type

III intermediate filaments are intermediate filaments, such as vimentin and desmin, that can form homopolymers and also heteropolymers with other Type III intermediate filament proteins. Type IV intermediate filaments are expressed mostly by neurons and muscle and includes the various neurofilament subtypes, nestin and synemin. Type VI includes CP49/phakinin and filensin, which are lens-specific intermediate filaments. Although CP49 can self-assemble *in vitro*, *in vivo* CP49 and filensin together form heteroligomeric filaments (Goulielmos et al., 1996). Here we will primarily focus on Type I-III cytoplasmic intermediate filaments, with special emphasis on keratin and vimentin, because of the emerging evidence for their influence over signal transduction, cellular function in a wide variety of cell types, and role in embryonic development.

Table 1.1: General Classification of Intermediate Filament Proteins

Intermediate Filament Type	General Categorization	Intermediate Filament Protein Members
Type I	Acidic Keratins	Acidic Keratins (28 genes in humans)
Type II	Basic Keratins	Basic Keratins (26 genes in humans)
Type III	Homodimerizing intermediate filaments, some capability of heterodimerizing	Vimentin, Desmin, GFAP
Type IV	Intermediate filaments mainly expressed in neurons and muscle	Neurofilaments, Nestin, Synemin
Type V	Nuclear intermediate filaments	Lamins
Type VI	Lens-specific beaded intermediate filaments	Phakinin (CP49), Filensin

All cytoplasmic intermediate filament proteins share a common tripartite molecular structure. Intermediate filament monomers are dominated by a conserved central α -helical domain (~310 amino acids) flanked by highly variable non- α -helical head and tail domains. Variability in the amino terminal head domain and the carboxy terminal tail domains account for much of the diversity, specificity and regulation of intermediate filaments. Meanwhile, the central domain is the primary dimerization region. The central rod domain is periodically interrupted by linker domains (L1 and L12) thus forming four helical subdomains (coil 1A, coil 1B, coil 2A and coil 2B) capable of forming coiled-coils (Chernyatina et al., 2012; Geisler and Weber, 1982; Nicolet et al., 2010). These sub-helices are predominantly rich in heptad repeats (abcdefg)_n where a & d are the small apolar residues (Leu, Ile, Met or Val). This amphipathic nature of the intermediate filament monomers allows them to readily form highly stable, parallel α -helical coiled-coil dimers without the assistance of any nucleating proteins *in vitro* (Quinlan et al., 1986).

Over the last few decades, several laboratories have elucidated the general mechanism for intermediate filament assembly *in vitro*. Cytoplasmic intermediate filament protein dimers laterally associate in an antiparallel fashion to form apolar tetramers. Once formed, tetramers further align to form unit length filaments (ULF's) that anneal longitudinally to yield long, flexible filaments, and subsequently undergo radial compaction to yield non-polar 10 nm filaments (Herrmann et al., 1996, 1999; Kirmse et al., 2007; Sokolova et al., 2006). Keratins spontaneously form obligate heterodimers from one Type I and one Type II intermediate filament protein (Steinert et al., 1976), whereas vimentin forms

homopolymers (Steinert et al., 1981b). In both instances, nucleation and polymerization can occur without aid from co-factors or nucleoside triphosphates (Herrmann et al., 2004). Although keratin heteropolymers can be formed from any combination of Type I acidic keratins and Type II basic keratins *in vitro*, assembly kinetics do show preferential pairing (Hatzfeld and Franke, 1985). Indeed, specific pairs of keratins are expressed *in vivo* (Franke et al., 1981) that parallel these assembly preferences. Such *in vitro* assembly studies of intermediate filaments, in addition to their remarkable insolubility in physiological buffers during *in vitro* experiments and resilient mechanical properties, led to the initial notion that intermediate filaments form stable networks in the cytoplasm.

While intermediate filament assemblages certainly have noteworthy physical properties, their assembly and disassembly are hardly static, unregulated, nor inconsequential to cell function. Contrary to *in vitro* assembly observations, *in vivo* pulse chase experiments suggest that intermediate filaments assemble from a soluble pool of tetrameric intermediate filament precursors/subunits (Blikstad and Lazarides, 1983; Schwarz et al., 2015; Soellner et al., 1985). Despite the tendency toward polymerization *in vitro*, in living cells intermediate filament proteins coexist both in filamentous form and as detergent-soluble filament precursors, of various varieties, including tetramers, ULFs, “particles”, and “squiggles”-short filamentous structures (Schwarz et al., 2015; Yoon et al., 1998, 2001). Intermediate filament precursors are most apparent in the peripheral region and protrusions of cells (Helfand et al., 2002; Prahlad et al., 1998; Schwarz et al., 2015; Yoon et al., 1998, 2001). As intermediate filament particles are transported, a subset of these are selected to

elongate to short filaments otherwise known as squiggles and further assemble into mature filaments, finally incorporating into the network (Schwarz et al., 2015; Windoffer et al., 2011; Yoon et al., 1998). Cytoplasmic intermediate filaments establish complex networks that form a central cage like structure encapsulating the nucleus and further radiates toward the cell periphery (Franke et al., 1978b, 1978a). Strikingly, when both the keratin and vimentin intermediate filaments are expressed in a cell type they display distinct spatial organization of intermediate filament arrays (Osborn et al., 1980). Typically keratin intermediate filaments are packaged into bundles called tonofibrils (Steinert et al., 1981a) and also form bifurcations (Nafeey et al., 2016). On the other hand, vimentin intermediate filaments are loosely arranged in a parallel or crisscross fashion forming a fine mesh network (Goldman et al., 1986). Polymerized filaments either become a part of the existing peripheral keratin intermediate filament network or get disassembled. Depolymerized precursors may be recycled in the cytoplasm and readied for the next cycle of assembly and disassembly or else undergo ubiquitin-mediated proteasomal degradation. Evidence points to a soluble pool of intermediate filament subunits as an important resource for the remodeling of intermediate filament networks. Keratin cycling uses disassembled soluble subunits for filament renewal, since inhibition of protein synthesis does not abolish filament formation nor subunit exchange (Kolsch et al., 2010). Similar cycling mechanisms are also seen for vimentin intermediate filaments, where vimentin precursors are translocated to the peripheral region of the spreading cells and display a stepwise formation of intermediate filaments (Prahlad et al., 1998).

In addition to dynamic assembly of intermediate filaments, established intermediate filament networks are subject to marked remodeling. Live imaging studies highlight the dynamic and motile properties of the intermediate filament networks and clearly show that vimentin and keratin fibrils exhibit undulations while constantly changing their configurations, appearing to collapse, extend and translocate over relatively short time intervals (Ho et al., 1998; Windoffer and Leube, 1999; Yoon et al., 1998). At the subunit level, the dynamic exchange of intermediate filament dimers is ever more complex. Predictably, severing and end-to-end annealing are major mechanisms for elongation and refurbishment of filaments (Hookway et al., 2015; Prahlad et al., 1998; Winheim et al., 2011; Wöll et al., 2005). Breaking with typical models of filament polymerization however, data show that intermediate filament subunits can also be added and removed from the entire length of the preformed filament as a mechanism for intermediate filament turnover (Coleman and Lazarides, 1992; Ngai et al., 1990; Vikstrom et al., 1992). Microinjection of soluble biotinylated keratin and vimentin (Miller et al., 1991; Vikstrom et al., 1989) and rhodamine-tagged vimentin followed by FRAP (Fluorescence Recovery After Photobleaching) analyses revealed that these subunits can rapidly incorporate in a well-established network (Vikstrom et al., 1992). Exchange of intermediate filament subunits is nonpolar and occurs along the entire length of the intermediate filament. Nevertheless, subunit swapping is highly dependent on the availability of a soluble pool. Collectively, this suggests that established intermediate filaments exhibit unique dynamic properties that allow for turnover of subunits, along with severing and end-to end annealing to maintain length and flexibility of the preformed filaments without compromising their structural integrity. Factors regulating and facilitating processes such as severing,

reannealing and subunit exchange are largely unknown and the underlying molecular mechanisms demand further attention given the disparate assembly dynamics *in vitro* compared to *in vivo*. As with their actin and microtubule counterparts, we speculate that a host of intermediate filament binding proteins that modulate polymerization are waiting to be elucidated.

Despite the ability of keratin and vimentin to polymerize so readily, cells clearly have regulatory controls that determine when and where intermediate filaments will form. A variety of post-translation modifications (PTMs) of intermediate filaments such as phosphorylation, ubiquitylation, acetylation, and sumoylation are emerging as crucial controllers of intermediate filament dynamics, stability and function (**Table 2**). [for review see (Snider and Omary, 2014)]. Phosphorylation status of cytoplasmic intermediate filaments is modulated by various kinases and phosphatases (Omary et al., 2006) depending upon the intermediate filament protein involved, cell and tissue type and specific physiological condition. Such phosphorylation/dephosphorylation events in general affect their conformation, solubility, filament organization and interaction with other signaling molecules consequently translating into various cellular functions. Site-specific serine/threonine phosphorylation of the head and tail region of intermediate filaments facilitate their structural reorganization mainly by promoting intermediate filament solubility. Conversely, tyrosine phosphorylation of the rod domain (Tyr 267) of K8 facilitates their proper filament formation and renders them insoluble (Snider et al., 2013b). Different PTMs on intermediate filaments can serve as docking sites for protein complexes

and allow for altered assembly dynamics or rearrangements of the network. For example, the chaperone protein Hsp27 interacts with K8 in a phosphorylation dependent manner (Kayser et al., 2013). Hsp27 manages keratin inter-filament interactions by inhibiting extensive bundling of filaments (Kayser et al., 2013), in essence by acting as a steric “spacer”. Such phosphorylation events not only correlate with, but have a functional role in cellular events such as mitosis, cell migration, cell growth and stress-mediated responses. Spatiotemporal localization of intermediate filaments is phosphorylation dependent. Different forms of intermediate filament proteins (e.g. non-filamentous particles versus filaments) reside in different subcellular compartments. During distinct cellular processes such as mitosis, site-specific hyperphosphorylation of cytoplasmic intermediate filaments, as determined by phospho-specific antibody labeling, affect their organization and distribution (Chou et al., 1991; Toivola et al., 2002). Epitope-specific phosphorylation can also segregate intermediate filaments to different compartments within a cell. In pancreatic acinar cells, K18 phosphorylated on Ser33 is necessary for specifically basal filament organization while the non-phosphorylated K18 localizes to the apical domain by default (Ku et al., 2002). Moreover, similar site-specific intermediate filament phosphorylation can be limited to specific cells within a tissue. For example, K20 Ser13 phosphorylation occurs specifically in small intestine goblet cells but not in other K20 expressing enterocytes (Zhou et al., 2006).

Phosphorylation of intermediate filaments promotes other PTMs, such as sumoylation of keratins. Both keratins and vimentin are extensively modified by SUMO2 and SUMO3 *in*

vitro, at multiple conserved rod domain sites. Monosumoylation of keratin increases protein solubility whereas hypersumoylation decreases it (Snider et al., 2011). Thus, sumoylation similar to phosphorylation is crucial for regulating solubility of cytoplasmic intermediate filaments. Similarly, acetylation of the conserved Lys residue (Lys 207) in the rod domain of K8 also decreases K8 solubility. Acetylation thus promotes the formation of a dense perinuclear intermediate filament network formation altering the mechanical properties of filaments (Snider et al., 2013a). A plausible reciprocal relationship exists between glycosylation and phosphorylation PTMs of intermediate filaments (Ku et al., 1996). Glycosylation of K18 (on Ser30/31/49 in the head domain) behaves as a cytoprotective PTM during stress and injury (Ku et al., 2010), whereas ubiquitylation is frequently detected in the context of hyperphosphorylated intermediate filaments. Ubiquitination of intermediate filament proteins promotes intermediate filament turnover; for example, increased K8 and K18 synthesis and phosphorylation predisposes these proteins to ubiquitination-dependent degradation (Ku and Omary, 2000). Thus, different PTMs by themselves or in combination not only alter the intermediate filament organization but also influence the recruitment of intermediate filament accessory proteins, in a context dependent fashion which subsequently regulate various cellular processes.

Table 1.2: Post-translational modifications of cytoplasmic intermediate filaments

Post-translational modification	General effect on intermediate filament	References
Ser/Thr phosphorylation	increases intermediate filament solubility	(Omary et al., 2006; Snider and Omary, 2014)
Tyr phosphorylation	promotes keratin insolubility	(Snider et al., 2013b)
Ser phosphorylation	induces compartmentalization of intermediate filaments	(Chou et al., 1991; Ku et al., 2002; Toivola et al., 2002; Zhou et al., 2006)
Sumoylation	alters filament dynamics	(Snider et al., 2011)
Acetylation	promotes formation of dense perinuclear network	(Snider et al., 2013a)
Glycosylation	protects against stress and injury	(Ku et al., 2010)
Ubiquitylation	regulates intermediate filament degradation and turnover	(Ku and Omary, 2000)

1.2 Intermediate filaments and the establishment of a cellular architectural framework

Throughout development, cells both exert and are subject to an array of forces. These physical interactions are initiated not only by the extra-organismal environment, but also by neighboring cells and extracellular matrix. To maintain the integrity of multicellular tissues, cells must 1) avoid rupturing due to mechanical strain and 2) remain adherent to one another. Intermediate filaments have unique features that not only distinguish them from the other two cytoskeletal elements, actin and microtubules, but also make them major contributors in providing mechanical resistance to the cells (**Table 3**). The persistence length of intermediate filaments is much shorter than both actin microfilaments and microtubules, thus classifying them as flexible polymers (Gittes et al., 1993; Lichtenstern et al., 2012; Mücke et al., 2004; Nöding et al., 2014; Pawelzyk et al., 2014; Schopferer et al., 2009). Cytoplasmic filaments along with being flexible and elastic are also highly extensible and can be stretched ~2.8 fold without rupturing (Kreplak et al., 2005). Microfilaments and microtubules are more fragile and tend to rupture at strains less than 50% (Janmey et al., 1991). Furthermore, intermediate filaments exhibit strain-induced strengthening without catastrophic failure, making them very suitable as intracellular load bearing springs (Ackbarow et al., 2009; Pawelzyk et al., 2014). Both *in vitro* and *in vivo* analyses corroborate this conceptual model of intermediate filaments as important contributors to cells' elasticity and tensile strength (Fudge et al., 2008; Janmey et al., 1991; Ma et al., 1999; Nolting et al., 2015). The dominant function of intermediate filaments in defining cell stiffness is emphasized in

keratinocytes devoid of the entire keratin cytoskeleton (Ramms et al., 2013; Seltsmann et al., 2013a). Indirect perturbation of cytoplasmic intermediate filaments likewise has detrimental effects on cell stiffness. Cells exposed to lipids such as sphingosylphosphorylcholine (SPC), induce perinuclear reorganization of keratins through site-specific phosphorylation, leading to a marked decrease in the elastic modulus (Beil et al., 2003). Studies using keratin mutants that either mimic or abrogate phosphorylation of keratins at specific sites further underscore the importance of phosphorylation on the mechanical properties of intermediate filaments (Fois et al., 2013; Homberg et al., 2015). Although tensile strength is most often attributed to the keratin filaments present in epithelial cells, vimentin also contributes to structural integrity, such that cell stiffness is reduced in vimentin depleted or disrupted cells (Gladilin et al., 2014; Sharma et al., 2017; Wang and Stamenović, 2000) and stiffness is increased in cells overexpressing vimentin (Liu et al., 2015). Vimentin further protects fibroblasts against compressive strain (Mendez et al., 2014).

Table 1.3: Comparison of the mechanical properties of cytoskeletal elements

	Keratin intermediate filaments	Vimentin intermediate filaments	Actin filaments	Microtubules
	Lp<L (flexible)		Lp-L (semi flexible)	Lp>>L (rigid)
Persistence length (Lp)	0.3-0.65 μm (Lichtenstern et al., 2012; Pawelzyk et al., 2014)	0.4-2 μm (Lin et al., 2010; Mücke et al., 2004; Nöding et al., 2014; Schopferer et al., 2009)	18 μm (Gittes et al., 1993)	1000-5000 μm (Gittes et al., 1993)
Contour length	10-20 μm	10-20 μm	$\leq 1 \mu\text{m}$	5-15 μm

Extensibility	~280 ⁺ % (Kreplak et al., 2005)	~300% (Qin et al., 2009)	~20% (Janmey et al., 1991) ~200% (native stress fibers) (Labouesse et al., 2016)	~50% (Janmey et al., 1991)
----------------------	---	---------------------------------	--	-----------------------------------

Along with maintaining the general mechanical integrity of the cytoplasmic volume, cytoplasmic intermediate filaments are also vital determinants of intracellular organelle organization. Vimentin plays a critical role in influencing actin and Rac1 driven (Dupin et al., 2011; Matveeva et al., 2015) localization of cytoplasmic organelles such as endoplasmic reticulum, Golgi complex, nucleus and mitochondria (Gao and Sztul, 2001; Guo et al., 2013; Nekrasova et al., 2011). In *Xenopus laevis*, vimentin intermediate filaments form a cage around melanophores and are involved in their transport and localization at distinct sites within the cells (Chang et al., 2009). Vimentin intermediate filaments are also involved in endoplasm spreading (Lynch et al., 2013). Nuclear position and shape have emerged as important downstream outcomes of mechanical stimuli. Changes in nuclear position relative to other organelles can determine cell polarity, and modulation of nuclear shape influences gene expression and stability. Cytoplasmic intermediate filaments physically link to the nuclear envelope via plectin (an intermediate filament-interacting protein) and SUN/nesprin complexes, also known as LINC (Linker of Nucleoskeleton and Cytoskeleton) complexes (Burgstaller et al., 2010; Ketema et al., 2007; Wilhelmssen et al., 2005). Targeted deletion of nesprin-3 or expression of dominant negative nesprin alters perinuclear intermediate filament organization, cell polarization and migration (Lombardi et al., 2011; Morgan et al., 2011; Postel et al., 2011). Plectin knockout or plectin mutations related to severe skin blistering disease (epidermolysis bullosa simplex) impair perinuclear keratin architecture, but not the linkages to the nucleus, nonetheless leading to misshapen nuclei and abnormal nuclear deformability (Almeida et al., 2015).

At the cell periphery, adhesions to neighboring cells and the surrounding extracellular matrix provide the interface with which cells interact. Intermediate filaments are most commonly known to be anchored to adjacent cells by desmosomes and to the extracellular matrix by hemidesmosomes. The classic view is that intermediate filaments simply provide internal scaffolding attachments to desmosome and hemidesmosome complexes, adhesive junctions that convey relatively long-term associations between a cell and its environment. However, the association of keratin intermediate filaments with desmosomes and hemidesmosomes is also mechanistically supportive of the molecular adhesive complex. That is, keratin filaments can promote the formation and maintenance of desmosomes and hemidesmosomes (Kröger et al., 2013; Loschke et al., 2016; Seltnann et al., 2015). Reciprocally, desmosomal adhesions act as organizing centers for *de novo* keratin network formation in native state tissues (Franke et al., 1980; Schwarz et al., 2015).

In addition to this classical view of intermediate filaments associating with hemidesmosomes and desmosomes, intermediate filaments interact with cell adhesions often inaccurately believed to be exclusively actin-linked, including junctions mediated by classical cadherins (Kim et al., 2005; Leonard et al., 2008; Weber et al., 2012) and focal adhesions (Tsuruta and Jones, 2003; Windoffer et al., 2006). Association of the intermediate filaments with these otherwise actin-linked adhesions is bolstered in response to physical forces applied to these adhesions (Tsuruta and Jones, 2003; Weber et al., 2012). As with desmosomes and hemidesmosomes, intermediate filaments modify the stability of actin-linked focal adhesions and classical cadherin adhesions. In endothelial cells, vimentin

regulates the size and adhesive strength of focal adhesions (Bhattacharya et al., 2009; Tsuruta and Jones, 2003). Vimentin is also implicated in the regulation of vesicular transport of integrin towards the cell membrane (Ivaska et al., 2005).

Intermediate filaments are physically linked to these various adhesion complexes. Vimentin intermediate filaments interact with integrins either directly with binding to $\beta 3$ integrin tail (Kim et al., 2016) or indirectly via linker proteins including plectin (Bhattacharya et al., 2009; Bouameur et al., 2014; Burgstaller et al., 2010) and BPAG (bullous pemphigoid antigens 1 and 2) by forming dynamic linkages with plakin repeat domains (Fogl et al., 2016). In *Xenopus laevis* mesendoderm (also known as anterior head mesoderm) cells, plakoglobin acts as recruitment signal for keratin intermediate filament association with cadherins (Weber et al., 2012). Similarly, in endothelial cells p120 catenin recruits vimentin intermediate filaments to cadherins (Kim et al., 2005). Both vimentin and keratin precursor assembly show dependence on focal adhesions as recruitment sites for motile precursors (Burgstaller et al., 2010). Tethering of adhesion complexes to intermediate filaments presents an ideal circumstance wherein intermediate filaments can serve as mediators of both tension and the coincident signaling that we now know occurs as a function of these adhesions.

Although intermediate filaments, microtubules and actin cytoskeletal networks are often viewed as three separate entities, these filamentous arrays cooperatively interact in more ways than not. Actin filaments and microtubules both have impacts on intermediate

filament organization through multiple direct, indirect and steric interactions. Bidirectional motility of both mature filaments and their non-filamentous precursors of intermediate filaments can occur on either microtubules or actin microfilaments (Helfand et al., 2002; Hookway et al., 2015; Kölsch et al., 2009; Liovic et al., 2003; Prahlad et al., 1998; Wöll et al., 2005). The filament network used to transport intermediate filament precursors is entirely dependent on context. Neither keratin nor vimentin seems to be exclusively limited to microtubules or actin. Motility of intermediate filament precursors can be both fast and slow, in retrograde and anterograde. Although the mechanism of transport seems to be well-defined in some cases (e.g. entirely dependent on actin or microtubules), defining trends have yet to emerge that reliably predict a mechanism of transport for intermediate filaments. Actin filaments are essential to retrograde motility of keratin precursors in some epithelial cells (Kölsch et al., 2009), yet actin cytoskeleton can restrict microtubule-dependent vimentin precursor movement, establishing a complex three-way cytoskeletal communication (Robert et al., 2014). Perturbing either microtubules, microfilaments, or their associated molecular motors can lead to intermediate filament collapse (Knapp et al., 1983; Wöll et al., 2005). Absence of vimentin intermediate filaments alters the microtubule network orientation, thus suggesting a function of vimentin in organizing the cytoskeletal architecture necessary for cell polarity (Liu et al., 2015; Shabbir et al., 2014). In addition, vimentin filaments, but not “non-filamentous” vimentin negatively regulate actin stress fiber assembly and contractility (Jiu et al., 2017). *In vitro* and *in vivo* studies have highlighted direct interactions between the tail domain of vimentin and actin (Cary et al., 1994; Esue et al., 2006). Furthermore, numerous cytoskeletal linkers have been identified that allow for indirect interaction among the cytoskeletal polymers. These proteins include

plectin (Osmanagic-Myers et al., 2015; Svitkina et al., 1996), myosin (Kölsch et al., 2009; Robert et al., 2014), fimbrin (Correia et al., 1999), filamin A (Kim et al., 2010), kinesin (Kreitzer et al., 1999; Prahlad et al., 1998), adenomatous polyposis coli (APC) (Sakamoto et al., 2013), dynein and dynactin (Helfand et al., 2002). Along with distinct cytoskeletal entities interacting with one another, vimentin and keratin intermediate filament networks have been observed to interact at the helical 2B domain of vimentin, and mutations in this region negatively impact collective cell migration (Velez-delValle et al., 2016).

Some data suggest specific roles for each of the cytoskeletal networks in how a cell normally manages different physical forces and stresses. And yet when systems are disrupted, cells often find ways to compensate using the available “protein toolkit”. Mechanical probing of fibroblasts shows that actin contributes to cortical stiffness, whereas vimentin dominates cytoplasmic stiffness (Guo et al., 2013). Disruption of vimentin intermediate filaments mandates that cells find other ways of dealing with imposed forces. In some cases, cells compensate to accommodate self-generated forces by increasing actin stress fibers and myosin activity to facilitate ECM substrate traction while exhibiting disruption of cell-cell adherens junctions (Jiu et al., 2017; Osmanagic-Myers et al., 2015). In response to increased externally-derived physical strain and mechanosensing of these forces, keratins can promote stress fiber formation and cell stiffness by activation of ROCK signaling pathway (Bordeleau et al., 2012). These data illustrate great versatility in how cells use the cytoskeletal networks available to facilitate adhesion, cohesion, and balance intracellular tension and externally-derived stresses. In the context of the complex

multicellular animal, keratin and vimentin establish an important scaffolding framework inside the cell. Cytoplasmic intermediate filaments enable the cells to resist deformation, localize organelles, change shape, and are integrally coupled to adhesion complexes (**Fig. 1.1**).

1.3 Intermediate filaments and modulation of signal transduction pathways

Intriguingly, a wide range of findings suggest that functions of intermediate filaments extend well beyond the mechanical and structural to direct participation in signal transduction. Interactions between cytoplasmic intermediate filaments and other cellular proteins initiate signaling cascades that regulate responses to process such as growth, migration and apoptosis- all cellular processes fundamental to development and embryogenesis.

Cytoplasmic intermediate filaments differentially regulate cellular adhesions through effecting signaling pathways. Vimentin intermediate filaments promote the formation, maturation and adhesive strength of maturing focal adhesions (Bhattacharya et al., 2009; Burgstaller et al., 2010; Liu et al., 2015; Lynch et al., 2013; Tsuruta and Jones, 2003). Vimentin regulates VAV2, a Rac1 GEF, phosphorylation and localizes phosphorylated VAV2 to focal adhesions to promote Rac1-mediated focal adhesion kinase (FAK) stabilization, which further stabilizes focal adhesions (Havel et al., 2015). PKC ϵ -mediated phosphorylation of vimentin governs efficient β 1-integrin recycling and motility (Ivaska et al., 2005), whereas Cdc2-mediated vimentin phosphorylation promotes β 1-integrin activation, leading to FAK phosphorylation (Chang et al., 2012). Likewise, keratins dynamically regulate focal adhesions through integrin/FAK-dependent signaling mediated either via PKC δ or Akt signaling (Bordeleau et al., 2010; Sankar et al., 2013). Reciprocally, during collective cell migration FAK is required for cadherin-dependent keratin intermediate filament organization (Bjerke et al., 2014). Keratins display isotype-specific

signaling functions and unique gene expression patterns of keratins can control stability and dynamics of adhesion complexes. For example, K5/K14 inhibit PKC α -mediated phosphorylation of desmoplakin via RACK1 and thus promote stability and maintenance of desmosomal junctions (Kröger et al., 2013). K6 similarly suppresses cell motility by sequestering Src from being activated and targeting focal adhesions (Rotty and Coulombe, 2012). In contrast, induction of K6/K17 expression produces PKC α -mediated desmosome disassembly (Loschke et al., 2016). Intermediate filaments are tightly coupled with signaling pathways to modulate cellular adhesions.

An ever increasing number of studies implicate intermediate filaments as signaling platforms and as scaffolds for signaling proteins. In fibroblasts, intermediate filament-associated plectin molecules sequester RACK1 on intermediate filaments to modulate PKC δ function (Osmanagic-Myers and Wiche, 2004). Similarly, in keratinocytes, plectin-mediated concentration of RACK1 further regulates ERK1/2 pathway (Osmanagic-Myers et al., 2006). In HER2 positive tumors, a positive feedback loop exists which induces K19 expression via HER2/ERK and further stabilizes HER2 on cell membrane by Akt mediated phosphorylation of K19 on Ser35 (Ju et al., 2015). Keratin 19 is also involved in shuttling β -catenin/Rac1 complex into the nucleus and thus modulating NOTCH signaling pathway in breast cancers (Saha et al., 2017). Collectively, these results support numerous scaffolding roles for keratin intermediate filaments. Vimentin intermediate filaments also function as scaffolds for ERK activation (Kumar et al., 2007). An interesting positive feedback loop exists between vimentin and ROCK2 activation. Activation of ROCK2

causes intermediate filament collapse with simultaneous release of inactive ROCK2. The released ROCK2 is translocated to the periphery where it gets activated again and acts on phosphorylated intermediate filaments (Sin et al., 1998). The vimentin interacting protein Raf-1 associated kinase in concert with other vimentin kinases induce extensive vimentin reorganization (Janosch et al., 2000). It is well known that intermediate filament architecture is reorganized in response to cell migration stimuli. α -Catulin, a scaffold for the ROCK signalosome (Park et al., 2002), co-localizes with vimentin intermediate filaments and contributes to vascular endothelial cell migration (Bear et al., 2016). In addition, vimentin filaments are also essential for VASP localization and phosphorylation by cGMP dependent kinase in endothelial cells (Lund et al., 2010). Many studies have emphasized the contributions of polymerized intermediate filaments, but a novel role of soluble vimentin precursors has been proposed that is not necessarily related to biogenesis of intermediate filament network. Here, soluble vimentin molecules bind to importin- β and phosphorylated ERK and thus enable their retrograde transport in sensory axons (Perlson et al., 2005, 2006). Polymerized intermediate filaments can function as scaffolds while even intermediate filament precursors can play a role of adaptors to transport signaling molecules.

Cytoplasmic intermediate filaments can also serve as phosphate “sponges or sinks”, with broad implications to all signal transduction events. In particular, their head and tail domain have been proposed to buffer excess kinase activity. Such hyperphosphorylation of intermediate filaments can be detrimental or advantageous for the cell depending on the

biological context (Ku and Omary, 2006; Lai et al., 1993). Phosphorylated cytoplasmic intermediate filaments can also act as sequestering reservoirs to accommodate stress response or physiological processes. Both phospho-vimentin and keratin provide binding affinity to sequester proteins like 14-3-3 and therefore limit their availability to other target proteins in order to regulate processes like mitosis and signal transduction (Kim et al., 2006; Margolis et al., 2006; Tzivion et al., 2000). Cell proliferation and size are closely coupled to the binding of adaptor proteins and kinases to cytoplasmic intermediate filaments serving as either molecular scaffolds or sequestration sinks. Perhaps the best example of phosphorylated intermediate filaments operating as docking sites for proteins is provided by members of the 14-3-3 protein family. Keratins and vimentin orchestrate the local interaction of 14-3-3 proteins with their multiple binding partners. 14-3-3 proteins bind keratin 18 (K18) at Ser33 in a cell-cycle and phosphorylation-dependent fashion (Ku et al., 1998) and trigger keratin filament solubilization during hepatocyte mitotic progression (Ku et al., 2002). K18 and 14-3-3 interaction is closely coupled to the association of 14-3-3 proteins with a host of phosphorylated signaling molecules that are involved in mitotic progression, such as Raf1 kinase and Akt (Deng et al., 2012). In the case of Raf, K8/K18 filaments regulate cell signaling via the known K18 and 14-3-3 complex and recruitment of Raf1 kinase by 14-3-3 (Ku et al., 2004). Similarly, phosphorylated vimentin also provides a binding sink for 14-3-3 adaptor proteins (Tzivion et al., 2000). Physical interaction of K10 with Akt and atypical PKC ζ inhibits intracellular translocation of these kinases, thus modulating PI-3 kinase signal transduction pathway and enabling K10 to function as a negative modulator cell cycle progression (Paramio et al., 2001). K17/14-3-3 complex has the ability to stimulate Akt/mTOR signaling and

influence epithelial cell growth and size by regulating protein synthesis (Kim et al., 2006). Thus, phosphorylation of intermediate filaments has broad impacts to both intermediate filament polymerization status as well as modulation of cell signaling pathway.

1.4 Role for intermediate filaments in mechanotransduction

Cellular mechanotransduction is an integration of multiple mechanical cues derived from sensing, transmission of force and transduction into a biochemical response. There is extensive evidence that cell-cell, cell-ECM and flow forces are actively sensed in different cellular contexts by the junctional protein complexes (Conway et al., 2013; Rivelino et al., 2001; Weber et al., 2012). Different mechanical forces alter the structure, assembly, adhesive strength, function and signaling of these adhesive complexes, which in turn has consequences to the cytoskeleton. Cytoplasmic intermediate filaments behave as an elastic and conductive network to transmit force and propagate mechanical stimuli within and between cells via adhesion complexes. As we detailed above, cytoplasmic intermediate filaments emerge as modulators of specific signal transduction pathways in a variety of biological contexts. Abundant availability, overall cytoplasmic presence and subcellular reorganization dependent on cellular context, allows the cytoplasmic intermediate filaments to partake in various signaling pathways in a multitude of ways. Such a view presents cytoplasmic intermediate filaments to be apt to transduce mechanical stimuli during development while integrating an ever changing physical environment with cell signaling (**Fig. 1.1**).

Fluid flow shear stress plays important roles in the developing vasculature system. Perhaps more surprisingly fluid flow shear stress is also an important mechanical stimulus in tissues not often intuitively associated with exposure to fluid flow shear stresses, such as bone and glandular epithelia. Fluid flow shear stress studies have shed some light on the role of

intermediate filaments in mechanotransduction pathways. Cytoplasmic intermediate filaments alter their network organization most likely by mechanisms such as conformational change, changes in assembly, PTMs and others. Mechanical forces such as shear stress can induce rapid reorganization of vimentin and keratin intermediate filament networks in various cell types, suggesting a role in spatial redistribution of intracellular force (Helmke et al., 2000, 2001; Sivaramakrishnan et al., 2008; Yoon et al., 2001). Shear stress increases the keratin intermediate filament network stiffness in the peripheral region of the cytoplasm (Sivaramakrishnan et al., 2008). Shearing also dramatically transforms the keratin intermediate filaments into more “wavy” tonofibril bundles, a process that is promoted by K8 and K18 phosphorylation on serine residues 73 and 33 respectively (Flitney et al., 2009; Sivaramakrishnan et al., 2009). This phosphorylation dependent reorganization of intermediate filaments is regulated by a variety of protein kinases including PKC δ and PKC ζ (Ridge et al., 2005; Sivaramakrishnan et al., 2009). Phosphorylation of keratins in the regulatory head domain (K18 pSer33) recruits binding of 14-3-3, which allow for dynamic exchange and remodeling of the network (Sivaramakrishnan et al., 2009). In order to control against hyperphosphorylation induced disruption, keratin intermediate filaments recruit epiplakin, which perhaps serves as a chaperone during filament reorganization (Spazierer et al., 2008). In addition to the local deformation of the intermediate filaments, there is increased association of vimentin intermediate filaments with β 3-integrin focal contacts, further stabilizing cell-matrix adhesions (Tsuruta and Jones, 2003). Similarly, in response to shear stress, endothelial cells trigger a transition from cell-cell adhesion loading on VE-cadherin to interaction of PECAM (Platelet endothelial cell adhesion molecule-1) with vimentin to stabilize cell-cell

junctions (Conway et al., 2013). In this manner, mechanical loads may be transferred from one cytoskeletal network to another. Indeed keratin intermediate filaments exhibit less motion when actin-myosin II rigidity is increased, likely a consequence of stress generated by actomyosin being transmitted to pre-stress the keratin intermediate filament network (Nolting and Koster, 2013).

Experimentally introduced physical forces, induced by optical tweezers and fibronectin beads on epithelial cells, promote the modulation of both the K8/K18 intermediate filaments and the actin network through Rho-ROCK pathway (Bordeleau et al., 2012). Tensile forces reinforce stress fibers by joint coordination between Solo protein a RhoA GEF and K8/K18 intermediate filament network (Fujiwara et al., 2016). Actin stress fiber assembly and contractility are likewise modulated by vimentin filament dependent regulation of RhoA and GEF-H1 (RhoA GEF protein) (Jiu et al., 2017). Decoupling the intermediate filaments from the mechanotransduction pathway has revealed hitherto unrecognized roles of intermediate filaments in this process. For instance, cells with inhibited vimentin expression display reduced mechanical resistance to the effects of flow (Tsuruta and Jones, 2003). Likewise mutant keratin intermediate filament network is unable to withstand mechanical stress (Ma et al., 2001), with marked reorganization of the filaments into discrete aggregates (Russell et al., 2004). In the absence of vimentin intermediate filaments or their displaced anchorage due to loss of plectin, cells display compromised activation of FAK and its downstream targets Src, ERK1/2 and p38 and thus impaired cell migration. Moreover, exploiting stress conditions in the absence of plectin,

triggers prominent fragmentation of the intermediate filament network (Gregor et al., 2014). In agreement with these findings, cytoplasmic intermediate filaments perceive tension relayed by the upstream mechanosensors and, in response, initiate rearrangements to function as stress buffers. How cytoplasmic intermediate filaments sense tension remains poorly understood. A speculative possibility is that cytoplasmic intermediate filaments alter their conformation or assembly upon stress to reveal cryptic sites crucial for sensing tension. For example, vimentin Cys327 site gets blocked under tension (Johnson et al., 2007; Pérez-Sala et al., 2015). Cytoplasmic intermediate filaments of all types exhibit plasticity in their structural folding which may offer both elasticity and potential for cryptic unmasking. These conformational changes in intermediate filament structure within the polymerized filament could have profound impacts to cell signaling as detailed earlier, and offers a bridge between managing the physical architecture and biochemical signaling.

1.5 Intermediate filaments as determinants of migration

With all of the above in mind, intermediate filaments must be considered as far more than just “intracellular rubberbands”. Attention must be given to intermediate filaments’ polymerization state, connections to adhesions, and influence on signal transduction pathways. Like their actin and microtubule counterparts, intermediate filaments have profound influence over cellular functions, with migration being amongst the most dynamic.

A traditional view of intermediate filaments, particularly keratins, is that their association with stable adhesions provides for a general inhibition of migratory potential. And indeed, depletion or mutation of keratin alters, often increasing, migration rates of cancer cells which is likely to contribute to metastasis (Busch et al., 2012), affect invasiveness (Fortier et al., 2013) and wound healing (Morley et al., 2003). Additionally, impaired directional migration has been observed in MCF-7, HeLa and Panc-1 epithelial cells lacking keratin expression (Long et al., 2006). In contrast, upregulation of vimentin is seen during wound healing (Eckes et al., 1998; Gilles et al., 1999; Menko et al., 2014; Rogel et al., 2011) and carcinoma invasion (Dmello et al., 2016). In addition to being an often used general marker of epithelial-mesenchymal transition (EMT), vimentin has a direct role in the migratory phenotype of cells having undergone EMT (Liu et al., 2015; Vuoriluoto et al., 2011), and declining vimentin levels decrease motility during mesenchymal-epithelial transition (MET) (Mendez et al., 2010). Furthermore, treatment of cells with diverse bioactive molecules such as withaferin A (Grin et al., 2012; Menko et al., 2014), acrylamide (Eckert,

1985), okadaic acid (Strnad et al., 2001), orthovanadate (Strnad et al., 2002) or sphingolipids (Beil et al., 2003; Hyder et al., 2015) simultaneously disrupts cytoplasmic intermediate filament arrays into to perinuclear collapse or soluble aggregates and alters the migration rates of cells.

The aforementioned view of keratins as inhibiting migration and vimentin as promoting migration, while convenient, greatly oversimplifies the actual role that intermediate filaments play in migration. In fact, some keratins, such as K14, can promote cell migration, and their expression is correlated with both invasive carcinomas and migration during embryonic development (Cheung et al., 2013, 2016; Sun et al., 2010). Still other keratins, like K19, seem to have multiple functionalities that may greatly depend on the expression levels and more nuanced roles in modification of signal transduction pathways (Ohtsuka et al., 2016; Saha et al., 2017). How then might intermediate filaments impact migration when they are doing more than simply resisting motility? Different modes of migration, whether random or directed, individual or collective, require the cytoskeleton to generate the structures that drive cell movement. Unique cytoskeletal structures determine and differentiate the protrusive cell front and a retracting rear. Akin to the differences that one sees in actin organization in the front versus the back (branched actin versus contractile stress fibers), it has become evident in recent years that cytoplasmic intermediate filaments establish a similarly polarized cytoskeletal network that regulates motility of single migratory cells.

Intermediate filaments extend through the rear and the perinuclear region of the cell, whereas vimentin particles are predominantly present in the lamellipodia (Helfand et al., 2011). Consistent with this correlational observation, it has been shown that increased presence of vimentin particles precedes lamellipodia formation (Helfand et al., 2011). Induced disruption of vimentin intermediate filament networks by microinjection of vimentin mimetic peptide (1A or 2B2) induces membrane ruffling at cell edges previously devoid of lamellipodia (Goldman et al., 1996; Helfand et al., 2011). Furthermore, non-filamentous vimentin or ULF's were shown to be in close proximity with smaller FAs while stable vimentin filaments were in vicinity of large FAs (Terriac et al., 2017). This suggests that assembly states of vimentin seem not only affect lamellipodia formation but may also be involved in establishing the anisotropy of focal contacts and focal adhesions to modulate efficient migration.

Notably, roles for intermediate filaments in migration are not limited to vimentin. In isolated keratinocytes, keratin particles primarily reside in the lamellipodia and keratin intermediate filaments extend through the cell body to the trailing edge (Kolega, 1986; Kolsch et al., 2010). Furthermore, these cells also exhibit asymmetric keratin dynamics, keratin particles prominently forming in the lamellipodia, further grow by elongation and fusion until integration into the peripheral network (Kolsch et al., 2010). In some non-epithelial cells that express keratins such as mesodermal cells, the correlation between cell protrusive polarity and reorganization of keratin intermediate filament network remains (Weber et al., 2012). In single multipolar mesodermal cells, lacking a definite protrusive

polarity, keratin intermediate filaments span across the cell cytoplasm and yet are notably absent from protrusions (Weber et al., 2012). It remains to be determined whether the location of the keratin filaments per se is a determinant of protrusive activity. However, in support of this hypothesis computational models predict that lamellipodia formation occurs in the direction opposite to keratin network formation (Kim et al., 2012). Keratins mediate stabilization of hemidesmosomes in some cells, and through promotion of these stable contacts, migration is inhibited (Seltmann et al., 2013b). However, not all cells that express keratins, especially during development while tissues are still establishing themselves, make hemidesmosomes and/or desmosomes. The influence of intermediate filaments on migration may have as much to do with the types of adhesions with which they are associated (focal contacts vs. hemidesmosomes) as it does the intermediate filament subtype expressed (vimentin vs. keratin).

How do intermediate filaments guide migration when cells are moving cohesively? Front-rear polarization depends on mechanical cues exerted at cell-cell junctions. Formation of adherens junctions, but not desmosomes, generates tensile stress in tissues (Harris et al., 2014). Perturbing such intercellular contacts either by function blocking antibodies, chelation of calcium or protein knockdown, attenuates stresses mediated by classical cadherins and collective cell migration (Bazellères et al., 2015; Ganz et al., 2006; Plutoni et al., 2016). Application of local tension on single mesodermal cells induces reorganization of the intermediate filaments at cell-cell adhesion sites via plakoglobin (Weber et al., 2012), coincident with the induction of polarized cell protrusions and

directional migratory behavior (Toyoizumi and Takeuchi, 1995; Weber et al., 2012). Similarly, *ex-vivo* embryonic *Xenopus* tissue explants arrange keratin intermediate filaments in a manner similar to single cells under tension (Weber et al., 2012). Reorganization of keratin cytoskeleton is also observed during epithelial sheet migration (Long et al., 2006). Intercellular tissue tension also contributes to integrin mediated traction forces (Dzamba et al., 2009); and conversely, integrin-fibronectin traction forces contribute to tissue tension and affect cell-cell tension by increasing the size of cadherin mediated cell-cell adhesions (Liu et al., 2010; Maruthamuthu et al., 2011). Thus, both cell-cell and cell-ECM interactions establish physicommechanical guidance cues. Extending lamellipodia of repair cells of wound healing are frequently enriched with vimentin particles (Menko et al., 2014). Likewise keratin particles are observed in the leading edge lamellipodia of epithelial cells (Kolsch et al., 2010). Thus, intermediate filaments break the symmetry and are arranged in an asymmetrical array to supporting polarized migration. We argue that this asymmetry may facilitate establishment of differential front and rear microenvironments necessary for efficient migration.

The small GTPase Rac1 is a probable mechanism for the differential localization of cytoplasmic intermediate filaments, and has direct implications to regulation of migration and polarity. Optimum levels of Rac1 play a critical role in protrusion formation to ensure directional cell migration (Pankov et al., 2005). Spatial and temporal activation of Rac1 is sufficient to promote collective cell migration in different models (Theveneau et al., 2010; Wang et al., 2010; Yoo et al., 2010). Additionally, leader cells of the MDCK collectives

not only show elevated levels of Rac1, integrin β 1 and PI3k, but also inhibition of any of these molecules disrupt the migratory phenotype. Activation of Rac1 which is downstream of integrin β 1 and PI3k drives the collective migration (Yamaguchi et al., 2015). In single migratory fibroblasts, local induction of Rac1, promotes disassembly of vimentin intermediate filaments, locally inducing membrane ruffles, while the assembled filaments are maintained in the rear (Helfand et al., 2011). Rac1 activity is negatively regulated by cadherin (Kitt and Nelson, 2011) and plakoglobin (Todorović et al., 2010), proteins which are both intermediate filament interacting molecules. These data suggest that cell-cell contacts may serve a mechanosensing and signaling function by stably recruiting intermediate filaments where they locally suppress Rac activity, and cell protrusions, at the posterior of collectively migrating cells (Figure 2).

The antagonistic relationship between cytoplasmic intermediate filaments and Rac1 may act as a mechanochemical switch that determines which of two mutually exclusive signaling states will occur. A similar switch exists between Merlin and Rac1. A negative feedback loop between Merlin-Rac1 controls the protrusion promoting state in the front end of the cell and protrusion inhibiting state at the rear end of the cells (Das et al., 2015). Stable cell-cell adhesions promote persistent directionality through this negative feedback loop (Das et al., 2015). Interestingly both intermediate filaments and Merlin are associated with stable cadherin-mediated cell-cell contacts. Perhaps future studies will find a molecular mechanistic link given their common function in regulating polarity of collectively migrating cells.

1.6 Functional roles for intermediate filaments during development

Elucidating the role of many cytoplasmic intermediate filaments in embryonic development has proven to be challenging due to functional redundancy and complexity within the family. Targeted deletion of K18 failed to block embryonic development in mice because of the presence of K19, demonstrating the functional redundancy within the protein family (Magin et al., 1998). However, double K18/K19 null mice display embryonic lethality due to disruption of the extraembryonic trophoctoderm (Hesse et al., 2000). Despite this dominant role in the extraembryonic tissue, various keratin knockouts have surprisingly mild developmental phenotypes considering the known roles intermediate filaments play in adhesion. Knockout of all Type II keratins (KtyII^{-/-}) still produces an embryo that survives through neurulation and begins organogenesis (Vijayaraj et al., 2009). Nonetheless it should be noted that there is a significant delay in the early development of these KtyII^{-/-} mice up to E8.5 that rapidly attempts to recover to E9.5 but ultimately ends in embryonic lethality (Vijayaraj et al., 2009). Defects in specific tissues at later stages where keratins are expressed argues a role for keratins in late tissue morphogenesis, homeostasis and physiological function (Bouameur and Magin, 2017), but a role for keratins in early embryogenesis has largely remained elusive in mouse models. As with many of the keratin knockout mice, mice lacking vimentin surprisingly undergo embryonic development quite normally, however, exhibit impaired wound healing (Eckes et al., 2000). In some cases, the role of cytoplasmic intermediate filaments only becomes evident upon mechanical and/or chemical stresses (Bouameur and Magin, 2017).

Genetic mouse models have yet to indicate a role for keratins or vimentin in early embryogenesis, but knockout mice have unequivocally revealed a definitive role for keratins in development and maintenance of skin (Bär et al., 2014; Kumar et al., 2015). The epidermal skin is broadly comprised of proliferative basal, stratified suprabasal, and terminally differentiated cornified layers. Each of these layers expresses a unique combination of Type I and II keratins. Additional keratins, such as K6, K7, K9, K17, K76, have limited expression in the specialized epidermal regions like the palms and hair follicles. In line with prior data that hemidesmosomes and desmosomes provide for mechanical strength of skin, keratin knockout mice have severely fragile skin and the barrier function of the skin is compromised (Bär et al., 2014; Kumar et al., 2015). What is more, perturbation of keratin expression in these layers also results in the disruption of the homeostasis of the epidermis as it matures into distinct layers. Although functional redundancy may obscure the role of specific keratins (Reichelt et al., 2001; Reichelt and Magin, 2002), dysregulation of cell proliferation is a common theme in several keratin knockouts (e.g. K7^{-/-}, K8^{-/-}, K9^{-/-}, K10^{-/-}) (Bouameur and Magin, 2017). Keratins also coordinate cell growth and protein biosynthesis by accurate localization of GLUT-1 and -3 and consequentially optimize regulation of mTOR pathway as evidenced by keratin Type II knockout mice (Vijayaraj et al., 2009). Collectively, these data point toward an important role for cytoplasmic intermediate filaments in modulating cell growth and proliferation through their impact on cell signaling pathways.

Cells migrate collectively in a coordinated manner to accomplish various tasks for development of the organism, from gametogenesis to morphogenesis to organogenesis. Collective cell migration allows whole groups of cells to move towards their final destination most efficiently while maintaining tissue cohesivity and tissue-specific characteristics. All the while, these cells can transmit signals to each other and effectively navigate the complex and changing environment within the developing embryo. Disruption of the keratin network in the amphibian embryo tells quite a different story than mice about the importance of intermediate filaments in early embryogenesis. Disruption of keratin by either targeting protein expression (Heasman et al., 1992; Weber et al., 2012) or filament assembly (Klymkowsky et al., 1992) impairs mesodermal involution and blastopore closure during gastrulation. Pointing to a role in collective migration events, polarized protrusive cell behavior of the mesoderm is lost in the absence of K8 expression in *Xenopus* embryos (Weber et al., 2012).

Collective cell movements are also perturbed in keratin mutant mice, albeit at stages of organogenesis and tissue maintenance. Vimentin plays a role in promoting stemness of mammary epithelial cells which provide the basis for mammary gland growth. Ductal outgrowth is significantly delayed in mammary glands from vimentin knockout mice and the lumen is slightly enlarged (Peuhu et al., 2017). Vimentin expression in stromal and basal epithelial layers is accompanied by expression of keratins in the basal (K14) and luminal (K8/18) layers of the mammary epithelia (Peuhu et al., 2017; Sun et al., 2010). Both populations of mammary cells are involved in the branching morphogenesis of the

tissue. Live cell imaging studies have shown that K8/18+ mammary epithelial cells collectively migrate during this process (Ewald et al., 2008) and other studies have indicated a pro-migratory role of K14 expressing mammary cells in collective invasion at the epithelial-stromal boundary (Cheung et al., 2013). Interestingly during the initial development of the mammary placode in the embryonic mouse, these invasive migratory cells express both K8 and K14 (Sun et al., 2010). Only recently have selective promoters for basal mammary epithelial cells become available. It will be interesting to determine whether knockout of K14 and/or K8 functionally inhibits mammary development.

Morphogenesis of epidermal and muscle tissue in *Caenorhabditis elegans* provides a particular elegant example of the interplay between intermediate filaments and mechanotransduction pathways during development. Muscle-generated tension within the epidermis induces recruitment of the adaptor protein GIT-1 and its partner PIX-1, a Rac GEF, to hemidesmosomes (Zhang et al., 2011). With PIX-1 at the hemidesmosome, Rac is activated, which further stimulates PAK-1 activity and subsequent phosphorylation of intermediate filaments (Zhang et al., 2011). Phosphorylation of intermediate filaments through this mechanism drives remodeling and maturation of the hemidesmosome and the associated intermediate filament network (Zhang et al., 2011). Hemidesmosomes behave as mechanosensors that further relay the tension by activation of specific signaling pathways that promote epithelial morphogenesis (Zhang et al., 2011). Indeed, coordination between the epidermis and muscle cells is absolutely essential to epidermal morphogenesis

that elongates the worm, and cytoplasmic intermediate filaments are vital to this process (Woo et al., 2004).

Migration driven by cell-cell adhesions has roles very early in development, even as early as development of gametes. Tension sensing through E-cadherin plays a critical role in controlling directionality of migration of border cells in the *Drosophila* ovary (Cai et al., 2014). As with many collectively migrating cells, asymmetric Rac activity also plays a key role in the steering of these migrating collectives (Wang et al., 2010; Yoo et al., 2010). For some time, cytoplasmic intermediate filaments were believed to be absent from many non-chordates including arthropods. Recently however, it was found that the tropomyosin-1 gene (Tm1) produces a unique isoform, Tm1-I/C, which has many cytoplasmic intermediate filament-like characteristics, including the tripartite head-rod-tail structure and the ability to anneal end-to-end and spontaneously polymerize into filaments of similar diameter to intermediate filaments (Cho et al., 2016). Knockdown of this Tm1 isoform impairs border cell migration, unlike knockdown of other Tm1 isoforms. Moreover, actin stress fiber organization is perturbed in cells lacking Tm1-I/C, despite that Tm1-I/C does not co-localize with actin (Cho et al., 2016). While the inhibition of border cell migration in Tm1-I/C knockdown cells could be entirely structurally related to facilitating adhesions and/or enabling protrusions, it certainly is appealing to speculate that Tm1-I/C, like keratin and vimentin intermediate filaments, tethers to cell adhesions and allows for mechanotransduction between these adhesions and signaling mechanisms regulating cell protrusive behavior

1.7 *Xenopus laevis*: model organism

Gastrulation is a crucial early phase process during embryogenesis. Here, the embryo reorganizes from a blastula (a hollow ball of cells) to a multilayered embryo with the three primary germ layers: ectoderm, mesoderm and endoderm. By the end of gastrulation, the mesoderm is located between the outer ectodermal layer and the inner endodermal layer. Gastrulation also is a key process that establishes the body plan of the embryo by specifying the anterior-posterior and dorsal-ventral axis. Morphogenetic tissue rearrangements mainly involve three modes of evolutionarily conserved migration patterns: 1) epiboly; 2) emboly or mesendoderm internalization and 3) convergent extension. These whole tissue movements are achieved by different directed cell behaviors including directed cell migration, radial intercalation and mediolateral intercalation. By performing these complex and mechanically coupled cellular reorganizations, the embryo undergoes gastrulation. The two modes of migration important from the stand-point of this study are epiboly and emboly.

Epiboly

During *Xenopus* gastrulation, the animal hemisphere of the embryo thins, expands and spreads vegetally. This morphogenetic movement is termed as epiboly. Here, the multilayered tissue is reduced by a process known as radial intercalation (Keller, 1978). Cellular movements of radial intercalation drive epiboly through the coordinated wedging of the several layers of cells between one another, thus exchanging neighbors and repositioning in the tissue. The movement of cells between adjacent planes (radially) and

toward the blastocoel roof forms a thinner tissue with increased diameter. Along with radial intercalation of the deeper layers, there is spreading and division of the superficial layer (Keller, 1978, 1980). Thus, epiboly entails the thinning and spreading of both ectodermal and mesodermal progenitors (Keller, 1975; Wilson and Keller, 1991) contributing to expansion of the embryo surface during early development. Both cell-matrix adhesions comprised of integrin $\alpha 5 \beta 1$ mediated interactions with fibronectin (Marsden and DeSimone, 2001) and cell-cell adhesions through E-cadherin (Choi and Gumbiner, 1989) are required for the cellular rearrangements during epiboly. In scenarios when mutated cadherin is expressed in animal cap cells or cadherin is knocked out, animal cap cells fail to undergo characteristic epibolic movements (Babb and Marrs, 2004; Kane, 2005). Within cells, the cytoskeleton, and in particular the keratin network, also seems to play a part to ensure satisfactory epiboly. Disruption of keratin network by anti-keratin antibodies induces gastrulation defects (Klymkowsky et al., 1992), notably a collapsed animal cap and extruded endodermal mass. A similar phenotype is observed when keratin expression is knocked down (Weber et al., 2012). Even though a functional role for keratin proteins has been demonstrated to ensure normal gastrulation, the role of keratin *filaments* remains uncertain.

Emboly

During *Xenopus* gastrulation, mesendoderm, a mixed population of mesodermal and endodermal cells, migrate beneath the ectodermal layer, in a process called emboly or internalization. Emboly involves apical constriction of bottle cells which shape the dorsal

blastopore lip. This is followed by mesodermal cells of the involuting marginal zone (IMZ) moving inward through the blastopore. At the onset of gastrulation, the vegetal endodermal cells are also moving animally towards the blastocoel roof (BCR). These combined movements bring the mesendodermal (the leading edge of the mesodermal mantle and the associated endoderm) cells migrating collectively as a cohesive sheet on the BCR (Keller et al., 2003). Thus, emboly entails morphogenetic movements such as involution and invagination to move the presumptive mesendodermal cells into the deeper layers.

Collective cell migration

Cellular movement of the internalized mesendoderm is a classic example of collective mode of migration. Collective migration of cells is defined as the ability of a group of cells to migrate simultaneously in a highly coordinate fashion. Unlike epiboly, collectively migrating cells do not exchange neighbors. Here, both leading edge cells and follower cells extend protrusions in the direction of migration. Follower cells' protrusions underlap those cells in front of them, creating a "shingled" arrangement such that the leading edges are in contact with fibronectin on the blastocoel roof and the trailing edges are within the mass (Davidson et al., 2002; Winklbauer et al., 1996). The collective migration of mesendodermal tissue starts dorsally and then progresses laterally and ventrally (Ibrahim and Winklbauer, 2001; Winklbauer and Schürfeld, 1999). Mesendoderm, also known as anterior head mesoderm, will contribute to interior structures of the head and foregut. It is well established that collective migration of mesendodermal cells depends on integrin based cell adhesion to the extracellular matrix protein fibronectin deposited on the inner

surface of blastocoel roof. Additionally, depletion of integrin associated focal adhesion kinase (FAK) causes failure of recruitment of keratin filaments to cell-cell adhesions at the rear of the cell and loss of oriented protrusions, leading to impaired collective migration (Bjerke et al., 2014). In parallel to cell-matrix adhesions, cell-cell contacts are also important for collective migration. In individual mesendoderm cells, application of C-cadherin mediated tension induces both polarized cell protrusion and directed migration of these cells (Weber et al., 2012). Along with the cellular adhesions, the importance of keratin filaments during collective cell migration has also emerged. Depletion of keratins disrupts important processes such as migration of tissues and embryogenesis in *Xenopus* (Torpey et al., 1992; Weber et al., 2012). Further, keratin filaments organize to sites of cell-cell contact only when tension is applied and are not induced to do so simply by cadherin engagement (Weber et al., 2012). These studies insinuate keratin *filaments* of having a role in mesendodermal collective migration to ensure normal gastrulation.

Hence to achieve successful gastrulation, both epiboly and collective migration of mesendodermal cells require cellular adhesions as well as keratin IFs. Due to these well-characterized cell and tissue movements, the *Xenopus* embryo is an excellent model to study the role of keratin filaments during embryogenesis.

Figure 1.1

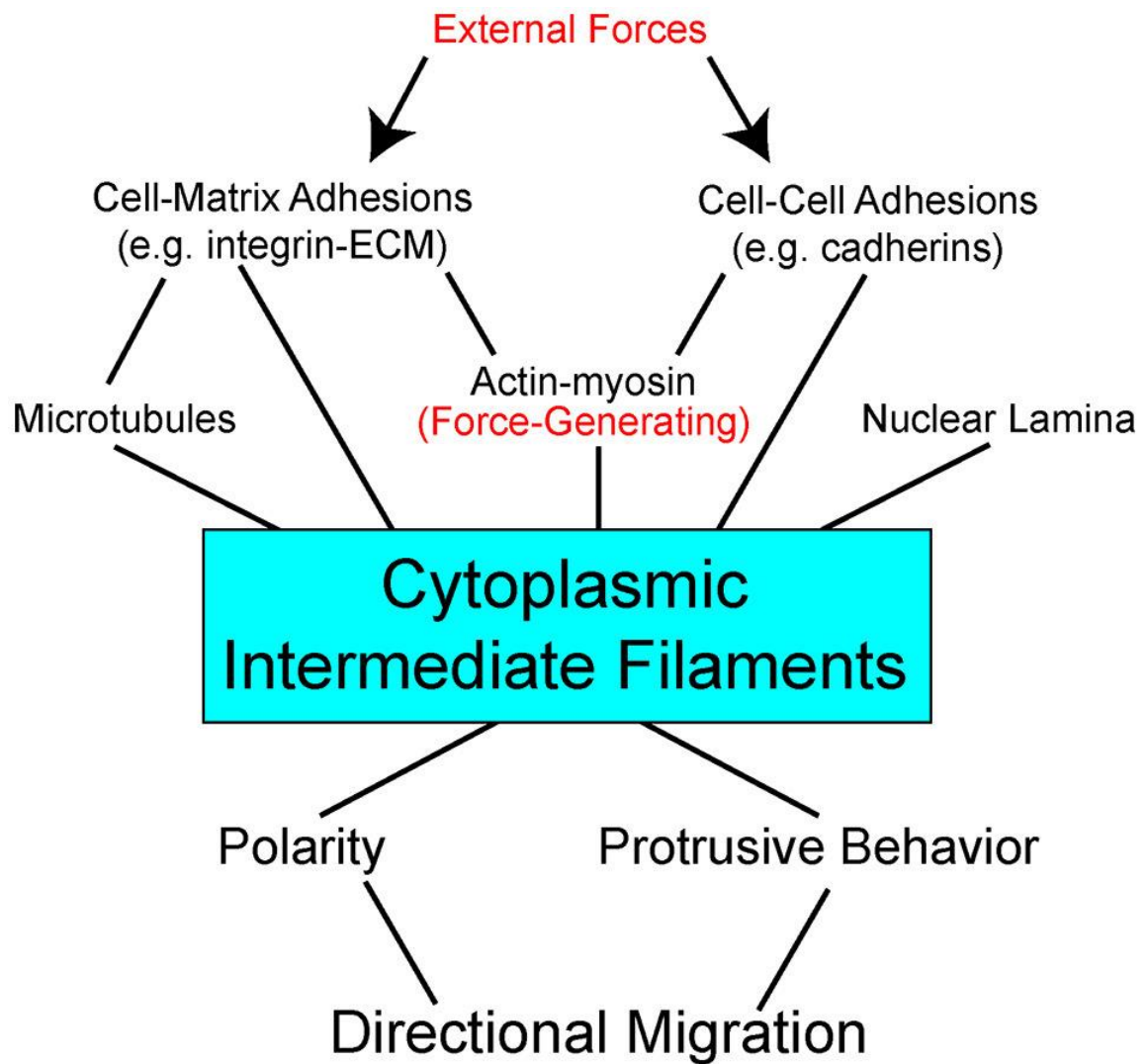


Figure 1.1: Interdependent network model of cytoplasmic intermediate filaments as a centerpiece between mechanical stimuli and directional cell migration.

External forces act on (arrows) adhesion molecules on the cell surface to impact a complex network of bidirectional interactions within the cell (lines). Adhesions are linked to the three major cytoskeletal networks. Of these, actin with its myosin motors is the primary force-generating apparatus. Intermediate filaments can be pre-stressed by actomyosin generated tension. Intermediate filaments also act to resist strains imposed on the cell. Through modulation of cell signaling pathways, direct and indirect, intermediate filaments effect cell polarity and protrusive behavior. Stabilization of distinct subcellular locales promotes persistent directional migration.

Figure 1.2

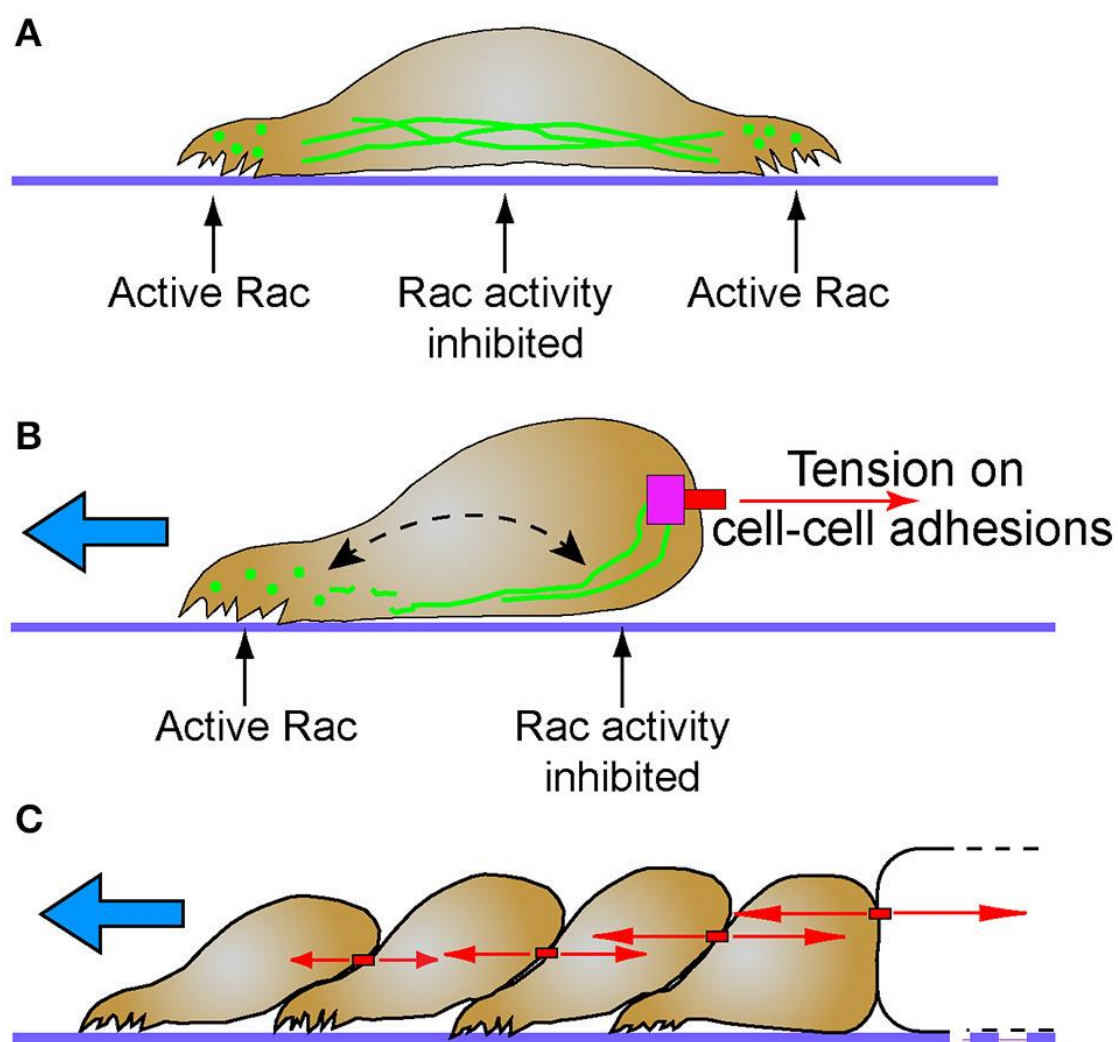


Figure 1.2: Intermediate filaments and the establishment of cellular subdomains to drive directional migration.

(A) Intermediate filaments exist in cells as monomer, filament precursors and mature filaments. While mature intermediate filaments connect to cell adhesions, the nuclear lamina and span across the cell body, they are often notably absent from protrusions. Filament precursors are abundant in protrusions where Rac is active. (B) Tension (red arrows) on cell-cell adhesions recruits intermediate filaments. Persistent localization of intermediate filaments proximal to cell-cell adhesions may establish distinct non-protrusive Rac-inhibited zones. Areas of the cell with lesser tension on cell-cell contacts do not recruit intermediate filaments, creating Rac-permissive zones that promote protrusions that lead to directional migration (blue arrow). Despite this subcellular localization, intermediate filaments remain dynamic through non-polar subunit exchange (dashed arrow). (C) Stable cell-cell adhesions and the differential intercellular tension present across tissues may promote persistent collective cell migration behavior (blue arrow). Intermediate filaments simultaneously maintain tissue integrity while influencing cell signaling pathways that determine cell polarity and protrusive behavior.

Chapter 2

Introduction

Introduction to the thesis project

Embryonic development entails orchestration of evolutionarily conserved morphogenetic movements of embryonic cells to form the germ layers and eventually sculpt the body. To accommodate such processes, cells interact with both neighboring cells and the extracellular matrix through adhesion receptors expressed on their surface. These adhesion receptors are linked inside the cell to a structural framework known as the cytoskeleton, made up of actin microfilaments, microtubules, and intermediate filaments (IFs). The former two filament systems, actin and microtubules, are well-known to be dynamically assembled, disassembled and remodeled through processes known as treadmilling and dynamic instability, respectively. In contrast, only through recent advances in live cell molecular imaging has it become increasingly apparent that intermediate filaments are also dynamic structures. Along with their dynamic behavior intermediate filament proteins, particularly keratins have been implicated in various cellular processes. The significance of cytoplasmic intermediate filament proteins has previously been examined largely through various genetic approaches, including knockdown, knockout and transgenic overexpression. Few studies to date have attempted to examine the role of specifically the filamentous keratin network in orchestrating various cell functions. However, its specific involvement during early development is questionable and needs further investigation.

Keratins are critical during embryogenesis, but the functional importance of the polymerized keratin filaments versus keratin proteins is still elusive (Klymkowsky et al.,

1992; Torpey et al., 1992; Weber et al., 2012). Conventional approaches used to study the role of keratins, whether they target protein synthesis or filament assembly, generate exogastrulation defects in *Xenopus* embryos (Klymkowsky et al., 1992; Torpey et al., 1992; Weber et al., 2012). These data hint towards the importance of keratins during embryogenesis, but fall short of identifying the functional significance of keratin filaments in early embryonic development. Recent studies highlight the role of keratin filaments as being important for specifying the directional protrusive behavior of migratory mesendoderm cells in gastrulating *Xenopus* embryos (Weber et al., 2012). Regardless of these studies, the functional significance of keratin filaments is least understood in early development, partly due to lack of available tools for interrogating IFs with subcellular resolution. In contrast to IF proteins, a multitude of small molecule compounds that specifically depolymerize or stabilize actin filaments and microtubules have been available for decades, which has led to major breakthroughs in their fields of research.

Using the *Xenopus laevis* (*X. laevis*) frog embryo as a readily accessible model system for embryogenesis and epithelial cell line Madin-Darby Canine Kidney (MDCK) cells as a model system for *in vitro* studies, this thesis explores different methods of keratin intermediate filament perturbation and the role of polymerized keratin filaments. Here, the focus is on morphogenetically active tissues such as ectodermal tissue that undergoes epiboly and collective migration of mesendoderm. The *Xenopus* model system is advantageous, owing to the external development of embryos, the earliest stages of embryogenesis are easily accessible for manipulations, such as microinjection of DNA,

mRNA or exposure to inhibitors. In addition, both dissociation of cells and explant preparations are easy to perform. Furthermore, they are ideal for studying keratin intermediate filaments for several reasons. In contrast to most keratin-expressing cells such as MDCK which are comprised of basic cytokeratins K5, K7, K8 as well as the type I acidic keratins K17 and K19 (Pollack et al., 1997), *X. laevis* ectodermal and mesodermal progenitor cells only express one type II basic cytokeratin keratin 8 (K8) and two type I acidic cytokeratins keratin 18 and 19 (K18 and K19), which greatly reduces the complexity of multiple intermediate filament networks. *X. laevis* progenitor cells also have relatively few filaments exhibiting a distinct keratin network.

Here I tested the central hypothesis that *polymerized keratin filaments have specific function in morphogenetically active tissues during early development*. The following specific aims were addressed with the goal of understanding the relationship of keratin intermediate filaments to cell-cell adhesions, coordinated migration and early embryonic development.

Specific Aim 1: To evaluate the effects of small molecule inhibitors on keratin intermediate filament network.

Specific Aim 2: Design and develop specific inhibitors to keratin filaments with spatiotemporal resolution.

Specific Aim 3: Investigate the functional role of keratin filaments during early development in *Xenopus laevis*.

Presentation of chapters

The following chapters will fundamentally impact the general understanding of keratin filament network function. The major innovation of this thesis is the development of novel tools to specifically inhibit keratin filaments with spatial and temporal precision. These genetic modules acutely disrupt the keratin filaments and thus allow to directly assess their role in regulating cellular behavior. Using this novel approach, significant progress has been made toward establishing a functional role for the keratin filament polymers during normal embryonic development.

Chapter 4 begins by studying the subcellular localization of keratin filaments in *ex vivo* migratory explants. Here, I show selective compartmentalization of keratin filaments and keratin particles in both *Xenopus* embryonic explants, ectodermal and dorsal mesendoderm. Moreover, the keratin network organization is dependent on the cellular context

A broad comparative study to establish global methods for effectively depolymerizing intermediate filaments has been accomplished in **chapter 5**. Here, small molecular inhibitors such as withaferin A and acrylamide are used to perturb intermediate filaments in cells with varying cell-cell interactions.

In **chapter 6**, I have developed a unique molecular tool to study function of keratin filaments with subcellular specificity. Here, photoactivatable disruptor of keratin filaments has been engineered, a fusion protein where a peptide derived from the 2B2 region of *Xenopus laevis* keratin 8 is appended with LOV-J α of the *Avena sativa* phototropin-1. Detailed studies about the engineering, characterization and verification of these tools are provided here.

Finally, **chapter 7** demonstrates the application of the photoactivatable 2B2 in native cellular environments. The study validates the use of this unique tool as a disruptor of keratin filaments in ectodermal progenitor cells. In addition, examination of embryonic phenotypes after targeted disruption of keratin filaments reveals a primary role of keratin filaments during early embryogenesis.

This thesis will then conclude with an overall discussion of results and preliminary data for future work in **chapter 8**.

Significance of the study

Morphogenetic movements of embryonic cells play a central role in the development of multicellular organisms. Keratin intermediate filaments have been implicated in facilitating early embryological development. However, their mechanistic functional role and subcellular localization needs further investigation. The unavailability of specific drugs to disrupt intermediate filament networks has impeded our understanding of their contribution to various cellular processes. The principal goal of the current thesis is to explore the functional importance of keratin filamentous network during early embryogenesis. To address this goal a new innovative method was developed, a genetic photoswitch which allows targeted disruption of keratin filaments with spatiotemporal efficiency. This study sheds light on the fundamental requirement of keratin filament polymers in morphogenetically active tissues during early embryogenesis through its role in fibronectin fibrillogenesis. The current tool will be transformative for the field of intermediate filaments, since similar acute acting methods to manipulate the actin filaments and microtubules have been a major source for advancing our knowledge of the roles of these other cytoskeletal networks. This study is anticipated to have a positive impact since the importance of keratin filament polymers can be further extrapolated to understand functional roles of keratin filamentous networks in normal development or pathological conditions.

Chapter 3

Materials and Methods

3.1 Cell culture and transfection

3.1.1. Cell lines and cell culture

Madin-Darby canine kidney (MDCK) epithelial cells and Human embryonic kidney 293T (HEK 293T) cells were obtained from ATCC (CCL-34 and CRL-3216, respectively). Cells were maintained in growth medium consisting of Dulbecco's modified Eagle's medium (DMEM) (Gibco, #31053028) containing 10% Fetal bovine serum (FBS) (Gibco, #10438026), Penicillin-Streptomycin (Gibco, #P0781), Glutamax (Gibco, #35050-061), 26.18 mM NaHCO₃ and filtered sterilized using 0.2 µm vacuum filter and grown at 37°C with 5% CO₂ in a humidified tissue culture incubator. Cells were cultured from frozen stock (stored in liquid N₂ or -80°C) and were not used beyond passage 20. Confluent cultures grown on plastic dishes were trypsinized (Life technologies, #15400054), dispersed into culture medium, and then the cells were replated onto dishes as per requirement of the experiment.

3.1.2. Plasmids and transfections

Xenopus keratin 8 plasmid C2-eGFP-krt8 construct was a kind gift from Dr. Victoria Allan and was subcloned into pCS2+ previously (Weber *et al.*, 2012). Keratin 19 plasmid pCS2+-eGFP-krt19 was made by Richard Mariani (Mariani *et al.*, 2018). mCherry plasmid (C1-mCherry) was from Clontech. PA-2B2 and I379E-2B2 were generated by cloning commercially synthesized Flag-tagged LOV-Jα-2B2 (Flag-PA-2B2) and LOV-Jα(I379E)-2B2 (Genewiz, NJ) (sequence provided elsewhere) into pCS2⁺ vector using EcoRI and XhoI restriction sites. Flag-tag was swapped for mCherry at the N-terminus using NheI

and BglII sites in pCS2⁺ Flag-PA/I379E-2B2 and C1-mCherry. Similarly, PA-1A and I379E-1A were also generated. In detail description about these plasmids is provided in the chapter 6.

3.1.3. Stable transfection and generation of cell lines

MDCK cell lines expressing eGFP-K8 were generated by transfection of the pCS2-eGFP-krt8 construct using lipofectamine 3000 (Invitrogen, Life Technologies) according to manufacturer's guidelines. Briefly, cells were seeded onto 96 well plates or 35 mm dishes to achieve 70-80% confluency at the time of transfection. For 96 well plates, 10 μ l of OPTI-MEM reagent was incubated with 0.3 μ l of lipofectamine, 0.2 μ l of P3000 and 0.1-0.2 μ g of DNA for 15 mins and then the DNA-lipid complexes were added on to the seeded cells. Whereas for 35 mm dishes, 150 μ l of OPTI-MEM reagent was incubated with 10 μ l of lipofectamine, 7.5 μ l of P3000 and 1-1.5 μ g of DNA for 15 mins and then the DNA-lipid complexes were added on to the seeded cells. The cells were then incubated for 6 hrs at 37°C before exchanging the cell culture medium.

For reverse transfection, in brief, the above-mentioned kit reagents were mixed and the Lipofectamine 3000-plasmid complexes were added to the cell suspension. Cells were then seeded and incubated for 24 hrs at 37°C until they were ready to be used for the assay.

Cells expressing eGFP-K8 were sorted based on homogeneous expression levels using Fluorescence-activated cell sorting facility (FACS) (Flow Cytometry Core Lab, NJMS,

Rutgers, Newark). Amongst the heterogenous expressing population, medium expressors were selected and enriched using FACS and used for experimental purposes.

3.1.4. Transient transfections

Transient transfections for WT MDCK and eGFP-K8 expressing MDCK cell lines, were performed using Lipofectamine 3000 (Invitrogen, Life Technologies) according to manufacturer's protocol. Cells transfected with light sensitive 2B2 and 1A constructs were handled in dark or under red light to avoid unintended 2B2 or 1A activation.

3.1.5. Sparse plating

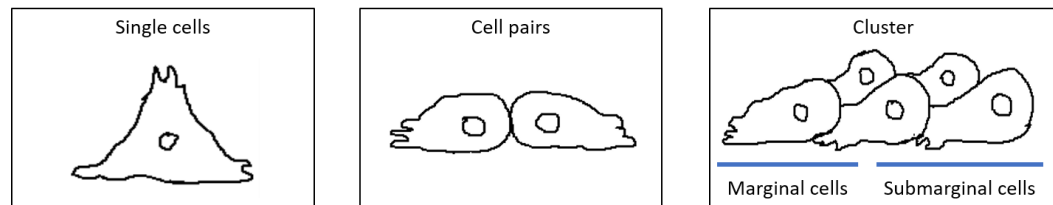
Plating densities are defined as ~ 60-70% confluent for 'sparse' and ~ 80-90% confluent for 'dense' cultures. For experiments under sparse culture conditions, cells were seeded at a density of 5000 cells per well in a 96-well plate and 80,000 cells per 35 mm glass bottom dishes. For dense culture assays, 100,000 cells per 35 mm glass bottom dishes. For lysate preparation, 0.5×10^6 (low density) and 1.5×10^6 (high density) per 100 mm dish. Once plated, cells were allowed to attach for at least 18 hrs before exposing to any treatment or transfection. Cells were grown at 37°C, 95% humidity and 5% CO₂.

These different MDCK conditions (**Fig. 3.1**) will be examined for chapter 5 and 6:

(1: Single cells) MDCK cells seeded at a density that single cells are obtained with multipolar protrusions and no cell-cell contacts exist.

(2: Cell pairs) here MDCK cells having cell-cell contacts, with cells polarized and protruding in opposite directions are considered as cell pairs.

(3: Clusters) cells will be allowed to form islands to achieve anisotropy of cell-cell contacts and protrusions towards the periphery. The cells in the outer edge of these clusters are designated as marginal cells and the cells within the cluster are designated as sub-marginal cells. Here clusters with cell density of 10 cells and above were only taken into consideration.

Figure 3.1**Figure 3.1 Varying cell-cell interaction conditions.**

3.2. Small molecule inhibitor treatments

For inhibitor treatments, Withaferin A (WFA) (Cayman chemicals, #CAS NO 5119-48-2) was dissolved in DMSO (Fischer scientific) at a stock concentration of 10 mM. Similarly, nocodazole (Cayman chemicals, #CAS NO 31430-18-9) was dissolved in DMSO at a stock concentration of 5 mM. While, acrylamide (Sigma, #A9099) was dissolved in water at a stock concentration of 1 M. Inhibitors were further diluted to a final concentration by adding them to the culture medium at indicated time intervals. For control experiments either H₂O or DMSO was added to the culture medium at the same dilutions. All treatments were performed at 37°C in 5% CO₂ for MDCK cells and at room temperature for mesendoderm cells.

3.3. Embryology/ *Xenopus laevis* embryo culture and microinjections

3.3.1. *Xenopus laevis* egg collection and testes preparation

Adult *Xenopus laevis* were obtained from Nasco (Fort Atkinson, WI) and housed at Rutgers University-Newark and used in accordance with institutional guidelines and the approval of the local Institutional Animal Care and Use Committee. Females were injected with a priming dose of human chorionic gonadotropin (hCG) 50 U (2U/μl) (MP Biomedicals, #198591) in the dorsal lymph sac 7-10 days preceding induction of ovulation. Females were induced to ovulate by injection of 500 U human chorionic gonadotropin and incubated at 15°C until ovulation commenced, typically 12 hours later. Spawning frogs were gently ‘squeezed’ and eggs were collected onto a dry petri-dish.

For testes collection, adult males were anaesthetized in 0.03% benzocaine solution (Sigma) for 17 mins. Dissected testes were maintained in testis medium (50% L-15 Leibowitz media with phenol red, 15 mM Hepes, 50 µg/ml gentamycin, 10% Fetal Bovine Serum) at 4°C for up to a month.

3.3.2. *In vitro* fertilization

To achieve synchronous fertilization, ~1 mm thick fragment of the testis was macerated and further homogenized in 1 ml 1x Modified Barth's Saline (1x MBS: 88 mM NaCl, 1.0 mM KCl, 2.4 mM NaHCO₃, 15.0 mM HEPES (pH 7.6), 0.3 mM Ca(NO₃)₂·4H₂O, 0.41 mM CaCl₂·2H₂O, 0.82 mM MgSO₄). Eggs were thoroughly mixed with the sperm suspension and allowed to sit for 3 minutes before flooding the Petri dish with deionized water. After 20 mins, fertilized eggs were dejellied by gently swirling (3-5 minutes) in a 2% cysteine hydrochloride (Amresco, #200-157-7), pH 7.8 solution in 0.1x MBS. Dejellied embryos were thoroughly rinsed, three times with deionized water, followed by three times with 0.1x MBS. Zygotes were then cultured in 0.1x MBS at 15°C until they were ready to be used for experiments.

3.3.3. Microinjection of embryos

Xenopus zygotes were either microinjected at one-cell stage in the animal hemisphere or at 2-cell stage at the presumptive mesendoderm site in the dorsal blastomere, to target ectodermal (animal cap) tissue and mesendoderm tissue respectively. 5 nl of appropriate DNA (K8/K19, 15 pg/nl; IE-2B2/PA-2B2, 50 pg/nl) or RNA (K8/K19, 100 pg/nl; IE-

2B2/PA-2B2, 20-50 pg/μl) diluted in deionized water was pressure injected using a Narishige IM-300 microinjection apparatus. Microinjection needles were fabricated from borosilicate glass capillaries (Drummond, #1000 0010) using a P-30 vertical micropipette needle puller (Sutter Instrument, CA) at settings 760 units for heat and 400 units for pull. Needles were calibrated to the desired injection pressure (20-30 PSI) and time (100-200 ms) settings to dispense 5 μl of injection volume. During injections and 20 minutes post injection, the embryos were kept in 3% Ficoll (Amresco, #E965-504). Embryos were rinsed thoroughly and transferred to 0.1x MBS and allowed to develop to gastrulation stage by maintaining in a 14°C incubator. Temperature was occasionally altered to 18-22°C to increase the speed of development. To avoid unintended photoactivation, embryos were maintained in the dark and all experimental steps were performed under red light only.

3.3.4. Preparation of dorsal marginal zone (mesendodermal) explant

Dorsal marginal zone (DMZ) explants were prepared from *Xenopus* embryos at gastrulae stage 10.5-11 in a 100 mm dish containing 0.1x MBS. Embryos were sorted out to ensure expression of the injected proteins based on eGFP or mCherry fluorescence. Care was taken to excise only the tissue expressing the injected proteins. First, the embryos were devitellinated from the animal side using forceps to avoid damaging the mesendoderm. Next, two incisions were made around the dorsal blastopore toward the animal hemisphere. The embryos were then oriented animal hemisphere up and a cut was made to separate the dorsal flap away from the animal hemisphere. Vegetal cells were scraped away using an eyebrow knife, leaving behind the mesendodermal, mesodermal, and bottle cells. Edges of

the tissue were trimmed to achieve the desired shape and dimensions of the explant. Since Fibronectin (FN) is the endogenous substrate for migration *in vivo*, the explanted tissues were then transferred to a 35 mm dish coated with ($1.4 \mu\text{g}/\text{cm}^2$) FN (Sigma, #F4759) containing 0.5x MBS using Pasteur pipettes. Here, the explants were arranged in such a way that the animal hemisphere flap is opened to expose the inner face of the dorsal marginal zone by using an eyebrow knife, however, remains attached to the explant at its vegetal end by the bottle cells of the blastopore lip. After arranging the explant on the substrate, they were secured under a cover slip supported by silicone grease at the four corners and compressed gently from above with forceps. The mesendodermal explants were then allowed to attach onto the FN substrate for at least 30 min before image acquisition.

3.3.5. Mesendoderm cell preparation

For dissociation of cells, dorsal mesendoderm tissue was excised at early gastrula stage as described above and dissociated to single cells on agarose surface using $\text{Ca}^{2+}/\text{Mg}^{2+}$ free 1x MBS. Dissociated cells were plated on 35 mm, FN ($1.4 \mu\text{g}/\text{cm}^2$) coated glass bottom dishes (MatTEK, USA) containing 0.5x MBS. The cells were then allowed to attach onto the substrate for at least 30 min before image acquisition.

3.3.6. Preparation of ectodermal tissue (animal caps) explants

Basic animal cap explants were prepared from *Xenopus* embryos at gastrulae stage 11-11.5 in a 100 mm dish containing 0.1x MBS. First, the embryos were devitellinated from the

vegetal side very gently using forceps to avoid damaging the animal cap. Next, the animal caps were excised using the eyebrow knife. The blastocoel side of the animal hemisphere was exposed from the vegetal side and then the region of the cap with fluorescence was identified and cut. To obtain the animal cap region expressing the injected proteins, the sides of the explants were shaved to appropriate size. The explanted animal caps were then transferred to a 35 mm dish coated with FN ($1.4 \mu\text{g}/\text{cm}^2$), containing 0.5x MBS using a Pasteur pipette. Explants were positioned with the deep layer facing the bottom of the chamber. The explants were secured flat beneath a small fragment of the cover slip supported by silicone grease at the four corners and compressed gently with forceps. The ectodermal explants were then allowed to attach onto the substrate for about 30 min before image acquisition.

3.3.7. Developmental phenotypes

Synchronously fertilized embryos were harvested for analysis at the desired developmental stage according to the external morphology as described by (Nieuwkoop and Faber, 1994). Embryos were kept at a density of maximum 50 embryos per 35 mm dish and 0.1x MBS was replaced daily. The unfertilized, dead or damaged eggs were quickly removed to minimize bacterial infection.

3.4. Biochemistry

3.4.1. Preparation of *Xenopus laevis* embryo lysates

Embryos at stage 10.5-11 were sorted for eGFP or mCherry fluorescence to ensure expression of proteins from the injected mRNA. Fluorescence-positive embryos were homogenized on ice with pre-chilled extraction buffer (100 mM NaCl, 50 mM Tris-HCl (pH 7.5), 1% Triton X-100, 1 mM phenylmethylsulfonylfluoride (PMSF), 10 mg/ml sodium β -glycerophosphate, 10 mM sodium fluoride, 1 mM sodium orthovanadate, 0.2 mM H_2O_2 , 3 mM sodium pyrophosphate, with mammalian protease inhibitor cocktail (Sigma, #P2714)). The embryo slurry was incubated on ice for 15 mins followed by centrifugation for 10 minutes at 14,000g at 4°C. To clarify the lysate, the yolk from the upper phase was aspirated. If a sequential aspiration was necessary the supernatant was centrifuged again with the same conditions. If the lysate was not used immediately, samples were frozen at -80°C, aliquoted for SDS/PAGE, and/or immunoprecipitated.

3.4.2. Co-immunoprecipitation

Immunoprecipitations were performed with RFP-Trap_MA (Chromotek, Germany, #rtma20) using 100 μl total lysates extracted from uninjected embryos or embryos injected with mCherry open-2B2 (100 pg/ ηl). Reactions were incubated for 1 hour at 4°C, beads were then magnetically separated and further washed 3 times with lysis buffer. Immunocomplexes were dissociated from beads by 40 μl 2x Laemmli buffer with 5% β -mercaptoethanol and boiling for 10 minutes. Samples were then separated by SDS-PAGE.

Immunoprecipitations to detect pSer71-Rac1 was done as follows:

For antigen-antibody capture, 500 µg of protein was incubated with 5 µg of antibody overnight at 4°C. Immunoprecipitation was done using Protein G agarose beads (Roche, #11243233001) incubated with the antigen-antibody overnight at 4°C. The beads were then separated using centrifugation at 3000g for 5 min and further washed with lysis buffer twice. Immunocomplexes were dissociated from beads by 40 µl 2x Laemmli buffer with 5% β-mercaptoethanol and boiling for 10 minutes. Samples were then separated by SDS page and Western blot procedure as described later.

3.4.3. SDS page and western blotting

Polyacrylamide gels of 12% or 14% concentration were prepared by mixing appropriate volumes of 1.5 M Tris-HCl pH 8.8, 30% Acrylamide-Bis acrylamide (Biorad), 10% SDS, 10% ammonium persulfate (Sigma), 0.02% TEMED (VWR). A 4% stacking gel was made by mixing appropriate volumes of 0.5 M Tris-HCl pH 6.8, 30% acrylamide (Biorad), 10% SDS, 10% ammonium persulfate (Amresco), 0.02% TEMED (VWR). Gels were loaded with protein samples and run at 80-100V. After separation, the proteins were either stained with Sypro Red dye (Invitrogen, S12000) or immunoblotted.

Running buffer: 25 mM Tris-HCl, 192 mM Glycine, 0.1% SDS, pH 8.3

Transfer buffer: 12 mM Tris Base, 96 mM Glycine, pH 8.3, 20% Methanol

After separation, the proteins were transferred to a nitrocellulose membrane using the transfer apparatus for 4 hrs at 290 milli amps, 4°C. To minimize unspecific binding, the nitrocellulose membrane was blocked for 1 hr at room temperature using 5% (w/v) milk powder in PBS buffer. Afterwards, the nitrocellulose membrane was incubated overnight at 4°C in 5% milk powder in PBS-T containing the primary antibody pSer71-Rac1 (sc12924-R, Santa Cruz). Following that, the membrane was washed with 3 times with 1x PBS-T for 10 min at room temperature. The nitrocellulose membrane was next incubated at room temperature in 5% milk powder in PBS-T containing the HRP conjugated secondary antibody (Jackson laboratories). After 1 h incubation at room temperature, the nitrocellulose membrane was again washed 3 times with 1x PBS-T for 10 mins at room temperature. For detection, the membrane was incubated with the chemiluminescent WesternBright Quantum HRP substrate (Advansta, CA) according to the manufacturer's protocol and then exposed to X-ray detection films (Genemate, #F-9024).

3.4.4. LC/MS-MS Proteomic Analysis

Prior to staining with Sypro Red dye, SDS-PAGE gels were incubated twice in fixative solution consisting of 50% methanol and 7% glacial acetic acid for 30 minutes per incubation. After decanting the second fixative solution, the gel was placed in a fresh dish and incubated in 60 ml of Sypro Red dye overnight. The staining solution was decanted and the gel was incubated in a wash solution of 10% methanol and 7% glacial acetic acid for 30 minutes. Afterwards, the gel was washed three times in 100 ml of commercial

ultrapure water before gel imaging and further preparation for LC/MS-MS. All incubations and washes were performed at room temperature on a flat rotator.

LC/MS-MS was performed by the Center for Advanced Proteomics Research (CAPR) at the Rutgers New Jersey Medical School. Sypro Red-labeled SDS-PAGE gel sections were excised at the facility and in-gel trypsin digestion was performed. The resulting peptides were C18 desalted and analyzed by LC/MS-MS on the Q Exactive instrument. The MS/MS spectra were searched against the NCBI *Xenopus laevis* database using MASCOT (v.2.3) search engines on the Proteome Discoverer (V1.4) platform. The protein false discovery rate is less than 1%. The mass spectrometry data were obtained from an Orbitrap instrument funded in part by NIH grant NS046593, for the support of the UMDNJ Neuroproteomics Core Facility. Information in tables was derived utilizing Scaffold 4.7.3 with a protein and peptide false discovery rate of <1%.

3.5. Molecular biology

3.5.1. DNA restriction digestion

Restriction digests were performed with restriction enzymes (New England Biolabs) according to the manufacturer's instruction. Dephosphorylation of the cloning vector was performed using Antarctic Phosphatase for 1hr at 37°C (New England Biolabs) in order to prevent recircularization during ligation.

3.5.2. Agarose gel electrophoresis

Analytical and preparative restrictions were analyzed by agarose gel electrophoresis (0.8% to 1%) prepared from agarose and 1x TAE running buffer (Tris/Acetate/EDTA: 40 mM Tris-Acetate, pH 8.5, 2 mM EDTA). For visualization of the DNA, either Gel Red (Biotium, #41003) or ethidium bromide (Amersco, #2810) were used and documented using Spectroline UV and UVP PhotoDoc-IT systems.

3.5.3. Purification of DNA fragments and linearized templates

Purification of DNA fragments from agarose gels or restriction digestions were performed with the Zymoclean Gel DNA Recovery kit (ZymoResearch, #D4002) or Nucleospin Gel and PCR clean up (Macherey-Nagel, #74060950) according to the manufacturer's instructions.

3.5.4. DNA ligation

Concentration of restriction-digested and gel purified vector and insert DNA fragments was determined by A260 on a spectrophotometer. 1:3 to 1:10 molar ratio of vector:insert was used in ligation reactions. Standard ligation reactions were carried out using T4 DNA Ligase (New England Biolabs, #MO202L) according to the manufacturer's instructions. The ligation was incubated for 45 minutes at room temperature or overnight at 15°C.

3.5.5. Transformation of bacteria cells

For chemical transformation of the ligation reaction, 5-alpha (New England Biolabs, #C2988J) or Express Iq competent *E. coli* cells (New England Biolabs, #C3037I) were used. The ligation reaction volume was added to 50 µl of the competent cells in a pre-chilled 14 ml round bottom tube on ice and incubated for 30 minutes. Cells were heat shocked at 42°C for exactly 2 min, followed by incubation on ice for 2 minutes. SOC medium (1 ml) was added and the transformed cells were incubated for 60 min at 37°C in a rotating shaker (~250 rpm) for recovery. Subsequently, different quantities of transformed cells were spread onto warm selection plates (LB agar plates supplemented with the appropriate antibiotic; ampicillin or kanamycin) and colonies were allowed to grow overnight at 37°C.

3.5.6. Plasmid DNA preparation

Depending upon the complexity of the ligation reaction 1-24 clones were picked under sterile conditions using a P200 pipette tip. For plasmid isolation, bacteria were grown in the required amount of LB or 2xYT media needed for miniprep or midiprep along with the selective antibiotic and cultured overnight in a shaker at 37°C.

For the plasmid preparation, 2.0 ml of the bacteria culture was centrifuged for 3 min at 14,000 rpm. Isolation of DNA in analytical amounts was performed using the "Plasmid Miniprep" kit (ZymoResearch) according to the manufacturer's protocol. Isolation of DNA in preparative amounts was carried out with the "NucleoBond®Xtra Midi" kit (Macherey-

Nagel) following the manufacturer's protocol. The DNA concentration was measured with the NanoDrop 2000 spectrophotometer (Thermo Scientific) using 1 μ l of the DNA sample.

3.5.7. *In vitro* transcription

To synthesize RNA for microinjection, 6 μ g of pCS2⁺-PA-2B2, pCS2⁺-IE-2B2, pCS2⁺-CA-2B2 or pCS2⁺-eGFP-krt8 DNA was linearized with Not I restriction enzyme (New England Biolabs) at 37°C overnight. pCS2⁺-eGFP-krt19 DNA was linearized with BssHII (New England Biolabs) at 50°C overnight. Linearization efficiency was verified by agarose gel electrophoresis. Digested DNA was extracted with phenol:chloroform:isoamyl alcohol (25:24:1) (Invitrogen) and precipitated with 10 μ l 3 M sodium acetate solution and 100% ethanol and incubated overnight at -20°C. DNA was pelleted by centrifugation at 14000 g for 10 min at 4°C and washed once using 100 μ l 70% ethanol and centrifuged for 5 min, 14000 g at 4°C. Ethanol was removed and the pellet was dried at 37°C. DNA was then solubilized in 16.5 μ l nuclease free water.

In vitro transcription was performed in a reaction mixture containing 5 μ l 10x transcription reaction buffer, 5 μ l 100 mM rATP, rCTP, rUTP ribonucleotide mix (Promega, #P1420) 5 μ l 1 mM rGTP, 5 μ l 10 mM m7G(5')G RNA Cap (New England Biolabs, #S1404S), 1 μ l RNase inhibitor (Promega, #P1420), and SP6 RNA polymerase (Promega, #P1420) and incubated at 37°C for 30 minutes. 1.25 μ l 10 mM rGTP was added and incubated for additional 1 hour at 37°C. To avoid degradation of the RNA, 0.5 μ l of the RNase inhibitor and 2.5 μ l RQ DNase1 (Promega, #P1420) were added followed by incubation for 15

minutes at 37°C. Free nucleotides and digested DNA were removed using Illustra ProbeQuant G-50 Microcolumns. Synthesized RNAs were purified by phenol:chloroform extraction and ethanol precipitation as above and stored at -80°C.

3.6. Direct Immunofluorescence

MDCK or HEK293T cells seeded on 35 mm glass bottom dishes (MatTek) were fixed in ice cold 100% anhydrous methanol for 10-15 mins on ice and subsequently washed 3 times with PBS. Ectodermal (animal cap) explants were fixed overnight in either ice cold 100% anhydrous methanol at -20°C or in 3.7 % paraformaldehyde in 0.1x MBS at 4°C. Explants were rehydrated 0.1x MBS and washed 3 times with 0.1x MBS, 10 min each time. Samples were permeabilized with 0.25% TritonX-100 diluted in PBS for 5 mins and rinsed 3 times with PBS. Blocking was done for 1hr at 37°C with 10% goat serum, 1% BSA and 0.1% Triton X-100 diluted in PBS/0.1xMBS, following which samples were incubated with primary antibodies diluted in blocking buffer for 30 mins at 37°C or overnight at 4°C. Samples were then thoroughly washed with PBS/0.1xMBS and incubated with secondary antibodies and Hoechst 34580 (1:1,000, Sigma Aldrich, #63493) for 30 mins at 37°C, rinsed again 3 times with PBS/0.1xMBS. Samples were then mounted with PBS/0.1xMBS and stored at 4°C in the dark until imaging was done.

Primary antibodies used include the following: pan-cytokeratin (1:100, C2562, Sigma-Aldrich), anti-FLAG M2 (1:500, F1804, Sigma-Aldrich), anti-FLAG (1:500, F7425,

Sigma-Aldrich), Lamin B (1:10, X223, Progen), pSer71-Rac1 (1:50, sc12924-R, Santa Cruz), fibronectin 4H2 (1:300, DSHB), mCherry polyclonal (1:700, Biovision #5993).

Secondary antibodies used were species-specific IgG conjugated antibodies:

Alexafluor-conjugates for confocal (1:1000) (Life technologies).

mCherry fluorescence was preserved through fixation and labeling.

3.7. Microscopy

3.7.1. Confocal microscopy and image analysis

Confocal images were acquired with Zeiss Cell Observer SD using Zen software (Zeiss) equipped with either Plan-Neofluar 40x/1.3 oil immersion objective or a Plan-Apochromat 63X/1.4 oil immersion objective, 1.0 or 1.6 optovar, 512x512. Z-stacks with a step size of 0.25-0.30 μm were acquired for each field. For optimal images, z-stack mean projections were processed from z-stacks collected through the entire cell and only linear adjustments were made to the brightness and contrast. Filter cube sets used were: Blue Channel: 49 (Zeiss), Green Channel: 38HE (Zeiss), Red Channel: 74HE.

Linescan analysis: Linescan measurements of fluorescence were conducted using the linescan tool in the profile tab of the Zen 2.3 lite software application. Measurements were taken in a region of cytoplasmic volume for a length of 15 μm near the nucleus. Intensities

were normalized to the intensity value at the beginning of the linescan in order to view intensity fluctuation.

3.7.2. Live cell microscopy

For live cell experiments, time-lapse images were acquired with Zeiss Cell Observer SD using Zen software (Zeiss) equipped with a Plan-Apochromat 63X/1.4 oil immersion objective, 1.0 or 1.6 optovar, 512x512. Time lapse images were taken for few hours at different time intervals as indicated for each experiment.

WT MDCK cells were plated on glass bottom 96 well plate/ 35 mm cell culture dishes (MatTEK, USA) and after 18-20 hrs they were treated with inhibitors as indicated. The stage was equipped with an incubator chamber (37°C, 95% humidity and 5% CO₂). Cells were kept in DMEM during the whole period of observation.

For mesendoderm cells, cells were kept in 0.5x MBS during the whole period of observation. Cells were seeded sparingly on glass bottom cell culture 35 mm dishes (MatTEK, USA) and after an hour were treated with inhibitors and their respective controls as indicated.

3.7.3. Photoactivation studies

For photoactivation studies, embryos were coinjected with mCherry PA-2B2 (DNA, 50pg/ηl) and eGFP-krt8 or eGFP-krt19 (DNA, 15pg/ηl). Ectodermal explants were

prepared as described previously. Because it was observed that high expression of PA-2B2 may disrupt keratin networks even when maintained in dark conditions, cells with apparently normal IF networks and general cell morphology and having moderate expression of mCherry PA-2B2 were selected for photoactivation. Briefly, cells were imaged with a Zeiss Cell Observer SD confocal microscope using a Plan-Apochromat 63X/1.4 oil immersion objective, 1.0 optovar and a DirectFRAP module. To induce PA-2B2 activation, a 458 nm laser was focused into a small circular area (diameter 10 μm) for 30-100s with 100% laser intensity. This combination of settings yielded an 8 μW blue light exposure. Images were acquired every 15 secs for 1 min before and between irradiation sessions, and then for 5-10 mins following the last irradiation.

3.7.4. Photoactivation of PA-2B2 in embryos

For blue light stimulation of whole embryos, 35 mm dishes containing either mCherry PA-2B2 or mCherry I379E-2B2 (I379E-2B2/PA-2B2, 20-50 $\text{pg}/\eta\text{l}$) injected embryos were placed underneath a home-built (50X40 mm) LED array (**Fig. 3.2**). Briefly, an LED array was constructed with 56 blue 5 mm LEDs (470 nm, 7065 millicandelas each max output) with a mean 100 μW measured output. The LEDs were powered through a 40 V power supply with a potentiometer for intensity control. Following microinjection of mCherry PA-2B2, the embryos were illuminated with oscillating pulses every sec with a minimum 53 μW and maximum of 154 μW intensity or maintained in the dark, until the embryos reached desired stages. Embryos were fixed in 4% paraformaldehyde at desired time points and analyzed for morphology. To examine external gross anatomical features, images of

embryos were collected using Zeiss steREO Discovery V12. To analyze internal gross anatomical features, control and experimental embryos were bisected sagittally with a scalpel.

For immunofluorescence labelling of ectodermal (animal cap) explants, the embryos were allowed to develop until gastrulation (stage 11/12) and then the explants were prepared and labelled as described earlier.

3.8. Experimental analyses

3.8.1. Software analyses of protein structure (In-silico analyses)

Protein sequences were analyzed for hydrophobic moment and amphipathicity using Heliquet (<http://heliquet.ipmc.cnrs.fr/>) (Gautier et al., 2008). Predicted secondary structure and 3D models of protein constructs were generated using PHYRE² (<http://www.sbg.bio.ic.ac.uk/phyre2/html/page.cgi?id=index>) (Kelley et al., 2015)

3.8.2. Filament and aggregation analysis tool (developed by Abid Haque)

In order to quantify the relative abundance of keratin filaments between the controls and the perturbed replicates, we developed a filament analysis tool. The tool employs a 7x7 pixel window, which sweeps over the image, and assigns a “Line Score” to the central pixel of the window. The line score acts as a measure of probability, that the focal pixel is part of a curvilinear structure, such as a keratin filament. Pixels located on line-like structures

(such as keratin filaments) yield a high line score, whereas other pixels yield low line scores. Therefore, the mean line score obtained from an image acts as a measure of the abundance of filamentous structures in the image. In this study, we compare the mean line scores obtained from various replicates to quantify the relative abundance of filaments in the respective images. Comparison between the experimental groups was performed using one-way ANOVA, followed by a post-hoc Tukey's honest significant test for pairwise comparison between the groups.

Aggregate detection was performed using an algorithm that sweeps through the image, and detects circular structures. The algorithm uses parameters such as area, circularity, convexity and inertia to filter aggregate-like structures. The sum of areas covered by detected aggregates is subsequently used to determine the total area covered by aggregates in an image. Similar to the line analysis tool described above, comparison between experimental groups was performed using one-way ANOVA, followed by a post-hoc Tukey's honest significant test for pairwise comparison of total area of keratinous aggregates in the experimental groups.

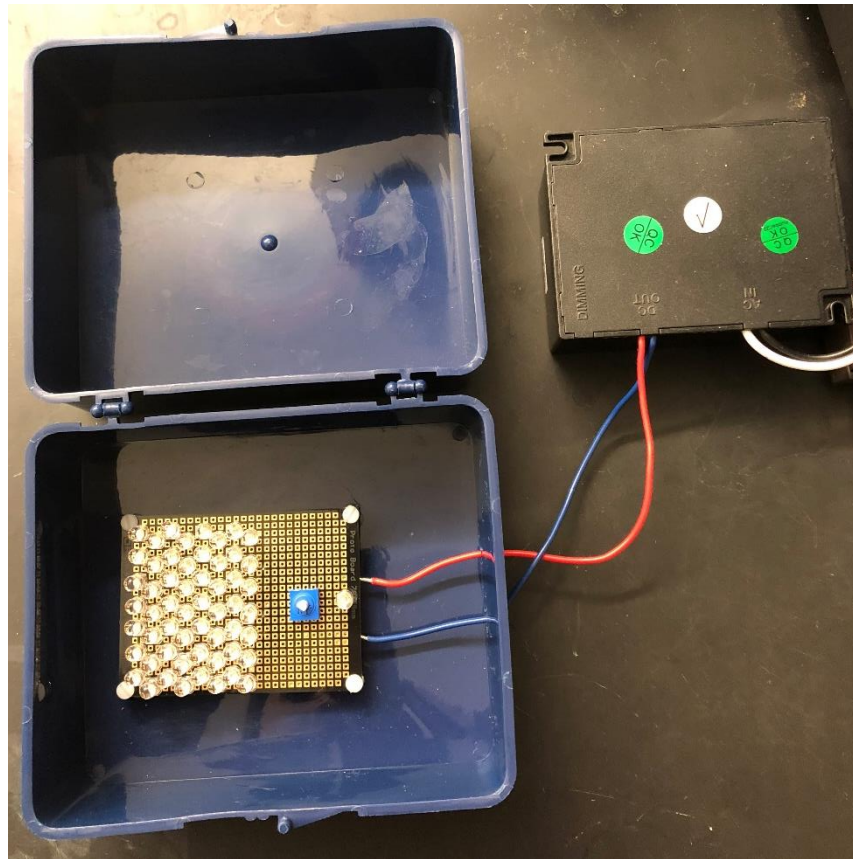
3.8.3. Statistical analyses

All experiments were replicated at least three times, and representative images were shown. Statistical testing was conducted using one-tail unpaired student's *t*-test (Microsoft Excel) to compare different data sets. The graphs show mean values, with error bars representing standard errors of the mean (S.E.M.), significance was reported according to the following

annotation: ns = not significant, p-values less than 0.05, 0.01 and 0.001 were denoted as “*”, “**” and “***” respectively.

Figures were composed using CorelDRAW X8.

Figure 3.2



(Created by Abid Haque)

Figure 3.2 Equipment for validation and application of PA-2B2 photoswitch.

Chapter 4

Keratin Filaments Maintain A Specific Subcellular Localization in migratory cells

Abstract

It has recently been recognized that single migratory cells with vimentin network, display distinct intermediate filament structures, localized in the front and back of the cell. However, it is unknown if the keratin network reorganizes during coordinated cellular movements required for gastrulation. Using amphibian models such as ectodermal (animal cap) explants and mesendodermal explants, migrating tissues were observed by confocal live-cell imaging. I demonstrate, that migratory cells in both the explants show differential subcellular localization of assembled keratin filaments and keratin precursors. Specifically, keratin filaments uniquely localize at the posterior end of the cell towards the points of cell-cell contacts. Whereas, keratin precursors predominantly accumulate in the protruding lamellipodia. This selective compartmentalization of keratin precursors and filaments exists in both the examined migratory cohorts. Contrary to the keratin organization in the leading edge of the migratory clusters, altered keratin organization is perceived with different cellular contexts. Altogether the data show that varying degrees of cell-cell contacts impacts spatial distribution of keratin filaments.

Introduction

Intermediate filaments, well-known for their role as one of the cytoskeletal components, have long been considered as static mechanical stabilizers of cells and tissues. On the contrary, similar to the other members of the cytoskeletal community, actin microfilaments and microtubules, IFs are also remarkably dynamic counterparts of the cell. While the asymmetrical distribution of both actin microfilament and microtubules have been studied in detail, very little attention has been given to the intermediate filaments and their subcellular distribution pattern, especially *in vivo*.

The networks formed by intermediate filaments are highly dynamic and flexible. For example, both keratin and vimentin network which typically extend throughout the cytoplasm are quite motile where filaments exhibit undulations while constantly changing their configurations, appearing to collapse, extend, and translocate over relatively short time intervals (Ho et al., 1998; Windoffer and Leube, 1999; Yoon et al., 1998, 2001). Remarkably, cytoplasmic IFs co-exist in different structural conformations, as filamentous form and as soluble non-filamentous precursors (Schwarz et al., 2015; Yoon et al., 1998, 2001). These non-filamentous assembly states, including tetramers and ULF's (Unit length filaments) are collectively termed as "IF particles". IF particles along with squiggles -short filamentous structures are known as "IF precursors" (Pahlad et al., 1998; Yoon et al., 1998, 2001). A spatially defined multistep *in vivo* assembly cycle for keratins has been proposed as follows. As IF particles are transported from the periphery, tetramers or ULF's convert

to short filaments or squiggles and further assemble into long mature filaments, finally incorporating into the network, which characterizes the spread-out network of the interphase cells (Kirmse et al., 2007; Strnad et al., 2001; Windoffer et al., 2004; Yoon et al., 1998). Adhesions such as nascent focal contacts and desmosomes, have been implicated as nucleation sites for these precursors (Schwarz et al., 2015; Windoffer et al., 2006). Along with fueling the formation of new keratin filaments, these keratin precursors also support filament renewal, since filament formation is not affected by inhibition of protein synthesis (Kolsch et al., 2010). Along with being essential players in network biogenesis and maintenance, it remains unknown if these precursors contribute to regulating any other cellular processes.

In addition to being highly dynamic, IFs display a dramatic organizational topography in cultured cells. Such that, vimentin precursors predominate the lamellipodia of fibroblasts, while the vimentin filaments are populated in the back of the cell (Helfand et al., 2011). Like vimentin, accumulation of keratin precursors in the lamellipodia was also observed in single migrating cells (Kölsch et al., 2009; Windoffer et al., 2004, 2006). In accordance with the presence of these non-filamentous assembly states in cells observed by fluorescence microscopy, these structures can also be isolated from cells grown on physiological-range stiffness (Murray et al., 2014). Similarly, IF precursors are preferentially found in the cell periphery and protrusions of cells in a variety of cell-context (Pralhad et al., 1998; Schwarz et al., 2015; Yoon et al., 1998, 2001). Keratin filaments reorganize to the posterior of the cell and establish cell directionality upon cell-cell

adhesion (Weber et al., 2012). Additionally, cellular tension and morphology influences the ratio between polymerized and non-polymerized forms of vimentin (Murray et al., 2014). The localization pattern of IF precursors observed so far is restricted to analysis of single migratory cells, and not much is known about the IF network organization in morphogenetically active tissues *in vivo*. Few studies of wound healing models, illustrate, a similar compartmentalization of IF precursors. The extending lamellipodia of wound healing cells are frequently enriched with vimentin precursors (Menko et al., 2014). Likewise, keratin precursors are observed in the lamellipodia of leading edge of the migrating epithelial cells (Kolsch et al., 2010).

While appreciating the presence of dynamic assembly states for soluble and polymeric IFs in different biological contexts as described earlier, these assembly states have mainly been characterized in cell lines. However, much is unknown about the keratin network organization during biological events such as embryogenesis. Thus, in order to fulfill the gap in knowledge, keratin network organization in different models of *in vivo* tissue movements need to be examined. During morphogenesis, epithelial-like cells often display surprisingly motile behavior while maintaining characteristic epithelial features such as cell-cell contact. *In vivo* examples of such migratory tissues during *Xenopus* gastrulation are the morphogenetic movements of ectodermal intercalation and mesendodermal internalization (**Fig. 4.1A**). Both these tissues undergo fundamentally distinct morphogenetic processes have certain striking similarities. For example, both ectodermal and mesendodermal migratory cohorts require cell-cell cohesions, cell-matrix adhesions

and intact keratin networks to perform directed migration (Bjerke et al., 2014; Klymkowsky et al., 1992; Marsden and DeSimone, 2001; Weber et al., 2012). One can draw similar parallels with the epithelial cell line MDCK. These cells are traditionally categorized as epithelial cells, but at lower density they have a fibroblast-like morphology. MDCK cells are commonly used as *in vivo* models for epithelial sheet migration. Similar to mesendoderm tissue, MDCK epithelial sheets extend cryptic lamellipodia to collectively drive cell movement (Farooqui and Fenteany, 2005; Winklbauer et al., 1996). Both these collectives also possess anisotropy of cell-cell and cell-matrix interactions. Thus, to determine and compare the distribution pattern of keratin structures, the above-mentioned models of migratory cell phenotypes were analyzed.

In this study, subcellular organization of the keratin network has been examined by undertaking time-lapse recordings of ectodermal (animal cap) and mesendodermal cultured explants. In both the explants selective compartmentalization of keratin particles and filaments was observed. Furthermore, keratin network organization in response to varying cell-cell interactions in *Xenopus* and MDCK cells is dependent on cellular context.

Results

4.1 Gastrulation movements and modes of migration of the *Xenopus laevis* explants

The gastrulation process entails morphogenetic movements such as epiboly and emboly which are defined by their morphogenetic outcome. Epiboly is the process that thins the animal hemisphere, to distribute the ectoderm such that it covers the embryo. Emboly or mesendoderm internalization transports the prospective mesoderm and endoderm cells underneath the future ectoderm layer (**Fig. 4.1A**). *Ex vivo* ectodermal (animal cap) and mesendoderm explants have distinct advantages over other culture models for investigating functional role of keratins in migrating cells. Mainly, there is presence of spatially distinct keratin (K8/K18/K19) network, which is not distinguishable in other systems. In brief, embryos expressing eGFP-K8/K19 in the ectoderm (animal cap) were sorted out and the respective tissue was excised and plated on fibronectin (FN) coated dishes. Here the cells exchange places throughout the thickness of a multilayered tissue, exchanging neighbors and repositioning in the tissue, thus driving tissue thinning and spreading (**Fig. 4.1B**). For dorsal mesendoderm explants, embryos expressing eGFP-K8/K19 were sorted out and the corresponding tissue was excised and plated on FN coated dishes. Here the cells migrate collectively as monopolar cells with protrusions toward the direction of migration (**Fig. 4.1C**).

4.2 Keratin precursors are predominant in the lamellipodia, while keratin filaments are excluded from the lamellipodia of migrating mesendodermal cells

To examine the distribution of keratins during collective cell migration, we investigated the subcellular organization of keratins in dorsal mesendodermal explants. Live cell observations of explants expressing eGFP-K8 show presence of several short filaments or squiggles and nonfilamentous keratin precursors predominantly in the lamellipodial protrusion (**Fig. 4.2a-e**). Whereas, the keratin filaments are concentrated at the rear of the cell at points of cell-cell contacts (**Fig. 4.2A-E**). Additionally, the presence of keratin precursors in the front of the cell changes in accordance with the formation of lamellipodia as the leading-edge cell migrates. The keratin precursors displayed bidirectional movement, both, in the anterograde (towards the cell surface) and retrograde (towards the nucleus) fashion. However, majority of the movements were in the retrograde direction at rates ranging from 0.01-0.02 $\mu\text{m}/\text{sec}$. While, precursors moving in the anterograde direction were in the range of 0.02-0.08 $\mu\text{m}/\text{sec}$.

4.3 Keratin precursors are predominant in the lamellipodia, while keratin filaments are excluded from the lamellipodia of ectodermal (animal cap) cells

Ectodermal (animal cap) explants were examined, to evaluate if the observed pattern of keratin organization during mesendoderm migration is common to other modes of migration. Similar localization pattern of keratin precursors and keratin filaments was detected. During live cell imaging of animal cap explants expressing eGFP-K19, keratin

filaments were observed predominantly in the rear of the cell (**Fig. 4.3A-E**) whereas abundant keratin precursors were seen in the lamellipodia (**Fig. 4.3a-e**). Analogous to mesendoderm tissue, ectodermal cells also exhibit bidirectional movement of keratin precursors. However, majority of particle movements were directed towards the nucleus (retrograde) at rates ranging from 0.01-0.04 $\mu\text{m}/\text{sec}$. Particles moving towards the cell periphery (anterograde) moved at rates ranging from 0.03-0.04 $\mu\text{m}/\text{sec}$.

4.4 Subcellular localization of keratin filaments is dependent on cell context in both *Xenopus* and MDCK cells

To evaluate if distribution of keratin structures was integral to the mesendodermal cells or a property of migrating collective tissue, the keratin organization was observed in single mesendodermal cells. Single dissociated cells prepared from embryos injected with eGFP-K8 show keratin filaments extended throughout the cytoplasm, however are excluded from the protrusions. Further, single cells lacked obvious keratin filament orientation and were multiprotrusive (**Fig. 4.4A**). Contrary, to the compartmentalized keratin network in the leading-edge cells of mesendoderm explants (**Fig. 4.2**), the back-row cells of mesendoderm tissue have a fully expanded keratin network (**Fig. 4.4B**). Next, the keratin organization was examined in the stable MDCK clones expressing eGFP-K8. Mid-expressor MDCK's show keratin filaments which circumscribe the nucleus and radiates out to the periphery with no exclusive regions predominant with keratin precursors (**Fig. 4.4C**). Most of the eGFP-K8 MDCK over-expressors display a normal keratin organization. However, many

of these cells show altered morphology and exhibit long crescent shaped processes at the rear of the cell with aberrant keratin bundles (**Fig 4.4D**).

4.5 Keratin filament organization is dependent on microtubule network in *Xenopus* mesendoderm cells

In order to investigate the involvement of microtubules in maintaining the keratin network, cells were treated with the microtubule depolymerizing drug-nocodazole. When *Xenopus* mesendoderm cells expressing EMTB-mCherry and eGFP-K8 were treated with nocodazole (5 μ m), the microtubule network gradually depolymerized within 80 mins of the treatment as depicted by the selected micrographs of a time lapse movie (**Fig 4.5A, B**). Under these conditions, keratin filaments also exhibit disruption and aggregation with eventual retraction towards the nucleus (**Fig. 4.5A, C**). These results demonstrate the dependence of keratin network on the microtubules.

Figure 4.1

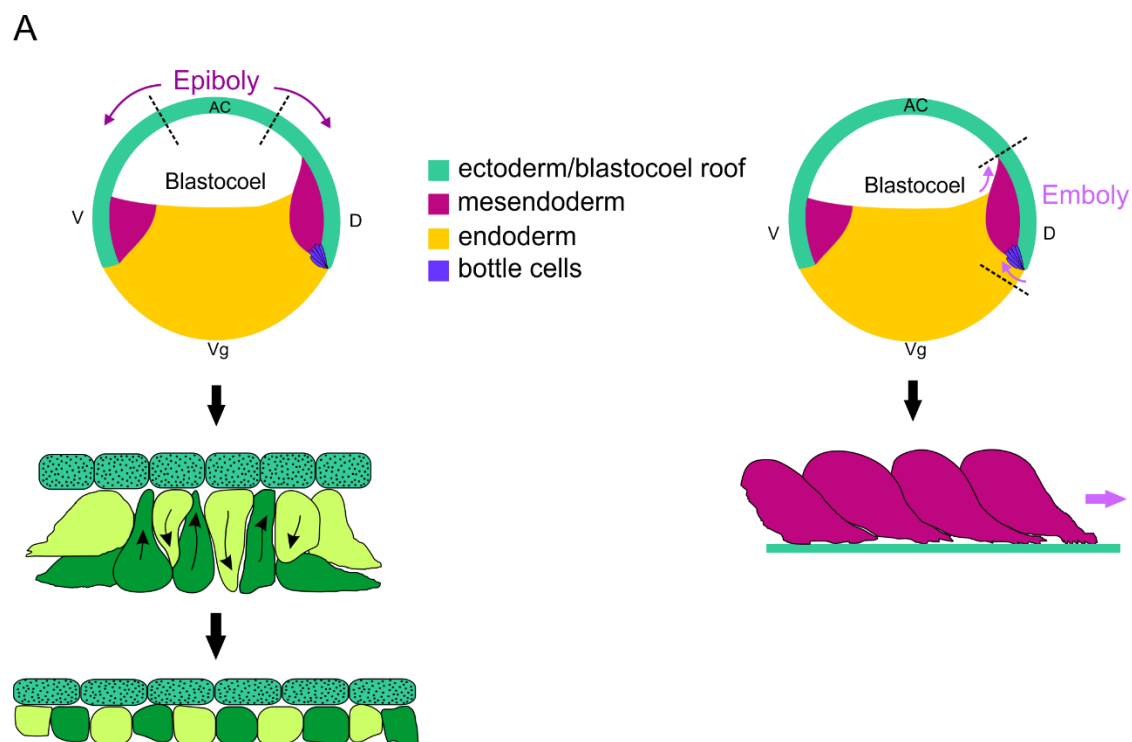


Figure 4.1

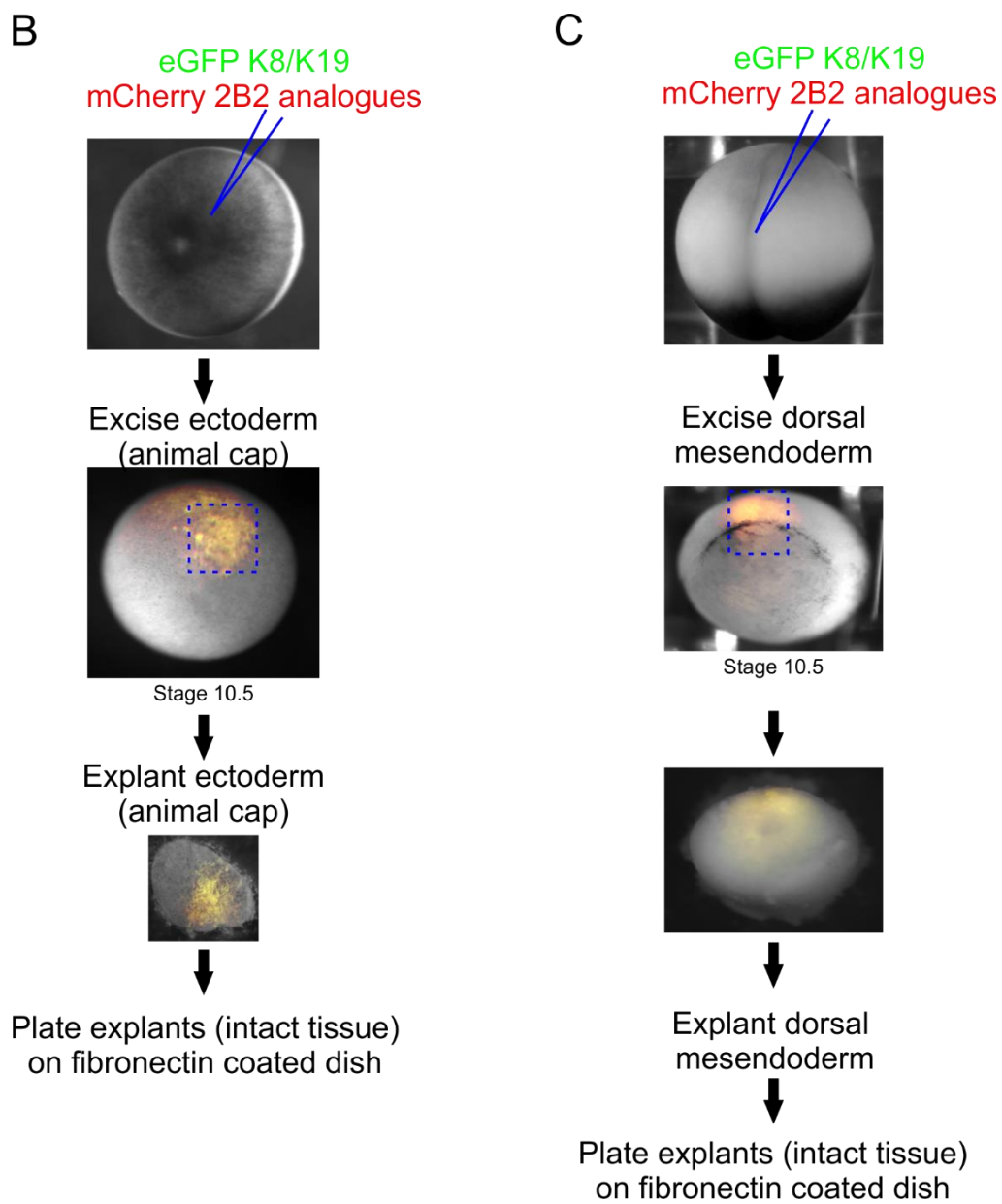


Figure 4.1: Gastrulation movements and modes of migration of the *Xenopus laevis*.

(A) Illustration depicts an early frog gastrula (stage 10.5) in sagittal section and show the early movements of epiboly and emboly during gastrulation (B) Experimental outline used to study ectodermal (animal cap) cells (C) Experimental outline used to study mesendoderm cells.

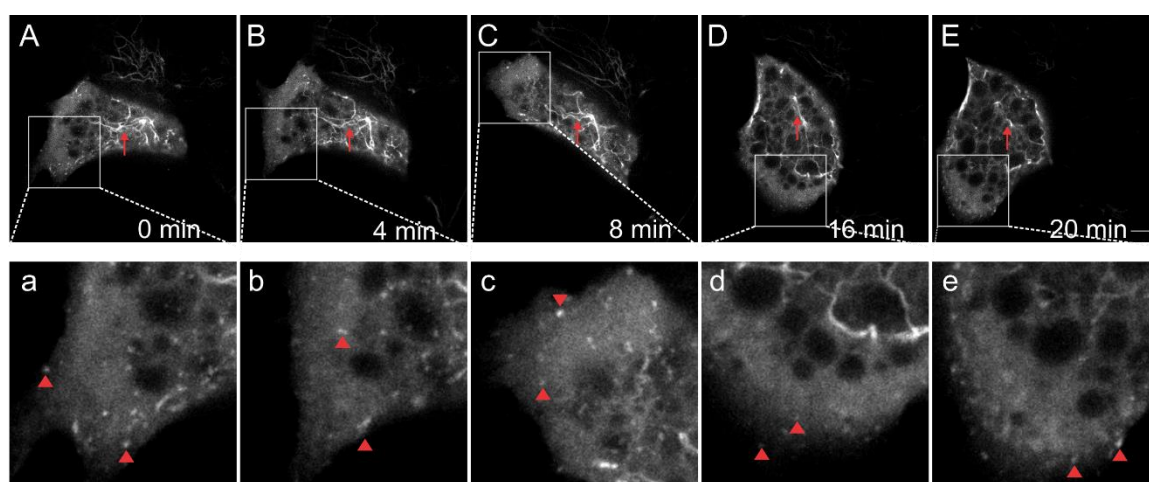
Figure 4.2

Figure 4.2: Keratin precursors are predominant in the lamellipodia, while keratin filaments are excluded from the lamellipodia of mesendodermal cells.

Xenopus embryos were microinjected with eGFP-krt8 RNA at two blastomere stage at the presumptive mesendoderm and permitted to develop until stage 10.5. Following, mesendodermal explants were prepared and plated on fibronectin-coated glass-bottom dishes. Cells expressing eGFP-K8 (green) were imaged every 10 s for the length of the movie of 20 mins using Zeiss Cell Observer spinning disk confocal microscope (63X/1.4 NA, 1.0X optovar). Representative inverse confocal images taken from a time series of leading-edge cells expressing eGFP-K8 (**A-E**) show keratin filaments in the posterior of the cells which appear to terminate in the anterior region (**arrows**). On the other hand, multiple keratin precursors are enriched in the lamellipodia which are shown by **boxed regions** and at higher magnification (**a-e**). The **arrowheads** indicate the keratin precursors emerging in the lamellipodia as the cells migrate.

Bars, 10 μm

Figure 4.3

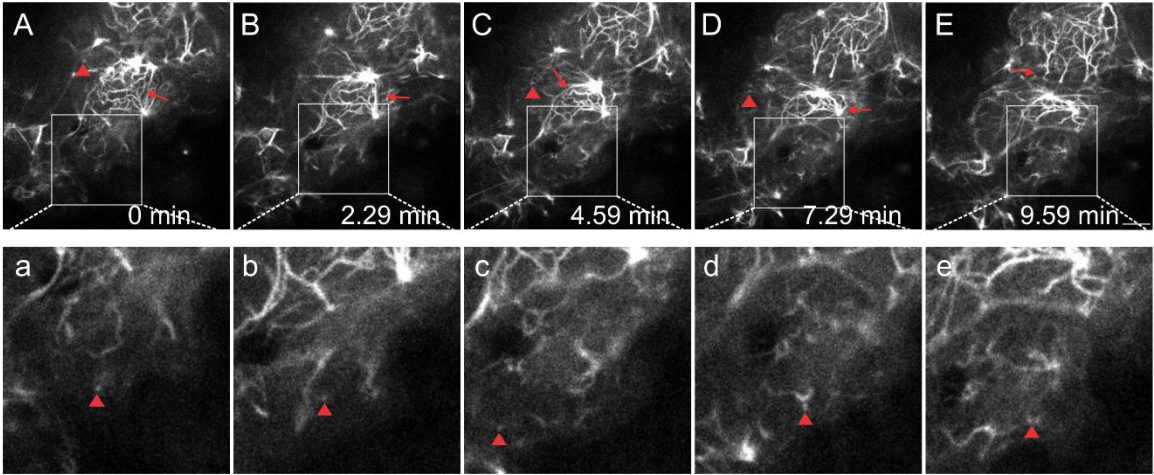


Figure 4.3: Keratin precursors are predominant in the lamellipodia, while keratin filaments are excluded from the lamellipodia of progenitor ectodermal cells.

Xenopus embryos were microinjected with eGFP-krt19 DNA at single cell stage at the presumptive ectoderm and permitted to develop until stage 11. Following, ectodermal animal caps were isolated and plated on fibronectin-coated glass-bottom dishes. Cells expressing eGFP-K19 (green) were imaged every 15 secs for the length of the movie of 10 mins, using Zeiss Cell Observer spinning disk confocal microscope (63X/1.4 NA, 1.0X optovar). Representative inverse confocal images taken from a time series of leading-edge cells expressing eGFP-K19 (**A-E**) show keratin filaments in the posterior of the cells which appear to terminate in the anterior region (**arrows**). Whereas, multiple keratin precursors are enriched in the lamellipodia which are shown by **boxed regions** and at higher magnification (**a-e**). The **arrowheads** indicate the keratin precursors emerging in the lamellipodia as the cells migrate.

Bars, 10 μ m.

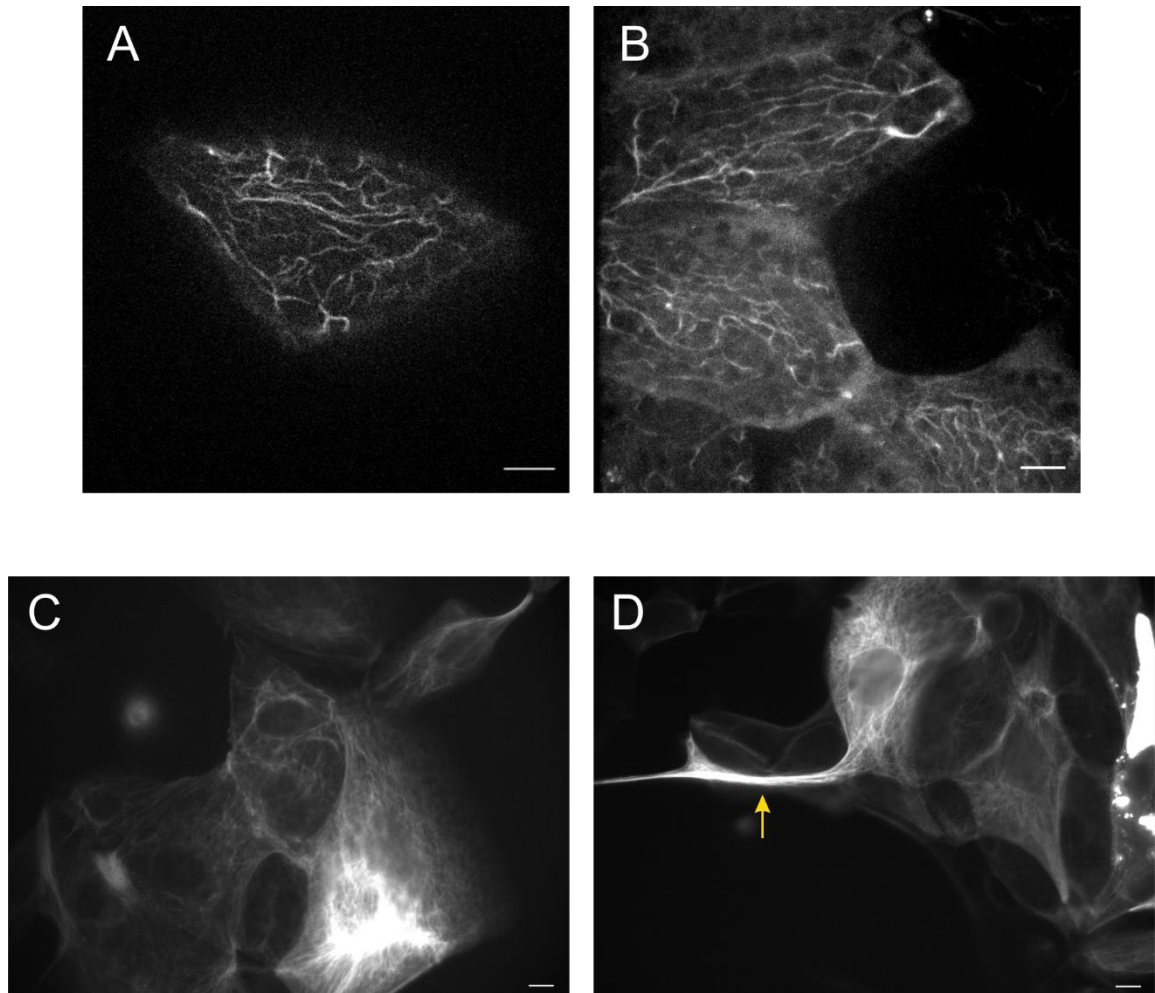
Figure 4.4

Figure 4.4: Subcellular localization of keratin filaments is dependent on cell context in both *Xenopus* and MDCK cells.

Xenopus embryos were microinjected with eGFP-krt8 RNA at two blastomere stage at the presumptive mesendoderm and permitted to develop until stage 10.5. Following, mesendodermal explants or single dissociated cells were prepared and plated on fibronectin-coated glass-bottom dishes. Cells expressing eGFP-K8 (green) were imaged using Zeiss Cell Observer spinning disk confocal microscope (63X/1.4 NA, 1.0X optovar). In single dissociated mesendodermal cells (**A**) keratin filaments expand throughout the cytoplasm, however are excluded from the protrusions. Whereas in back row cells of mesendoderm explant (**B**) keratin filaments are organized in a network that spans the whole cytoplasm.

Keratin network was examined in sparsely plated stably expressing eGFP-K8 MDCK cells using Vivatome microscope (63X/1.4 NA, 1.0X optovar). In comparison to *Xenopus* mesendoderm cells, keratin filaments conform a denser network which extends from the perinuclear region to cell periphery in stably expressing eGFP-K8 mid-expressor MDCK cells (**C**) and eGFP-K8 over-expressor MDCK cells (**D**). **Arrow** depicts the extended tail more commonly seen in over-expressors. Panels show representative widefield images of two independent experiments.

Bars, 10 μ m

Figure 4.5

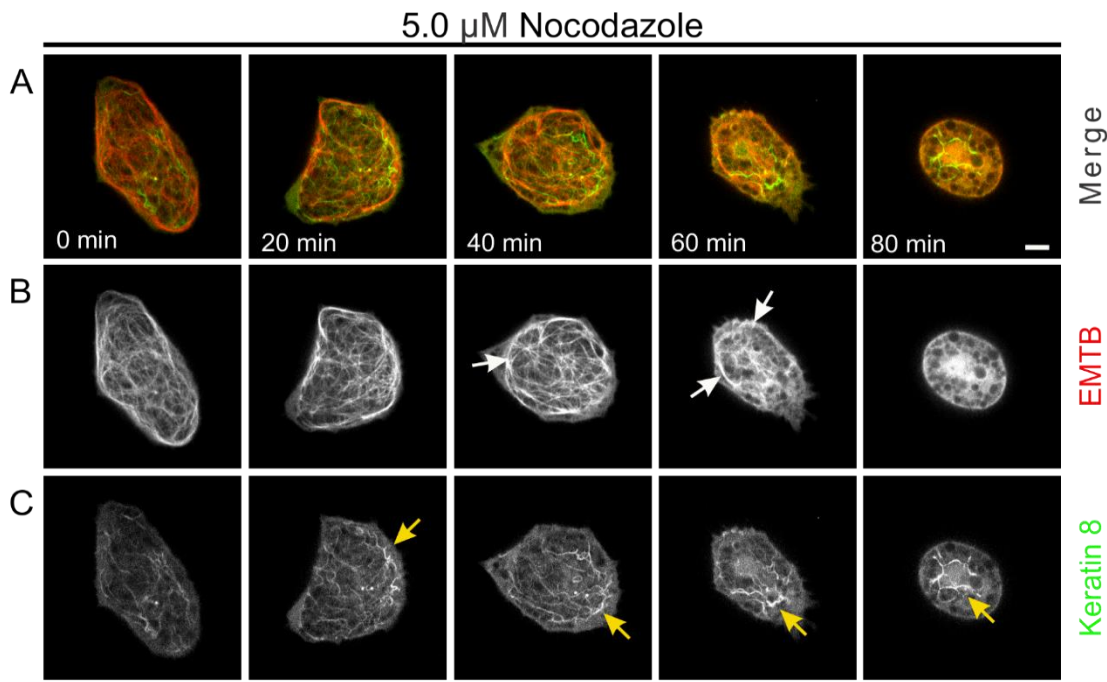


Figure 4.5: Keratin filament organization is dependent on microtubule network in *Xenopus* mesendoderm cells.

Xenopus embryos were co-injected with eGFP-krt8 and microtubule binding domain of ensconsin (EMTB)-mCherry RNA at two blastomere stage at the presumptive mesendoderm and permitted to develop until stage 10.5. Following, dissociated single mesendoderm cells were prepared and plated on fibronectin-coated glass-bottom dishes. Cells expressing eGFP-K8 (green) and EMTB-mCherry (red) were imaged every 5 min for the length of the movie of 90 mins using Zeiss Cell Observer spinning disk confocal microscope (63X/1.4 NA, 1.0X optovar). Select confocal images of a time series of dissociated mesendoderm cells document the response of keratins and microtubules exposed to 5.0 μ M nocodazole (**A-C**). The **arrows** show the disruption and aggregation of the cytoskeletal filaments. Panels show representative images of four independent experiment.

Bars, 10 μ m

Discussion

Migratory explants have provided a unique opportunity to observe the keratin network organization *in vivo*. Here, both explants, mesendoderm and ectoderm (animal cap), demonstrate a spatially defined keratin network organization. A considerable amount of keratin filaments accumulated at the back of the cell, near the sites of cell-cell contacts and nonfilamentous keratin particles were enriched in the lamellipodia regions (**Fig. 4.2 & 4.3**). This data closely resembles results demonstrated earlier in keratinocytes, where highly polarized single migratory cells have IF particles in lamellipodia versus stable filaments at the trailing end (Kolsch et al., 2010). Such reorganization of intermediate filament network during migration is not an integral property of keratins, but rather is quite common. Vimentin network also reorganizes in a similar fashion in single migratory cells. An apparent gradient of the assembly forms of vimentin is established, such that the highest concentration of vimentin particles is in lamellipodia, while the highest concentrations of long vimentin filaments is in the tail and perinuclear regions (Helfand et al., 2011). Other examples of tissue migration such as wound healing also show a similar pattern of keratin and vimentin filament organization (Kolsch et al., 2010; Menko et al., 2014). The functional significance of the considerable enrichment of keratin precursors in the lamellipodia and the presence of keratin filaments at the back of the cells is unknown.

However, there is significant precedence about the observation that intermediate filaments reorganize under tension in migrating tissue. Upon cell-cell contact formation, keratin

filaments previously distributed randomly lacking any apparent orientation, get recruited to the sites of cell contacts. This spatial distribution of polymerized keratin filaments promotes polarized cell migration in mesendoderm cells (Weber et al., 2012). Similar observation was made in this study, where in single mesendodermal cells, keratin filaments fill the entire cytoplasm, however are excluded from the protrusive regions (**Fig. 4.4A**). Whereas, in the leading-edge cells of mesendoderm tissue, keratin filaments are localized near the cell-cell contacts (**Fig. 4.2**) but are excluded from the lamellipodia. Correlative evidence suggests that vimentin filaments inhibit protrusion formation (Helfand et al., 2011). Moreover, a mathematical model also predicts that cell-protrusion formation should be stimulated in a direction opposite that of the keratin network (Kim et al., 2012). Thus, suggesting that tension dependent spatial localization of polymerized keratin filaments maybe required to inhibit protrusion formation at the sides and rear of the cells.

Keratin precursor particles may have a completely different function from keratin filaments. The keratin particles have been shown as precursors to formation of mature filaments (Kolsch et al., 2010; Windoffer et al., 2004; Windoffer and Leube, 1999). In an emanating lamellipodia, focal adhesions function as centers for keratin nucleation (Windoffer et al., 2006). Thus, the presence of keratin precursors in the protrusions is owing to continuous cycling of keratin network to allow for persistent migration. Even in the present study, both mesendodermal and ectodermal tissues exhibit retrograde movement of small particles further fusing to form squiggles or short filaments and eventually merging to form mature filaments. The keratin precursors do not exclusively

move towards the cell center rather show bidirectional motility, both anterograde and retrograde. Similar bidirectional motility has been previously shown for keratins (Liovic et al., 2003; Windoffer and Leube, 1999; Yoon et al., 2001) and vimentin (Helfand et al., 2002; Prahlad et al., 1998; Yoon et al., 1998). Motility of non-filamentous IF particles relies on either microtubules or microfilaments (Hookway et al., 2015; Kölsch et al., 2009; Liovic et al., 2003; Wöll et al., 2005). The filament network used for movement of IF is context dependent and does not exclusively depend on either microtubules or microfilaments. The disruption and retraction of keratin filaments upon nocodazole treatment (**Fig. 4.5**), suggests the involvement of microtubule network for the motility of keratin particles and thus maintenance of keratin network in our system.

The lack of spatially distinct distribution of the assembly states of keratin in the other cellular contexts observed in this study (**Fig. 4.4**), further highlights that the selective compartmentalization of keratin precursors and filaments is a feature of monopolar migratory cells. Perhaps, the mechanical tension in the migratory explants induces the striking reorganization pattern of keratin filaments. Similar to the importance of front-back polarity established by actin and microtubule cytoskeletal elements to facilitate migration, the specific subcellular localization of keratin IFs may also be essential for cell migration. In support of this it has previously been shown that altering keratin organization leads to increased cell migration (Beil et al., 2003; Busch et al., 2012). Additionally, knockdown of K8 results in failure of epithelial sheet migration (Long et al., 2006). Whereas, the data

here shows that overexpression of K8 in MDCK cells alters keratin network organization (**Fig. 4.4D**), and induces formation of long crescent tails at the rear end of the cell.

In conclusion, subcellular localization of assembled keratin filaments is dependent on cell context such that keratins filaments are localized at the rear end in monoprotusive cells and are absent from the lamellipodia.

Chapter 5

Withaferin A and Acrylamide Alter Keratin Intermediate Filament Network Organization in MDCK and *Xenopus* cells

Abstract

Keratin intermediate filaments form a fibrous polymer network primarily thought to be functional mainly to provide structural support in the cytoplasm. Now, however, keratin is known to form a dynamic and flexible network that play an important role in several cellular processes suggesting that keratins also perform non-structural roles. Here, I describe various chemical inhibitors that have been developed to investigate cellular functions of keratins. Previously, chemical inhibitors such as withaferin A (WFA) and acrylamide have been used to disrupt intermediate filaments, however, these studies lack a comprehensive analysis of the inhibitors in use. Here, I asses the use of both WFA and acrylamide to disrupt keratin filaments in cultured MDCK cells. The analysis done here reveals that both the inhibitors disrupt keratin network with cells being more sensitive to WFA than acrylamide, but there are important exceptions to this trend. The results show that extent of disruption is dependent not only on the choice of drug but also on the time of exposure, dose of the inhibitor, cell type and number of cell-cell contacts maintained by the cells. This study provides a decisive insight on the use of chemical inhibitors to study the contributions of keratin intermediate filaments in essential cellular processes.

Introduction

Intermediate filaments and Withaferin A

Withaferin A (WFA) is a steroidal lactone isolated from the plant *Withania somnifera* (**Fig. 5.1A**). WFA induces the aggregation of vimentin filaments in cultured endothelial cells (Bargagna-Mohan et al., 2007). *In silico* and biochemical studies suggest that WFA binds to vimentin covalently at the cysteine residue of the 2B region in the central rod domain (Bargagna-Mohan et al., 2007). Interestingly, WFA causes vimentin aggregation, by targeting soluble vimentin particles (Bargagna-Mohan et al., 2013). Contrary to this, another study suggests that WFA induced alteration of vimentin network does not appear to require cysteine modification (Grin et al., 2012), but rather the disassembly is phosphorylation dependent. In this described mechanism, serine 38 phosphorylation of vimentin (pSer38Vim) causes the perinuclear condensation of vimentin IFs by generation of pSer38Vim squiggles and particles. In addition to vimentin, WFA also alters distribution of a variety of intermediate filament networks, including keratin, peripherin, neurofilaments and GFAP (Glial fibrillary acidic protein) (Bargagna-mohan et al., 2010; Grin et al., 2012) (**Table 5.1**). WFA effects on intermediate filaments show cell type selectivity that is dose and time dependent followed by changes in cell shape and motility (Grin et al., 2012). Unlike some other IF proteins, keratins lack the cysteine residue in their rod domain and thus the mechanism of action of WFA dependent keratin network redistribution is unknown. Nonetheless, disruption of keratin intermediate filaments has been observed in some cell types.

Table 5.1 Summary of Withaferin A targets.

Target IFs	Withaferin A effective dose and time	Cell type	Effect on IF network	References
Vimentin	3 μ M (18hrs)	Endothelial cells	Perinuclear filament retraction	(Bargagna- Mohan et al., 2007)
	1 μ M (24hrs)	Fibroblasts	Perinuclear filament retraction, depolymerization into dots and squiggles	(Bargagna- Mohan et al., 2013)
	1 μ M (3hrs)	Breast cancer cells	Perinuclear filament retraction	(Thaiparambil et al., 2011)
	2 μ M (3hrs)	Fibroblasts	Perinuclear filament retraction, depolymerization into dots and squiggles	(Grin et al., 2012)

GFAP	2 μ M (2hrs)	Astrocytes	Perinuclear filament retraction	(Bargagna- mohan et al., 2010)
Keratin	4 μ M (3hrs)	Epithelial cells	Juxtanuclear filament retraction	(Grin et al., 2012)
	6 μ M (3hrs)	Human lung cancer cells	Perinuclear filament retraction	(Grin et al., 2012)
Peripherin	1 μ M (3hrs)	PC 12	Perinuclear filament retraction	(Grin et al., 2012)
Neurofilament	1 μ M (3hrs)	PC 12	Perinuclear filament retraction	(Grin et al., 2012)

Intermediate filaments and acrylamide

Acrylamide, a small chemical compound, is a highly water-soluble vinyl monomer (**Fig 5.1B**). Reorganization of IFs has also been reported in cells exposed to small molecule inhibitors such as acrylamide. Although the mechanism of action for acrylamide is unknown, it has been used to depolymerize intermediate filaments (Eckert, 1985). Acrylamide can be used for disruption of IFs including keratin, vimentin and neurofilaments (**Table 5.2**). The severity of the IF collapse is highly dependent on the dose and period of exposure of the drug and also the cell type under consideration.

Table 5.2 Summary of acrylamide targets.

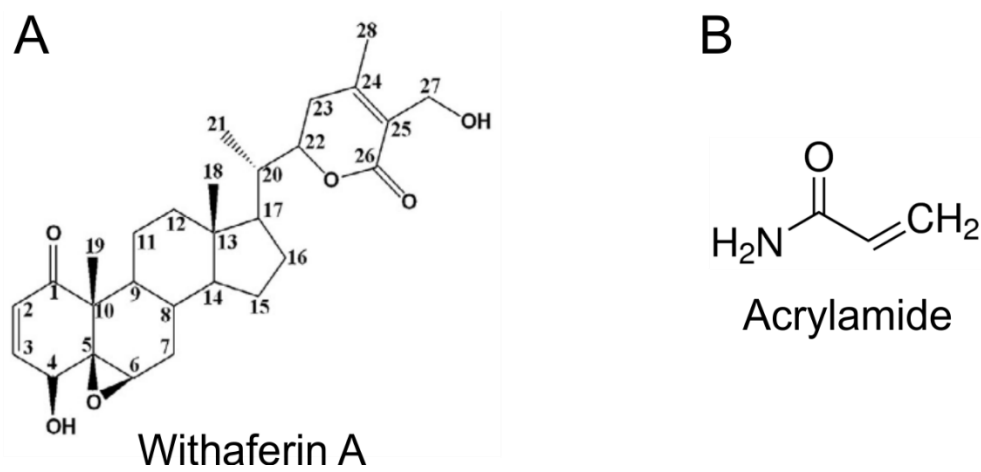
Target IFs	Acrylamide effective dose and time	Cell type	Effect on IF network	References
Vimentin	1-5 mM (20hrs)	Fibroblasts	Perinuclear filament retraction	(Klymkowsky, 1988)
	5 mM (17hrs)	PtK ₂	Perinuclear filament retraction	(Sager, 1989)
	5 mM (4hrs)	PtK1	Juxtannuclear filament retraction	(Eckert, 1985)
	5 mM (4hrs)	Epithelial cells	Perinuclear filament retraction	(Arocena, 2006)

Keratin	5 mM (4hrs)	PtK1	Juxtannuclear filament retraction	(Eckert, 1985)
	5 mM (17hrs)	PtK ₂	Filaments are bundled and clumped	(Sager, 1989)
Neurofilament	(0.1/2/10 mM) (48/24/4hrs)	Neuroblastoma	Perikaryal inclusion bodies	(Hartley et al., 1997)

As mentioned above, few studies have employed inhibitors such as WFA and acrylamide to probe the cellular functions of IFs. Most of these studies were done using *in vitro* cell line models for evaluating the effect of drugs on IFs and fail to accurately model the *in vivo* state, such as embryogenesis. The morphogenetically active tissues during early embryogenesis are cell clusters with an inherent anisotropy of cell-cell and cell-matrix interactions. The topology of cellular interactions, that is where the cell is placed within the cluster, influences its activity and behavior. Furthermore, results from the previous chapter, clearly illustrate that keratin network organization is strongly influenced by cell-cell contacts. Therefore, an important feature in the present study was to evaluate the response of keratin network(s) in cells with varying degrees of cellular interactions.

Here, the effect of small molecular inhibitor treatments on keratin IFs in context with different cell-cell interactions by fixed and live cell microscopy was examined. Moreover, with the goal to develop reliable and useful inhibitors to IFs a broad comparison of the inhibitors to IFs has been undertaken. I examined the utility of WFA and acrylamide as disruptors of intermediate filament organization. I used MDCK cells because of their epithelial-like characteristics, including the ability to form stable cell-cell contacts and their high expression levels of keratin intermediate filament proteins. I also used *Xenopus* mesendodermal cells since they have a simpler keratin network made up of type I keratin 18/19 and type II keratin 8. Both the cell types- MDCK and *Xenopus* mesendodermal cells were exposed to small molecule inhibitor WFA at different time points and dosage and in a variety of cell-cell interactions. Similar study was also

conducted with the use of acrylamide. The comprehensive analysis done here identifies that keratin network disruption is dependent on the choice of the small molecular inhibitor, time of exposure, dosage of the inhibitor, the cell type and the number of cell-cell contacts maintained by the cell.

Figure 5.1**Figure 5.1: Chemical structure of small molecular inhibitors.**

Withaferin A (A) and acrylamide (B)

Results

5.1 Small molecule inhibitor WFA alters keratin filament organization dependent on time and cell-cell contacts

The effects of WFA on keratin IF network were determined in MDCK cells by immunofluorescence. In controls, keratin network extends throughout the cytoplasm from the nucleus to the peripheral regions (**Fig. 5.2A, 5.3A, 5.4A**). After 1 hr exposure to 6.0 μ M WFA, keratin filamentous network collapsed away from the periphery and accumulated all around the nucleus. The keratin filaments appeared to be bundled or clumped. The extent of retraction varies with the cell density, such that, there was most retraction in single cells and least in submarginal cells (**Fig. 5.2A**). In cell pairs and marginal cells, the retraction of filaments was more at the cell free edges and least at the cell-cell contact region (**Fig 5.2A**).

Next, cells were exposed to the inhibitors for longer time, 3 hrs (**Fig. 5.3B**) and 6 hrs (**Fig. 5.4B**) to examine if keratins retract in submarginal cells. Similar observations were made as fig. 5.2A. After 3 hrs and 6 hrs exposure, keratin network retracts towards the nucleus in single cells, cell pairs and marginal cells but not in submarginal cells (**Fig. 5.3B & 5.4B**). Thus, suggesting that keratin filaments in the protrusive regions were more sensitive to WFA in comparison to keratin filaments near the cell-cell contacts. Plausibly, the cell-cell contacts confer protection to keratins and therefore keratin filaments do not retract in these regions.

5.2 Small molecule inhibitor acrylamide alters keratin filament organization dependent on time and cell-cell contacts

To examine the effect of acrylamide on keratin network organization, cells were treated with 6 mM acrylamide for 1 hr, 3 hrs and 6 hrs and then immunolabeled with anti-keratin antibodies. Control cells exhibit abundant keratin filaments extending throughout the cytoplasm (**Fig. 5.2B, 5.3A & 5.4A**). In contrast to the control cells, acrylamide treatment induces aggregate formation (**Fig. 5.2B, 5.3C & 5.4C**). The effect was more pronounced at 6 hrs in both single cells and cell pairs (**Fig. 5.3C**). However, marginal and submarginal cells treated for 1 hr do not show appreciable disruption of keratin filaments (**Fig. 5.2B**). By 3 hrs, marginal cells display some aggregation of filaments (**Fig. 5.3C**). But submarginal cells with most cell adhesions do not show any disturbance in keratin network even after 6 hrs of treatment with acrylamide (**Fig. 5.4C**).

5.3 WFA induces disruption of keratin network in MDCK single cells

Time lapse microscopy was performed with eGFP-K8 MDCK single cells to visually observe the collapse of keratin network during WFA treatment. In control experiments, cells treated with DMSO did not show any effects on keratin network (**Fig. 5.5A**). However, single cells treated with 6.0 μ M WFA lost their normal keratin network organization (**Fig. 5.5B**). Visual disruption of the keratin network was first observed to begin on an average at about 15 mins (n=12) after treatment and concludes with the formation of a perinuclear ring (a ring around the nucleus) (**Fig. 5.5B**) or a juxtannuclear

aggregate (aggregate on one side of the nucleus) (**Table 5.3**). Visually the filaments exhibited severe undulations and simultaneous thickening and aggregate formation and moved inward to collapse around the nucleus (**Fig. 5.5B**). Comparison of control with treated cells by DIC microscopy, revealed that cytoplasmic granules, normally distributed throughout the cytoplasm accumulate around the nucleus leaving a very thin layer of peripheral cytoplasm. The response of different single cells to the same treatment conditions is detailed in **Table 5.3 and 5.4**.

5.4 WFA induces disruption of keratin network in MDCK cell pairs

In contrast to the control cells (**Fig. 5.6A**), treated cells exhibited alterations of keratin network organization (**Fig. 5.6B**). Similar observations to single cells were made when eGFP-K8 MDCK cell pairs were treated with 6.0 μ M WFA. The keratin filaments localized near the cell-cell adhesion sites were protective against WFA induced keratin network disruption (**Fig. 5.6B**). However, the keratin filaments residing in the cell free edges formed filament clumps and aggregates in response to WFA treatment (**Fig. 5.6B**). Along with perinuclear and juxtannuclear aggregates, the filament aggregates also accumulated around the clumped cytoplasmic organelles (**Fig. 5.6B**). Even after 5.0 hr treatment complete collapse of keratin network and cell-cell dissociation was not observed. The response of different cell pairs to the same treatment conditions is detailed in **Table 5.5 and 5.6**.

5.5 Acrylamide induces keratin network alterations in MDCK single cells

In the presence of 6 mM acrylamide, the keratin network alterations were analyzed by live cell imaging of eGFP-K8 MDCK cells. Untreated cells had abundant keratin filaments extending across the cytoplasm (**Fig. 5.7A**). Acrylamide treated cells exhibit altered keratin network. Visually keratins began to collapse at ~ 50 mins (n=5) and ended up forming perinuclear or juxtannuclear aggregates or cytoplasmic organelles trapped within the keratin aggregates around the nucleus (**Fig. 5.7B**). Here, keratin filaments first formed discrete aggregate hot spots and then accumulated towards the nucleus. Along with altered keratin network, cell shape changes were also observed. Comparison of control with treated cells by DIC microscopy, revealed that cytoplasmic organelles appear to accumulate around the nucleus leaving a thin layer of agranular cytoplasm. The response of different single cells to the same treatment conditions is detailed in **Table 5.9 and 5.10**.

5.6 Acrylamide induces keratin network alterations in MDCK cell pairs

Similar observations to acrylamide treated single cell were made. However, keratin filaments near the cell-cell contact do not seem to get affected as much. Even after 8hrs of treatment, complete network collapse or dissociation of cell pairs was not seen (**Fig. 5.8B**). The response of different cell pairs to the same treatment conditions is detailed in **Table 5.11 and 5.12**.

5.7 Withaferin A Treatment Alters Keratin Filament Organization and Cell Morphology of *Xenopus* mesendoderm cells

The objective of this study was to investigate the functional role of keratin filaments in cells more relevant to *in vivo* processes. Thus, single dissociated mesendoderm cells expressing eGFP-K8 were plated on fibronectin (FN) and treated with different doses of WFA. The cells were exposed to either DMSO or a range of concentrations (2-6 μ M) of WFA for 30 mins (**Fig. 5.9**). The effects of WFA on keratin filaments were determined by live-cell imaging. WFA induced dose-dependent disassembly and aggregation of keratin filaments in mesendoderm cells. These concurrent alterations in keratin organization and changes in cell shape were observed. The results show a correlation between change in cell morphology and the extent of keratin network disruption. Control DMSO treated cells exhibited intact cytoplasmic keratin IF network (**Fig. 5.9A**). Lower dose, 2.0 μ M WFA had minimal effects on the keratin organization and cell morphology (**Fig. 5.9B**). While treatment with 4.0 μ M WFA displayed disruption and aggregation of keratin filaments (**Fig. 5.9C**). Extensive disruption of keratin network and a more rounded cell morphology was observed following exposure to 6.0 μ M WFA for 30 mins (**Fig. 5.9D**). Thus, WFA induces reorganization of keratin network and alters the cell morphology in a dose-dependent fashion.

Next, to visually observe the effects of WFA on keratin network, single dissociated mesendoderm cells were obtained from a 10.5-11 stage embryo expressing eGFP-K8, plated on FN substrate and exposed to DMSO or 4.0 μ M WFA for 1hr. Live cell imaging

was performed and confocal images were taken every 5 mins. Selected images from the time-lapse experiment are shown in **figure 5.9E, F**. The extensive cytoplasmic keratin network disrupted to less filamentous state within 10 mins of WFA treatment. The keratin filaments started to disassemble and aggregate, also small protrusions were generated around the entire periphery by 10 min. Subsequently, keratin puncta were observed, which could be lower order structure keratin particles (**Fig. 5.9F, 10 min**). By 30 min keratin filaments had disassembled even further with more aggregate formation (**Fig. 5.9F, 30 min**). Followed by extensive keratin disruption and aggregation, random protrusion formation was observed at 50 min (**Fig. 5.9F, 50 min**). By 1 hr the keratin network had collapsed and aggregated to the nucleus and this drastic effect also changed the cell morphology to more rounded one (**Fig. 5.9F, 60 min**). In control DMSO treated cells, keratin IFs show a random cytoplasmic orientation and the filaments were unaffected over the time with no dramatic changes to the cell morphology (**Fig 5.9E**).

5.8 WFA treatment induces alterations of the microtubule filament organization in *Xenopus mesendoderm cells*

Next it was determined if WFA treatment can induce alteration of microtubule network. Single dissociated mesendoderm cells expressing EMTB-mCherry were treated with 4.0 μ M WFA and live cell imaging was done. In control cells, normal microtubule arrays extending the entire cytoplasm were observed through the length of the movie (**Fig. 5.10A**). In cells exposed to WFA, microtubules aggregate and by 60 min they get arranged in a

whorled array pattern near the nucleus. The cell membranes were showing rough edges with formation of small projections leading to massive cell shape changes (**Fig. 5.10B**).

Figure 5.2

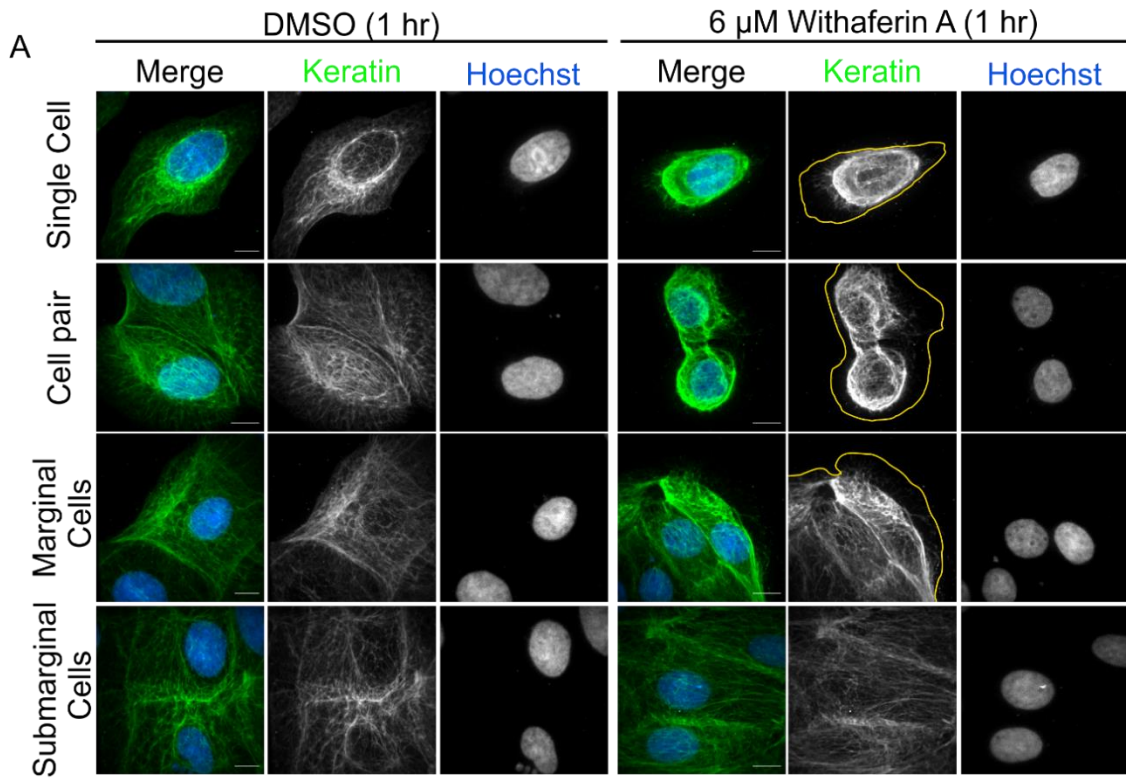
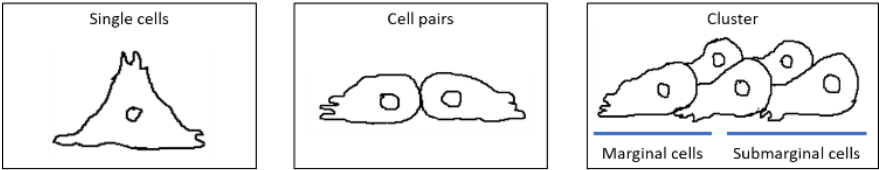


Figure 5.2

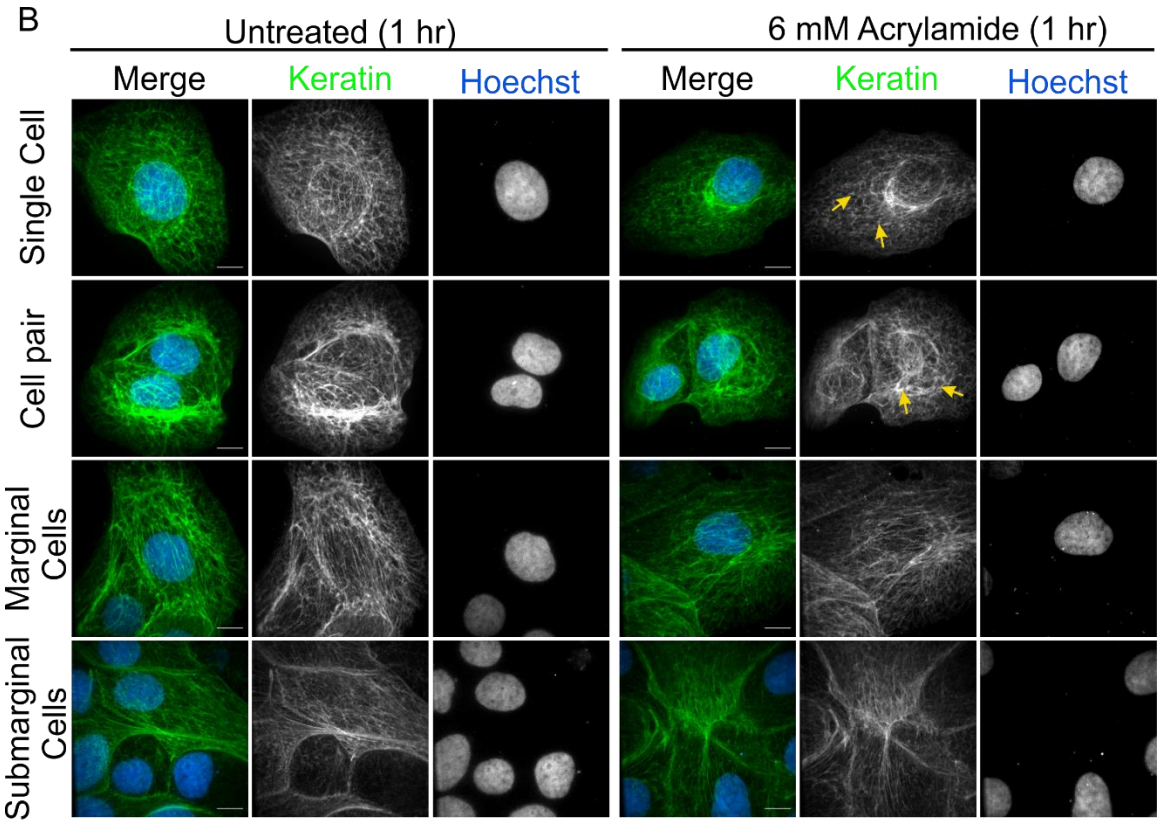


Figure 5.2: Small molecule inhibitors withaferin A and acrylamide alter keratin filament organization dependent on cell-cell contacts within 1hr.

WT MDCK cells treated with 6.0 μ M WFA (**A**) and 6.0 mM acrylamide (**B**) for 1 hr were methanol fixed and immunolabeled using pan-keratin antibody and nuclei were counterstained with Hoechst dye (merge). Keratin network (green) organization and nuclear (blue) morphology were examined using Zeiss Cell Observer spinning disk confocal microscope (63X/1.4 NA, 1.6X optovar). Confocal images (maximum intensity projections of 0.25-0.28 μ m thick optical sections) show that keratin organization is more sensitive to WFA than acrylamide and is also dependent on the number of cell-cell contacts. Within 1 hr of the WFA treatment keratin filaments have retracted from the edge of the cells to the perinuclear region. The cell boundary is traced in **yellow line** to show the lamellipodial region. Whereas the **arrows** depict mild aggregation and disruption of the keratin network in cells treated with acrylamide. Panels show representative images of two independent experiments. (DMSO, n=116; WFA, n=220; untreated n=68; acrylamide, n=120).

Bars, 10 μ m

Figure 5.3

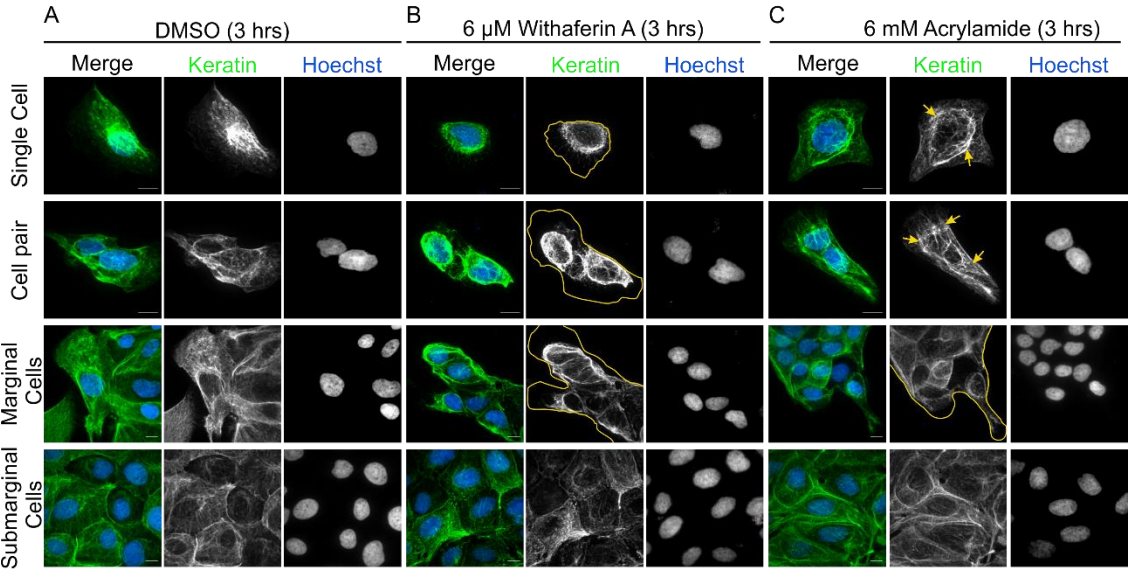
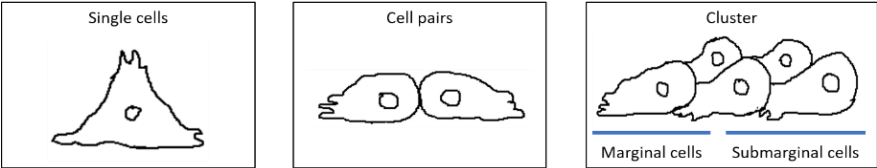


Figure 5.3: Small molecule inhibitors WFA and acrylamide alter keratin filament organization dependent on cell-cell contacts within 3hrs.

WT MDCK cells treated with DMSO (**A**) 6.0 μ M WFA (**B**) and 6.0 mM acrylamide (**C**) for 3 hrs were methanol fixed and immunolabeled using pan-keratin antibody and nuclei were counterstained with Hoechst dye (merge). Keratin network (green) organization and nuclear (blue) morphology were examined using Zeiss Cell Observer spinning disk confocal microscope (63X/1.4 NA, 1.6X optovar). Confocal images (maximum intensity projections of 0.25-0.28 μ m thick optical sections) show that even after 3 hrs of the inhibitor treatment keratin filaments are not affected in submarginal cells. The cell boundary is traced in **yellow line** to show the lamellipodial region where keratin filaments have retracted from the edge of the cells to the perinuclear region. Whereas the **arrows** depict aggregation and disruption of the keratin network in cells treated with acrylamide. Panels show representative images from one experiment (DMSO, n=131; WFA, n=184; acrylamide n=113).

Bars, 10 μ m

Figure 5.4

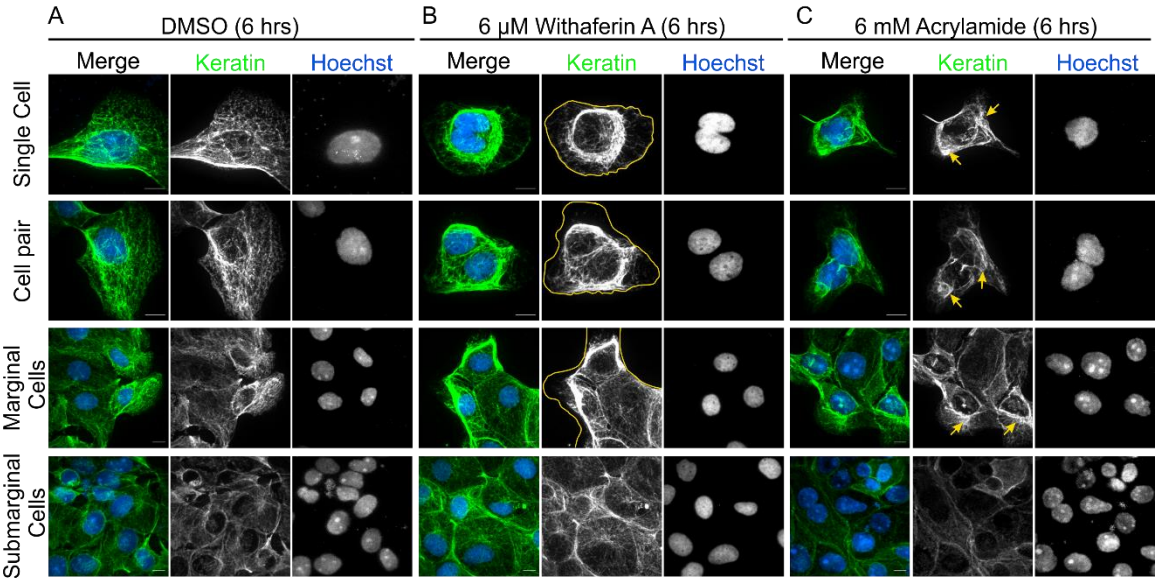
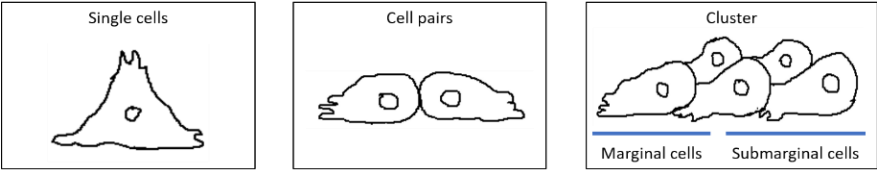


Figure 5.4: Small molecule inhibitors WFA and acrylamide alter keratin filament organization dependent on cell-cell contacts 6hrs.

WT MDCK cells treated with DMSO (**A**) 6.0 μ M WFA (**B**) and 6.0 mM acrylamide (**C**) for 6 hrs were methanol fixed and immunolabeled using pan-keratin antibody and nuclei were counterstained with Hoechst dye (merge). Keratin network (green) organization and nuclear (blue) morphology were examined using Zeiss Cell Observer spinning disk confocal microscope (63X/1.4 NA, 1.6X optovar). Confocal images (maximum intensity projections of 0.25-0.28 μ m thick optical sections) show that even after 6 hrs of the inhibitor treatment keratin filaments are not affected in submarginal cells. The cell boundary is traced in **yellow line** to show the lamellipodial region where keratin filaments have retracted from the edge of the cells to the perinuclear region. Whereas the **arrows** depict aggregation and disruption of the keratin network in cells treated with acrylamide. Panels show representative images from one experiment (DMSO, n=126; WFA, n=184; acrylamide, n=102).

Bars, 10 μ m

Figure 5.5

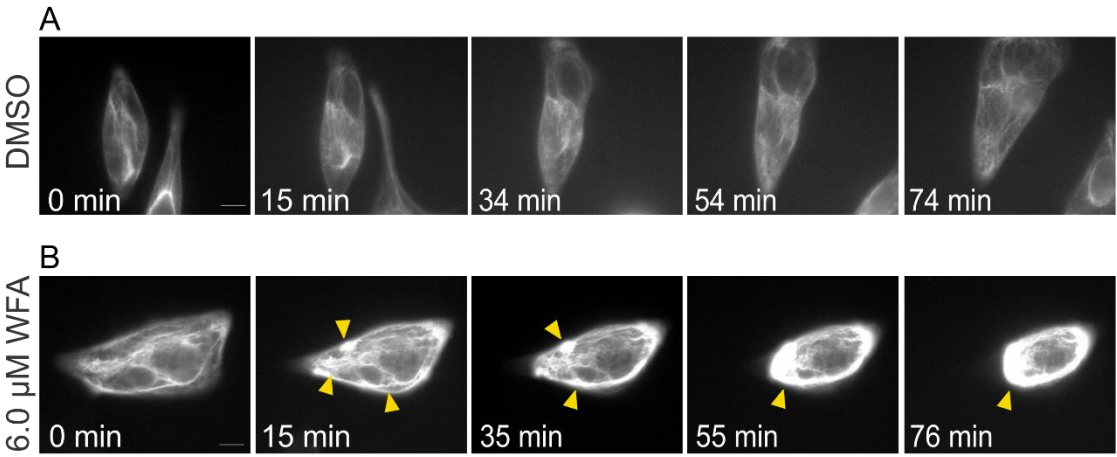


Figure 5.5: WFA induces disruption of keratin network in MDCK single cells.

eGFP-K8 mid-expressor MDCK were sparsely plated and the response of keratin network was documented during DMSO treatment (**A**) and 6.0 μ M WFA treatment (**B**). Single cells expressing eGFP-K8 were imaged every 2 min for the length of the movie of 120 mins using Zeiss Cell Observer spinning disk confocal microscope (63X/1.4 NA, 1.0X optovar). Select confocal images representative of a time series reveal typical dynamics of a spread-out keratin network during DMSO treatment, whereas, cells treated with WFA show changes in the distribution of eGFP-K8. The keratin network is distributed throughout the cytoplasm prior to addition of WFA as seen in the image (0 min). However, in the presence of WFA, the centripetal movement of peripheral fluorescence continues, with filaments showing severe undulations and simultaneous thickening and aggregate formation (**arrowheads** at 15 min and 35 min) which eventually forms a dense perinuclear ring (**arrowheads** at 55 min and 76 min). (DMSO, n= 3; WFA, n=4).

Bars, 10 μ m

Figure 5.6

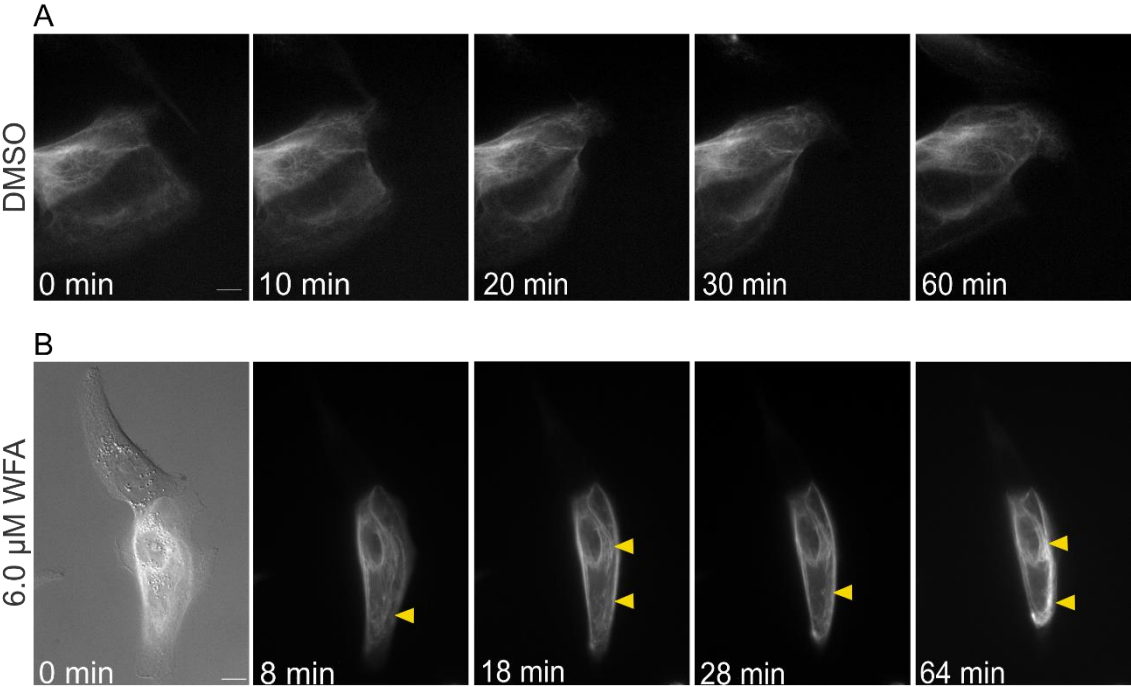


Figure 5.6: WFA induces disruption of keratin network in MDCK in cell pairs.

eGFP-K8 mid-expressor MDCK were sparsely plated and the response of keratin network was documented during DMSO treatment (**A**) and 6.0 μ M WFA treatment (**B**). Cell pairs expressing eGFP-K8 were imaged every 2 min for the length of the movie of 4 hrs using Zeiss Cell Observer spinning disk confocal microscope (63X/1.4 NA, 1.0X optovar). Select confocal images representative of a time series reveal characteristic dynamics of a spread-out keratin network from perinuclear region to cell periphery during DMSO treatment, whereas, cells treated with WFA show changes in the distribution of eGFP-K8. The keratin network is distributed throughout the cytoplasm prior to addition of WFA as seen in the image (0 min). However, in the presence of WFA, the filaments fuse together and form aggregate (**arrowheads** at 8 min, 18 min and 28 min). Eventually, a juxtannuclear aggregation is formed, the filament aggregates also accumulate around the clumped cytoplasmic organelles (**arrowheads** at 64 min). (DMSO, n= 4; WFA, n=3).

Bars, 10 μ m

Figure 5.7

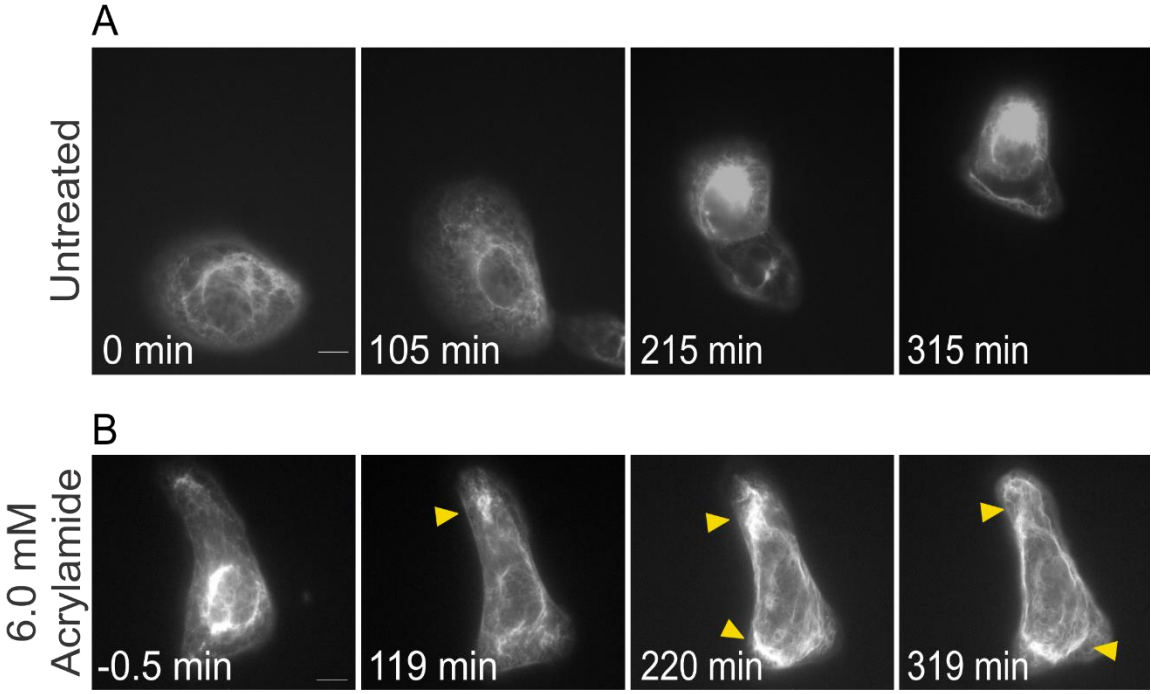


Figure 5.7: Acrylamide induces disruption of keratin network in MDCK single cells.

eGFP-K8 mid-expressor MDCK were sparsely plated and the response of keratin network was documented in normal conditions (**A**) and during 6.0 mM acrylamide treatment (**B**). Single cells expressing eGFP-K8 were imaged every 5 min for the length of the movie of 7 hrs using Zeiss Cell Observer spinning disk confocal microscope (63X/1.4 NA, 1.0X optovar). Select confocal images representative of a time series reveal typical dynamics of a spread-out keratin network during normal conditions, whereas, cells treated with acrylamide show changes in the organization of eGFP-K8. Characteristic dynamics of the spread-out network prior to addition of acrylamide is seen in the image (-5 min). In the presence of acrylamide, keratin filaments first form discrete aggregate hot spots (**arrowheads** at 119 min, 220 min) and concurrently accumulate towards the nucleus (**arrowheads** at 319 min). (Untreated, n= 6; acrylamide, n=3).

Bars, 10 μm

Figure 5.8

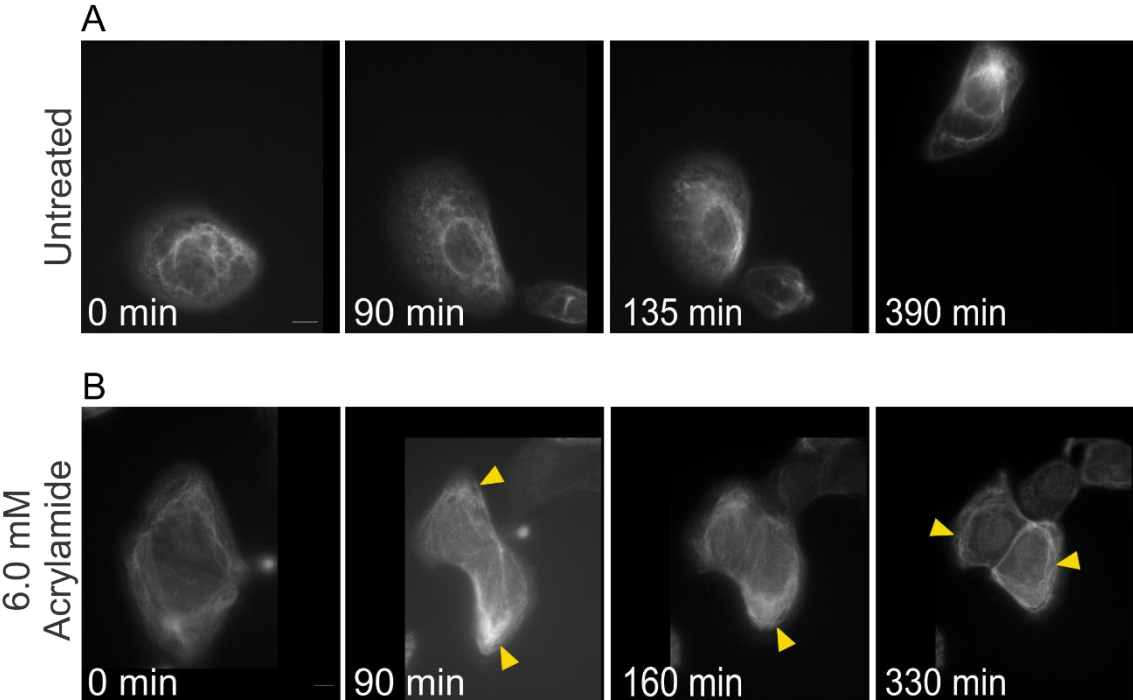


Figure 5.8: Acrylamide induces disruption of keratin network in MDCK cells pairs.

eGFP-K8 mid-expressor MDCK were sparsely plated and the response of keratin network was documented in normal conditions (**A**) and during 6.0 mM acrylamide treatment (**B**). Cell pairs expressing eGFP-K8 were imaged every 5 min for the length of the movie of 8 hrs using Zeiss Cell Observer spinning disk confocal microscope (63X/1.4 NA, 1.0X optovar). Select confocal images representative of a time series reveal typical dynamics of a spread-out keratin network during normal conditions, whereas, cells treated with acrylamide show changes in the distribution of eGFP-K8. Characteristic dynamics of a wide spread network prior to addition of acrylamide is seen in the image (-5 min). In the presence of acrylamide, keratin filaments first form aggregates at discrete spots (**arrowheads** at 90 min and 160 min) and eventually, the filaments accumulate around the nucleus (**arrowheads** at 330 min). (Untreated, n=3; acrylamide, n=3).

Bars, 10 μ m

Figure 5.9

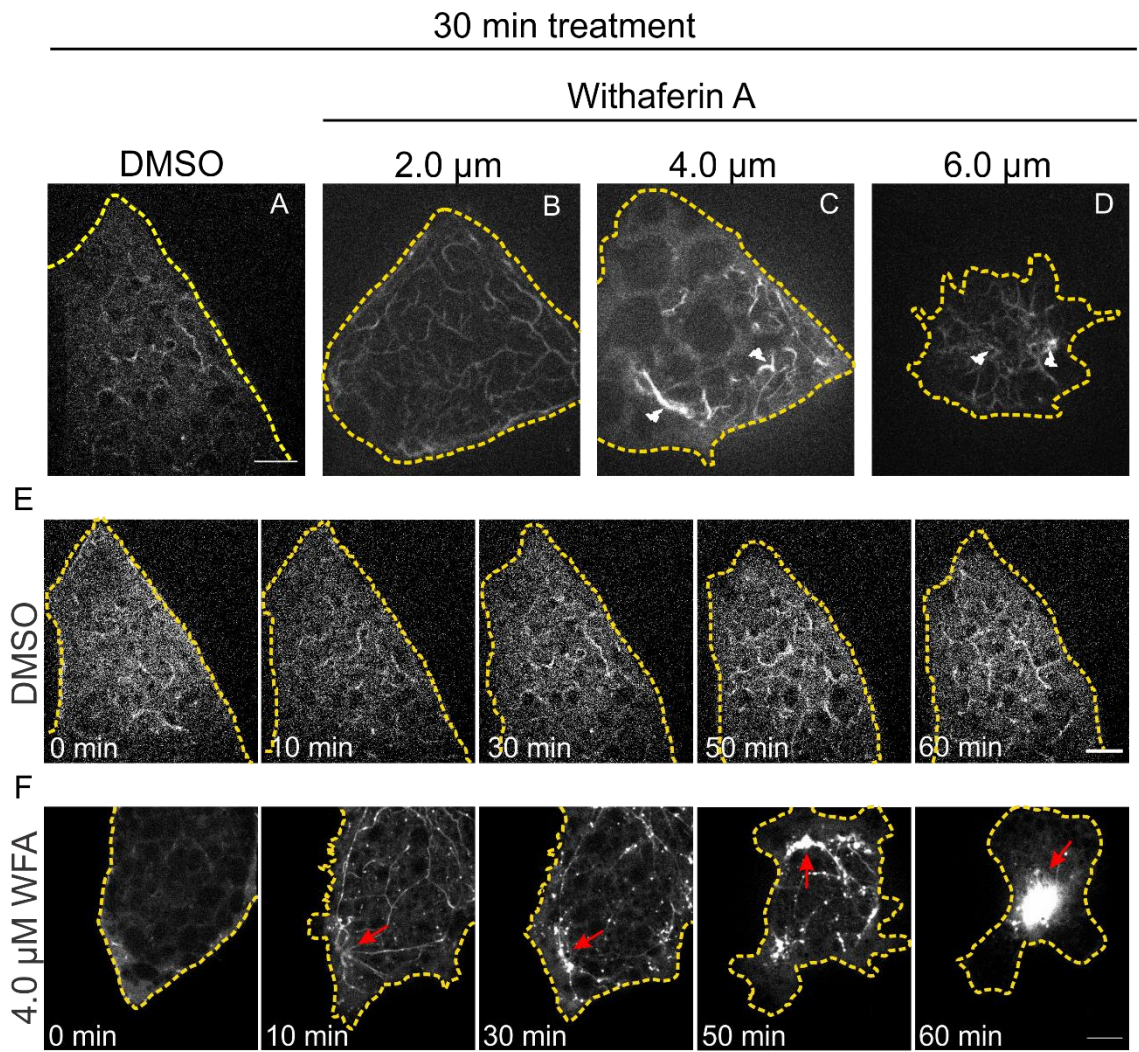


Figure 5.9: Withaferin A treatment alters keratin filament organization and cell morphology of *Xenopus* mesendoderm cells.

Xenopus embryos were microinjected with eGFP-krt8 RNA at two blastomere stage at the presumptive mesendoderm and permitted to develop until stage 10.5. Following, mesendodermal tissue was dissociated to single cells and prepared and plated on fibronectin-coated glass-bottom dishes. Cells were imaged using Zeiss Cell Observer spinning disk confocal microscope (63X/1.4 NA, 1.0X and 1.6X optovar). Representative inverse confocal images of dissociated mesendoderm cells expressing eGFP-K8 treated with DMSO (**A**), 2.0 μ M WFA (**B**), 4.0 μ M WFA (**C**), 6.0 μ M WFA (**D**) show a dose-dependent increase in disruption of keratin filaments. The **arrowheads** show the extensive aggregation of keratins at the highest concentration. Select confocal images representative of a time series of dissociated mesendoderm cells expressing eGFP-K8 exposed to DMSO (**E**) and 4.0 μ M WFA (**F**), show progressive disruption and aggregation of keratin intermediate filaments with maximum retraction at 60 min (**arrows**). The cell boundary traced in **yellow dotted line** shows changes in cell shape coincident with degree of keratin network alteration by WFA treatment, with no effect of DMSO (negative control) on the treated cell. (Control, n=3; WFA, n=3). Bars, 10 μ m

Figure 5.10

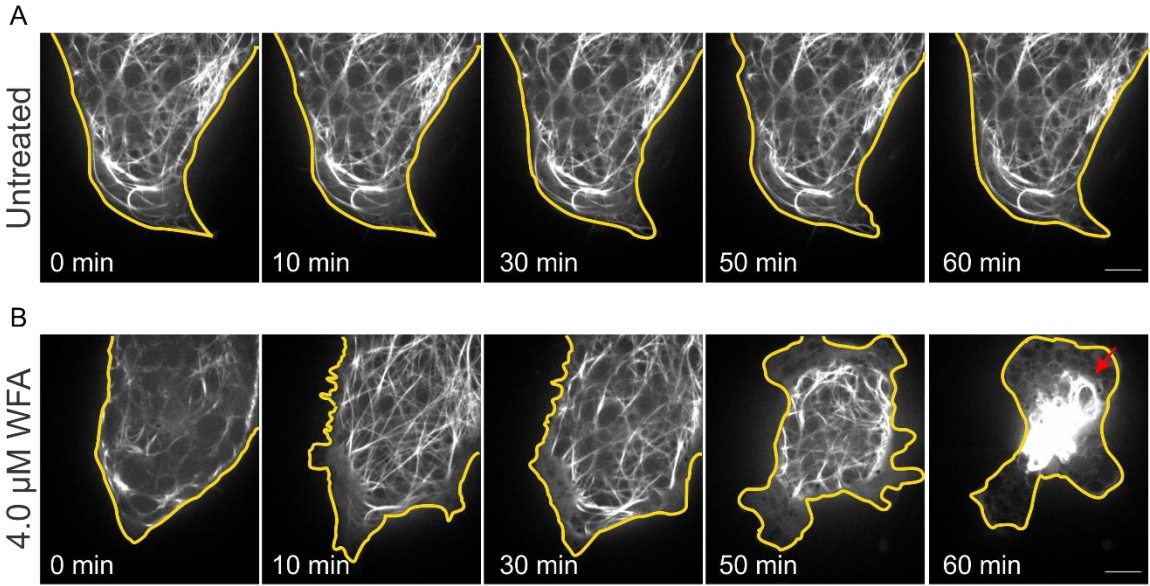


Figure 5.10: WFA treatment induces alterations of the microtubule filament organization in *Xenopus* mesendoderm cells.

Dissociated single cells were obtained from *Xenopus* embryos expressing EMTB-mCherry and plated on fibronectin-coated glass-bottom dishes. Cells were imaged every 5 min for the length of the movie of 80 mins using Zeiss Cell Observer spinning disk confocal microscope (63X/1.4 NA, 1.0X optovar). Select confocal images representative of a time series of dissociated mesendoderm cells expressing EMTB-mCherry untreated (**A**) and exposed to 4.0 μ M WFA (**B**), reveal the microtubule network in different conditions. Cells treated with WFA show progressive disruption and aggregation of microtubules with acute disassembly and aggregation of the microtubule filaments by 60 mins (**arrow**). The cell boundary traced in **yellow dotted line** shows changes in cell shape coincident with degree of microtubule network alteration by WFA treatment, with no effect in untreated cell. (control, n=3; WFA, n=3).

Bars, 10 μ m

Table 5.3 Effect of Withaferin A on MDCK single cells.

NO	Concentration	Time points					Activity at edges	Type of IF collapse	Morphology
		IF collapse start time	IF collapse end time	Protrusions start time	Protrusions end time	Cell collapse start time			
1	6 uM WFA	25 mins i.e 1st image	270 mins	25 mins i.e 1st image	385 mins	25 mins	Transient: microspikes, blebbing, concave lamellipodia	Juxtannuclear aggregation	"fried egg" with trailing edge, tiny vacuoles
2	3/6 uM WFA	10 mins	385 mins	15 mins	475 mins	215 mins	Microspikes, broad protrusions, concave lamellipodia	Perinuclear aggregation	"fried egg", vacuoles
3	3/6 uM WFA	10 mins	145 mins aggeration/ 455 mins perinuclear ring	15 mins	protrusions until 225 mins after that blebbing	205 mins	Transient: micro spikes, small broad protrusions, blebbing	Juxtannuclear aggregation	"fried egg", tiny vacuoles
4	3/6 uM WFA	10 mins	200 mins	15 mins	425 mins	260 mins	Transient: microspikes (at rigid edges), small broad protrusions	Perinuclear aggregation	"fried egg", big n tiny vacuoles
5	6 uM WFA	14 mins	158 mins	23 mins	240 mins	53 mins	Transient: small broad protrusions	Perinuclear aggregation	Trailing edge
6	6 uM WFA	9 mins	360 mins	29 mins	264 mins	210 mins	Transiet: small broad protrusions	Perinuclear aggregation	"fried egg" with trailing edge, tiny vacuoles
7	6 uM WFA	22 mins	180 mins	40 mins	170 mins	200 mins	small protrusions	Perinuclear aggregation	"fried egg", tiny vacuoles
8	6 uM WFA	22 mins	90 mins	22 mins	50 mins	50 mins	microspikes, small protrusions	Juxtannuclear aggregation	"fried egg", tiny vacuoles
9	6 uM WFA	16 mins	36 mins	21 mins	N/A	N/A	Blebbing	Juxtannuclear aggregation	Rounded cell
10	4 uM WFA	240 mins	537 mins	368 mins	inconclusive	681 mins	protrusions	Perinuclear aggregation	In b/w rounded cell and fried egg
11	6 uM WFA	6 min	60 mins	6 mins	110 mins	inconclusive	blebbing	Perinuclear aggregation/ perinuclear ring	Fried egg
13	6 uM WFA	2 min	90 mins	6 mins	85 mins	60 mins	Microspikes mainly at ridge edges, small protrusions	Perinuclear aggregation	Fried egg
14	6 uM WFA	6 min	120 mins	8 mins	inconclusive	32 mins	Blebbing	Perinuclear aggregation	Fried egg
15	6 uM WFA	2 min	58 mins	8 mins	inconclusive	84 mins	Lots of microspikes, small protrusions	Incomplete perinuclear collapse	Fried egg

Table 5.4 Effect of DMSO on MDCK single cells.

No.	Treatment	Time points						Morphology
		IF collapse start time	IF collapse end time	Protrusions start time	Protrusions end time	Cell collapse start time	Total treatment time	
1	DMSO	NO	NO	NO	NO	NO	600 mins	Normal
2	DMSO	NO	NO	NO	NO	NO	285 mins	Normal
3	DMSO	NO	NO	NO	NO	NO	240 mins	Normal
4	DMSO	NO	NO	NO	NO	NO	675 mins	Normal

Table 5.5 Effect of Withaferin A on MDCK cell pairs.

No.	Concentration	Time points						Activity at edges	Type of IF collapse	Morphology
		IF collapse start time	IF collapse end time	Protrusions start time	Protrusions end time	Cell-cell contact changes	Cell collapse start time			
1	6 uM WFA	10 mins	Cell 1- 35 mins Cell 2- 155 mins	Cell 1-10 mins Cell 2- 15 mins	Cell 1- 35 mins Cell 2- 100 mins	100 mins	Cell 1- 35 mins Cell 2- 90 mins	transient: microspikes, blebbing, small protrusion	aggregation	cell rounded
2	3/6 uM WFA	Cell 1- 10 mins Cell 2- 10 mins	Cell 1- 55 mins Cell 2- 392 mins	15 mins	Cell 1- 300 mins Cell 2- 300 mins	contacts get thinner but not completely lost	Cell 1- 50 mins Cell 2- 170 mins	transient: microspikes, blebbing, small protrusion	perinuclear aggregation	fried egg, small and big vacoules
3	3/6 uM WFA	10 mins	Cell 1- 120 mins Cell 2- 300 mins	15 mins	480 mins	NO	215 mins	transient: microspikes, small protrusion	perinuclear aggregation	fried egg, small and big vacoules
4	3/6 uM WFA	15 mins	300 mins	20 mins	470 mins	contacts get thinner but not completely lost	470 mins	transient: microspikes, small protrusion	juxtannuclear aggregation	fried egg, small and big vacoules
5	6 uM WFA	14 mins	104 mins	24 mins	200 mins	N/A	120 mins	transient: microspikes, small protrusion, concave lamellipodia	perinuclear aggregation/perinuclear ring	fried egg, small and big vacoules
6	6 uM WFA	9 mins	Cell 1- 44 mins Cell 2- 600 mins	9 mins	660 mins	NO	120 mins	transient: microspikes, small protrusions, blebbing	perinuclear aggregation	fried egg, small and big vacoules
7	6 uM WFA	28 mins	40 mins	21 mins	inconclusive	NO (IF b/w cell contact collapse at 224 mins)	28 mins	blebbing, microspikes	perinuclear aggregation	fried egg and rounded cell
8	6 uM WFA	19 mins	76 mins	28 mins	inconclusive	NO	inconclusive	transient: blebbing, microspikes small protrusions	perinuclear aggregation	rounded cell
9	4 uM WFA	396 mins	Cell 1- 603 mins Cell 2- partial collapse			Yes	400 mins	microspikes, slightly broader protrusions	perinuclear aggregation for one cell	cell1 -apoptosis
10	6 uM WFA	4 mins		10 mins	240 mins/ 360 mins	contacts get thinner but not completely lost		transient: small protrusions, microspikes	incomplete perinuclear aggregation	fried egg, small vacoules
11	6 uM WFA	6 mins	Cell 1- 22 mins Cell 2- 60 mins Cell 3- 70 mins	12 mins	No	No	32 mins	transient: small protrusions, microspikes	juxtannuclear aggregation	fried egg, small vacoules

Table 5.6 Effect of DMSO on cell pairs.

No.	Treatment	Time points					Total treatment time	Morphology
		IF collapse start time	IF collapse end time	Protrusions start time	Protrusions end time	Cell collapse start time		
1	DMSO	NO	NO	NO	NO	NO	300 mins	Normal
2	DMSO	NO	NO	NO	NO	NO	554 mins	Normal
3	DMSO	NO	NO	NO	NO	NO	586 mins	Normal
4	DMSO	NO	NO	NO	NO	NO	675 mins	Normal

Table 5.7 Effect of withaferin A on MDCK cell clusters.

No.	Concentration	Time points						Activitiy at edges	Type of IF collapse	Morphology
		IF collapse start time	IF collapse end time	Protrusions start time	Protrusions end time	Cell-cell contact changes	Cell collapse start time			
1	6 uM WFA	180 mins	600 mins	260 mins	uncertain	260 mins	370 mins	No	aggregation	normal

Table 5.8 Effect of DMSO on MDCK cell clusters.

No.	Treatment	Time points					Total treatment time	Morphology
		IF collapse start time	IF collapse end time	Protrusions start time	Protrusions end time	Cell collapse start time		
1	DMSO	NO	NO	NO	NO	NO	620 mins	Normal

Table 5.9 Effect of acrylamide on MDCK single cells.

NO.	Concentration	Time points						Cell-cell contact	Activity at edges	Type of IF collapse	Morphology
		IF collapse start time	IF collapse end time	Protrusions start time	Abnormal Protrusions start time	Protrusions end time	Cell collapse start				
1	6mM Acrylamide	45 min	655 mins	85 mins	500 mins	933 mins	715 mins	single cell forms cell-cell pair	spikes seen towards the end of the movie	perinuclear aggregation, juxtanuclear aggregation	fried egg, granules collapse towards nucleus
2	6mM Acrylamide	40 mins	459 mins		360 mins	510 mins	120 mins	No	spikes seen towards the end of the movie	aggregation	vacuoles, cytoplasmic granules accumulation, eventually long spikes as protrusions
3	6mM Acrylamide	15 mins	320 mins	25 mins	270 mins	315 mins	225 mins	No	spiked broad protrusion	perinuclear aggregation	broad protrusions with microspikes, granules collapse to nucleus, fried egg
4	3mM Acrylamide	uncertain	uncertain	uncertain	uncertain	uncertain	uncertain	single cell forms cell-cell pair	uncertain	uncertain	uncertain

Table 5.10 Control MDCK single cells.

NO.	Treatment	Time points					Type of IF collapse	Morphology
		IF collapse start time	IF collapse end time	Protrusions start time	Protrusions end time	Cell collapse start time		
1	Untreated	No	No	No	No	No	No	Normal
2	Untreated	No	No	No	No	360 mins	No	Normal
3	Untreated	No	No	No	No	No	No	Normal
4	Untreated	No	No	No	No	No	No	Normal
5	Untreated	No	No	No	No	No	No	Normal
6	Untreated	No	No	No	No	650 mins	No	Normal
7	Untreated	No	No	No	No	170 mins	No	Normal

Table 5.11 Effect of acrylamide on MDCK cell pairs.

NO	Concentration	Time points						Cell-cell contact	Activity at edges	Type of IF collapse	Morphology
		IF collapse start time	IF collapse end time	Protrusions start time	Abnormal Protrusions start time	Protrusions end time	Cell collapse start time				
1	6mM Acrylamide	20 mins	Cell 1- 240 mins, Cell 2- 480 mins, Cell 3- ?	40 mins	180 mins	360 mins	144 mins	cell-cell contact tethers lost almost at the end	long spikes with no broad protrusions	aggregation, perinuclear aggregation	vacuoles, long spikes, most likely apoptosis
2	6mM Acrylamide	210 mins	600 mins	390 mins	No	930 mins	430 mins	cell-cell contact tethers lost almost at the end	No	perinuclear aggregation	vacuoles, fried egg
3	6mM Acrylamide	20 mins	Cell 1- 420 mins, Cell 2- 460 mins	50 mins	120 mins	465 mins	155 mins	No	small spikes formed at the end	peculiar perinuclear aggregation absent	vacuoles, fried egg
5	3mM Acrylamide	Uncertain	Uncertain	Uncertain	Uncertain	Uncertain	Uncertain	Cell-cell pair break and formed a new cell-cell pair	Uncertain	Uncertain	Uncertain
6	3mM Acrylamide	Uncertain	Uncertain	Uncertain	Uncertain	Uncertain	Uncertain	Cell-cell pair break and formed a new cell-cell pair	Uncertain	Uncertain	Uncertain

Table 5.12 Control MDCK cell pairs.

NO	Concentration	Time points						Cell-cell contact	Type of IF collapse	Morphology
		IF collapse start time	IF collapse end time	Protrusions start time	Abnormal Protrusions start time	Protrusions end time	Cell collapse start time			
1	12 mM Acrylamide	20 mins	360 min	50 mins	70 mins	210 min	cell border: 90 min	NO	perinuclear aggregation	big n small vacuoles, most likely apoptosis
2	6mM Acrylamide	40 min	uncertain	uncertain	200 mins	305 mins	210 min	yes	aggregation	organelles collapse, spikes and vacuoles seen at the end
3	6mM Acrylamide	50 mins	900 mins	300 mins	No	uncertain	No	No	aggregation	organelles collapse, spikes and vacuoles seen at the end
4	6mM Acrylamide	70 min	600 mins only one cell	190 min	n/a	n/a	420 min	gaps b/w cell pair	aggregation	cells did not completely collapse

Discussion

In contrast to a number of selective drugs which are readily available for the actin and microtubules, there are no comparable drugs for selective inhibition of IFs. Despite the reservations regarding the specificity of the IF inhibitors, a large number of studies have used them as tools to elucidate the role of intermediate filaments. Here a broad analysis was undertaken to examine the effects of drugs such as WFA and acrylamide on keratin IFs. This study included examination of four variables 1) cell type: *in vitro* model MDCK and *in vivo* model *X. laevis* mesendoderm cells; 2) cell density: single cells, cell pairs, marginal cells and submarginal cells; 3) pharmacological inhibitors: withaferin A and acrylamide and 4) time of exposure.

WFA induces a marked disorganization of keratin filaments in MDCK cells from their normal arrays extending throughout the cytoplasm, into collapsed keratin filament aggregates around the nucleus. In some cases, keratin filaments aggregate and rearrange in the perinuclear region of the cytoplasm. While in other cases, keratin filaments collapse and reorganize as juxtanuclear aggregates. Similar WFA induced redistribution of keratin filaments was also observed in MCF-7 epithelial cells and A549 human lung cancer cells (Grin et al., 2012). However, in these cells reorganization of keratin network was obtained with 6.0 μ M WFA treatment for 3hrs. The difference in the time of exposure could be because of the different cell type (Grin et al., 2012). Other conditions that induce similar collapse of keratin network include microinjection of anti- α -keratin antibodies

(Klymkowsky et al., 1983) and exposure to microcystin-LR (serine/threonine protein Phosphatases) (Toivola et al., 1997). This phosphatase inhibitor causes hyperphosphorylation induced reorganization and disassembly of keratin polymers (Toivola et al., 1997). Likewise, WFA induces increase in vimentin phosphorylation which is coincident with the perinuclear accumulation of vimentin filaments (Grin et al., 2012). These studies suggest that the observed WFA induced keratin filament collapse might be hyperphosphorylation dependent. However, further experiments are required to elucidate the molecular mechanism of keratin filament retraction in presence of WFA.

The time lapse movies shown here revealed that keratin redistribution followed a specific pattern. In MDCK cells, the filaments were constantly undulating and aggregating, similar to forming thicker filament cables. Further along, the filaments seem to be recoiling to form a perinuclear mass. However, in mesendoderm cells the keratin redistribution pattern in response to WFA treatment appear to be different. Here, the fluorescence pattern showed a simultaneous formation of small keratin granules and filament aggregation which ultimately curled up near the nucleus. Moreover, WFA also induces similar whorled array of microtubules following their aggregation. The aggregation of keratin filaments was accompanied by changes in cell shape. Similar changes in cell morphology were observed when vimentin or keratin filaments were disrupted by WFA treatment (Grin et al., 2012). Thus, in addition to keratin filaments, WFA also alters the organization of other IF family members (**Table 5.1**), as well as the microtubules (Fig 5.10) and microfilaments (Grin et al., 2012).

Hence, a possible multistep sequence in keratin filament reorganization begins with phosphorylation dependent filament bundling and aggregation of filaments and formation of smaller nonfilamentous aggregates and thus collapse of keratin network. This is followed by pulling up of filament bundles in conjunction with microtubules into perinuclear or juxtannuclear mass. This coiling of keratin and microtubule filaments may cause pulling of cytoplasm and organelles around the nucleus since both IFs and microtubules are involved in organelle subcellular organization (Leterrier et al., 1994; Nekrasova et al., 2011).

In MDCK cells the keratin network was affected within minutes (~15 min) of WFA treatment. In comparison with timescale for keratin disruption as reported by other studies (Grin et al., 2012), this study suggests that at least in MDCK cells there is speedy response to WFA. Moreover, the timescale for disruption of other members of the IF family are also not comparable (**Table 5.1**). This difference in response time can be due the cell type and the presiding IF(s) and also the cell density used during the experiments. The present study shows density dependent keratin filament retraction from cell periphery to the nucleus. The keratin network in the submarginal cells which has maximum cell-cell contacts is most resistant to WFA. Whereas, filaments of the single cells which have no cell-cell contacts are most susceptible to WFA induced keratin reorganization. Next, in marginal cells and cell pairs, the filaments collapsed from the peripheral region and accumulated in the perinuclear zone, however, keratin filaments in the vicinity of cell-cell contacts did not

disrupt as readily and were more resistant. This indicates that cell-cell contacts exert a protective effect against WFA induced keratin disruption.

Extensive rearrangement of keratin filament organization is also observed in MDCK cells upon acrylamide treatment. However, acrylamide does not cause the drastic collapse of keratin network as observed with WFA treatment. As with WFA treatment the keratin network disruption happened in a time dependent fashion. Minimal disruption was observed in cells exposed for 1hr with acrylamide where very small puncta or aggregates were formed. But by 6 hrs of treatment further aggregates formed and filaments accumulated in the perinuclear region. Live cell imaging revealed that unlike WFA, acrylamide treatment promotes formation of distinct aggregates throughout the cytoplasm which become more concentrated, the filaments show undulations and inward movement of the aggregates and filaments then ultimately concentrate surrounding the nucleus. Reorganization of keratin filaments in response to acrylamide has also been reported, however, these studies show more severe disruption pattern(Durham et al., 1983; Eckert, 1985; Sager, 1989). Similar to WFA, acrylamide also shows cell-density dependent keratin network collapse. Keratin filaments in submarginal cells were most protected against acrylamide induced redistribution. In all sample sets, filaments close to cell-cell contacts did not show severe disruption pattern. Thus, small molecule inhibitors deform keratin network organization in a cell-density dependent manner.

In spite of the advances towards the understanding of the relationship of keratin intermediate filaments to cell-cell adhesions and redistribution of keratin organization to cell shape changes by the comprehensive comparison done here, the study clearly shows that keratin disruption is not consistent and varies due to differences in cell types, cell density, time of exposure and dose of the inhibitor. Additionally, along with the studies done here and comparative literature survey of the studies where these tools have been used (Introduction), the small molecular inhibitors do not emerge as specific tools for selective inhibition of IFs. Along with having a broad specificity for intermediate filaments (Table 5.1), WFA does not exclusively affect IFs but also has other effects at doses less than that required for IF disruption. For example, at low doses (IC_{50} 12 nM) WFA causes antiproliferative activity in endothelial cells (Mohan et al., 2004) whereas at high doses (IC_{50} above 2 μ M) induces apoptosis (Bargagna-Mohan et al., 2007; Grin et al., 2012). Taken together, likely WFA does not specifically interfere with IF structure and function. Acrylamide, similar to WFA, also has a broad specificity to intermediate filaments (Table 5.2) and is not just an IF disrupting agent but has anti-proliferative activity, affects NAD- and NADP- dependent metabolic pathway, protein synthesis inhibition (Aggeler and Seely, 1990; Sager, 1989) and desmosome internalization (Shabana et al., 1994). Due the broad utility and ease of use, these small molecule inhibitors should be used as a prelude or in conjunction with other specific approaches to interrogate intermediate filaments.

Chapter 6

Rational Design and Development of Photoactivatable Inhibitory Peptides to Specifically Disrupt Keratin Filaments

This chapter is, in part, adapted from manuscript:

Sanghvi-Shah, R., Paranjpe, S., Baek, J., Dobrowolski, R., and Weber, G. (2018). A novel photoactivatable tool for intermediate filament disruption indicates a role for keratin filaments in early embryogenesis. *bioRxiv*. doi:10.1101/484246.

(PA-2B2 and PA-dIF are equivalent names for mCherry-LOV-J α -2B2, open-2B2 and CA-dIF are equivalent names for mCherry-LOV-J α -(I379E)2B2)

Abstract

The significance of keratin intermediate filaments has previously been discerned using traditional tools such as genetic techniques and chemical inhibitors. Few studies to date have attempted to examine the role of polymerized keratin filaments and their contribution to various cell behaviors. To directly assess the role of polymerized keratin filaments, Photoactivatable-2B2 (PA-2B2) and constitutively active open-2B2 genetically encoded photoswitches were generated. These novel tools take advantage of the disruptive effects of the mimetic peptides derived from the 2B2 region of the central rod domain of *Xenopus* keratin 8. Sequence analysis and molecular modeling were used to embed the peptide 2B2 into the J α segment of the photosensitive AsLOV2 domain of *Avena sativa* phototropin-1. The 2B2 peptide can efficiently disrupt keratin filaments in multiple species and cell types.

Introduction

Although intermediate filaments are one of the major cytoskeletal elements of a cell, their functional significance remains least understood. Despite extensive research, specific roles of keratin filaments remain elusive especially in complex tissue processes such as morphogenesis during embryological development. Recently it has been shown that keratins are important for specifying the directional protrusive behavior of migratory mesendoderm cells in gastrulating *Xenopus* embryos. Correlative evidence suggests that localization of polymerized keratin filaments determines the non-protrusive posterior of the migratory cell (Weber et al., 2012). However, the specific role of keratin filaments versus keratin protein is unknown. Deciphering the role of keratins is difficult due to functional redundancy and complexity within the protein family, generation of exogastrulation or embryonic lethal phenotypes in IF deficient animal models, and thirdly due to lack of specific inhibitors characterized for IFs. In contrast, variety of tools are readily available for the other two cytoskeletal elements, actin and microtubule, which has allowed for major breakthroughs in their respective fields of research. As described in chapter 5, there are a few small molecule inhibitors that disrupt IFs and none have well understood mechanisms of disruption specific to IFs. Such small molecule inhibitors have broad impacts to cell signaling and result in cell-wide disruption of the IF network. Future investigation of intermediate filaments necessitates the development of tools to specifically disrupt keratin filaments.

In the last decade, there has been a considerable progress in the use of naturally occurring photosensitive proteins to generate photoswitches that are genetically encoded and reversible. These photoswitches manipulate a wide range of protein functions with unprecedented spatiotemporal resolution. The LOV2 (light, oxygen, voltage) domain from *Avena sativa* phototropin-1 (AsLOV2), has light sensitive ability to photomodulate the binding affinity of the peptides linked to them for their targets (Huala, 1997). AsLOV is a subclass of the Per-ARNT-Sim (PAS) superfamily of protein-protein interaction domains (Crosson and Moffat, 2001). In the center of the PAS domain there is a conserved central antiparallel β -sheet within which resides the flavin mononucleotide (FMN) acting as a chromophore for the protein. A segment attached to the C-terminal of the fold forms a novel α -helix, termed J α -helix. This J α -helix is docked on the β -sheet of the LOV domain (Harper et al., 2003; Möglich et al., 2009). Upon irradiation with blue light, excitation of the flavin molecule leads to formation of a covalent adduct between cysteine residue in the LOV domain and the carbon atom of the FMN (Swartz et al., 2001). This conformational change leads to the dissociation of the J α -helix from the β -sheet and subsequent unwinding of the α -helical structure (Harper et al., 2004; Swartz et al., 2001). This photoadduct is reversible and recovery is achieved in the absence of light within seconds to minutes, depending on the LOV domain ortholog (Swartz et al., 2001). There are successful examples where the light-sensitive LOV domain has previously been harnessed to create photoswitches either by embedding short peptides (Lungu et al., 2012) or entire proteins (Wu et al., 2009). In either case, the J α -helix conformational change allows for the steric block of the peptide of interest and its release in presence of light. Advantages of using the

LOV domain include its small size (15 kDa), light induced conformational change and prevalence of the flavin cofactor which occurs in cultured cells and *in vivo*.

All intermediate filaments share the common tripartite structure that includes the α -helical rod domain flanked by the non-helical head and tail regions. Despite some sequence divergence among IF proteins, the helical rod domain invariably has highly conserved 1A and 2B segments located at the N-terminal and C-terminal respectively. These segments are critically involved in the formation of coiled-coil α -helical dimers (Strelkov et al., 2002) and are referred to as the 'helix initiation domain' and 'helix termination domain', respectively.

Helix initiation domain -1A

Mimetic peptides homologous to the 1A portion of the rod domain display substantial efficacy as disruptors of the IF network and thus can be developed as tools to inhibit IF structure and function. Synthetic keratin peptides (35 aa) mimicking the 1A rod segment at 1:1 molar ratio promotes *in vitro* disruption of the preformed keratin IFs after 60 mins (Steinert et al., 1993a, 1993b). Similarly, *in vitro*, vimentin 1A mimetic peptide (35 aa) has been shown to disrupt the preexisting vimentin IFs into smaller oligomeric and monomeric subunits within 30 mins and also interfere with vimentin IF assembly (Goldman et al., 1996). In addition, disruption of the vimentin IF network was also detected when 1A peptides (0.5-2.0 mg/ml) were microinjected in fibroblasts (Goldman et al., 1996). Thus, helix initiation-1A peptides induce disruption of IF networks both *in vitro* and *in vivo*.

Helix termination domain -2B (2B2)

Mimetic peptide 2B2 (the C-terminal most segment of 2B domain) also has a central role in IF assembly, and thus can be developed as a tool to disrupt IF structure and function. *In vitro*, 2B2 mimetic peptides (20 aa) have been shown to disrupt pre-assembled filaments of keratins and also inhibit keratin filament assembly (Hatzfeld and Weber, 1992; Steinert et al., 1993a, 1993b). Likewise, both a synthetic 20 aa peptide (Kouklis et al., 1992) and a 57 aa peptide (Strelkov et al., 2002) corresponding to the highly conserved region of the vimentin 2B segment interfere with vimentin IF assembly, and disrupt preformed IFs when added at 10-70 fold molar excess. *In vivo*, microinjection of 2B2 peptide (0.5-2.0 µg/ml) in fibroblasts causes disruption of vimentin network into short filaments and ULF like structures (Helfand et al., 2011). These studies demonstrate the efficacy of helix termination domain 2B2 in disrupting IFs in both *in vitro* and *in vivo* conditions.

Collectively, these results indicate that due to the affinity and efficacy of the mimetic peptides to interfere with both preformed IFs and IF assembly, 1A and 2B2 peptides are equally excellent candidates to be developed as dominant negative tools. Some of these approaches are invasive methods such as cell loading achieved via disruption of the cell membrane and none of the methods confer spatial and temporal specificity. Hence, as a logical extension I developed unique genetically encoded photoactivatable derivatives of 1A and 2B2 peptides to manipulate the disruption of IFs *in vivo*.

To that end, I developed a rational design strategy to generate the current tools while taking into consideration several strategies noted by other laboratories while developing similar tools (Lungu et al., 2012; Wu et al., 2009). First, *X. laevis* krt8 peptides corresponding to the 1A and 2B2 segments compatible with LOV caging were identified and their ability to disrupt keratin filament network was verified in cultured cells. Next, the photoactivatable 1A (PA-1A) and 2B2 (PA-2B2) constructs and their light insensitive derivatives were constructed. The ability of the 2B2 constructs to disrupt keratin filaments was validated in living cells. Such a biological tool with photocontrol of inhibitory peptides provides a method to probe the cellular functions of keratin in a variety of physiological processes in a way that is inaccessible by current approaches.

Results

6.1 Identifying peptides to generate photoswitchable disruptor of keratin filaments

The two segments, 1A at the N-terminal and 2B2 domain at the C-terminal of the helical rod domain are highly conserved sequences and critically important for dimer-dimer interactions (Strelkov et al., 2002). Previously, *in vitro* and *in vivo* studies show the efficacy of peptides resembling the 1A (Goldman et al., 1996; Steinert et al., 1993a) and 2B2 (Hatzfeld and Weber, 1992; Helfand et al., 2011; Kouklis et al., 1992; Steinert et al., 1993a; Strelkov et al., 2002) peptides in disrupting the IF networks. These studies suggest that as few as 18 amino acids from the 1A segment and 20 amino acids from the 2B segment are sufficient to induce disruption of IFs *in vitro* (Goldman et al., 1996; Hatzfeld and Weber, 1992; Steinert et al., 1993a). Based on these studies 18 residues of the conserved α -helical segment 1A of the N-terminal end and 22 residues of the α -helical segment 2B situated at the C-terminal end of the central rod domain were derived from *X. laevis* krt8 as template for 1A and 2B2 peptides respectively (**Fig 6.1A**). To be more specific, while the 2B2 fragment harbors the so-called IF consensus motif YRKLLEGEE (Herrmann et al., 2002) the peptide spans 16 residues of the α -helical segment 2B situated at the very end of the rod domain and the remaining 6 residues overlap the initial part of the tail domain (**Fig. 6.1A**). Nonetheless, the sequences used here are relatively smaller in comparison to the similar mimetic peptides (1A-35 aa and 2B2-57 aa) utilized for *in vivo* disruption of the IF network (Goldman et al., 1996; Helfand et al., 2011). The 2B2 amino acid sequence is highly conserved across intermediate filament proteins (**Fig 6.1B**) and species (**Fig. 6.1C**).

In comparison to 2B2, 1A fragment is less conserved among the *X. laevis* intermediate filament proteins. (**Fig. 6.1D**).

6.2 Keratin 8 mimetic peptides 2B2 and 1A readily promote keratin network disruption

Previous experiments with similar mimetics were mostly *in vitro* and the few *in vivo* experiments were performed with high concentrations of peptides directly microinjected in the cell. Microinjection possess a limitation of cell injections per experiment along with cell loading with high concentrations of protein and damaging the cell membrane. Thus, I examined, whether keratin disruption can still be achieved even when DNA of *X. laevis* krt8 mimetic peptide 2B2/1A is introduced by approaches such as transfection. Constructs 3X-FLAG 2B2 and 3X-FLAG 1A generated under the control of a CMV promoter (**Table 6.1 and 6.2**) were expressed in MDCK cells and disruption of keratins was verified. Transfected cells were methanol fixed and immunolabelled with anti-FLAG antibody and counterstained with Hoechst dye, 24 hrs post-transfection. Quite contrary to the control (mock treated) cells, which have keratin filaments widely distributed throughout the cytoplasm, the cells expressing either 2B2 or 1A peptide exhibit formation of filamentous aggregates (**Fig. 6.2**). Both 2B2 and 1A peptides readily disrupt keratin filamentous network; however, to achieve an acute disruption of keratin filaments it would be highly advantageous to cage the peptides and develop molecular tools whose activity can be spatiotemporally controlled.

6.3 *In silico* analyses and molecular modeling to design PA-2B2 and PA-1A

To create a photoactivatable fusion protein containing 2B2 or 1A that could acutely disrupt keratin filaments, 2B2 and 1A inhibitory peptides were fused at the C-terminal of the J α -helix. Several strategies noted by other laboratories were used in the design in order to maximize caging while allowing 2B2 to be available for binding upon photoirradiation (Lungu et al., 2012; Wu et al., 2009; Zimmerman et al., 2016). Tighter caging was suggested to be enhanced by minimizing peptide sequence that extends beyond the LOV-J α interface. In order to promote fusion of inhibitory peptides with LOV-J α along with functional blocking of the peptides against globular LOV domain a series of *in silico* analyses were performed. Optimal caging can be achieved by embedding the inhibitory peptide with the J α helix, however accessibility of peptide could be limited, even in the lit state (Lungu et al., 2012). Therefore, the 2B2 and 1A peptides were fused directly to the J α sequence. All three segments J α , 2B2 and 1A are amphipathic α -helices (**Fig. 6.3, 6.4**). The fusion of 2B2 to J α was predicted to create a contiguous α -helical domain (**Fig. 6.5**).

Helical wheel diagrams for J α -2B2 showed that the amphiphilic properties were conserved and a continuous helix was modeled when 2B2 helical peptide was tethered to J α -helix (**Fig. 6.3**). Thus, no further adjustments were done. Similar Heliquist analyses were done to optimize the threading of J α -helix and 1A helical peptide. The 1A helical peptide packed unfavorably against J α -helix giving a slightly distorted α -helix. Thus, 1A helical peptide was pushed more N-terminally into the J α -helix, such that a small segment

comprising of 3 amino acids (KEL) was removed from the J α -helix. The J α -1A peptide thus obtained had conserved α -helix amphiphilic properties (**Fig. 6.4**).

6.4 Design of 2B2 and 1A peptide photoswitches

The sequence of the peptides used for generation of photoswitches are as follows:

- 2B2- KLALDIEIATYRKLLEGEESRL (22 aa)
- 1A- KEQIKTLNNKFASFIDKV (18 aa)

The photoswitches were constructed by ligating LOV domain via its carboxy terminal to J α -2B2 and J α -1A (**Fig.6.6A & B**). Fluorescent protein mCherry was attached at the N-terminus of the LOV domain to gauge expression level and localization. These two domains were fused with a short linker GS (serine and glycine) to maintain peptide flexibility (**Fig.6.6A & B**). Constructs were inserted into a pCS2⁺ vector for transient expression in *X. laevis* as well as in cell lines. An additional construct containing a mutation within the J α domain of I379E yielded a ‘lit/open-state’ variant. (**Fig.6.6A & B**). To mimic the lit state conformation of LOV domain in a manner analogous to light activation, a point mutation was introduced at the Ile379 residue which lies in the J α -helix. The hydrophobic amino acid was changed to a glutamate residue, so the negative charge at the interface would prevent the docking of the J α -helix onto the β -sheet of the LOV domain (Harper et al., 2004; Wu et al., 2009).

Cloning strategy in brief

In silico sequences for genes LOV-J α -2B2, LOV J α -(I379E)2B2, J α -1A and J α -(I379E)1A tagged with an N-terminal FLAG were designed using pDRAW32 software. These genes were synthesized and cloned into the pUC57 vector (Genewiz). The obtained plasmids were transformed into DH5-alpha *E. coli* competent cells and further subcloning was done using the protocols as mentioned in materials and methods section. The J α -1A and J α -(I379E)1A genes were swapped in place of J α -2B2, J α -(I379E)2B2 to obtain LOV-J α -1A and LOV J α -(I379E)1A. These plasmids were then transformed into BL21 and/or *Iq* competent cells. Further, the N-terminal FLAG tag was swapped with mCherry fluorescent protein from C1mCherry vector using NheI and BglII sites. Once the plasmids for the 2B2 peptide [mCherry-LOV-J α -2B2 (referred to as PA-2B2), mCherry-LOV-J α -(I379E)2B2 (referred to as mCherry open-2B2)], and 1A peptide [mCherry-LOV-J α -1A (referred to as PA-1A), mCherry-LOV-J α -(I379E)1A (referred to as mCherry open-1A)] were generated, they were subcloned into a pCS2⁺ vector using EcoRI and XhoI restriction sites and transformed into *Iq* cells.

Generation of PA-2B2 2.0 and open-2B2 2.0 versions:

The previous versions of PA-2B2 and open-2B2 were expressing a short ‘junk’ peptide in addition to the protein of interest. The unwanted sequence was removed and replaced with a part of the pCS2⁺ backbone using a different pCS2⁺ plasmid. Thus the 2.0 versions are the older PA-2B2 and open-2B2 versions rectified to express only the protein of interest.

NOTE: It was decided to discontinue with the development of 1A molecular tools because early preliminary results displayed no substantial difference in keratin disruption by 1A or 2B2. Moreover, 1A also presented with construct design and cloning problems. It was also taken into consideration that literature supporting the usage of 2B2 peptide was stronger.

Predictive 3D modeling of sequences encoding mCherry-LOV-J α -2B2 was performed using Phyre2 (Kelley *et al.*, 2015). Modeling of LOV-J α closely resembles other predicted and actual X-ray crystallography- and solution NMR spectroscopy-based structures of the domain (**Fig. 6.7A**) (Harper *et al.*, 2003; Lungu *et al.*, 2012; Wu *et al.*, 2009). The addition of the intermediate filament 2B2 domain extended the J α helix (**Fig. 6.7B**). Interestingly the addition of a mCherry fluorophore to the fusion protein generated a loop and turn in the J α -2B2 helix (**Fig. 6.7C**). However, in either case of LOV-J α -2B2 or mCherry-LOV-J α -2B2, the 2B2 domain is predicted to be helical in structure and associate with the globular LOV domain. The 'lit/open-state' variant (**Fig. 6.7D**) with I379E mutation cannot fold properly due to steric hindrance of the LOV-J α interaction (Harper *et al.*, 2004; Wu *et al.*, 2009; Zimmerman *et al.*, 2016). These strategies yielded two constructs: 1) a Photoactivatable disruptor of Intermediate Filaments (PA-2B2) and 2) a Constitutively active disruptor of Intermediate Filaments (open-2B2).

6.5 Hypothesized mechanism for keratin network disruption

The LOV- J α sequence was fused to the amino terminus of the krt8 mimetic peptides 2B2, in anticipation that the LOV domain in its closed conformation would block the binding of krt8 2B2 peptide to its dimerization partners, and that light induced unwinding of the helix would release the steric inhibition leading to “peptide activation”. Hence the mechanism of action of these photoactivatable tools is expected to be as follows. While PA-2B2 is in its closed state, the keratin filaments remain intact. However, upon irradiation with blue light (458 nm) 2B2 peptide gets relieved from the allosteric block and can now bind to its dimerization partners keratin 18/19. Since the 2B2 peptide behaves as a truncated K8 dominant negative protein it fails to form true heterodimers with K18/19 leading to a more general filament disruption and aberrant aggregation (**Fig. 6.8B**). The light insensitive open/lit mutants are expected to be unwind, so the inhibitory peptide 2B2 would be available to bind with the keratin 18/19 and disrupt the keratin network (**Fig. 6.8C**).

6.6 Constitutively active open-2B2 disrupts keratin filaments in cultured MDCK cells

Although several prior studies have demonstrated the ability of 2B2 peptides to bind and disrupt endogenous intermediate filaments, fusion peptide of 2B2 linked to epitope tags or fluorophores have not been tested for IF disruption potential. To test the ability of the developed tools, specifically if the 2B2 mimetic peptide would still remain functional after the addition of moieties such as LOV-J α and mCherry, WT MDCK cells were transfected with either mCherry open-2B2 or mCherry PA-2B2 and keratin disruption was analyzed

by immunofluorescence. Cells were methanol fixed and immunostained with pan-keratin and counterstained with Hoechst dye, 12 hrs post transfection. Although the sequence of 2B2 used originates from frog krt8, the high homology suggested that this sequence should disrupt keratin intermediate filaments across species and cell types (**Fig. 6.1C**). MDCK cells originating from canine kidney epithelia are enriched with a diverse number of keratin intermediate filament proteins. Normal untransfected MDCK cells exhibited a well spread keratin network and robust oval nuclei (**Fig. 6.9A**). Similarly, MDCK cells transfected with PA-2B2 and maintained in the dark (not activated) exhibited normal widespread keratin network. Nuclei in these cells were similarly normal and oval in shape (**Fig 6.9B**). In contrast, mCherry open-2B2 expressing cells showed a perinuclear clustering of the keratin network and aberrant nuclear morphology (**Fig. 6.9C**). Line scan analyses of the keratin filaments in control cells showed high fluorescence intensity fluctuations created by the presence of distinct keratin filament in the network (**Fig 6.9 D**). Filaments in mCherry open-2B2 expressing cells were shorter, aggregated and overall less distinct, which produced lesser intensity fluctuations by line-scan analyses of keratin labelling in the cytoplasm (**Fig. 6.9 E**). A comparison of the variances of normalized line scans indicated a statistically significant decrease in the variance of keratin immunofluorescence in mCherry open-2B2 expressing cells compared to controls (**Fig. 6.9F**).

\

6.7 Constitutively active open-2B2 disrupts keratin filaments in HEK293T cells

Similar to MDCK cells, HEK293T cells contain an extensive cytoplasmic network of keratins. Here, HEK293T cells were transfected with either mCherry PA-2B2 or mCherry open-2B2 and the keratin disruption was observed by immunofluorescence. Like MDCK cells, HEK293T cells transfected with PA-2B2 and maintained in the dark exhibited normal spindly keratin networks typical for this cell line (compare untransfected mCherry- cells to transfected mCherry+ cells, Fig. 6.10A). Nuclei in these cells were similarly normal and oval in shape. In contrast, mCherry open-2B2 expressing cells show perinuclear aggregate formation (**Fig. 6.10E**) and abnormal lobular nuclear morphology (**Fig. 6.10G**).

6.8 Expression of open-2B2 binds to and disrupts keratin filaments in embryonic *Xenopus* cells

Previously, I show that open-2B2 can disrupt keratin filaments in MDCK and HEK293T cells and similar work has used 2B2 peptide to disrupt vimentin in fibroblasts (Helfand et al., 2011). However, no studies to date have used the 2B2 inhibitory peptides to disrupt intermediate filaments *in vivo* in whole organisms. To evaluate the ability of mCherry open-2B2 to interfere with keratin network in an animal model, mRNA coding for 2B2 derivatives were coinjected with mRNA coding for eGFP-krt8 or eGFP-krt19 in *Xenopus* ectodermal (animal cap) embryos. Unlike MDCK and HEK293T cells, expression of intermediate filament proteins is limited to K8, K18, and K19 into the early morphogenetic events of gastrulation with vimentin emerging in the ectodermal layers only in late

gastrulation and later stages. The K8/18/19 keratin complement is present in all tissues of the embryo from egg through gastrula. Ectodermal animal cap explants were prepared at gastrulation and keratin intermediate filaments were imaged in live cells of the deep cell layers. Keratin intermediate filament networks were distributed throughout the cell body of ectodermal cells (**Fig. 6.11A**), similar to that previously described in unpolarized mesendoderm cells (Weber *et al.*, 2012). Likewise, coalescence of keratin filaments was seen occasionally near cell-cell contacts. Similar to control cells (**Fig. 6.11A**), explants expressing mCherry PA-2B2 (not activated) (**Fig. 6.11B**) have a normal fully extended keratin filamentous network. In contrast to the control cells, explants expressing mCherry open-2B2 and eGFP-K8 exhibit disruption of keratin filaments with formation of punctate aggregates and shorter filaments.

Comparable analyses were also conducted with ectodermal (animal cap) explants co-expressing 2B2 peptide derivatives and eGFP-K19. The results show similar disruption and formation of aggregates in explants expressing mCherry open-2B2 (**Fig. 6.12B**). In comparison the normal keratin filamentous network extended throughout the cell body in ectodermal cells of control explants (**Fig. 6.12A**) and explants expressing mCherry PA-2B2 (not activated) (**Fig. 6.12C**).

It was noted that cells with high expression of mCherry PA-2B2 show some disruption of keratin filaments even in dark, i.e. without activation of the photoswitch. This may be because these fusion proteins are not covalently docked; they therefore exist in two

populations; the docked and the undocked state, and both confirmations exist during presence and absence of light (Strickland et al., 2010). This introduces a leaky expression of the active PA-2B2 leading to disruption of keratins even in dark. To overcome this issue, the expression levels of the photoactivatable protein needs to be titered. Nonetheless, the current PA-2B2 is sufficient to prevent disruption of keratin filaments in dark and under moderate expression levels.

To confirm the molecular target of our 2B2 constructs when expressed *in vivo*, we immunoprecipitated mCherry open-2B2 from injected *Xenopus* gastrula and looked for enrichment of proteins in mCherry open-2B2 samples (**Fig. 6.13A**). Protein bands were enriched in the molecular weight range of 37-75kD. These bands were isolated and liquid chromatography tandem mass spectroscopy analyses were performed to identify endogenous proteins that were binding to mCherry open-2B2. Keratin 18 isoforms originating from both *X. laevis* alleles predominated in terms of both unique peptides identified, spectral counts, and were identified as the top target proteins of our construct with few other proteins enriched (**Fig. 6.13B**).

Altogether, these data show the capacity of the constitutively active mutant mCherry open-2B2 to specifically disrupt keratin intermediate filaments in multiple cell types and species. Thus, showing the utility of open-2B2 as a versatile keratin filament disrupting tool. In principle, by caging this 2B2 peptide with the photoactivatable LOV-J α module, our developed tool could be light-activated in living cells to disrupt intermediate filaments at

the subcellular spatial scale. The results shown here encourage further development of PA-2B2 as a photoactivatable tool to interrogate keratins in whole organisms.

6.9 Keratin 8 2B2 mimetic peptide is a specific inhibitor of keratin filaments

To examine whether expression of 2B2 specifically affected keratin IFs and not microtubules, microtubules were examined in open-2B2 expressing cells. Ectodermal explants were generated from embryos expressing lit/open state mutant open-2B2 and EMTB-GFP (a reporter for microtubules in live cells). Despite the disruption of keratin network induced by open-2B2 shown in previous results, unperturbed array of microtubules was evident in cells expressing open-2B2 with no obvious cell shape change (**Fig. 6.14**). Thus, due to the specificity to keratin filaments, 2B2 peptides are excellent tools to be used as polymerized keratin filament inhibitors.

Figure 6.1

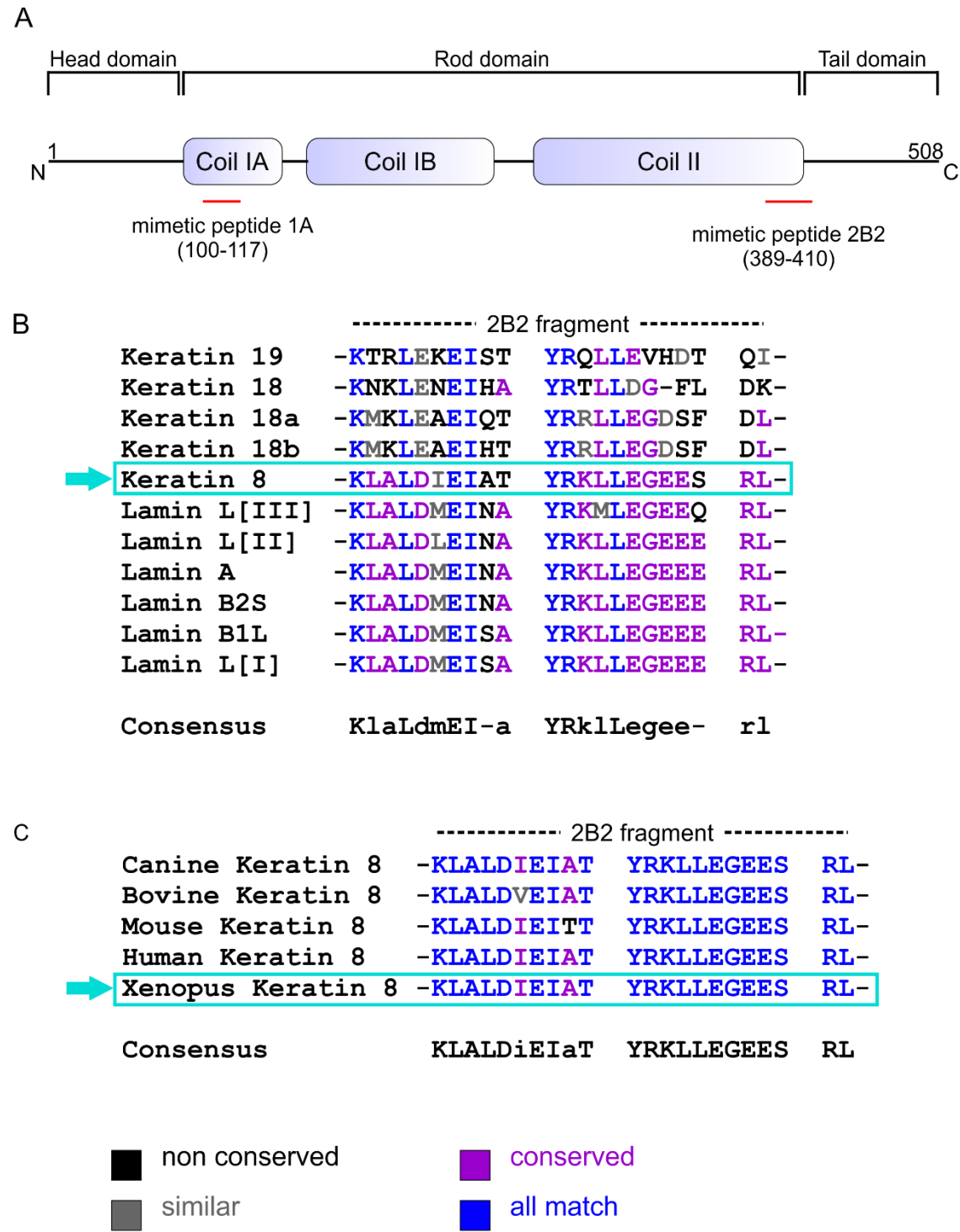


Figure 6.1

D

	----- 1A fragment-----
Keratin 19	-KATMQNLNDR LASYLDKV-
Keratin 18	-QEVMQGLNER LAGYLKRV-
Keratin 18a	-KETMQDLNDR LASYLERV-
Keratin 18b	-KETMQDLNDR LASYLERV-
Lamin L[II]	-KEDLRHLNDR LAAYIERV-
Lamin L[III]	-KEELRHLNDR LAVYIDRV-
Lamin B1L	-KEELRHLNDR LAVYIDRV-
Lamin B2S	-KSDLQELNDR LAVYIDKV-
Lamin L[I]	-KVDLQELNDR LALYIDTV-
Lamin A	-KEDLQGLNDR LAVYIDKV-
→ Keratin 8	-KEQIKTLNKK FASFIDKV-
Consensus	-kedlq-LNdr lA-yidkV-
■ non conserved	■ conserved
■ similar	■ all match

Figure 6.1: Identification of peptides to generate photoactivatable disruptor of keratin filaments.

(A) Schematic representation of primary structure of keratin IF proteins. (B) Sequence alignment of 2B2 segments of *Xenopus laevis* IF proteins including keratin 8, keratin 18/19 and nuclear lamins A, B and L showing that keratin 8 2B2 segment has more homology with the lamins than keratin 18 or keratin 19. (C) Sequence alignment of 2B2 segments of keratin 8 IF proteins. Protein sequence alignment reveals that the 2B2 peptide is highly conserved across different species including *Xenopus*, Canine, Bovine, Mouse and Human. (D) Similar sequence alignment of the 1A segments of *Xenopus laevis* IF proteins including keratin 8, keratin 18/19 and nuclear lamins A, B and L showing that keratin 8 1A segment has subtle differences with other 1A segments.

Figure 6.2

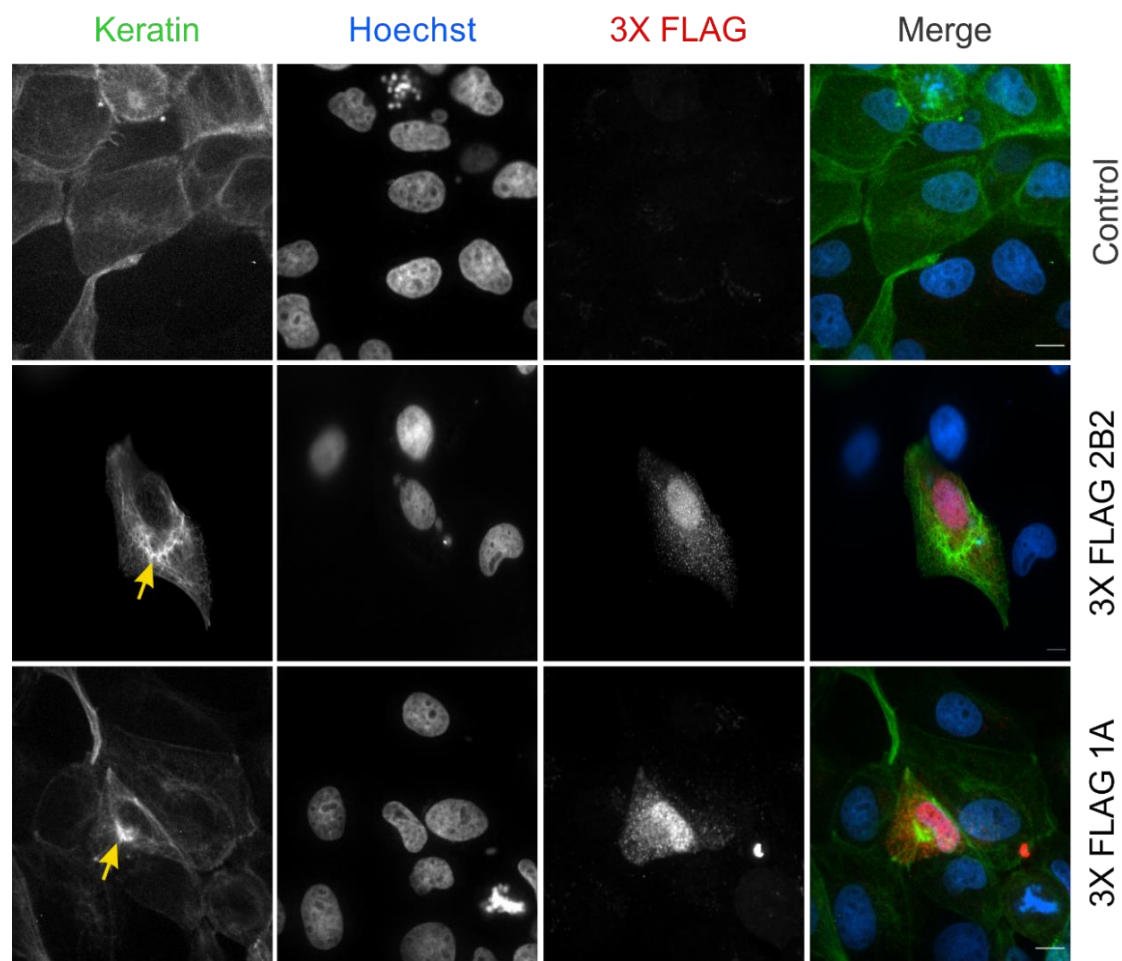


Figure 6.2: Keratin 8 mimetic peptide 2B2 readily promotes keratin network disruption.

Immunofluorescence images of eGFP-K8 MDCK cells expressing 3X-FLAG 2B2 or 3X-FLAG 1A construct, stained with FLAG antibody and counterstained with Hoechst dye depict disruption of the keratin network (**yellow arrows**). Cells were imaged using Zeiss Cell Observer spinning disk confocal microscope (63X/1.4 NA, 1.0X optovar). Panels show representative images of two independent experiments. (Control, n= 46; 3X FLAG2B2, n=70, 3X FLAG1A, n=76).

Bars, 10 μ m

Figure 6.3

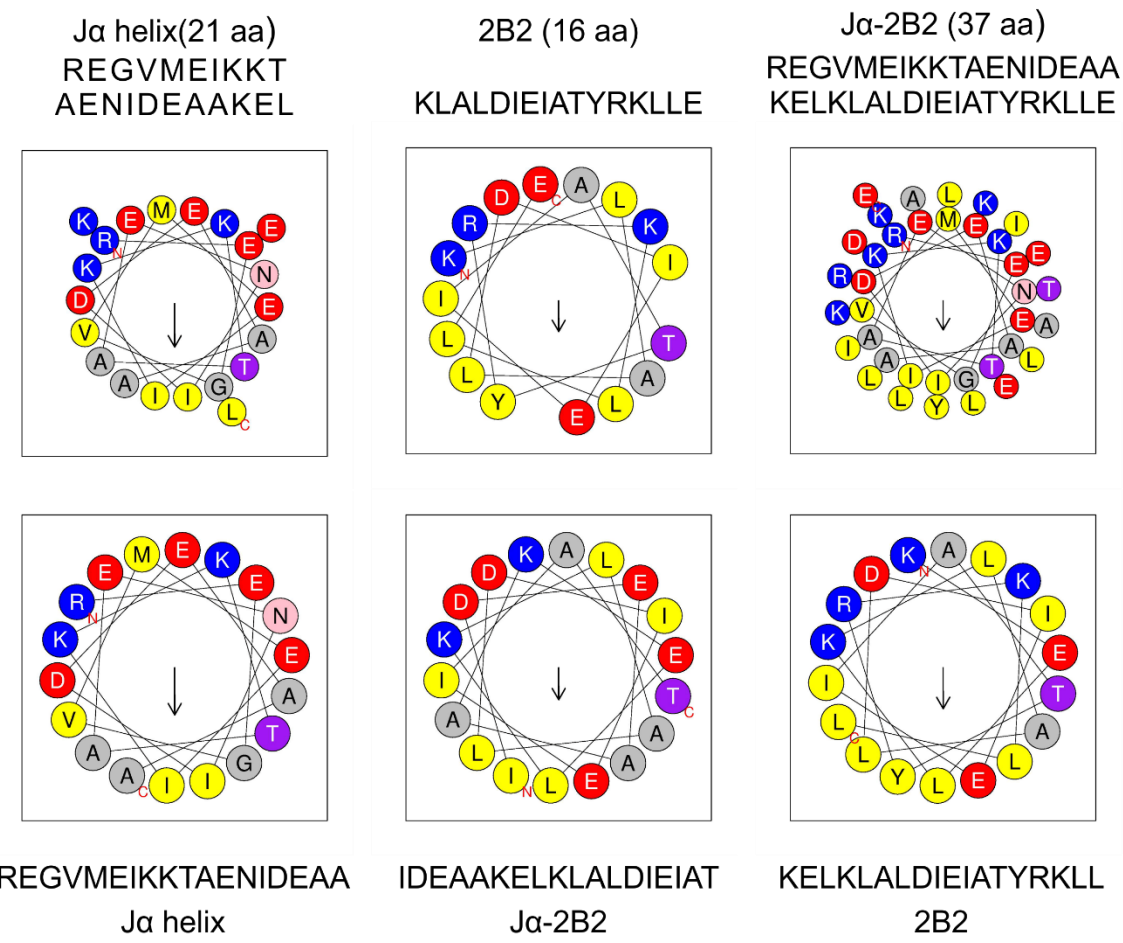
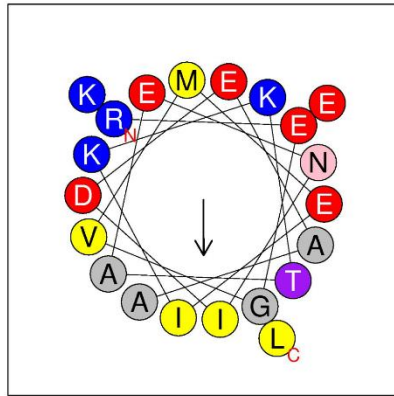


Figure 6.3: Conserved amphipathic pattern in J α -helix facilitates interactions between 2B2 and J α -helix.

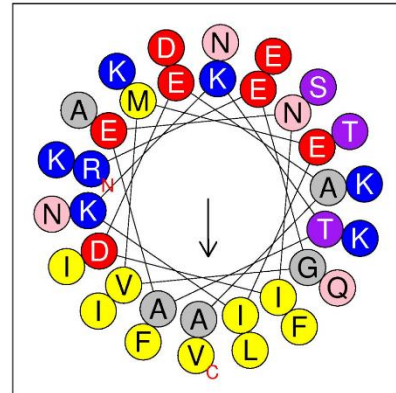
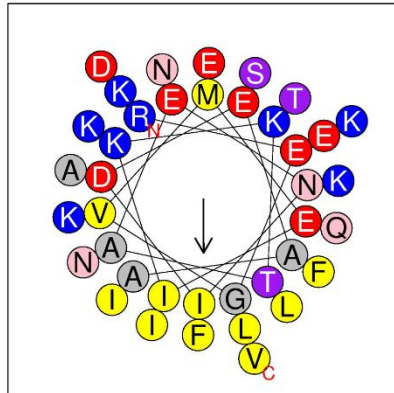
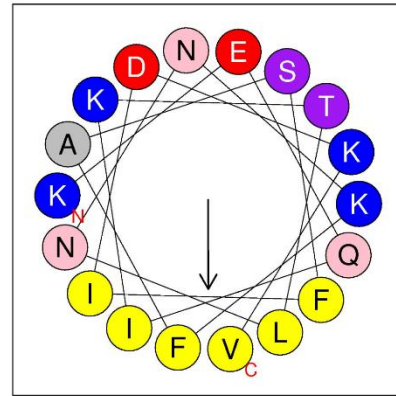
Heliquet software molecular modeling was done to optimize the α -helix formation for J α -2B2. Helical wheel projection of J α -helix, 2B2 and 2B2 appended to J α -helix are shown here.

Figure 6.4

J α (21 aa)
REGVMEIKKTAENIDEAAKEL



1A (18 aa)
KEQIKTLNKNKFASFIDKV



REGVMEIKKTAENIDEAAKELKEQIKTLNKNKFASFIDKV REGVMEIKKTAENIDEAAKELKEQIKTLNKNKFASFIDKV
J α -1A (39 aa) J α -1A (36 aa)

Figure 6.4 Conserved amphipathic pattern in J α -helix facilitates interactions between 1A and J α -helix.

Heliquet software molecular modeling was done to optimize the α -helix formation for J α -1A. Helical wheel projection of J α -helix, 1A and 1A appended to J α -helix are shown here. Highlighted sequence indicates the modification done to embed 1A helical peptide into J α -helix.

Figure 6.5

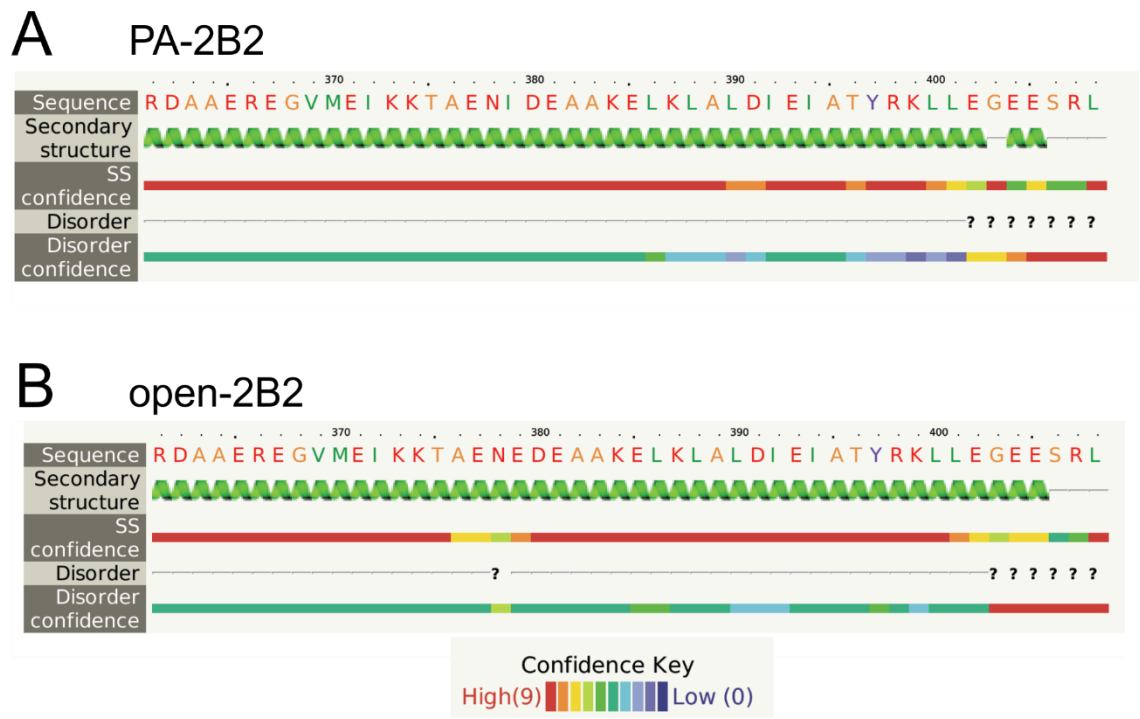
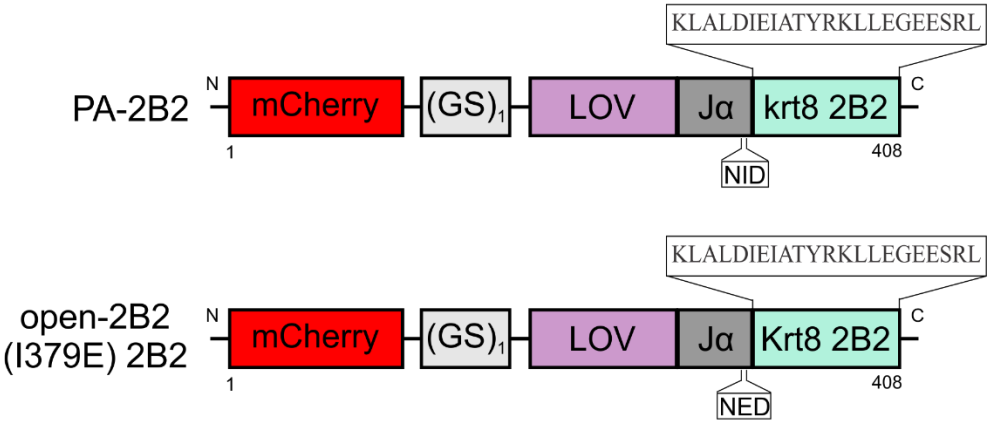


Figure 6.5: Secondary structure shows continuous α -helical domain.

Fusion of J α to 2B2 retains the α -helical structure in both PA-2B2 (**A**) and open-2B2 (**B**).

Figure 6.6

A



B

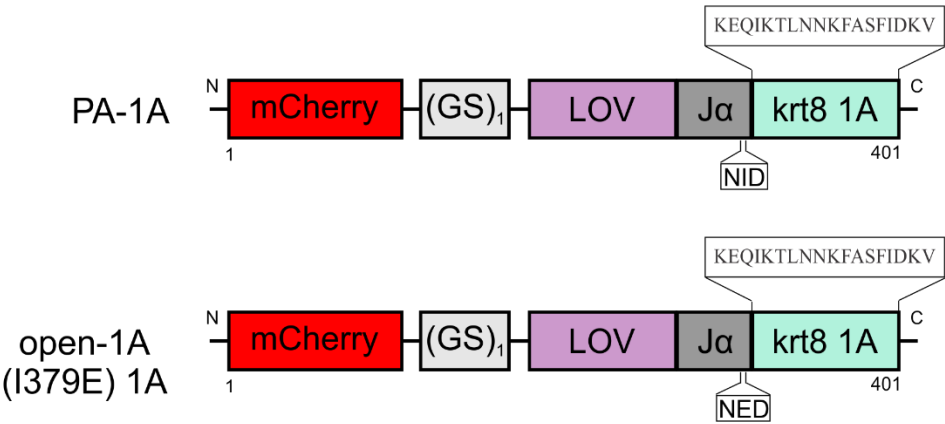


Figure 6.6: Design of 2B2 and 1A peptide photoswitches.

(A) Schematic representation of 2B2 modules. The 2B2 modules comprise a mCherry fluorophore to gauge the expression levels, which is connected to the LOV-J α photosensitive domain by a GS linker, and a krt8 2B2 (22aa) peptide which is directly appended to J α . The open-2B2 has a point mutation in the J α domain as illustrated by NED. (B) Schematic representation of 1A modules. The 1A modules comprise a mCherry fluorophore to gauge the expression levels, which is connected to the LOV-J α photosensitive domain by a GS linker, and a krt8 1A (18aa) peptide directly tethered to J α . The open-2B2 has a point mutation in the J α domain as illustrated by NED.

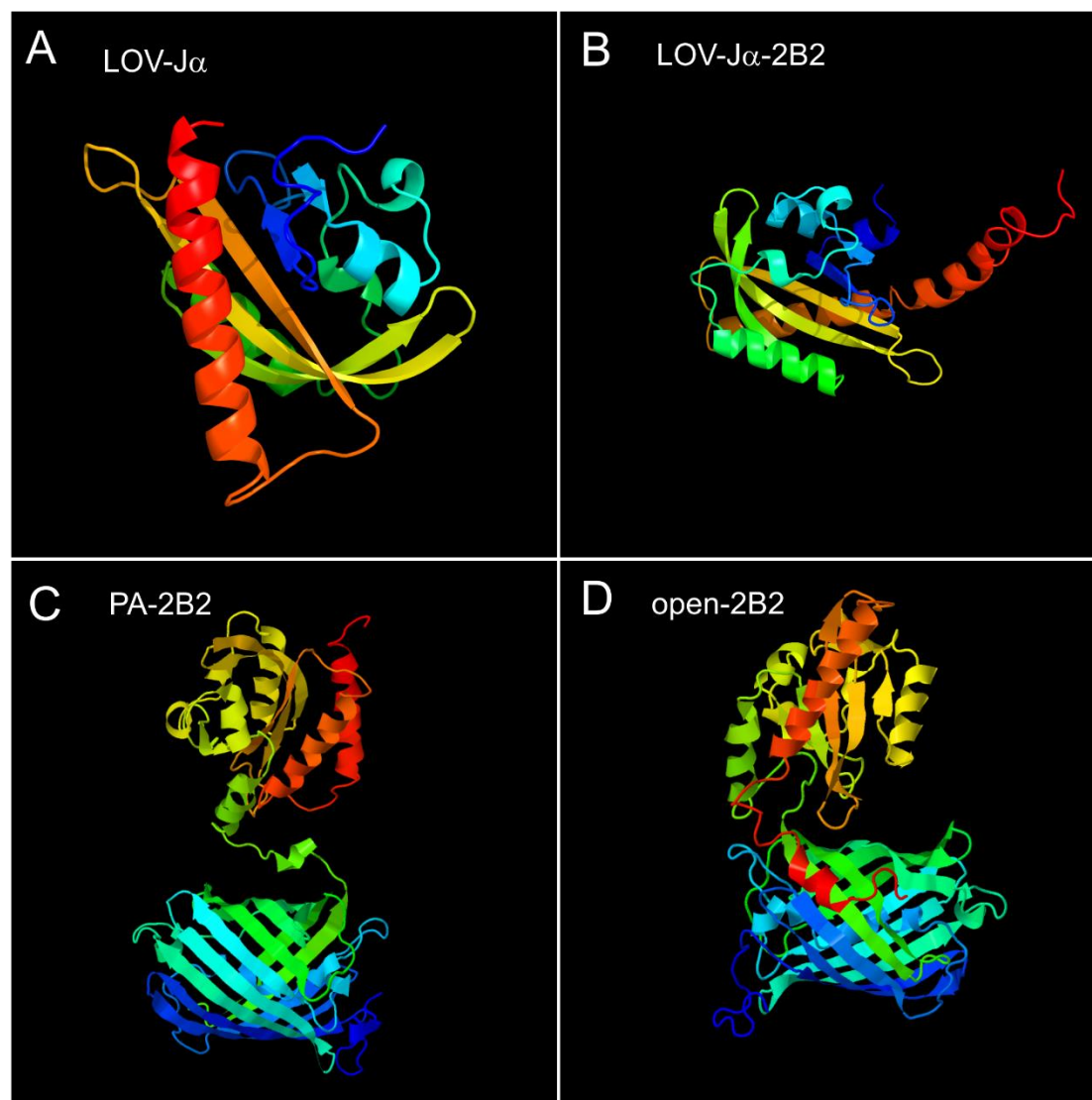
Figure 6.7

Figure 6.7: Structural modelling shows a nearly contiguous α -helical domain.

In both LOV-J α (**A**) and LOV-J α -2B2 (**B**) the 3D structural analysis shows a continuous helical structure of J α and also of J α -2B2. However, in PA-2B2 (mCherry LOV-J α -2B2) (**C**), and open-2B2 (mCherry LOV-J α (I379E)2B2) (**D**) the addition of mCherry generates a loop and turn in J α -2B2. The presence of mutation I379E in (D) induces a steric hindrance of the LOV-J α interaction not allowing the protein to fold properly. The protein is color coded from N-terminal (blue) to C-terminal (red).

Figure 6.8**A**

2B2- KLALDIEIATYRKLLEGEESRL (22 aa)

1A- KEQIKTLNNKFASFIDKV (18 aa)

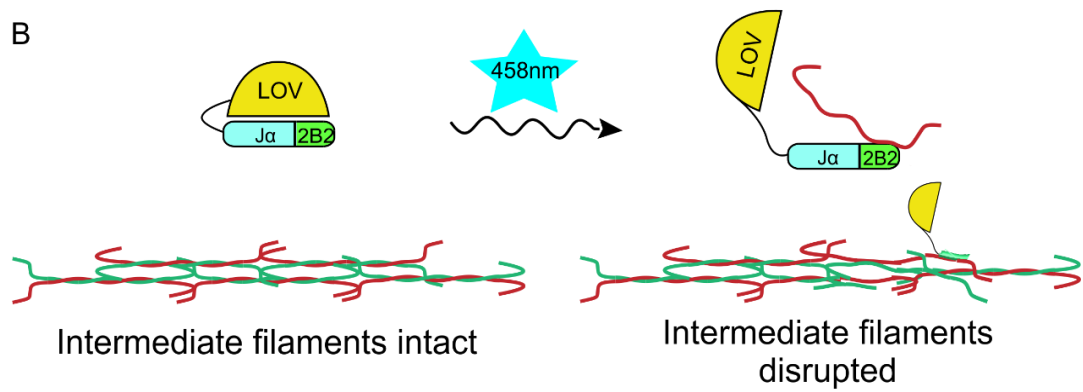
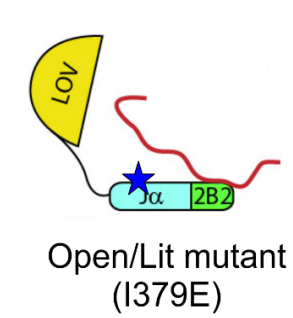
B**C**

Figure 6.8: Strategy for mechanism of action.

(A) Sequence of the *Xenopus laevis* mimetic peptide 2B2 and 1A. (B) Strategy for caging 2B2 or 1A mimetic peptides and mechanism for keratin network disruption. In principle, upon irradiation with 458 nm light the LOV-J α should uncouple and the 2B2 peptide should be available to bind to its dimerization partners keratin 18 and 19 and thus disrupt the keratin filaments. (C) Design of light insensitive mutant open-2B2

Figure 6.9

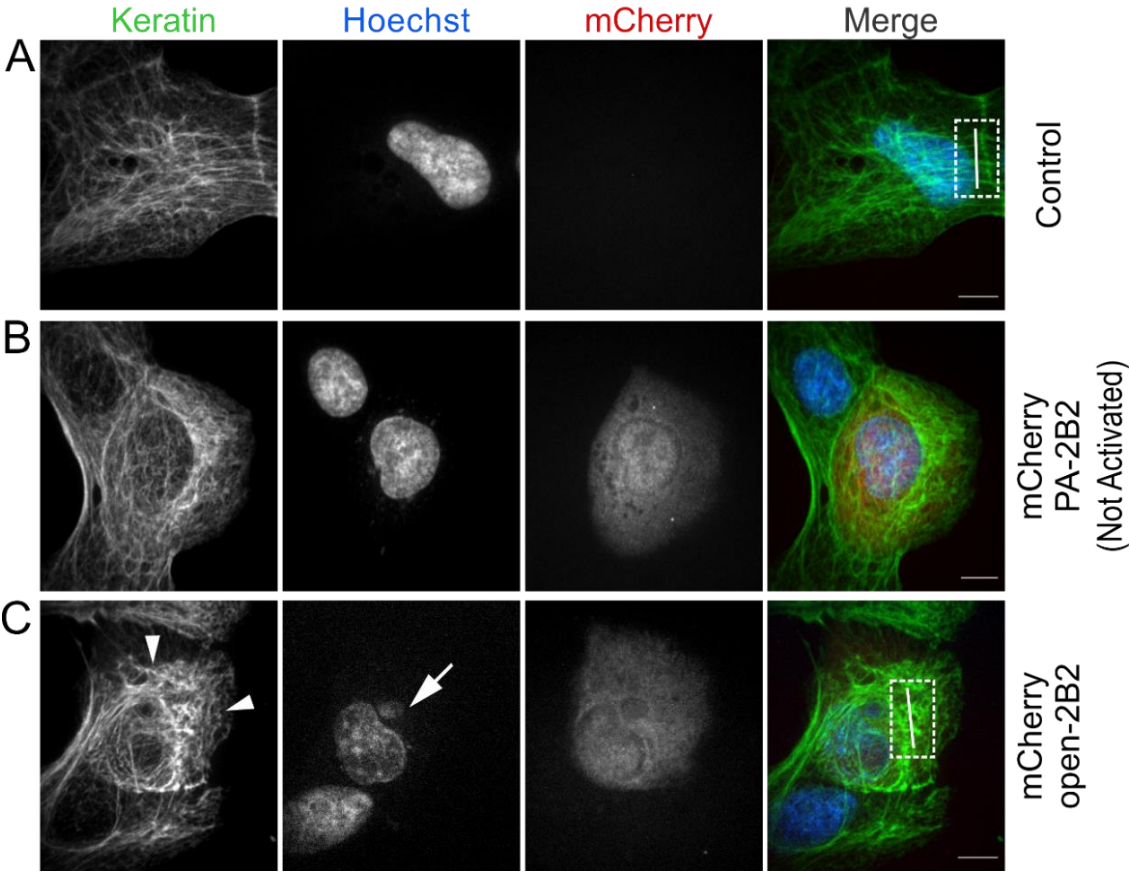


Figure 6.9

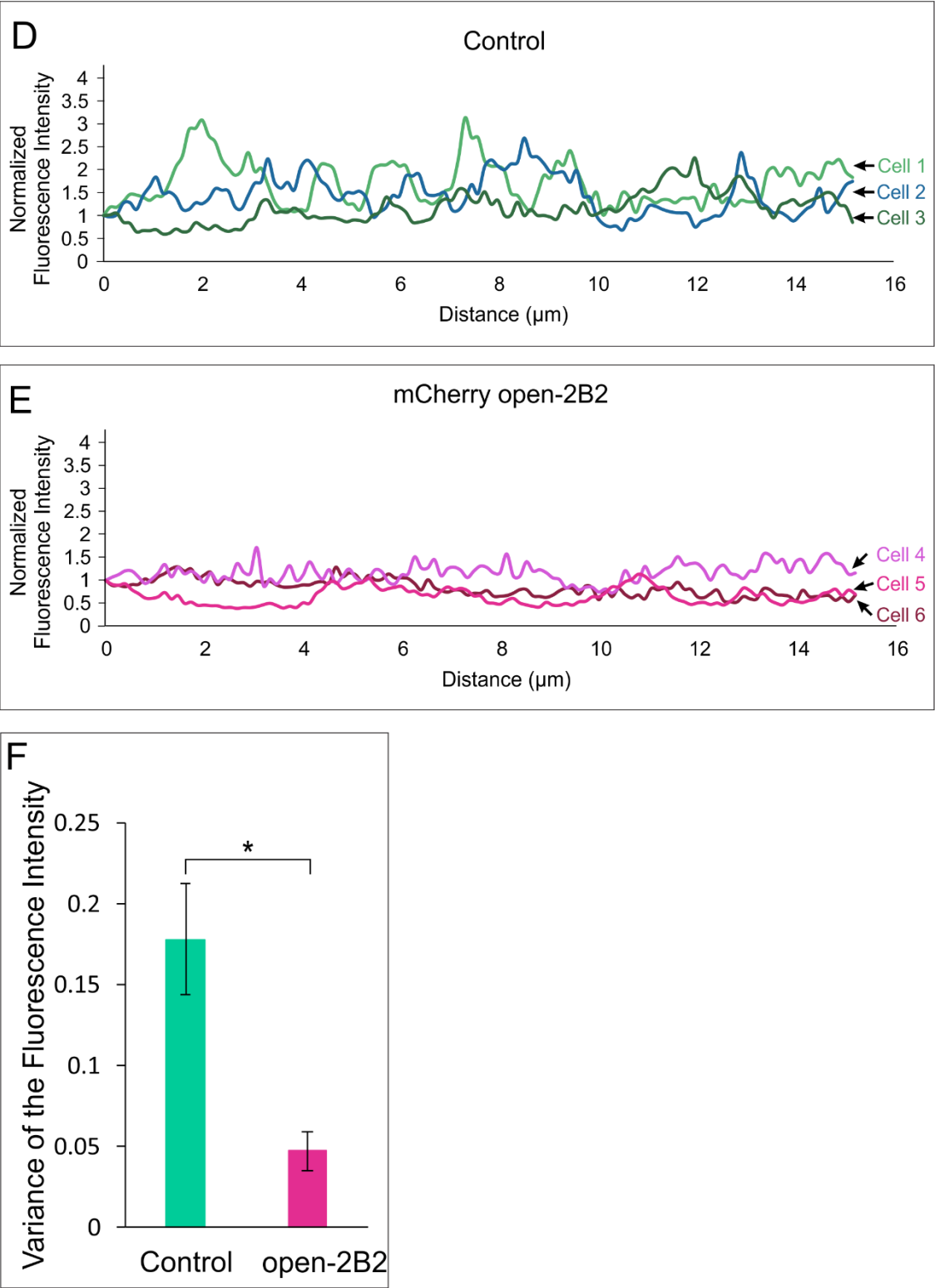


Figure 6.9: Constitutively active open-2B2 disrupts keratin filaments in MDCK cells.

MDCK cells were either mock transfected (control) (**A**) or transfected with mCherry PA-2B2 (**B**), mCherry open-2B2 (**C**), 12 hrs post transfection. Confocal images (maximum intensity projections of 0.28 μm thick optical sections) of cells immunostained with pan-keratin antibody and counterstained with Hoechst dye display keratin network (green) organization and expression of 2B2 modules (red) and nucleus (blue). Images were taken using Zeiss Cell Observer spinning disk confocal microscope (63X/1.4 NA, 1.6X optovar). **Arrowheads** show disruption of keratin filaments and **arrows** show aberrant nuclear morphology. **Yellow bar line** in merged image indicates example region of line scans shown in graphs in (**D**) and (**E**). Distinct filaments are seen in control line scans as evidenced by periodic intensity fluctuations (**D**), whereas keratin filaments in mCherry open-2B2 transfected cells are more aggregated and/or less distinct as shown by less varied intensity fluctuations (**E**). Variance of the fluorescence intensity between line scans of control and mCherry open-2B2 expressing cells. Graph represents mean \pm S.E.M., results from unpaired student's t-test are indicated (**F**). Panels show representative images of three independent experiments.

Bars, 10 μm

Figure 6.10

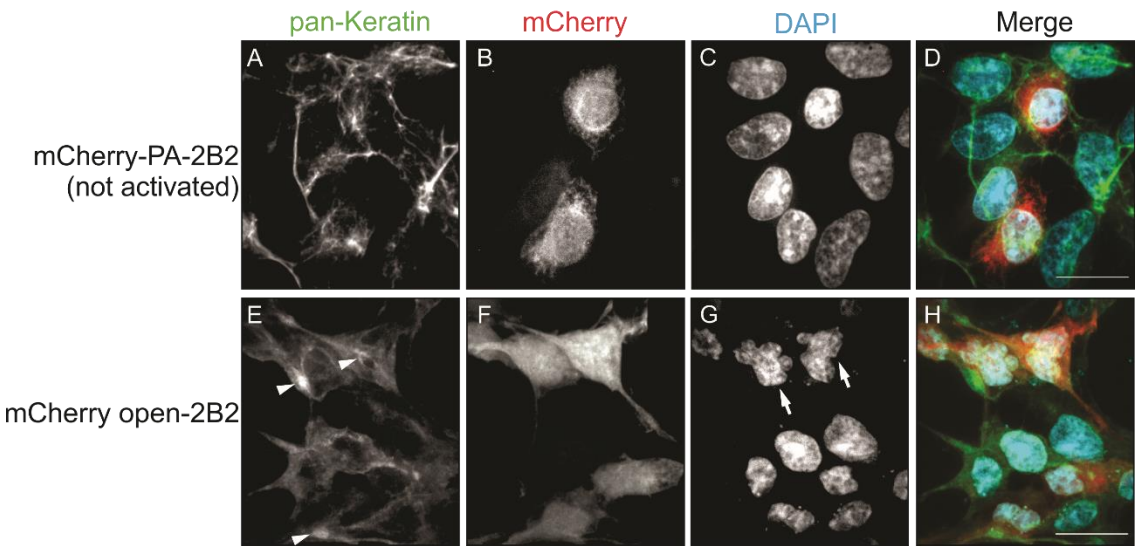


Figure 6.10: Constitutively active open-2B2 disrupts keratin filaments in HEK293T cells

The keratin network was examined in HEK293T cells transfected with either mCherry PA-2B2 (**A-D**) or mCherry open-2B2 (**E-H**), 24 hrs post-transfection. Cells were immunostained with pan-keratin antibody and counterstained with DAPI dye. **White arrowheads** show disruption of keratin filaments and **white arrows** show aberrant nuclear morphology.

Bars, 20 μm .

Note: Figure prepared by Jiyeon Baek.

Figure 6.11

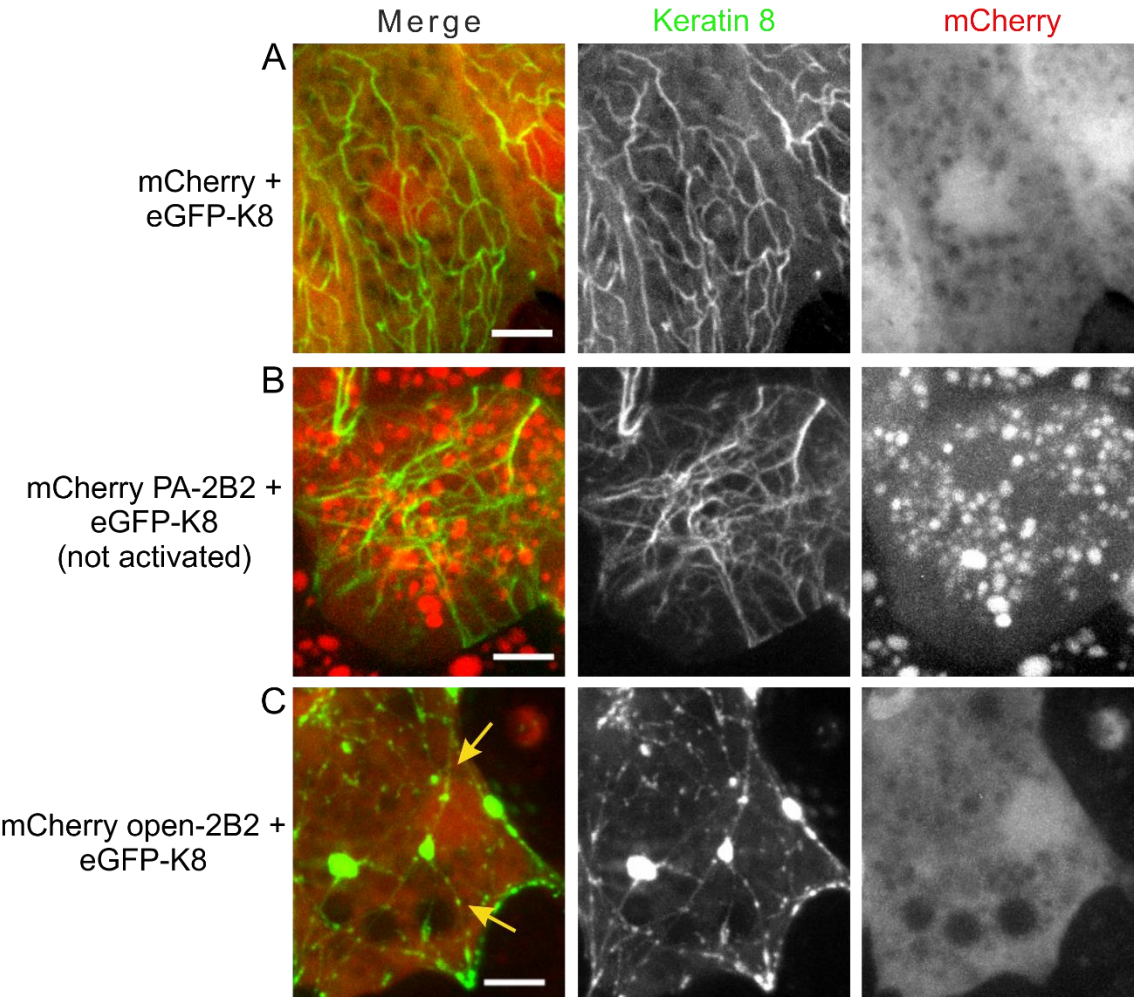


Figure 6.11: Constitutively active open-2B2 disrupts keratin filaments in *Xenopus* ectodermal cells.

Xenopus embryos co-injected with eGFP-krt8 and either mCherry or mCherry PA-2B2 or mCherry open-2B2 plasmid DNA targeting the presumptive ectoderm were allowed to develop until stage 10.5-11. Next ectodermal explants were isolated and plated on fibronectin-coated glass-bottom dishes. Cells expressing eGFP-K8 (green) and either control or 2B2 modules (red) were imaged using Zeiss Cell Observer spinning disk confocal microscope (63X/1.4 NA, 1.0X optovar). Maximum intensity projections from serial confocal sections of 0.28 μm collected from the top to the bottom of the cells are shown. Representative confocal images of *Xenopus* progenitor ectodermal explants (stage 11) expressing eGFP-K8 and either mCherry (**A**), mCherry PA-2B2 (**B**), mCherry open-2B2 (**C**). In contrast to the control and PA-2B2 expressing cells which show a widespread keratin network, cells expressing open-2b2 exhibit disrupted keratin network. **Arrows** show the formation of punctate aggregates in cells. (mCherry N= 6, n=12; mCherry PA-2B2 N=10, n= 28, mCherry open-2B2, N=8, n= 18). Bars, 10 μm .

Figure 6.12

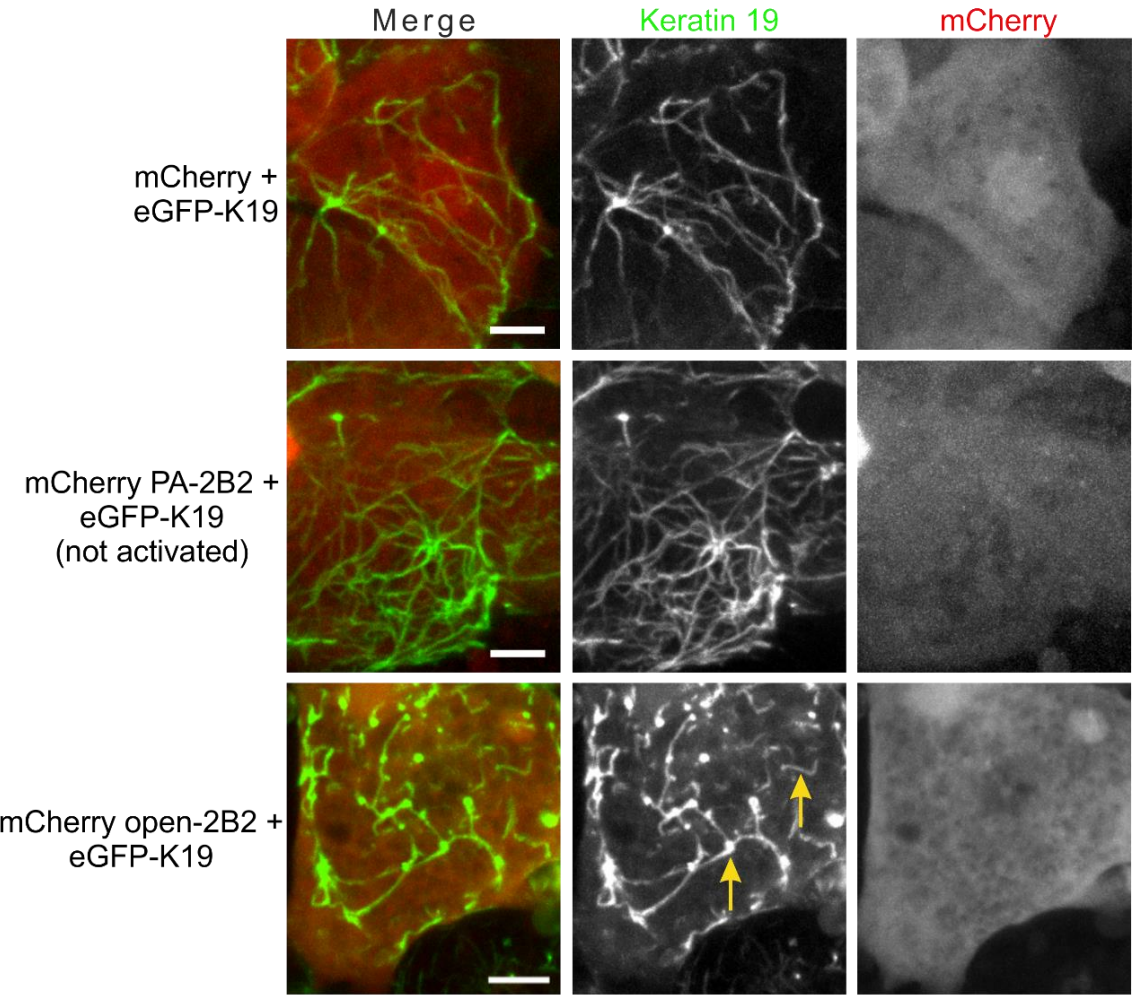


Figure 6.12: Constitutively active open-2B2 disrupts keratin 19 filaments in *Xenopus* ectodermal cells.

Xenopus embryos co-injected with eGFP-krt19 and either mCherry or mCherry PA-2B2 or mCherry open-2B2 targeting the presumptive ectoderm were allowed to develop until stage 10.5-11. Following, ectodermal explants were isolated and plated on fibronectin-coated glass-bottom dishes. Cells expressing eGFP-K19 (green) and either control or 2B2 modules (red) were imaged using Zeiss Cell Observer spinning disk confocal microscope (63X/1.4 NA, 1.0X optovar). Maximum intensity projections from serial confocal sections of 0.28 μm collected from the top to the bottom of the cells are shown. Representative confocal images of *Xenopus* progenitor ectodermal explants (stage 11) expressing eGFP-krt19 and mCherry (**A**), mCherry PA-2B2 (**B**) and mCherry open-2B2 (**C**). **Arrows** indicate the disruption of keratin filaments in cells. Images are representative of at least four independent experiments (mCherry N= 4, n=7; mCherry PA-2B2 N=6, n= 15).

Bars, 10 μm .

Figure 6.13

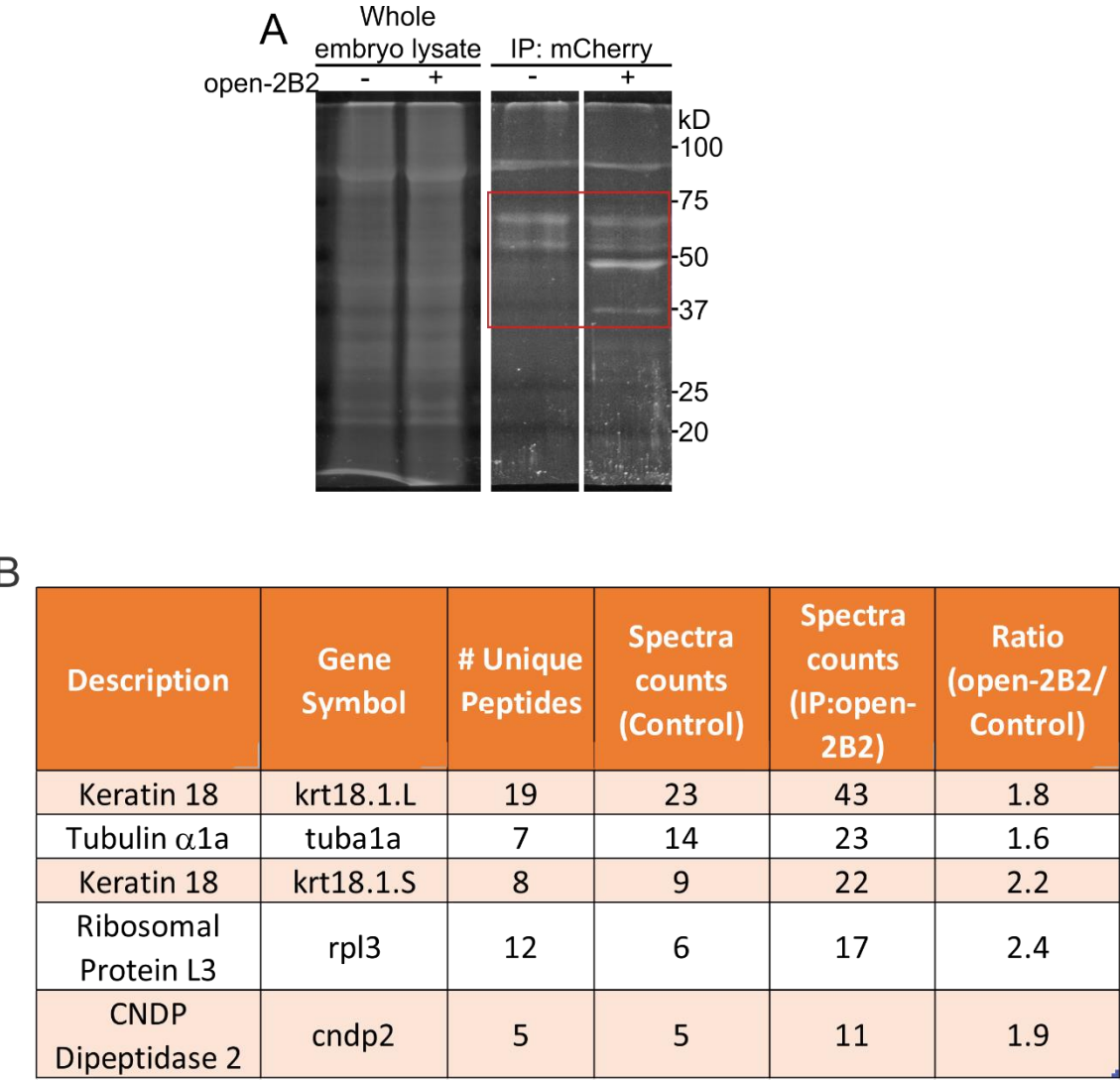


Figure 6.13: Keratin 8 2B2 mimetic peptide target keratin 18 to induce disruption of filaments.

Xenopus embryos were microinjected with mCherry open-2B2 (500 pg) mRNA at one cell stage in the animal hemisphere. **(A)** Lysates from embryos in gastrula stage were subjected to immunoprecipitation to isolate mCherry open-2B2 complexes and separated by SDS-PAGE. Protein bands within the region outlined by the red box were excised, in-gel trypsinized and analyzed by LC-MS/MS. **(B)** Table summary of abundant proteins detected in LC-MS/MS samples.

Figure 6.14

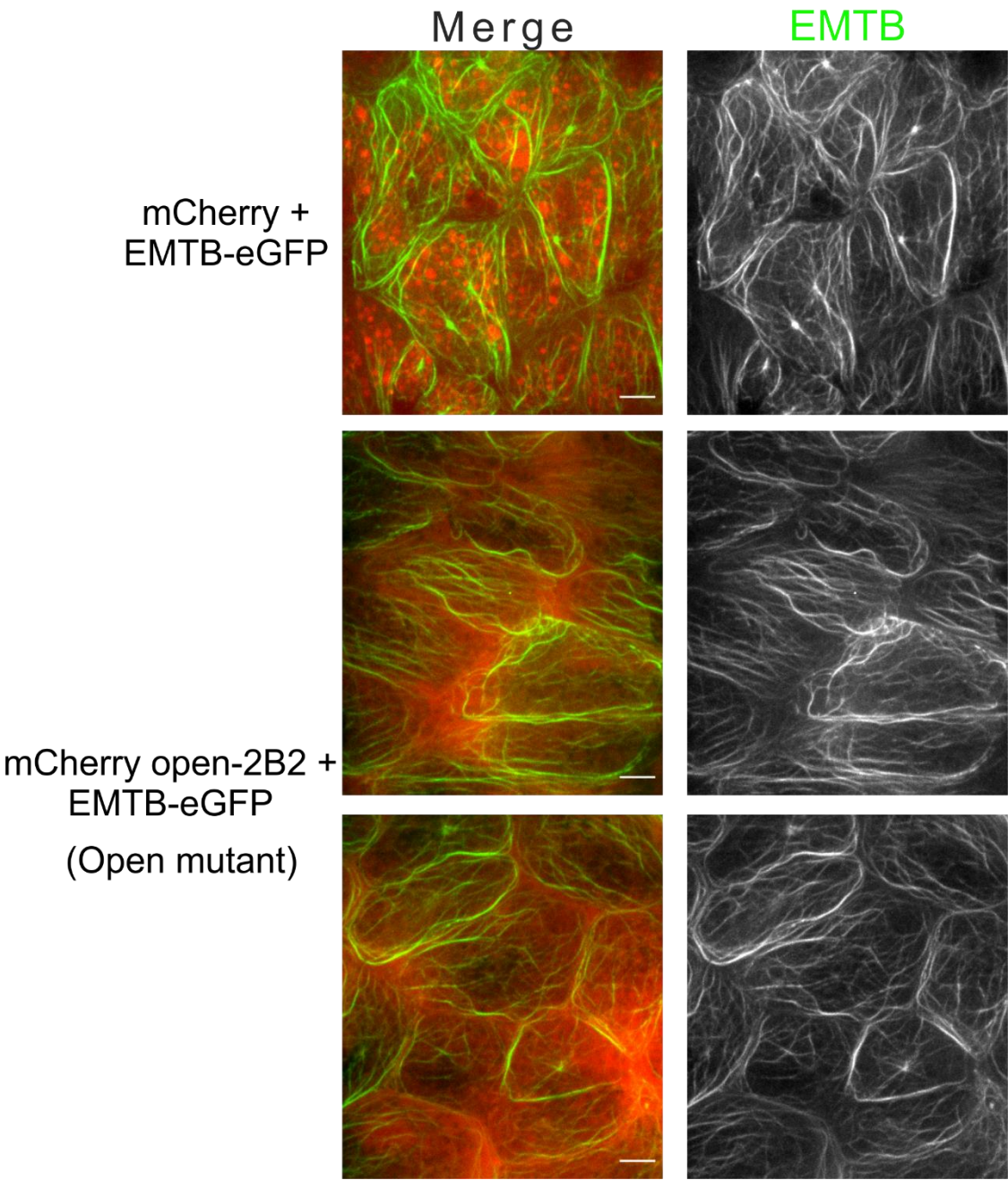


Figure 6.14: Keratin 8 2B2 mimetic peptides are specific inhibitors to keratin filaments.

Xenopus embryos co-injected with EMTB-eGFP and either mCherry or mCherry open-2B2 RNA targeting the presumptive ectoderm were allowed to develop until stage 10.5-11. Next, ectodermal explants were prepared and plated on fibronectin-coated glass-bottom dishes. Cells expressing EMTB-eGFP (green) and either control or open-2B2 (red) were imaged using Zeiss Cell Observer spinning disk confocal microscope (63X/1.4 NA, 1.0X optovar). Maximum intensity projections from serial confocal sections of 0.26 μm collected from the top to the bottom of the cells are shown. In comparison to controls, confocal images of *Xenopus* progenitor ectodermal explants (stage 11) microinjected with EMTB-eGFP and mCherry open-2B2 do not show any obvious alterations in the microtubule network. Images are representative of at least three independent experiments.

Bars, 10 μm .

Table 6.1: Protein Sequences for keratin 8 2B2 mimetic analogues

Construct	Sequences
3X FLAG-2B2	MDYKDDDDKDYKDDDDKDYKDDDDKGSLLALDIEIATY RKLLERGEESRL
mCherry- LOV-Jα-2B2 (mCherry PA-2B2)	MVSKGEEDNMAIIKEFMRFKVHMEGSVNGHEFEIEGEGEG RPYEGTQTAKLKVTKGGPLPFAWDILSPQFMYGSKAYVKH PADIPDYLKLSFPEGFKWERVMNFEDGGVVTVTQDSSLQD GEFIYKVKLRGTNFPDGPVMQKKTMGWEASSERMYPED GALKGEIKQRLKLDGGHYDAEVKTTYKAKKPVQLPGAY NVNIKLDITSHNEDYTIVEQYERAEGRHSTGGMDELYKSGSL RSGSLATTLERIEKNFVITDPRLPDNPIIFASDSFLQLTEYSRE EILGRNCRFLQGPETDRATVRKIRDAIDNQTEVTVQLINYT KSGKKFWNLFHLQPMRDQKGDVQYFIGVQKDGTEHVRDA AEREGVMEIKKTAENIDEAAKELLLALDIEIATYRKLLERGE ESRL
mCherry- LOV-Jα- (I379E)2B2	MVSKGEEDNMAIIKEFMRFKVHMEGSVNGHEFEIEGEGEG RPYEGTQTAKLKVTKGGPLPFAWDILSPQFMYGSKAYVKH PADIPDYLKLSFPEGFKWERVMNFEDGGVVTVTQDSSLQD GEFIYKVKLRGTNFPDGPVMQKKTMGWEASSERMYPED GALKGEIKQRLKLDGGHYDAEVKTTYKAKKPVQLPGAY

(mCherry open-2B2)	<div>NVNIKLDITSHNEDYTIVEQYERAEGRHSTGGMDELYK</div> <div>SGL</div> <div>RSGS</div> <div>LATTLERIEKNFVITDPRLPDNPIIFASDSFLQLTEYSRE</div> <div>EILGRNCRFLQGPETDRATVRKIRDAIDNQTEVTVQLINYT</div> <div>KSGKKFWNLFHLQPMRDQKGDVQYFIGVQKDGTEHVRDA</div> <div>AEREGVMEIKKTAENE</div> <div>DEAAKELKLALDIEIATYRKLLEGE</div> <div>ESRL</div>
-------------------------------	---

Table 6.2: Protein Sequences for keratin 8 1A mimetic analogues

Construct	Sequence
3X FLAG-1A	MDYKDDDDKDYKDDDDKDYKDDDDKGSLEQIKTLNNK FASFIDKV
mCherry- LOV-Jα-1A (mCherry PA-1A)	MVSKGEEDNMAIIKEFMRFKVHMEGSVNGHEFEIEGEGEG RPYEGTQTAKLKVTKGGPLPFAWDILSPQFMYGSKAYVKH PADIPDYLKLSFPEGFKWERVMNFEDGGVVTVTQDSSLQD GEFIYKVKLRGTNFPDGPVMQKKTMGWEASSERMYPED GALKGEIKQRLKLKDGGHYDAEVKTTYKAKKPVQLPGAY NVNIKLDITSHNEDYTIVEQYERAEGRHSTGGMDELYKSGL RSGSLATTLERIEKNFVITDPRLPDNPIIFASDSFLQLTEYSRE EILGRNCRFLQGPETDRATVRKIRDAIDNQTEVTVQLINYT KSGKKFWNLFHLQPMRDQKGDVQYFIGVQKDGTEHVRDA AEREGVMEIKKTAENIDEAAEQIKTLNNKFASFIDKV
mCherry- LOV-Jα- (I379E)1A (mCherry open-1A)	MVSKGEEDNMAIIKEFMRFKVHMEGSVNGHEFEIEGEGEG RPYEGTQTAKLKVTKGGPLPFAWDILSPQFMYGSKAYVKH PADIPDYLKLSFPEGFKWERVMNFEDGGVVTVTQDSSLQD GEFIYKVKLRGTNFPDGPVMQKKTMGWEASSERMYPED GALKGEIKQRLKLKDGGHYDAEVKTTYKAKKPVQLPGAY NVNIKLDITSHNEDYTIVEQYERAEGRHSTGGMDELYKSGL

	RSGSLATTLERIEKNFVITDPRLPDNPIIFASDSFLQLTEYSRE EILGRNCRFLQGPETDRATVRKIRDAIDNQTEVTVQLINYT KSGKKFWNLFHLQPMRDQKGDVQYFIGVQKDGTEHVRDA AEREGVMEIKKTAENEDEAAKEQIKTLNNKFASFIDKV
--	--

Discussion

This study documents the generation of PA-2B2 and open-2B2 genetically encoded molecular tools. The effective disruption of keratin filamentous network in living cells by 2B2 peptide, makes 2B2 an excellent inhibitory peptide. I show that the K8 mimetic 2B2 can be efficiently embedded in the LOV-J α helix so that their affinity to effector proteins can be lowered in the dark but enhanced upon photoirradiation. Therefore, these genetically encoded 2B2 modules were further developed as photoactivatable tools in order to study functional role of keratin filaments in living cells (chapter 8). Simultaneously, the PA-1A and open-1A were also generated, however their functionality was not validated. Based on previous studies (Steinert et al., 1993b; Goldman et al., 1996), the 1A peptide is also a promising candidate to disrupt keratin filaments. Therefore, these genetically encoded modules should be developed as functional photoactivatable tools for future applications to determine the role of filamentous keratin networks.

The krt8 mimetic peptide used in this study has sequence similar in length to synthetic 2B2 peptides previously used in *in vitro* studies to interfere with both keratin intermediate filament assembly and disrupt pre-assembled filaments (Hatzfeld and Weber, 1992). Similarly vimentin 2B2 peptide, *in vitro* (Strelkov et al., 2002) and *in vivo*, disrupts assembled intermediate filaments to smaller structures such as unit length filaments (Helfand et al., 2011). Unlike this previous *in vivo* study where disruption of intermediate filaments is achieved by microinjecting the inhibitory peptides directly in cells under study

and damaging their cell membrane, here the disruption of the keratin filaments is achieved by a least invasive method. In this study we primarily see disruption of keratin filaments to more nonfilamentous substructures by the pseudo lit state mutant open-2B2 in multiple species and cell types. The specificity of these effects on keratin filamentous network is further supported by the *in vivo* analysis where the microtubule network is unaffected in the presence of open-2B2. The details of keratin filament perturbation and nature of the effects on polymerization remain to be determined. Presumably, the tools developed here exploit dualistic approach to target disruption of keratin filamentous network. One possibility being, open-2B2 in its open configuration can bind to the keratin precursors and thus prevent filament assembly while forming protein aggregates. Second possibility could be that 2B2 fragments in their “active state” interfere with the proper dimer-dimer interactions within the filaments, thus compromising the polymerized IFs and thereby causing destabilization and disruption of the IFs. Thus, the disruption of the keratin filaments observed here could be the result of usage of either or both mode of actions by the mimetic peptides. Further experiments such as *in vitro* keratin filament disassembly in the presence of the 2B2 peptide and electron microscopy analysis would be more beneficial to establish the nature of perturbation and the effects of such inhibitory peptide on filament assembly. Nonetheless, this study is the first report wherein the keratin filamentous network is acutely targeted *in vivo* using the *Xenopus* K8 2B2 peptide.

Intriguingly, cells expressing open-2B2 also displayed aberrant nuclear phenotypes. Considering that the nuclear lamins possess 2B2 motif that is homologous with the keratin

8 (**Fig. 6.1**), possibly the 2B2 modules are transported to the nucleus driven by their affinity for the nuclear lamins. Thus, insinuating possible lamin disruption in cells transfected with 2B2 peptide modules. This nuclear morphology may have resulted from either direct perturbation of nuclear lamins or, more likely, indirect effects on the nucleus that resulted as a consequence of keratin disruption in the cytoplasm. Given the highly conserved sequence homology, we expect that 2B2 constructs may also disrupt multiple intermediate filament networks. In the LC-MS/MS analyses, vimentin and nuclear lamins were associated with open-2B2; however, they were found at a much lesser extent and did not meet our stringent proteomics criteria. While it is difficult to determine that the effects of 2B2 are due exclusively to disruption of the keratin network, this possible affinity of 2B2 to multiple intermediate filament proteins suggests that the tool may broadly be used to disrupt intermediate filament networks. In this respect, 2B2 constructs are among a very limited set of tools that can be used for the interrogation of intermediate filaments (Zwenger *et al.*, 2015; Ridge *et al.*, 2016). Nonetheless, K18 appeared to be the primary target for our 2B2 constructs in the early *Xenopus* embryo. Interestingly, did not find K19 particularly enriched in open-2B2 expressing samples even though other recent work from our laboratory indicates an important role for 14-3-3 binding to K19 for intermediate filament recruitment to cell-cell adhesions (Mariani *et al.*, 2018). Conversely, in that study, we did not find K18 associated with 14-3-3. It is not yet clear why K19 was not associated with 2B2 constructs but tentatively speculate that the association of 14-3-3 with K19 and/or subcellular compartmentalization may diminish 2B2-K19 interaction. Even though the complete details of the keratin filamentous network disruption are yet to be understood, based on the LC-MS analysis open-2B2 targets K18. We observed that open-2B2 disrupts

K8/K19 filaments as a proxy of the keratin filaments more broadly. This permitted observation of the keratin network without altering the expression of the main keratin target of open-2B2, K18. The disruption of the keratin network we observed (Fig 6.12) is likely an indirect effect of open-2B2 binding to K18.

The mCherry open-2B2 can be used as a “constitutively active” tool to specifically disrupt keratin filaments and thus examine the structure and function of keratin filamentous network in a variety of processes. On the other hand, mCherry PA-2B2 can be further developed as a photoactivatable tool to disrupt keratin filaments with spatio-temporal specificity and thus investigate the function of keratin filaments at a subcellular localization and specific processes. In these ways, both these tools can be useful to interrogate the functional role of keratin filaments without altering the expression levels of endogenous IFs or introducing mutations in them.

Chapter 7

Targeted Disruption of Keratin Filaments in the Progenitor Ectodermal Tissue Alters Keratin Network Organization and Induces Major Defects During *Xenopus* Early Development

This chapter is, in part, adapted from manuscript:

Sanghvi-Shah, R., Paranjpe, S., Baek, J., Dobrowolski, R., and Weber, G. (2018).
A novel photoactivatable tool for intermediate filament disruption indicates a role for
keratin filaments in early embryogenesis. *bioRxiv*. doi:10.1101/484246.

(PA-2B2 and PA-dIF are equivalent names for mCherry-LOV-J α -2B2,
open-2B2 and CA-dIF are equivalent names for mCherry-LOV-J α -(I379E)2B2)

Abstract

To specifically examine the role of keratin filaments in early embryogenesis, I developed and employed a novel genetic tool to acutely disrupt keratin filament polymers with spatial and temporal specificity. Since the krt8 mimetic 2B2 peptide was validated as a keratin filament disrupting tool in both cultured cells and *ex vivo* ectodermal tissues, the photoactivation regime was optimized for application of PA-2B2 in morphogenetically active tissues. Upon 458 nm photoirradiation, PA-2B2 disrupts keratin intermediate filaments in ectodermal tissues. Marked remodeling of keratin filament network accompanies morphogenetic movements of gastrulation and neurulation during *Xenopus* embryogenesis. Light-based activation of PA-2B2 was able to disrupt keratin intermediate filaments in *Xenopus* cells and lead to tissue-specific disruption of morphogenetic processes. Specific disruption of keratin filaments in the presumptive ectoderm induces drastic neural tube defects, suggesting the fundamental requirement of keratin filaments during early embryogenesis. Localized disruption of keratin filaments in the ectoderm inhibited fibronectin fibrillogenesis along the blastocoel roof. Altogether my data show a fundamental requirement for keratin intermediate filaments in orchestrating morphogenetic movements during early embryonic development that have yet to be revealed in other model systems. Moreover, the data presented here validate the use of photoactivatable 2B2 as effective tools *in vivo*, which allow the disruption and examination of keratin intermediate filaments with spatiotemporal specificity.

Introduction

In the prior chapter, I have shown that 1A and 2B2 peptides induce the disruption of keratin filaments in cells. However, the photoactivatable component was not exploited in those experiments. Here, I sought to determine whether perturbation of keratin filaments could be optically controlled by targeted photoirradiation of PA-2B2.

Classical genetic approaches including knockdown, knockout and transgenic overexpression have been utilized to evaluate the functional role of keratin intermediate filaments. Such methods may implicate keratins in a particular process but fail to assess the of role keratin filamentous network. Moreover, methods such as application of pharmacological inhibitors have proven to be unreliable (chapter 5), since these inhibitors are non-specific and have cell-wide changes. In contrast to these past strategies used to study keratin intermediate filaments, the unique photoactivatable tools developed here can be applied more rapidly and with tunable effects. Moreover, these tools have the potential to provide precise control over the location and timing of protein disruption, allowing elucidation of the spatial and temporal roles of keratin filaments, without introducing mutations or altering the expression levels of keratins.

The early expression of keratins (K8 and K18/19) during embryo development in *X. laevis*, suggest keratins may have an important function during embryogenesis (Franz et al., 1983; Franz and Franke, 1986). The importance of keratins in efficient morphogenetic

movements comes from the studies targeting keratin protein expression during *Xenopus* development (Heasman et al., 1992; Torpey et al., 1992; Weber et al., 2012). Similarly, disruption of keratin network by anti-keratin antibodies also induces gastrulation defects (Klymkowsky et al., 1992). Polymerized keratin filaments are suggested to have a functional role during collective cell migration as being important for specifying the directional protrusive behavior of migratory mesendoderm cells (Weber et al., 2012). While these studies strongly argue for a role of keratins in early *Xenopus* development, genetic mice models have yet to identify the role for keratins in early embryogenesis.

In parallel to *Xenopus*, early expression of keratins (K8 and K18) during mouse development also suggests they have important function during embryogenesis (Jackson et al., 1980). However, knockout mouse for K18 (Magin et al., 1998) and K19 (Harada et al., 1999) do not display early embryonic defects, due to functional redundancy and complexity within the keratin family. The double knockout mice (K18/K19) display embryonic lethality due to extraembryonic defects (Hesse et al., 2000). Whereas, knockout of all Type II keratins (KtyII^{-/-}) show mild early development phenotypes, since these embryos survive through neurulation and begin organogenesis, but ultimately end in embryonic lethality (Vijayaraj et al., 2009).

Thus, the animal models put forth contradictory views about the importance of keratins during early embryogenesis. Despite the evidence supporting the importance for assembled keratin filaments in cell migration (Weber et al., 2012), the precise function of keratin

filamentous network during early development remains obscure. Early *Xenopus laevis* embryos provide a useful model organism in which to investigate the developmental and cell biological roles of intermediate filaments.

Using the currently developed novel biomolecular tool, I demonstrate the ability to acutely disrupt intermediate filaments with subcellular spatial resolution, and identify important functions for keratin filaments during early embryonic development. Thus, for the very first-time specific tools were used to interrogate the function of keratin filaments with spatial and temporal precision.

Results

7.1 Photoactivation of PA-2B2 induces disruption of endogenous keratin filaments

Previous results with MDCK, HEK293T and *Xenopus* ectodermal cells show that the fusion of LOV-J α to 2B2 is able to suppress the inhibitory 2B2 activity in dark. I next evaluated if the PA-2B2 could be photoregulated to disrupt keratin filaments in a blue light dependent manner. In principle, when in the dark state the LOV-J α would sterically inhibit 2B2 peptide interaction with keratin filaments, and release this inhibition when stimulated with blue light resulting in disrupted polymerized keratin filaments. Therefore, uninjected or *Xenopus* embryos expressing PA-2B2 or open-2B2 were either exposed to blue light or kept in dark until mid-gastrulation (stage 11). Animal caps were isolated and distribution of the endogenous keratin network was examined using immunofluorescence. As expected, both in the presence and absence of the blue light stimulation, normal uninjected ectodermal cells have a fully extended filamentous keratin network (**Fig 7.1A, B**). In the dark or absence of photostimulation, cells expressing PA-2B2 show some degree of disruption (**Fig 7.1C**) (also compare to figure 7.1 A). In contrast photoactivation with blue light induces acute disruption of the filamentous keratin network in ectodermal cells expressing PA-2B2 (**Fig 7.1D**) (compare to figure 7.1B). However, the ectodermal tissue is not falling apart and the cells seem adherent. A significant increase in disruption of keratin filaments after photoactivation of PA-2B2 was observed as indicated by the line score parameter (**Fig 7.1 D, F**), compared to the dark condition (**Fig 7.1C, F**). Consistently,

the constitutively active 2B2 induced keratin disruption in the open-2B2 expressing ectodermal cells (**Fig 7.1E, F**).

7.2 Localized activation of PA-2B2 induces rapid disruption of keratin filaments

An important advantage of PA-2B2 is its ability to control precisely the subcellular location of keratin filament disruption. I tested this ability of PA-2B2 in *Xenopus* ectodermal explants expressing PA-2B2 and eGFP-K8. The photoactivation regime was determined for the localized activation of PA-2B2, where cells were photoirradiated with repeated pulses of 458 nm laser for a period 30 seconds in ~10 μ m diameter spots while performing time-lapse imaging. Due to the leakiness of the construct, for these experiments it was made sure that the cells with visually intact keratin network were selected to evaluate the disruption of keratin filaments in response to activation of PA-2B2. No change to the intermediate filament network was observed in cells expressing eGFP-K8 and mCherry. This is also evident by the quantitative analysis where there was no significant increase in network collapse and aggregate formation (**Fig. 7.2A, G**). Similarly, when ectodermal cells are not stimulated and kept in dark the keratin filament network remains intact and there is no aggregate formation (**Fig. 7.2B, G**). In cells expressing PA-2B2, exposure to blue light induced the rapid collapse of keratin filaments specifically in the immediate vicinity of illumination (**Fig. 7.2C-D, G**). While total collapse of the keratin filaments was isolated to the region of photoirradiation, this localized perturbation had widespread consequences for the intermediate filament network beyond the local effect, causing filaments nearby to

appear more tortuous rather than taut. However, only in the area where illumination occurred did filaments completely collapse and aggregate. To further explore the capability of PA-2B2 to disrupt the intermediate filament network in an acute manner, we performed repeated illuminations of a single cell where we systematically targeted filaments that remained until the entire intermediate filament network was collapsed. Repeated photoirradiation was able to acutely disrupt the entire intermediate within a cell in a period of less than 10 minutes (**Fig. 7.2E**). There is a significant increase in aggregate formation post activation of PA-2B2, indicating that light-based activation of PA-2B2 disrupts keratin network (**Fig. 7.2G**). In both series A and B, as internal control other cells of the explant and their respective keratin networks were observed to behave normally, suggesting that, experimental conditions did not have any obvious effect on their keratin network. The engineered PA-2B2 is appended to the LOV-J α helix in anticipation that their affinity to effector proteins is lowered in the dark but enhanced upon irradiation. These data suggest that although, blue light stimulation allows 2B2 to disrupt keratin filaments, PA-2B2 action on the keratin network is not readily reversed even when light stimulation ceases.

Similarly, blue light stimulation did not promote any obvious effects on the keratin network in ectodermal cells expressing control construct mCherry and eGFP-K19 (**Fig. 7.3A**). Photoactivation of PA-2B2, by repeated pulses of 40 seconds elicits K19 network disruption, quite similar to K8 disruption (**Fig. 7.3B**). Taken together, these results demonstrate that photoactivatable PA-2B2 can induce rapid subcellular disruption of keratin filaments in morphogenetically active tissue

7.3 Keratin filaments are necessary for normal *Xenopus* embryo development

Having demonstrated the ability of PA-2B2 to disrupt the intermediate filament network in individual cells, we next sought to examine the consequences of intermediate filament disruption on early development. *Xenopus* embryos were co-injected with cDNA encoding eGFP-krt19 and mCherry alone or mCherry open-2B2 in the animal hemisphere at one cell stage and allowed to develop to tadpole stage in dark. Both uninjected and mCherry expressing control embryos developed normally (**Fig. 7.4A, B**). In contrast, the open-2B2 injected embryos exhibited worsening abnormal phenotypes as development progressed from gastrulation to tadpole (**Fig. 7.4C**). Embryos showed extruding yolk as they progressed to neurulation. By early tailbud and continuing through late tailbud stages, open-2B2 embryos had an open dorsal region, likely originating from the failed blastopore closure. In tadpoles, this open dorsal aspect persisted in open-2B2 injected embryos. Thus, the open-2B2 tadpoles with open dorsal side and/or ventral edema were characterized with abnormal phenotype. Additionally, these embryos often had underdeveloped head structures, poor midline separation, a bifurcated shortened tail (**Fig. 7.4C**). There is no significant difference between uninjected and mCherry + eGFP-K19 injected embryos (**Fig. 7.4A, B, D**) suggesting that developmental abnormalities in the embryos are due to keratin filament disruption induced by open-2B2 (**Fig. 7.4C, D**). Expression of open-2B2 in *Xenopus* embryos contributed significantly to the formation of defects during development (**Fig. 7.4C, D**).

Next, to determine if photoactivation of PA-2B2 can induce similar developmental defects, uninjected or *Xenopus* embryos injected with mRNA encoding PA-2B2 were grown to tadpole stages in the dark or in the presence of blue (458 nm) light. *Xenopus* embryos injected with 100-175 pg mRNA encoding PA-2B2 and maintained in the dark appeared largely like their wildtype and mCherry injected counterparts (**Fig. 7.5(B-E)**). Developmental defects paralleling the open-2B2 phenotypes were induced when PA-2B2 embryos were grown under blue light conditions (**Fig. 7.5B, C, F**). Fluorescence images show that spatial expression of mCherry PA-2B2 in embryos that were injected at one cell stage in the animal hemisphere coincided with the dorsal defects (**Fig. 7.6**). Expression of PA-2B2 (175 pg) caused significant increase in the percentage of embryos developed with developmental defects in comparison to uninjected embryos kept in dark or exposed to blue light (**Fig. 7.5F**). Additionally, the significant difference in percentage of embryos with abnormalities between dark and photoactivated states of PA-2B2 suggests PA-2B2 is an excellent photoswitch for probing keratin functional role *in vivo* (**Fig. 7.5F**). Injection of greater amounts of PA-2B2 mRNA (250-500 pg) resulted in developmental abnormalities irrespective of blue light exposure that were only mildly enhanced by blue light exposure as it did not significantly increase the average percentage of abnormal embryos (**Fig. 7.5D-F**). Nonetheless, the developmental perturbations due to photoactivation of PA-2B2 and its expression at higher levels were consistent with those observed by open-2B2 expression. Altogether, these data show an important role for intermediate filaments during development of the ectoderm in the early embryo.

To understand the consequences of photoactivation of PA-2B2 on different aspects of early development the internal gross morphology of embryos was assessed. Uninjected or *Xenopus* embryos injected with mRNA encoding PA-2B2 were allowed to develop in the dark or in the presence of blue (458 nm) light and bisected sagittally at desired stages. During embryo development, the blastocoel becomes apparent which then gets displaced with the formation of archenteron as the mesendodermal cells involute through the blastopore during gastrulation. The formation of the blastopore ring encircles the endodermal cells at the vegetal hemisphere called the yolk plug which eventually gets internalized into the embryo as involution progresses. As the embryos progress from gastrulation through neurulation the archenteron elongates along with formation of the notochord, elongation of neural plate and elevation and apposition of neural folds and fusion of the folds at dorsal midline. Both in the presence and absence of photo-stimulation, sagittally bisected control uninjected embryos during gastrula stage appeared normal with smooth formation of blastocoel, archenteron and yolk plug. As the embryos progressed to neurulation, the embryos elongate with the formation of notochord along with the gut cavity or archenteron (**Fig. 7.7A**). Similarly, PA-2B2 expressing embryos in the absence of blue light underwent gastrulation and neurulation normally (**Fig. 7.7B**). In contrast, photoactivation of PA-2B2 caused a more spherical blastocoel formation, and later the normal archenteron failed to form and the blastocoel was retained and extruding yolk plug formed during gastrulation. Furthermore, the sagittal bisections revealed gaps between the migrating mesendodermal cells and blastocoel roof (BCR) (**Fig. 7.7B**). Embryos that did not gastrulate normally showed cascading effects that were apparent at the neurula stage, the embryos had underdeveloped head structure, failure of archenteron expansion and

extruding yolk plugs (**Fig. 7.7B**). The failure of these early morphogenetic processes during gastrulation and neurulation culminated in improper closure of neural tube and thus embryos display the open dorsal aspect and bifurcated tail evident at the late neurula and tadpole stage (**7.4, 7.5, 7.6, 7.7B**). Comparable defects are seen in sagittally bisected embryos expressing open-2B2 both during gastrula and neurula stages (**Fig. 7.7C**). Remarkably, the defects manifesting during early embryo development stem from keratin filament disruption in the ectodermal tissue induced by photo-stimulation of PA-2B2. These results indicate that the keratin filamentous network in the ectodermal tissue is critically important for normal early development.

7.4 Disruption of keratin filamentous network affects fibronectin fibrillar organization

The sagittal bisections revealed gaps between BCR and the migrating cells suggesting either defective cell migration or defects with ECM substrate (**Fig. 7.7B, C blue arrows**). A network of fibronectin (FN) fibrils covers the inner surface of the BCR (Lee et al., 1984; Nakatsuji et al., 1985; Nakatsuji and Johnson, 1983). Perturbations that disrupt fibrillar fibronectin on the BCR induces exogastrulation (Davidson et al., 2006; Marsden and DeSimone, 2001; Ramos, 1996; Rozario et al., 2009) indicating that FN plays important roles in multiple morphogenetic processes. FN fibrils support endoderm migration (Wen and Winklbauer, 2017), mesendoderm migration (Lee et al., 1984; Winklbauer, 1998), radial cell intercalation and epiboly (Rozario et al., 2009) and mediolateral cell intercalation during convergent extension (Davidson et al., 2006; Marsden and DeSimone,

2003; Rozario et al., 2009). Since interfering with polymerized keratin filaments induced similar developmental abnormalities such as extruding yolk plug (**Fig. 7.4-7.7**), I next tested whether FN fibrillogenesis on the BCR was affected by keratin disruption. Uninjected or *Xenopus* embryos injected with mRNA encoding PA-2B2 and open-2B2 were allowed to develop in the dark or in the presence of blue (458 nm) light and FN fibrillogenesis along the BCR was visualized at mid-gastrulation (stage 11/12). Fixed and immunostained ectodermal explants reveal that, unlike the uninjected control embryos (**Fig. 7.8A**), or PA-2B2 maintained in dark (**Fig. 7.8B (a-c)**), FN fibrillogenesis is markedly perturbed in cells where keratin disruption is induced by photoactivation of PA-2B2 (**Fig. 7.8B(d)**) or by expression of open-2B2 (**Fig. 7.8C(g)**). Cells displayed a pericellular distribution of FN and lacked a clearly defined fibrillar network. A complete blocking of FN fibril assembly is observed in the presence of FN functional antibodies (Marsden and DeSimone, 2001) with a similar pericellular arrangement when only FN fibrillogenesis is perturbed (Rozario et al., 2009). Additionally, the tissue area with mosaic expression of PA-2B2 or open-2B2 have partial FN fibrillogenesis (**Fig 7.8B(e), C(h)**), while the most distal uninjected cells have intact FN fibrillogenesis (**Fig 7.8B(f), C(i)**). This suggests that specific disruption of keratin filaments hinders FN assembly into a fibrillar network. It was noted that dark (-) PA-2B2 condition also exhibited some level of disruption of FN fibrillogenesis; however, not comparable to photoactivated (+) PA-2B2 condition. This was likely due to the leakiness of the PA-2B2 construct and its ability to some induce minimal keratin filament disruption even in dark. Thus, the results indicate that intact keratin filamentous network is required for FN fibrillogenesis on the BCR surface.

Figure 7.1

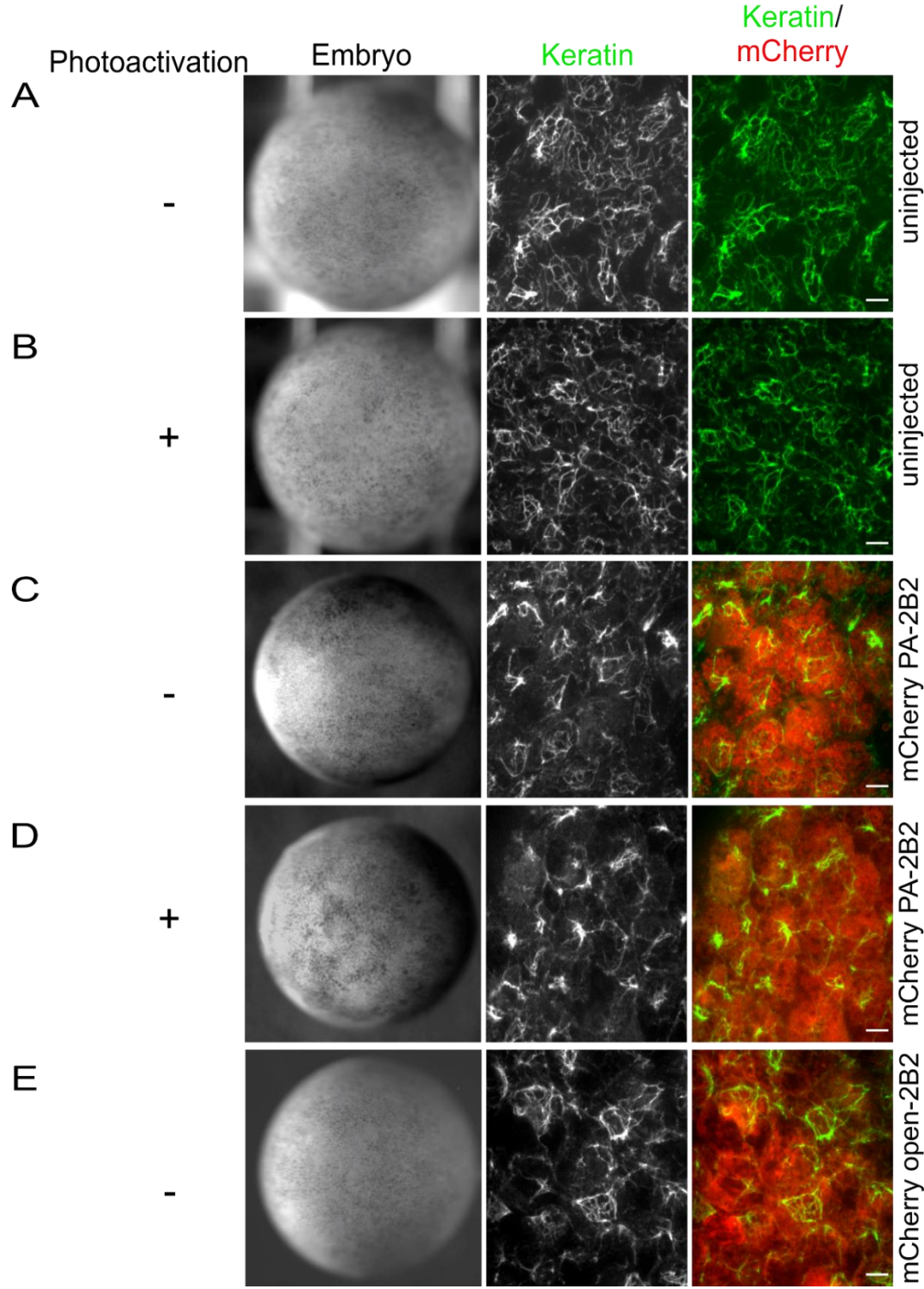


Figure 7.1

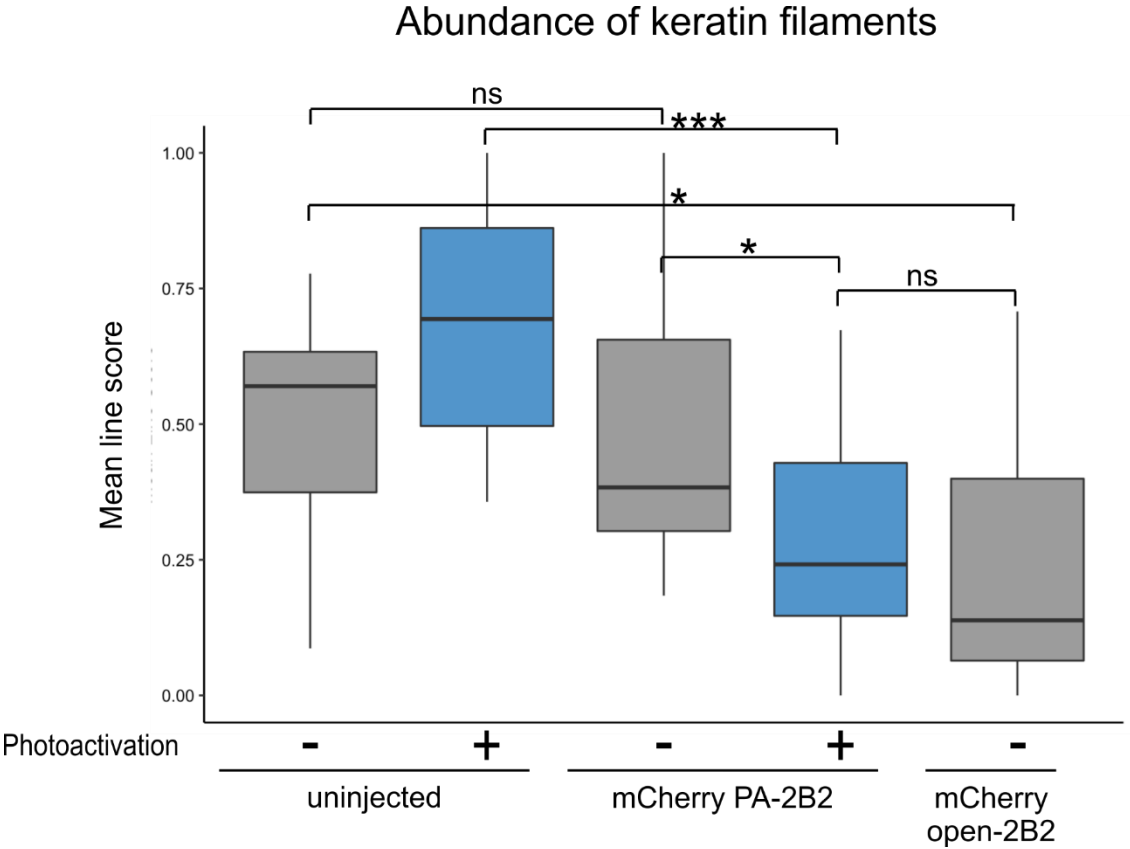


Figure 7.1 Photoactivation of PA-2B2 induces disruption of endogenous keratin filaments.

Fertilized *Xenopus* eggs uninjected or injected with mCherry PA-2B2 (red) or mCherry open-2B2 (red) at one cell stage were allowed to develop until gastrulation either in the presence or absence of blue light. Animal caps were isolated and immunostained for keratin network (green). **(A & B)** Uninjected control embryos display a widespread keratin network regardless of exposure to blue light. mCherry PA-2B2 expressing cells in absence of photoactivation **(C)** show some widespread keratin network, while in the presence of photoactivation **(D)** all cells show disrupted and aggregated network. **(E)** Expression of open-2B2 show some disruption of keratin network **(F)** Quantitation showing the line score of presence of keratin filaments in different conditions.

Figure 7.2

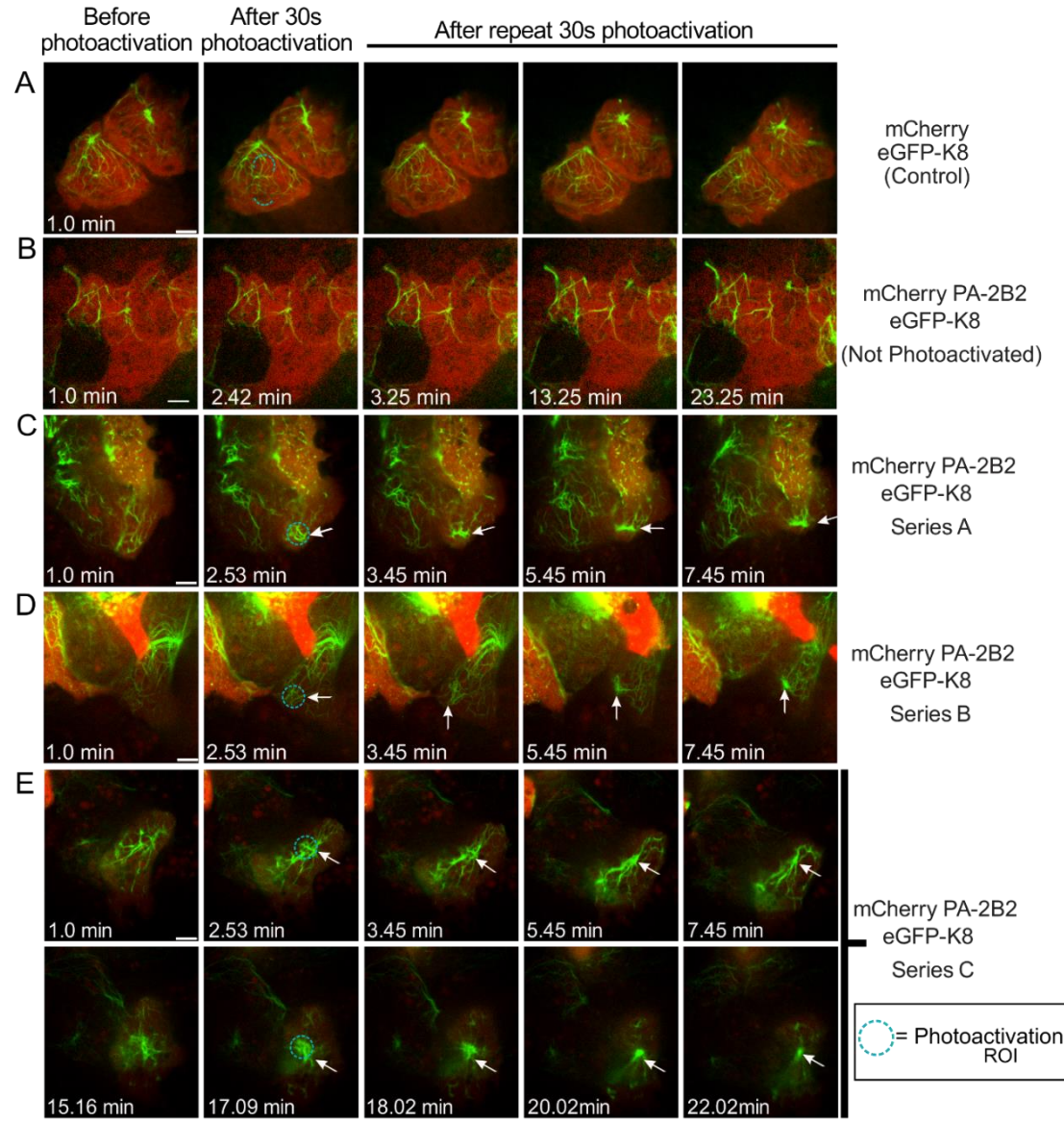


Figure 7.2

F

Keratin network collapse and aggregation after light based activation of PA-2B2

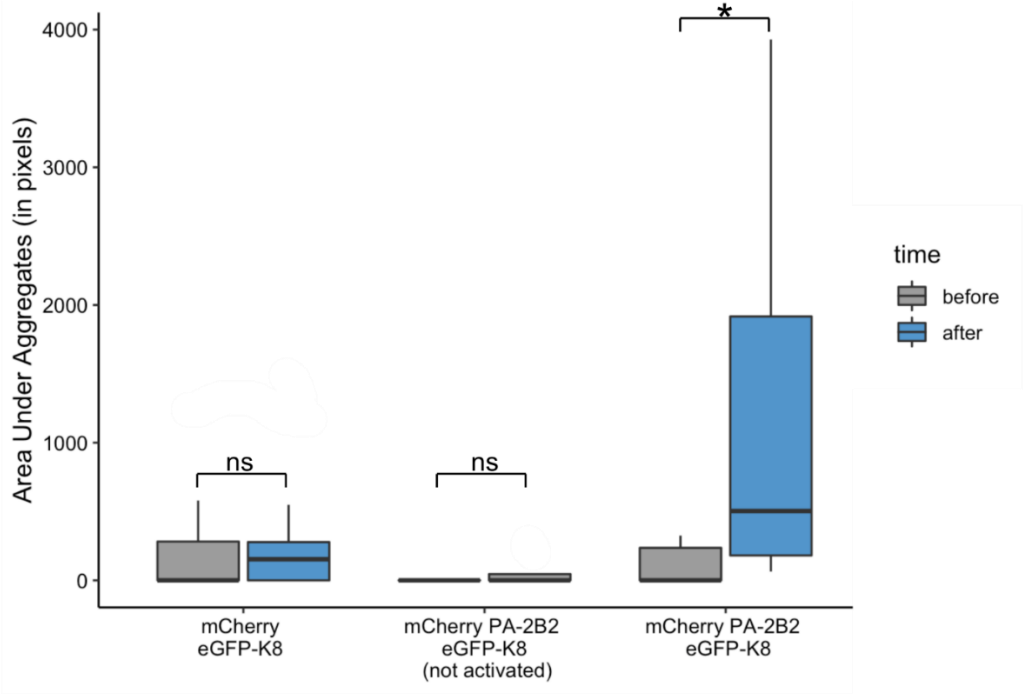


Figure 7.2: Localized activation of mCherry PA-2B2 induces rapid disruption of keratin filaments.

Xenopus embryos co-injected with eGFP-krt8 and either mCherry or mCherry PA-2B2 or mCherry open-2B2 plasmid DNA targeting the presumptive ectoderm were allowed to develop until stage 10.5-11. Following ectodermal animal caps were isolated and plated on fibronectin-coated glass-bottom dishes. Ectodermal cells expressing eGFP-K8 (green) and the respective control or 2B2 modules (red) were illuminated at different subcellular positions with 458 nm light using a 10 μ m diameter (teal circle) and 3 secs pulses for 30s twice with image acquisition between photoirradiation events. Photoactivation and imaging were done using Zeiss Cell Observer spinning disk confocal microscope (63X/1.4 NA, 1.0X optovar). Selected confocal images of a time-lapse movie of the response of ectodermal progenitor cells to localized photoirradiation are illustrated above. **(A)** mCherry controls show no keratin disruption nor aggregation either locally or throughout the cell. **(B)** In the absence of photostimulation PA-2B2 expressing cells show no keratin disruption either locally or elsewhere in the cell. **(C and D)** Two independent examples of light sensitive PA-2B2 expressing cells exhibit local disruption and aggregation formation of keratin filaments. **(E)** An extended photoactivation regime induces complete collapse of the keratin network. **Arrows** indicate region of collapsing keratin network. In the absence of photostimulation PA-2B2 expressing cells show no keratin disruption either locally or elsewhere in the cell. **(F)** Quantitation showing the

aggregation of keratin filaments in different conditions post-stimulation of PA-2B2.

Circles indicate where the 458nm laser light was applied. Bars, 10µm

(mCherry PA-2B2 + eGFP-K8, N=11, n=13 explants, 45 cells); (C1mCherry + eGFP K8, N=3, n=5 explants, 21 cells)

Figure 7.3

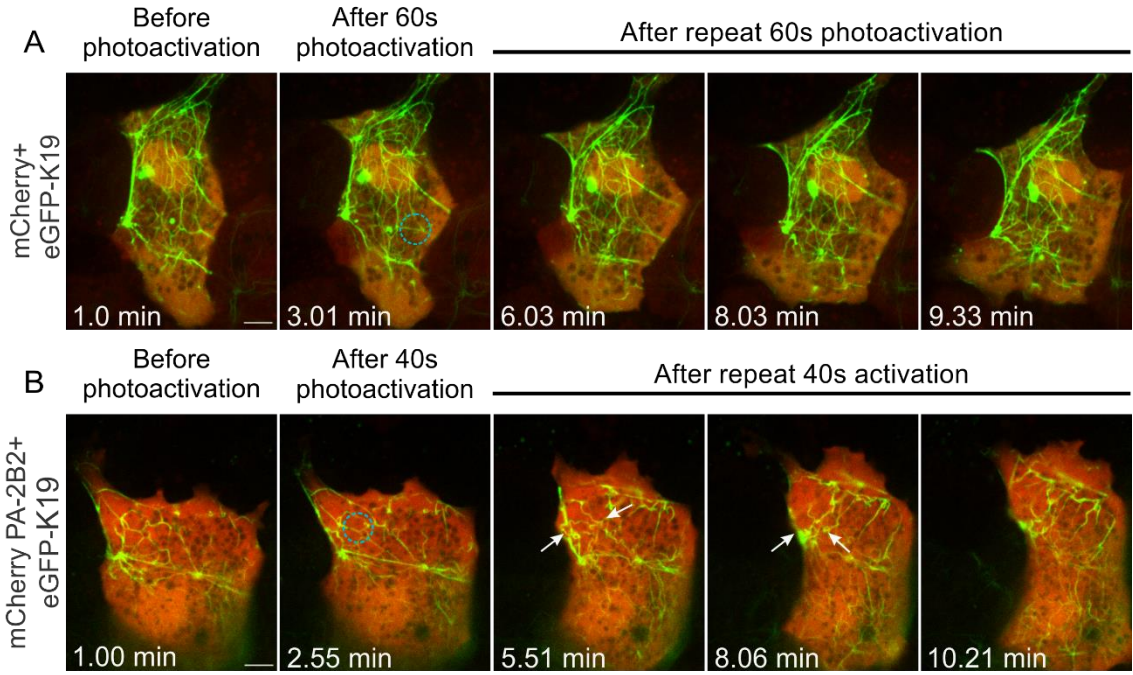


Figure 7.3: Localized photo stimulation of mCherry PA-2B2 induces rapid disruption of keratin filaments.

Xenopus embryos co-injected with eGFP-krt19 and either mCherry or mCherry PA-2B2 plasmid DNA targeting the presumptive ectoderm were allowed to develop until stage 10.5-11. Following, ectodermal explants were prepared and plated on fibronectin-coated glass-bottom dishes. Ectodermal animal cap cells expressing eGFP-K19 (green) and the experimental or control constructs (red) were illuminated at different subcellular positions with 458 nm light using a 10 μ m diameter (teal circle) and 10 secs pulses for 40 secs or 60 secs, twice with image acquisition between photoirradiation events. Photoactivation and imaging was done using Zeiss Cell Observer spinning disk confocal microscope (63X/1.4 NA, 1.0X optovar). Selected confocal images of a time-lapse movie of the response of ectodermal progenitor cells to localized photoirradiation are illustrated above. **(A)** mCherry controls show no keratin disruption nor aggregation either locally or throughout the cell. **(B)** light sensitive PA-2B2 expressing cells exhibit local disruption and aggregation formation upon light stimulation as indicated by **arrows**. **Circles** indicate where the 458nm laser light was applied.

Bars, 10 μ m.

(mCherry PA-2B2+ eGFP-K19, N=3, n=6 explants, 24 cells); (mCherry + eGFP-K19, N=2, n=5 explants, 30 cells)

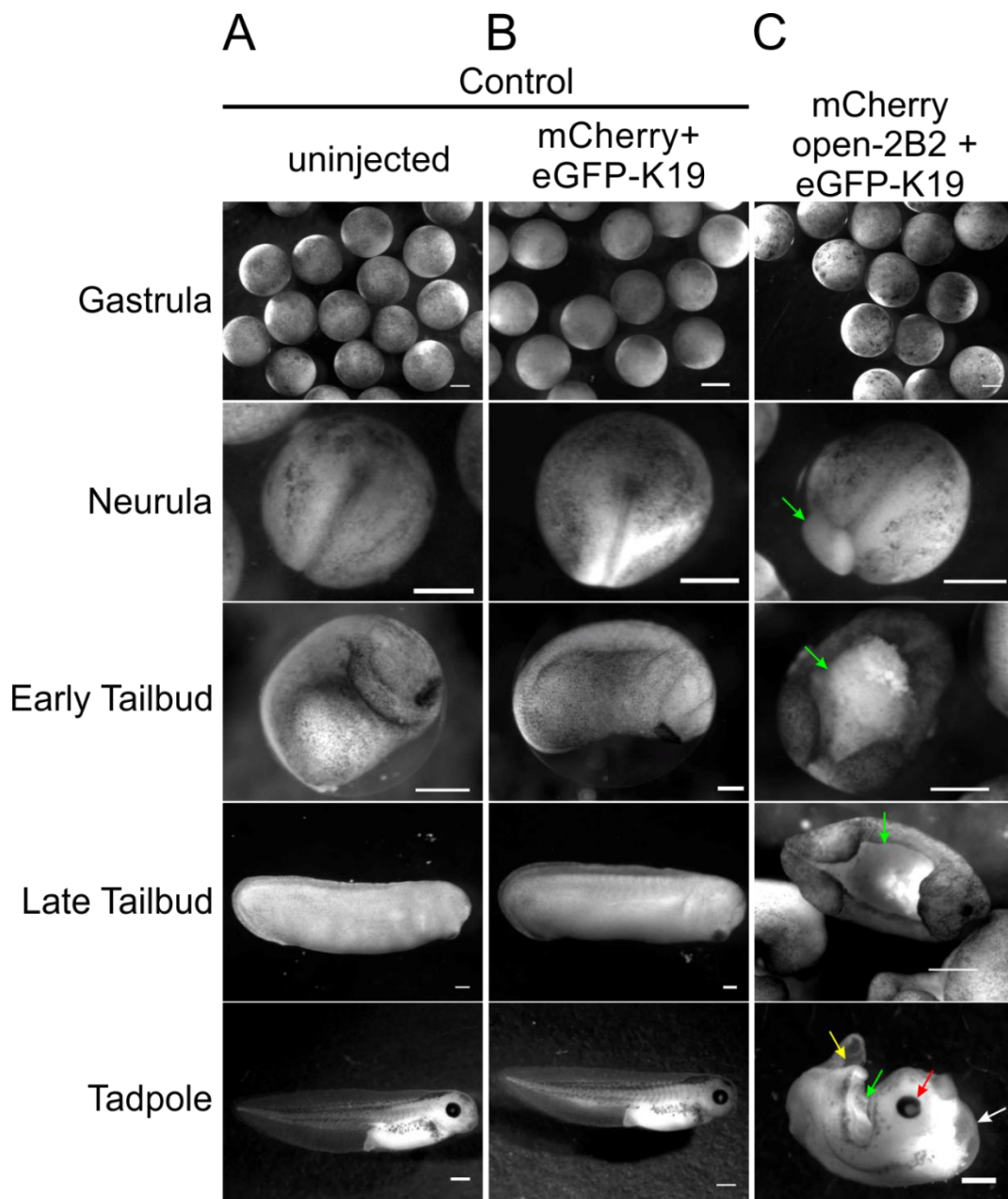
Figure 7.4

Figure 7.4

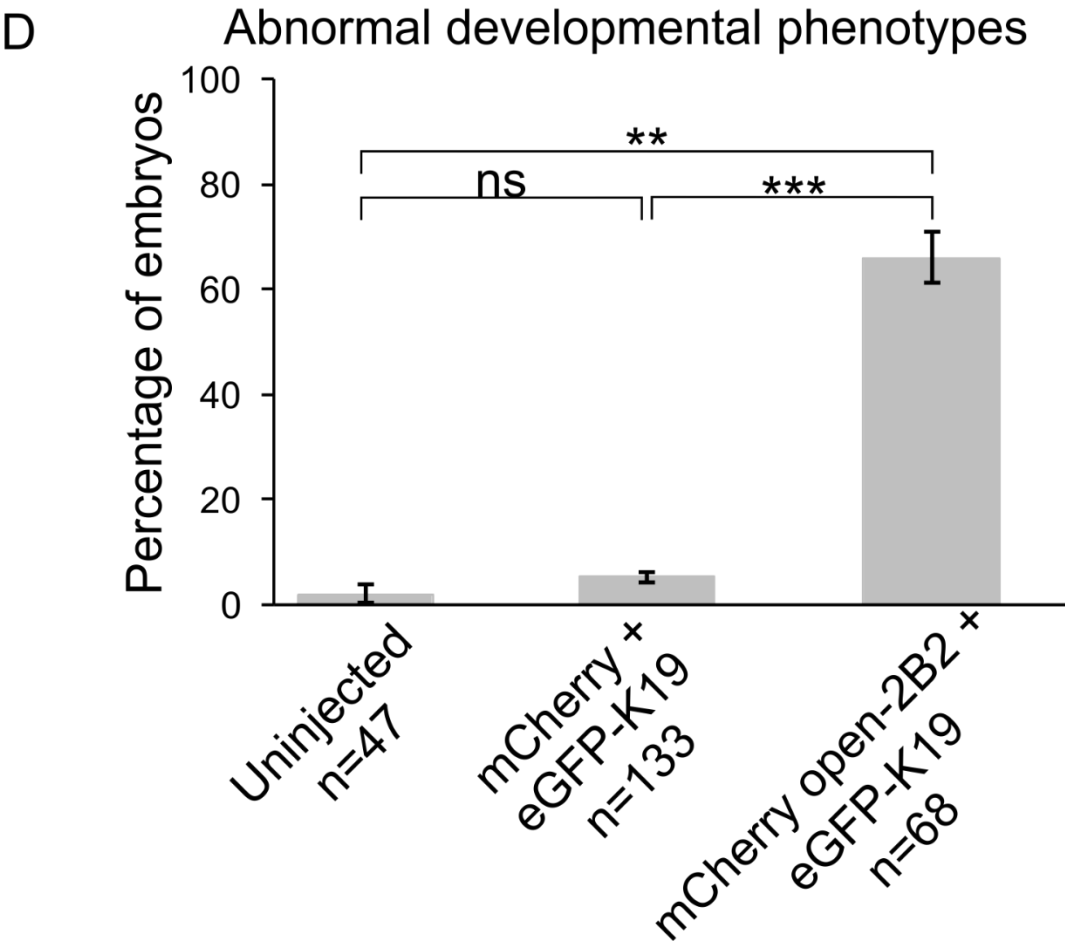


Figure 7.4: Keratin filaments are necessary for normal *Xenopus* embryo development.

(A) Uninjected control embryos or (B) embryos injected with control constructs (mCherry+ eGFP-krt19) demonstrate normal morphological development from gastrulation, neurula, early tailbud, late tailbud, and tadpole stages. (C) Expression of mCherry open-2B2 in the ectodermal cells comprising the animal cap induces various developmental defects. Arrows point to defects such as defective yolk plug closure (green arrow), regressed eye development (red arrow), bifurcated tail (yellow arrow), and ventral edema (white arrow). Bars, 500 μ m. (D) Quantitative representations of abnormal phenotypes. Data shown are the standard errors of the means of the average percentages from at least three repeats. Statistics were calculated by one-tail unpaired student's t-test as indicated.

Figure 7.5

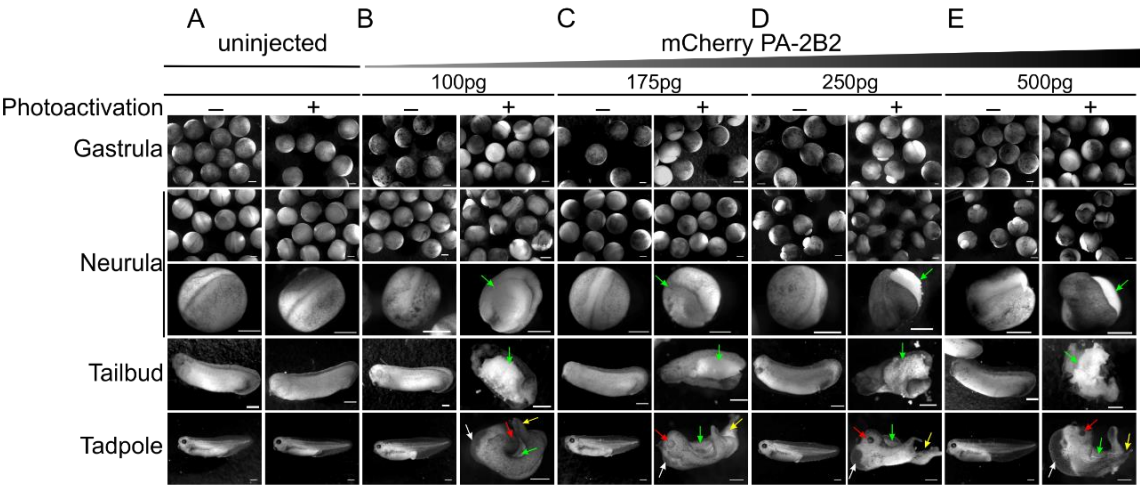


Figure 7.5

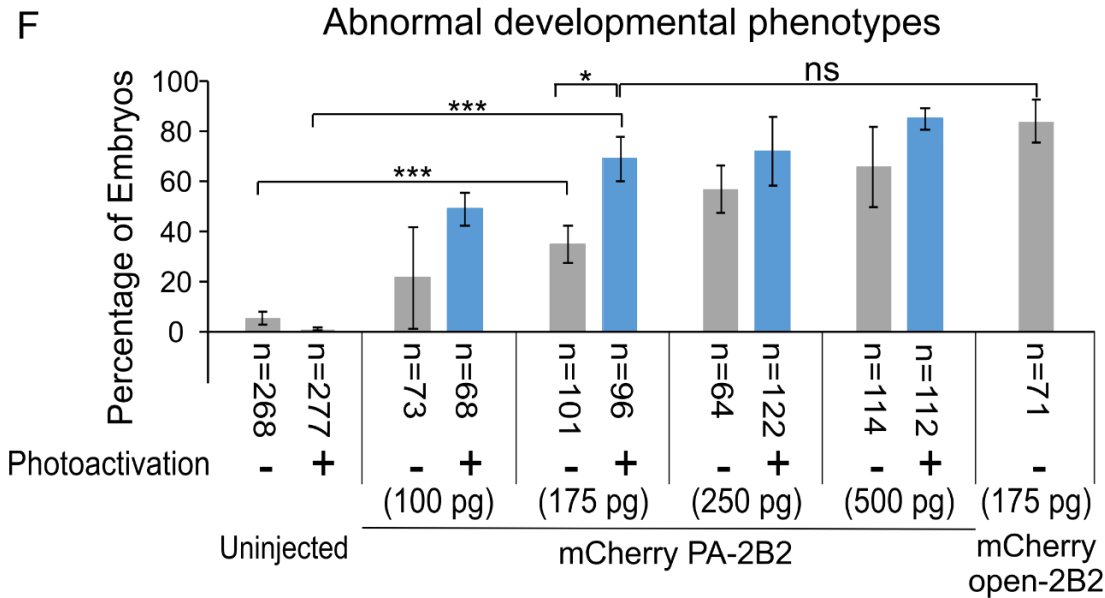


Figure 7.5 Light induced disruption of keratin filaments elicits abnormal *Xenopus* development.

Fertilized *Xenopus* eggs uninjected or injected with PA-2B2 at one cell stage were either protected from light or exposed to blue light. Phenotypes were assessed from gastrulation to tadpole stage. **(A)** Uninjected control embryos display a normal phenotype regardless of exposure to blue light. **(B)** Embryos were injected with 100 pg PA-2B2, **(C)** 175 pg PA-2B2, **(D)** 250 pg PA-2B2, **(E)** 500 pg PA-2B2. Embryos were grown under blue light conditions as indicated (+ or -). Developmental defects of open yolk plug/open dorsal side (green arrows), underdeveloped eye or no eye (red arrows), bifurcated tail (yellow arrows), ventral edema (white arrows) are indicated. Bars, 500 μ m. **(F)** Quantitative representations of abnormal phenotypes. Data shown are the standard errors of the means of the average percentages from at least three repeats. Statistics were calculated by one-tail unpaired student's t-test as indicated.

Figure 7.6

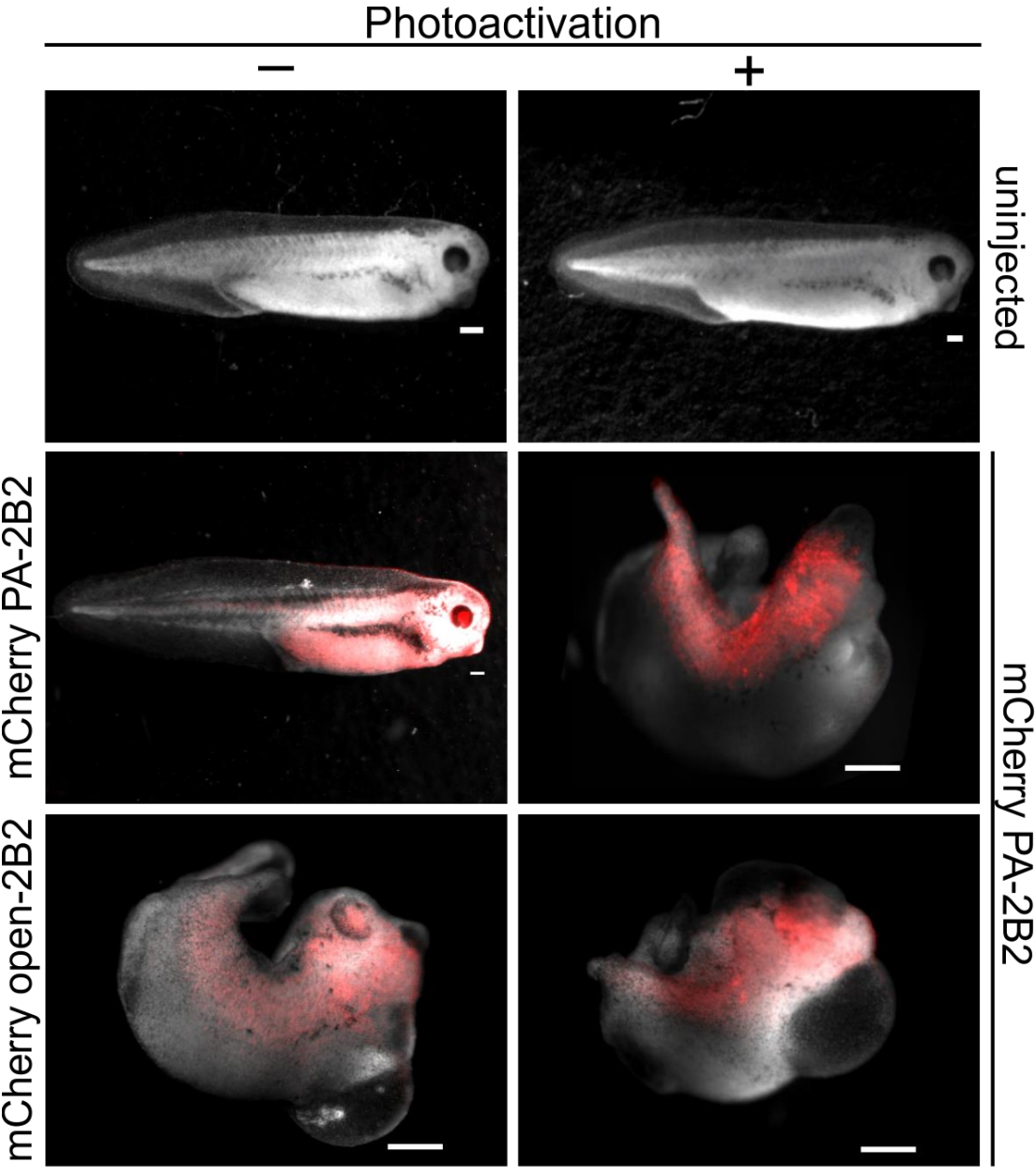


Figure 7.6 mCherry fluorescence is present in dorsal most tissues in embryos expressing PA-2B2.

Fertilized *Xenopus* eggs uninjected or injected with PA-2B2 or open-2B2 at one cell stage were either subjected to blue light or not and spatial expression of mCherry PA-2B2 or mCherry open-2B2 was detected. Embryos were grown under blue light conditions as indicated (+ or -). mCherry fluorescence is present in dorsal region of the embryo.

Bars, 200 μ m

Figure 7.7

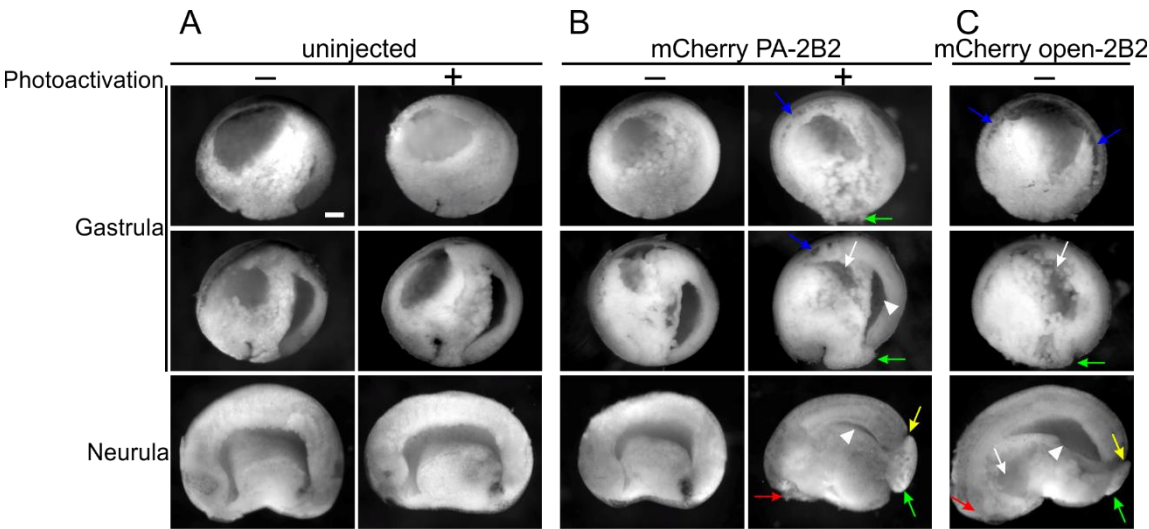
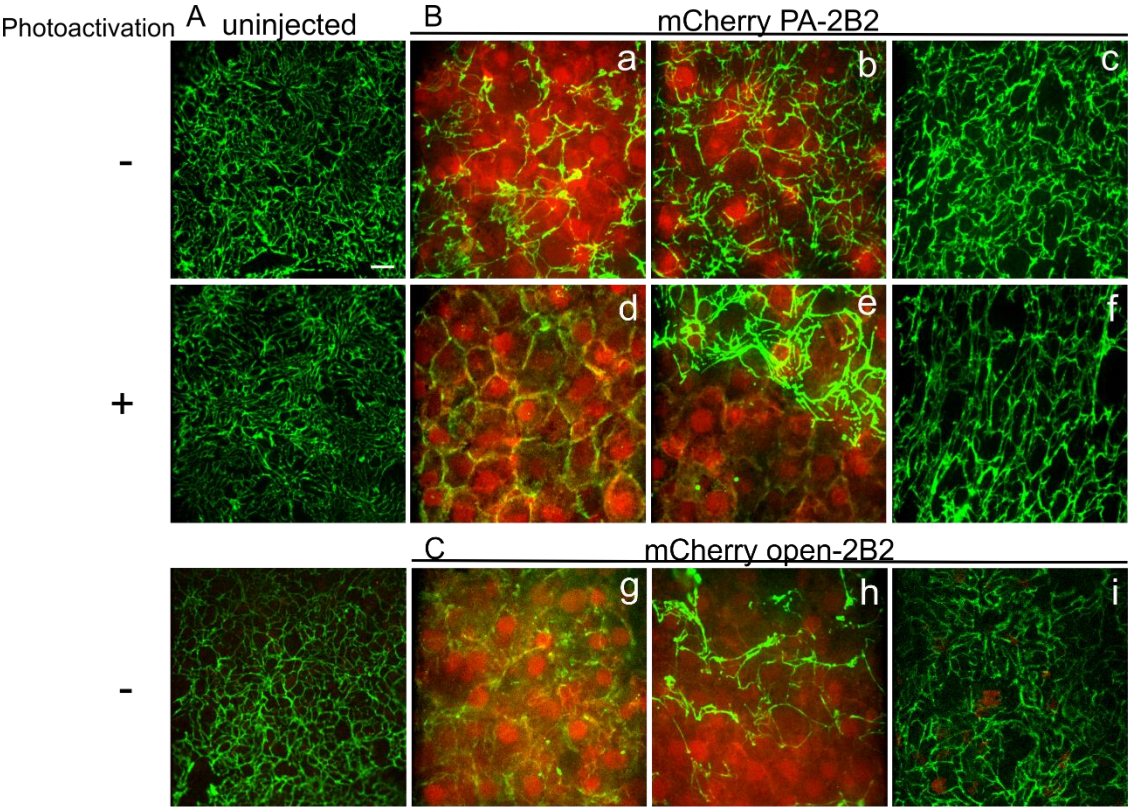


Figure 7.7: Light induced disruption of keratin filaments perturbs internal morphology of embryos.

Fertilized *Xenopus* eggs uninjected or injected with PA-2B2 or open-2B2 at one cell stage were either protected from light or exposed to blue light, fixed and bisected sagittally. Internal gross anatomical features were assessed from gastrulation to neurulation stages. **(A)** Uninjected control embryos display a normal phenotype regardless of exposure to blue light. Embryos injected with **(B)** 175 pg PA-2B2, **(C)** 175 pg open-2B2 were grown under blue light conditions as indicated (+ or -). Photoactivation of PA-2B2 perturbed blastopore closure/extruding yolk plug (green arrows), induced underdeveloped head area (red arrows), posterior bifurcated neural tube (yellow arrows), deformed blastocoel (white arrows), gaps between migrating cells and BCR (blue arrows), failed archenteron expansion (white arrowhead) are indicated. Panels show representative images of three independent experiments. Bars, 200 μm .

Figure 7.8



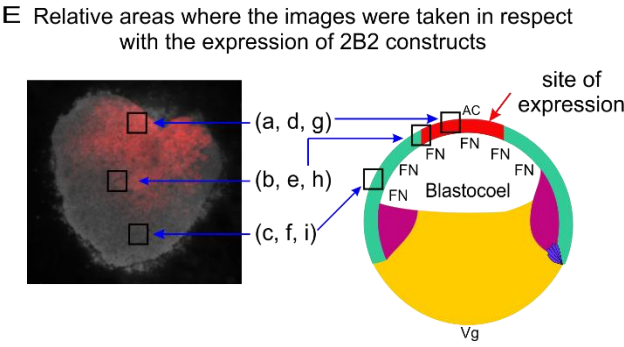
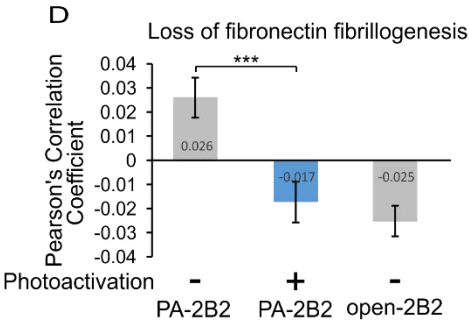


Figure 7.8 Keratin filamentous network is required for fibronectin assembly.

Fertilized *Xenopus* eggs uninjected or injected with 175pg mRNA of PA-2B2 (red) or open-2B2 (red) at one cell stage were either protected from light or exposed to blue light. Animal caps were isolated and immunostained for FN fibrils (green). **(A)** Uninjected control embryos regardless of exposure to blue light or **(B (a-c))** Embryos expressing (175pg) mCherry PA-2B2 in the absence of blue light display a normal FN fibril assembly, **(B (d-f))** Embryos expressing mCherry PA-2B2 in the presence of blue light have complete loss of FN fibrils (d), while the uninjected cells are able to assemble fibrils (e, f) **(C)** Expression of mCherry open-2B2 in the ectodermal cells comprising the animal cap induces perturbation of FN fibrils (g), while the uninjected cells are able to assemble FN fibrils (h, i); Bars, 10 μ m. **(D)** Quantitative representation showing the loss of FN fibrillogenesis, bar graphs show the mean Pearson's correlation coefficient for colocalization of FN fibrils with mCherry. Data shown are the standard errors of the means of the average percentages from three repeats. Statistics were calculated by one-tail unpaired student's t-test as indicated. **(E)** Cartoon showing relative positions from where the images were taken from the PA-2B2 or open-2B2 expressing ectodermal explants

Discussion

By engineering a LOV2 domain fusion with a short 2B2 peptide that can be made available for disruption through photomanipulation and titrated as necessary, I have developed a unique biomolecular tool to disrupt keratin filaments. Through this approach, these constructs can be used to target intermediate filaments at a subcellular scale or more broadly disrupt filaments in cells and tissues where the tools are expressed and photoactivated. Furthermore, this study fortifies *Xenopus laevis* as an instrumental model system to study the role of keratin filaments during early development.

Deciphering the role of keratins in early embryonic development has thus far been difficult, due to functional redundancy and complexity within the family, generation of exogastrulation or embryonic lethal phenotypes in intermediate filament knockout and knockdown animal models, and a lack of specific polymerization inhibitors characterized for intermediate filaments. This study develops a unique photoactivatable tool using the K8 mimetic peptide and show primarily disruption, collapse and aggregation of the filaments at the site of PA-2B2 activation. Although the mechanisms underlying the filament perturbation and kinds of the effect on polymerization remain to be determined, as expected, open-2B2 yields a more widespread disruption and the intermediate filaments appear sparser, less well-defined and often punctate. Questions remain as to how exactly PA-2B2 is incorporating and disrupting the existing filamentous network. Nonetheless, this

tool when acutely activated by exposure to blue light induces disruption of keratin filaments which widely remained within the region of photoactivation.

From preliminary observations it was apparent that in all cell types PA-2B2 did not disrupt keratin filaments in dark or under moderate expression levels. However, high expression levels of PA-2B2 was sufficient to cause disruption even in dark conditions, similar to open-2B2. Titration of PA-2B2 to appropriate expression levels was sufficient to maintaining dynamic light responsiveness. In view of this, improving caging by introducing further mutations in LOV-J α (Zimmerman et al., 2016) and/or expressing PA-2B2 under a titratable expression system will be necessary for greater utility across other cell systems. Future work will be aimed at determining the cell biological consequences of intermediate filament perturbation using these tools.

For the first time it has been shown that keratin filaments are critical for early embryogenesis by the utilization of PA-2B2 and open-2B2. Other methods used to disrupt keratins fail to provide any functional significance of keratin filaments. For instance, morpholinos injected in the mesendoderm to interrupt keratin protein expression induce exogastrulation of the embryos (Weber et al., 2012). Similarly, targeting keratin 8 protein expression by antisense oligonucleotides also causes exogastrulation of embryos (Torpey et al., 1992). Likewise, anti-keratin antibodies injected anmally to disrupt keratin filament assembly induces defective blastopore lip closure or exogastrulation (Klymkowsky et al., 1992). On the other hand, by biasing the targeted keratin filament disruption induced by

PA-2B2 and open-2B2 in the ectoderm, generates remarkably distinct phenotypes, that have not been reported so far. Here, I describe a more targeted method of disrupting intermediate filaments. Unique to the usage of 2B2 constructs versus prior knockdown methods is that the present tool distinguishes the role of intermediate filaments as a cytoskeletal network from intermediate filament proteins more generally. The results presented here identify a novel role of keratin filaments required for the appropriate morphogenetic movements of the *Xenopus* embryo. It is curious since involution and blastopore constriction are primarily directed by morphogenetic movements in the vegetal and marginal zones (Keller et al., 2003). And here I show that restricted disruption of the keratin filaments in the subset of cells in the ectodermal region impacts the disparate morphogenetic movements. Intriguingly, disruption of the keratin filaments in the presumptive ectodermal tissue results in the predominant phenotypes that include failure of blastopore closure, abnormal blastocoel displacement and defective archenteron formation. These induced defects further lead to the manifestation of the defective neural tube closure, AP axis shortening and dorsal flexure and defective eye development. These defects were similar to gastrulation phenotypes obtained by morpholino knockdown of FN (Davidson et al., 2006), mAbs directed against FN cell-binding domains (Marsden and DeSimone, 2001, 2003), inhibition of FN fibril assembly (Rozario et al., 2009) or indirect inhibition of FN (Dzamba et al., 2009).

The current study shows that normal FN fibrillogenesis is perturbed following disruption of keratin filaments in cells by mere expression of open-2B2 or by photoactivation of PA-

2B2. Likewise, depletion of vimentin IFs in wound healing models impairs collagen expression and dynamic reorganization (Challa and Stefanovic, 2011; Cheng et al., 2016; LeBert et al., 2018). Despite the importance of keratin filaments in the assembly of FN fibrillar matrix, the detailed mechanism of how keratin filament disruption leads to FN matrix perturbation is not very clear. However, similar disruption of the FN fibrillogenesis is observed in plakoglobin morphants (Hirsh et al., 2018). Plakoglobin is required for normal keratin filamentous network organization and their recruitment to C-cadherin in the event of stress application (Weber et al., 2012). Thus, it would not be too far-fetched to speculate that disruption of keratin filamentous network affects the plakoglobin-cadherin mediated FN fibrillogenesis and thus morphogenetic movements during *Xenopus* gastrulation. Nevertheless, keratin filaments are functionally essential in tissue morphogenesis during early development through its role in FN fibrillogenesis.

Collectively, my data shows the fundamental requirement of keratin filaments during morphogenetic movements and thus early embryogenesis in *X. laevis*. Additionally, unlike the approaches used thus far, such as genetic manipulations or chemical inhibitors, to inspect the function of keratins, the tools developed here have far more advantages. The most important being the use of light, which affords a spatiotemporal and noninvasive control over inhibition of keratin filaments. Moreover, by controlling the light intensity and area of irradiation, the extent of keratin disruption can be regulated. A more targeted inhibition can be achieved rather than a global one, enabling teasing out precise roles of keratin filaments not only in specific cellular compartments but also specific biological

processes. Furthermore, this study validates the use of genetically encoded photoactivatable 2B2 tool which enables precise spatial and temporal inhibition of keratin filaments in live cells, with photoactivation at 458 nm. Finally, the photoactivatable proteins employed in this study provide a powerful tool to study aspects of keratin filaments at spatiotemporal specificity that has been, so far, difficult to address.

Chapter 8

Discussion and Future Directions

Discussion

This study was initiated to examine the functional role of keratin intermediate filaments during early embryonic development. First, a distinct subcellular localization of keratin filaments and keratin precursor particles was identified in morphogenetically active tissues. In order to specifically study the functional role of keratin filaments I engineered PA-2B2, a novel genetically encoded photoactivatable peptide that can be used to rapidly disrupt intermediate filaments with subcellular spatial resolution. Since comparative broad analysis of small molecule drugs such as withaferin A and acrylamide done here confirm that these drugs are not specific inhibitors to IFs; I also developed a constitutively active inhibitor of keratins, the open-2B2, to disrupt keratin filaments more persistently.

The keratin network organization was observed to be different based on the cellular contexts (Fig. 4.4) suggesting that cellular connections both cell-cell and cell-ECM and thus differential intercellular tension, dictate the keratin network organization. Evidently, in the migrating tissues, such as the mesendoderm and the ectoderm, which have an anisotropy of cellular adhesions the keratin network organization in the leading cells versus the back-row cells was distinctly different (**Fig. 4.2, 4.3 and 4.4**). The front row cells of the tissues have a defined subcellular localization of keratin filaments and keratin precursors. The keratin filaments preside at the back of cells near the cell-cell contacts whereas the keratin precursor particles predominate in the lamellipodia (**Fig. 4.2, 4.3**). Similar intermediate filament network organization for both vimentin and keratin has been

observed previously (Helfand et al., 2011; Kölsch et al., 2009). In order to understand the mechanism behind such a distinct subcellular localization of the keratin network, it is important to identify the functional roles of both the keratin filaments and keratin precursor particles in these tissues. While the exact origin of keratin particles in the morphogenetically active tissues of *Xenopus* is still to be determined. It is likely that some of these may represent newly synthesized precursors since similar accumulation of keratin precursors is seen in the peripheral regions of epithelial cells during network biogenesis (Windoffer et al., 2004, 2006; Wöll et al., 2005; Yoon et al., 2001). Even in the present study, both mesendodermal and ectodermal tissues exhibit retrograde movement of small particles further fusing to form squiggles or short filaments and eventually merging to form mature filaments (**Fig. 4.2 and 4.3**). The other possibility is that at least some of these keratin precursors in the lamellipodia arise from disassembly of existing keratin filaments. This disassembly most likely is induced by protein kinases, since phosphorylation of keratin filaments is known to affect their assembly states and organization (Omary et al., 1998). Some of the kinases that induce phosphorylation dependent reorganization of keratins include PKC δ (Ridge et al., 2005), PKC ζ (Sivaramakrishnan et al., 2009), MEK-ERK (Busch et al., 2012), p38-mitogen activated kinase (Feng et al., 1999), c-Jun N-terminal kinase (JNK) (He et al., 2002). Furthermore, based on the observation made here and in previous studies, that both vimentin filaments and keratin filaments are always absent from the protrusions one can speculate that polymerized intermediate filaments locally suppress the formation of protrusions, aiding in the establishment of directional cell migration. In further support to this hypothesis is the correlative evidence suggesting that

keratin filaments reorganize to the posterior of the cell and establish cell directionality upon cadherin mediated stress application (Weber et al., 2012).

In contrast to the peripheral keratin filaments, keratin filaments that were linked to the cell-cell contacts were more resistant to disruption by small molecular inhibitors withaferin A and acrylamide. In comparison with acrylamide, WFA exhibited a drastic keratin inhibitory activity. The present study describes an extensive comparative study with the above-mentioned small molecule inhibitors. The results presented here show that the effect of the drug, concentration and time of drug application. The present and previous studies (Eckert, 1985; Grin et al., 2012; Sager, 1989) unambiguously demonstrate that these drugs not only affect other IFs but also other cytoskeletal networks and have cell-wide effects. Furthermore, attempts to understand the functional role of keratins in genetic models have failed largely due to functional redundancy and complexity within the keratin family, generation of exogastrulation and embryonic lethal embryos. These limitations further emphasize the need to develop reliable specific inhibitors to intermediate filaments.

Therefore, a large part of this study was to establish specific tools to inhibit keratin filaments with spatiotemporal specificity and thus analyze their function during early embryogenesis. The vimentin 2B2 peptide, interferes with intermediate filament assembly (Strelkov et al., 2002). This peptide disrupts the IF network to unit length filaments rather than smaller identifiable units (Helfand et al., 2011). Similar, keratin 2B2 mimetic peptides also inhibit both assembly of intermediate filaments and disrupt preassembled filaments

(Hatzfeld and Weber, 1992). *In vivo* microinjection of vimentin 2B2 peptides disrupts vimentin filaments to unit length filament like structures (Helfand et al., 2011). In this study, using a keratin 2B2 peptide similar in length to Hatzfeld and Weber, keratin filament disruption, collapse and aggregation were observed upon photo-stimulation of PA-2B2. The detailed mechanism of this disruption remains unclear at present. Nonetheless, using the *Xenopus* krt8 2B2 I developed a photoactivatable-2B2 which can be acutely activated by blue light stimulation to disrupt keratin filaments and an open-2B2 which is a constitutively active inhibitor to keratin filaments.

Unlike, the small molecule inhibitors WFA and acrylamide (Chapter 5) used to disrupt keratins the photoactivatable tools developed here have far more advantages. The most important, the use of light, which affords a spatiotemporal and noninvasive control over disruption of keratin filaments. Moreover, by controlling area of irradiation, the extent of keratin disruption can be regulated. Contrary, with the use the chemical inhibitors it was noted that disruption of keratin filamentous network was cell-wide and lacked spatiotemoral specificity. Thus, with the use of PA-2B2 more targeted disruption can be achieved rather than a widespread one, enabling teasing out precise roles of keratin filaments not only in specific cellular compartments but also specific biological processes. Unlike chemical inhibitors which lack specificity to IFs, PA-2B2 specifically targets K18 and induces disruption of keratin filamentous network. Both WFA and acrylamide are known to have non-specific cellular effects which can be avoided by using PA-2B2 as a disruptor of IFs. Furthermore, even though the detailed mechanism of action is not known

for either of the inhibitors, PA-2B2 most likely affects filament formation and stability, however the chemical inhibitors could be affecting both the intermediate filament protein and filamentous network. Along with specifically targeting keratin filamentous network, PA-2B2 has utility in studying keratin filament function in morphogenetically active tissues during development; such an introspection of keratin filaments cannot be done with small molecule inhibitors.

The keratin filaments have critical importance in *Xenopus* early embryogenesis, as revealed by the use of PA-2B2 and open-2B2. Striking similarities were observed between the gastrulation phenotypes induced by keratin disruption (**Fig. 7.4, 7.5, 7.7**), FN loss of function studies (Marsden and DeSimone, 2001; Ramos, 1996; Rozario et al., 2009), and PG morphant embryos (Hirsh et al., 2018). The embryos displayed exogastrulation along with more severe defects as they progressed through gastrulation and beyond. In the bisected gastrulae it was also observed that occasionally the blastocoel was more spherical rather than the normal hemispheric appearance (**Fig 7.7**). This change in the shape of the blastocoel is indicative of a more symmetrical tension in the perimeter of the blastocoel, instead of the normal asymmetrical tension between the blastocoel roof and blastocoel floor. Additionally, FN did not efficiently assemble into fibrils along the roof of BCR when specific disruption of keratin filaments was induced by light stimulation of PA-2B2 or expression of open-2B2 (**Fig. 7.8**). These results strongly suggest a role for keratin filaments in FN fibrillogenesis during early embryogenesis (**Figure 8**). The assembly of FN into fibrils is dependent on cell tension at cell-cell and cell-matrix adhesions and

transduced through cytoskeleton (Dzamba et al., 2009; Pankov et al., 2000). Since keratin filaments are known to associate with C-cadherin in *Xenopus* embryos at this stage of development (Weber et al., 2012), the function of keratin filaments in FN fibrillogenesis is likely through keratin-cadherin mediated tension. Plakoglobin anchors both actin filaments via actin-binding proteins such as α -catenin (Nieset et al., 1997) and keratin filaments (Weber et al., 2012) to cadherin adhesions. Parallel observations were recently made in regards with developmental phenotypes and FN fibrillogenesis, in both PG morphants (Hirsh et al., 2018) and during keratin filamentous network disruption by PA-2B2 or open-2B2 in our work shown here. Together, this suggests that disruption of keratin filamentous network perturbs plakoglobin-cadherin mediated FN fibrillogenesis and thus morphogenetic movements during *Xenopus* gastrulation. Additionally, Rac1 and Pak signaling in relation to cadherin adhesions and tissue tension have been implicated in FN fibrillogenesis (Dzamba et al., 2009; Hirsh et al., 2018). Perturbation of Rac1 and Pak signaling leads to actin reorganization and affects myosin contractility, culminating in defective FN fibrillogenesis (Dzamba et al., 2009). The transmission of actin- and myosin-dependent tension via integrin $\alpha_5\beta_1$ promotes FN fibril assembly (Baneyx et al., 2002; Pankov et al., 2000; Wu et al., 1995; Zhong et al., 1998). The effects of perturbation of Rac1 and Pak on keratin filaments are unknown. However, disruption of keratin network leads to dramatic reorganization of actin network and altered myosin contractility (Sonavane et al., 2017). Nonetheless, despite the apparent compensatory reorganization of actin filaments in response to keratin knockdown or keratin filament disruption, actin is unable to rescue the morphogenetic consequences of keratin perturbations (Sonavane et al., 2017; Weber et al., 2012, Fig. 7.6 & 7.7). These studies make it appealing to speculate that

disruption of the filamentous keratin network interrupts the local tension transmitted by keratin-cadherin mechanosensitive complex to $\alpha 5 \beta 1$ integrin bound to FN dimers, causing the failure of FN fibril assembly. Consequently, this absence of FN fibrillogenesis affects the morphogenesis during early development and introduces defects in the embryos.

In summary, the study demonstrates that keratin IFs have definitive subcellular domains, such that keratin filaments reside in the rear and the sides of the cells and keratin precursors populate the front during migration. Nonetheless, keratins are resistant to disruption by small molecule drugs such as withaferin A and acrylamide in the presence of cell-cell contacts. Here, I report the engineering and application of a photoactivatable inhibitor to keratin filaments. By employing these novel tools, an important role of keratin filaments in normal morphogenesis during *Xenopus* embryonic development has been identified.

Future experiments will determine the contribution of intermediate filaments to morphogenetic movements in other tissues. Furthermore, we now have the capability to examine the role of intermediate filaments in stages beyond gastrulation by simply waiting to expose embryos to blue light until developmental stages of choice. With the flexibility of both spatial and temporal disruption using PA-2B2, the utility of PA-2B2 for examining functional developmental roles of intermediate filaments is limitless.

Figure 8

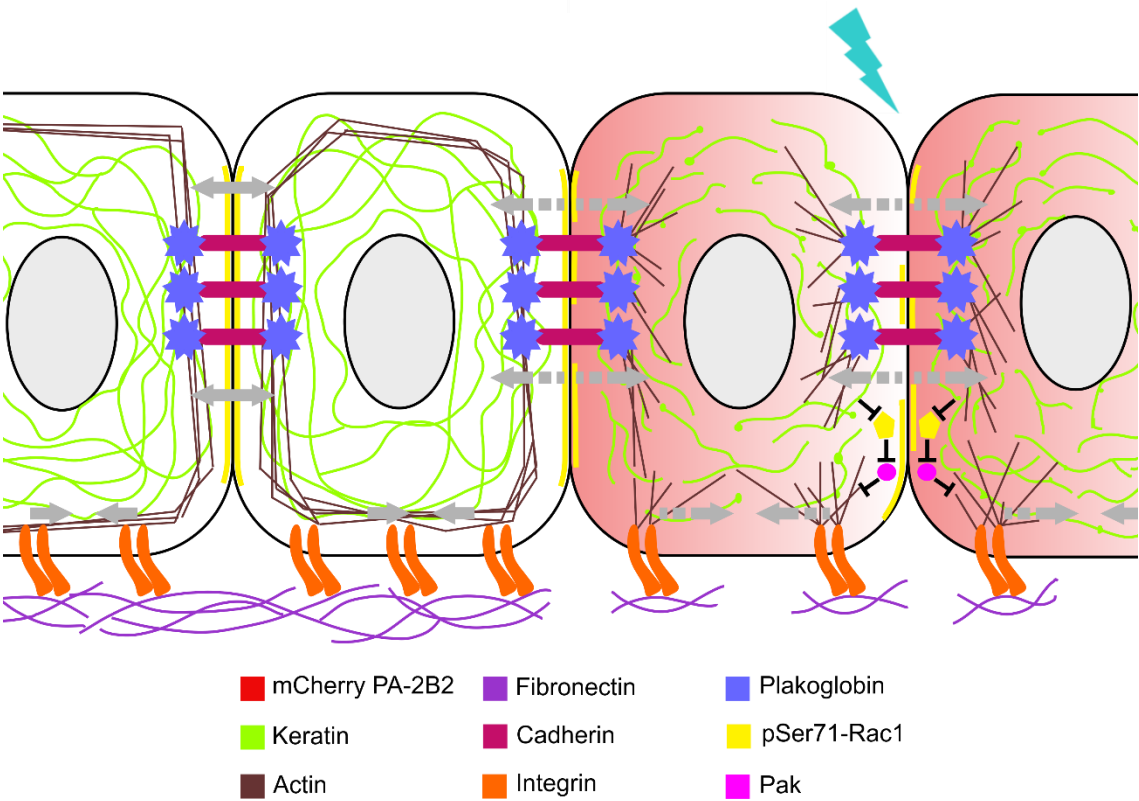


Figure 8 Role for keratin filaments in fibronectin fibrillogenesis during early embryogenesis.

During gastrulation, fibronectin fibrillogenesis is regulated by keratin filamentous network. Cells of the ectodermal tissue pull on each other through cadherin adhesions to increase local mechanical tension. Cadherin dependent forces recruit keratin filaments to cadherin adhesions in a PG-dependent fashion. Along with keratin filaments, PG/ α -catenin additionally anchors actin filaments to cadherin adhesions. Tissue tension increases as cell-cell cadherin adhesions result in reorganization of cortical actin cytoskeleton, which are contractile actin-myosin filaments. The cytoskeletal tension is transmitted to integrin $\alpha 5 \beta 1$ with bound FN dimers which causes the clustering of integrins and formation of FN fibrils from pericellular FN that initially assembles at cell-cell boundary in a Rac1/Pak dependent process. Light induced specific disruption of keratin filamentous network perturbs FN fibrillogenesis. Specific disruption of keratin filaments perturbs the local mechanical tension and thus affects the efficient transmission of force to integrins needed to promote FN fibril assembly. This in part could be by altered actin organization, since knockdown of IFs results in drastic reorganization of actin network. Disruption of keratin filamentous network also reduces the localization of pSer71-Rac1 at cell-cell boundary, which in turn would affect the Rac1 dependent crosstalk between cadherin and integrin adhesions. Concomitantly perturbing the Rac1/Pak dependent contractile event required for translocation of integrin bound FN

dimers from sites of cell-cell contacts and thus affecting the FN fibril assembly which then remains pericellular.

Future directions

This study has led to the following key questions:

1. *Here, the subcellular localization of keratin filaments in the mesendodermal and ectodermal tissue has been shown, however what are their precise functional roles during migration?*
2. *Whether keratins, specifically in their filamentous state, negatively regulate Rac1 activity to establish cellular non-protrusive behavior?*
3. *To rationally improve the PA-2B2 photoswitch for applicability across other cell systems.*
4. *I show that the photoactivatable proteins are effective tools in vivo, however these tools can be further developed to specifically inhibit other classes of intermediate filaments, for example lamins, for a wide application in biology.*

1. Keratin filament polymers establish protrusive polarity essential for directed migration

The data presented in chapter 4, show that keratin precursors and keratin filaments have specific subcellular localization in the front edge cells of the mesendoderm and ectoderm explant. Whereas, the dissociated mesendoderm single cells exhibit frequent presence of long mature filaments throughout the cytoplasm but are definitely absent from the protrusions. Similarly, in fibroblasts, vimentin filaments assemble along the rear and the perinuclear region of the cell whereas nonfilamentous vimentin particles are predominant in the lamellipodial region. Further, targeted disassembly of the vimentin filaments is coincident with the formation of ruffles (Helfand et al., 2011). Whereas, keratin filaments reorganize to the back of the cell and establish cell directionality upon cell-cell adhesion (Weber et al., 2012). Based on these findings; I speculate that this antagonism is not limited to the vimentin network, and that a similar reciprocal relationship between the keratin filaments and protrusive regions of motile cells exists. Thus, polymerized keratin filaments may locally suppress the formation of protrusions. This hypothesis can be tested by using the optogenetic tools, PA-2B2 and open-2B2, engineered and developed here. Light based activation of PA-2B2 can be used to induce specific subcellular disruption of keratin filaments, and thus evaluate contributions of keratin filaments to essential cellular processes such as migration.

2. *Keratin filaments maintain non-protrusive regions of polarized migratory cells by regulating Rac1 activity*

Rac1, a member of the Rho family small GTPase, is a pivotal regulator of protrusion formation. The Rac1 protein is conformationally regulated by the binding of GTP and GDP, such that they exist as an active GTP-bound form and an inactive GDP-bound form. In their active conformation, they interact with their downstream target proteins, which include protein kinases, lipid-modifying enzymes, and activators of the Arp2/3. In response to biochemical signals, Rac1 is activated by guanine nucleotide exchange factors (GEFs) and inactivated by GTPase activating proteins (GAPs). The importance of Rac1 in single cell motility (Ridley 2011) have long been recognized. However, only recently has the function of Rac1 has been investigated in *in vivo* collectives during embryogenesis (Theveneau et al., 2010; Wang et al., 2010).

Rac1 is important for collective cell migration (Ren et al., 2006; Theveneau et al., 2010; Wang et al., 2010; Yamaguchi et al., 2015), since spatial temporal activation of Rac1 promotes both motility and directionality of these collectives. Along with being under tight spatiotemporal control to mediate protrusion formation, Rac1 has been implicated in reinforcement and stabilization of newly formed protrusions. In order to facilitate the onset of new protrusions in the upcoming migratory cycle, Rac1 maintains a significant level of activity during the retraction phase of the cycle (Machacek et al., 2009). However, at the rear end of the cell the initial elevated level of Rac1 activity at the site of cell-cell contact

is rapidly suppressed (Yamada and Nelson, 2007), implicating cadherins (Kitt and Nelson, 2011) and plakoglobin (Todorović et al., 2010) as negative regulators of Rac1 activity. Both these proteins are required by keratin filaments to maintain cell protrusive behavior and directional migration (Weber et al., 2012). In keratin morphants, the Rac1 activity gradient gets disrupted (Sonavane et al., 2017), further suggesting a relationship between Rac1 and keratins. Moreover, targeted Rac1 activation induces disassembly of keratin filaments, which is coincident with the local membrane ruffling at the edges of mesendoderm explants (Sonavane et al., 2017). Likewise, in single migrating fibroblasts the vimentin IFs and Rac1 are reciprocally inhibitory to each other (Helfand et al., 2011). However, it is unknown whether keratins, specifically in their filamentous state, negatively regulate Rac1 activity to establish cellular non-protrusive behavior.

In contrast to the importance of active Rac1 in lamellipodia formation, phosphorylation of Rac1 at serine 71 negatively affects its activity by modulating its downstream effector binding and thus the ability of Rac1 to stimulate protrusion formation (Schwarz et al., 2012). To steer from random to persistent migration, Rac1 activity must be reduced in the peripheral lamellae (Pankov et al., 2005), suggesting optimal levels of active Rac1 in specific subcellular domains are critical for migration. Presumably, Rac1 in the front end and p-Ser71-Rac1 at the rear function to maintain migratory polarity. Therefore, I hypothesize that assembled keratin filaments at cell-cell contacts regulate pSer71-Rac1 expression.

Preliminary results

Localization of pSer71-Rac1 is influenced by cell-cell contacts

To initiate these studies, density dependent regulation of pSer71-Rac1 expression was investigated. Increased levels of pSer71-Rac1 correlate with high confluent MDCK cultures (**Fig. 8.1A**). Indicating that cell density and therefore cell-cell contacts trigger the increased expression of pSer71-Rac1. Therefore, the localization of pSer71-Rac1 in a variety of cell-cell contacts was examined. WT MDCK cells were plated sparsely to obtain single cells, cell pairs and cell clusters. Next, the cells were immunolabelled using antibodies against keratin, pSer71-Rac1 and counterstained with Hoechst dye. In contrast to the cytoplasmic localization of pSer71-Rac1 in single cells, pSer71-Rac1 localized at cell-cell contacts in cells pairs and cellular clusters (**Fig. 8.1B**).

Acute disruption of keratin filaments reduces pSer71-Rac1 localization at cell-cell contacts

To test the hypothesis, the expression of pSer71-Rac1 was analyzed after disruption of the keratin network using small molecular inhibitors. WT MDCK cells were plated at different density and the expression of pSer71-Rac1 before and after 6.0 μ M WFA or 6 mM acrylamide treatment was determined. Here, the keratin organization and the expression of pSer71-Rac1 were examined using a pan-keratin antibody and antibody specific for pSer71-Rac1 respectively. Confocal images of control samples showed localization of p-

Ser71 Rac1 at cell-cell contacts of MDCK cells (**Fig. 8.2A, B**). Whereas, following 6.0 μ M WFA or 6.0 mM acrylamide treatment for 1 hr, pSer71-Rac1 staining was perturbed (**Fig. 8.2A, B**). To quantify such alterations, average pixel intensity of pSer71-Rac1 staining at the cell-cell contacts was measured. Next, ratio of intensity in treated cells to intensity in control cells was calculated. As shown in **Fig. 8.2A, B** keratin filament disruption correlates with pSer71-Rac1 staining and a significant reduction in average staining intensity at cell-cell contacts (**Fig. 8.2C**). In WFA treated cells pSer71-Rac1 signal intensity (0.59) was weakened at cell-cell contacts in cell pairs, whereas marginal cells had moderate intensity (0.73). Since WFA had least effect on the keratin network of submarginal cells, pSer71-Rac1 fluorescence intensity was also not reduced as much (0.98). Similar pattern of staining was observed when MDCK cells were treated with 6.0 mM acrylamide for 1 hr, with ratio of staining intensity for cell pair: 0.76, marginal cells: 0.94 and submarginal cells: 1.35. Taken together, the data indicates that the keratins are involved in regulating pSer71-Rac1 expression at cell-cell contacts.

Specific disruption of keratin filaments reduces pSer71-Rac1 localization at cell-cell contacts

Previously, it was shown that disruption of keratin network alters pSer71-Rac1 expression which is dependent on the cell density. This suggests that keratins have a functional role in maintenance of non-protrusive regions of cells by negatively regulating Rac1 activity via pSer71-Rac1. To examine the role of keratin filaments in regulating pSer71-Rac1, keratin

filaments were disrupted in MDCK cells using open-2B2. MDCK's were plated at different density and expression of pSer71-Rac1 in control and transfected cells was determined using an antibody specific for pSer71-Rac1. In contrast to the control samples and cells expressing PA-2B2 (not activated) that showed localization of p-Ser71 Rac1 at cell-cell contacts of MDCK cells (**Fig. 8.3A, B**), cells expressing open-2B2 display perturbed pSer71-Rac1 staining along with disruption of keratin filaments (**Fig. 8.3C**). pSer71-Rac1 staining throughout cell-cell interface had a discontinuous distribution. Also, it was difficult to discern from which side of the cell-cell adhesion the pSer71-Rac1 staining had accumulated. To quantify such alterations, average pixel intensity of pSer71-Rac1 staining at the cell-cell contacts was measured in mCherry positive cells and control cells within the same image. Next, ratio of intensity in mCherry positive cell to intensity in control (mCherry negative) cells was calculated. The pSer71-Rac1 signal intensity was weakened at cell-cell contacts, such that ratio of fluorescence staining intensity for mCherry open-2B2: 0.8 and mCherry PA-2B2: 1.0. Thus, the reduction in signal intensity is reciprocal to the extent of keratin disruption in the cells. Taken together, the data indicates that the keratin filaments are involved in regulating pSer71-Rac1 expression.

Figure 8.1

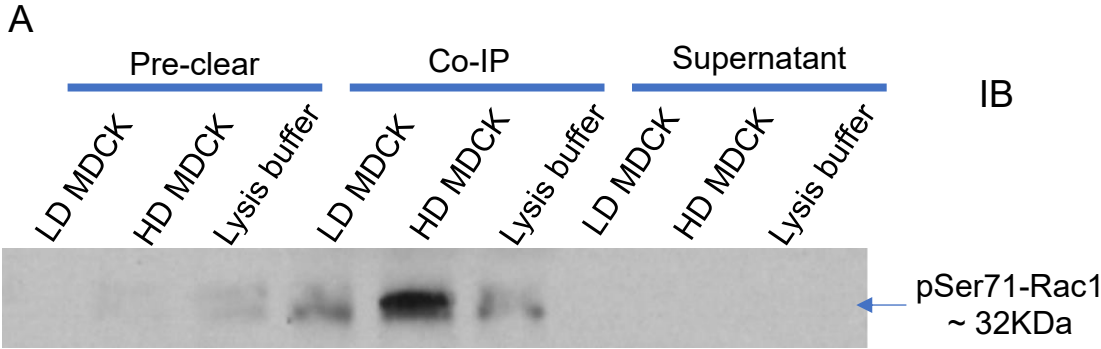


Figure 8.1

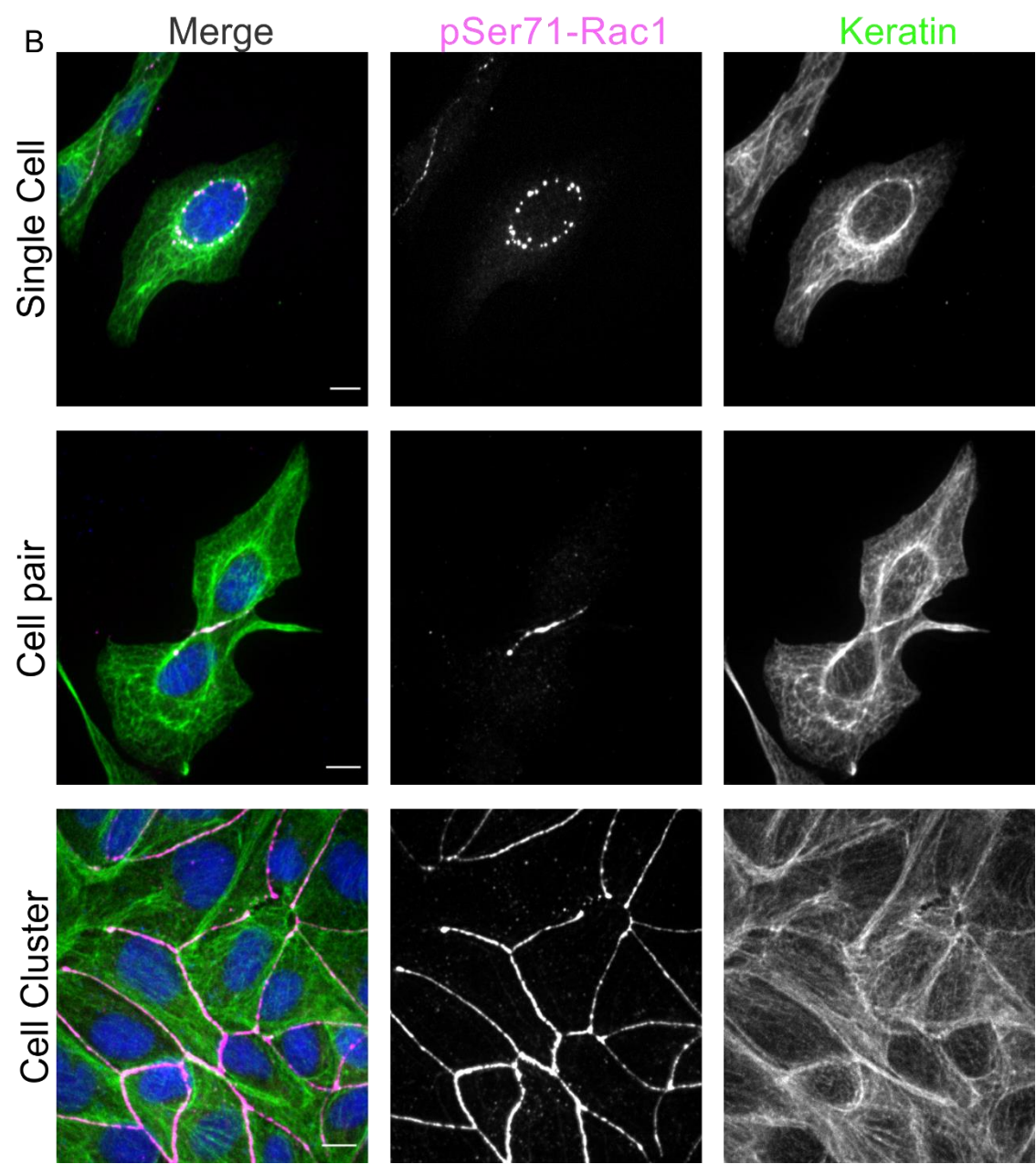


Figure 8.1: Localization of pSer71-Rac1 is influenced by cell-cell contacts.

(A) Increase in expression of pSer71-Rac1 is dependent of cell density. WT MDCK cells were harvested at low density (0.5×10^6) and high density (1.5×10^6) and lysates were subjected to coimmunoprecipitation with anti Rac1 antibody, followed by immunoblotting to detect precipitation of pSer71-Rac1. Representative blot image is of one independent experiment.

(B) pSer71-Rac1 localization is dependent of the presence of cell-cell contacts. pSer71-Rac1 localization was examined in WT MDCK cells with varying degree of cell-cell contacts. Cells were immunostained with pan-keratin, anti-pSer71-Rac1 and counterstained with Hoechst dye. Bars, $10\mu\text{m}$

Figure 8.2

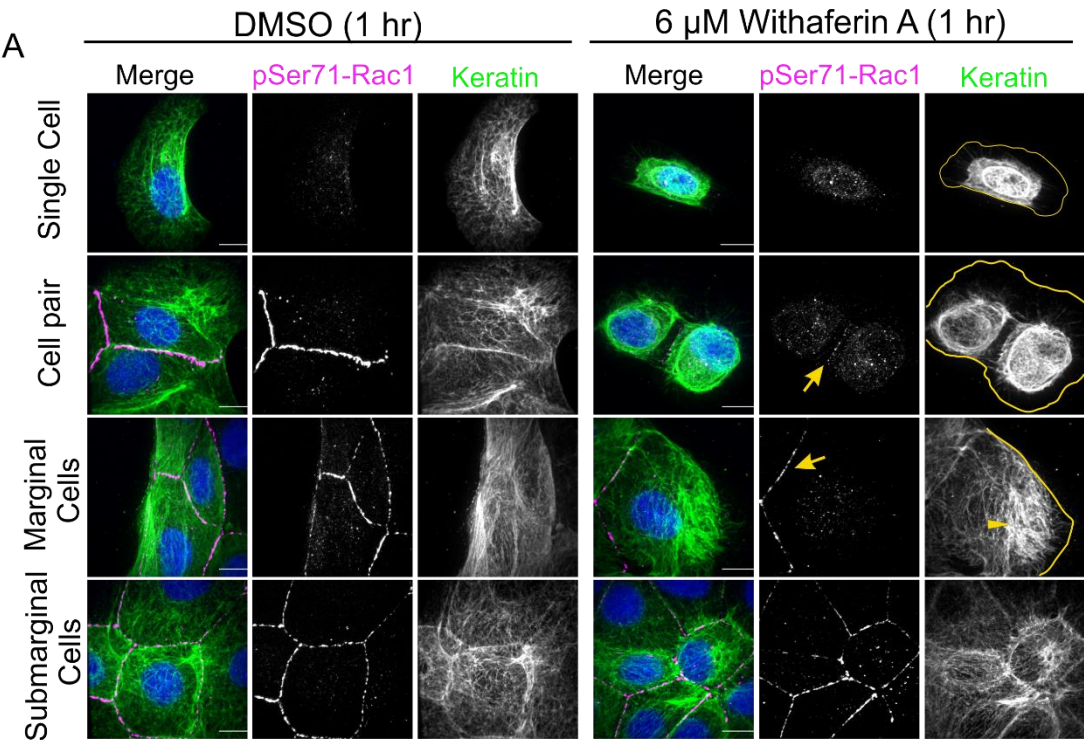


Figure 8.2

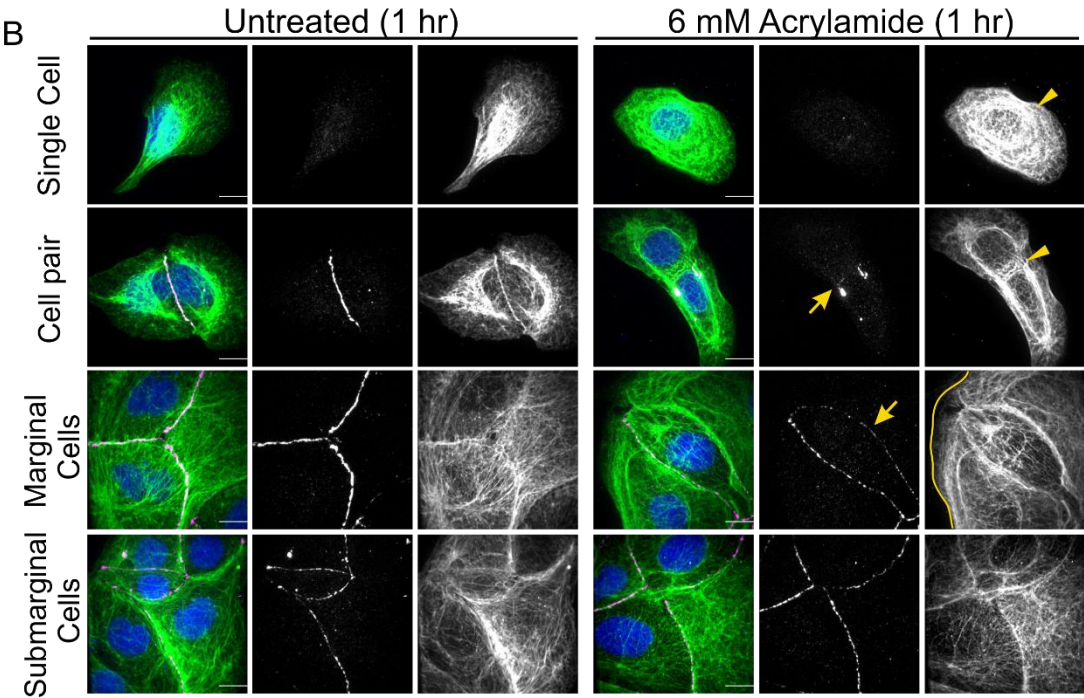


Figure 8.2

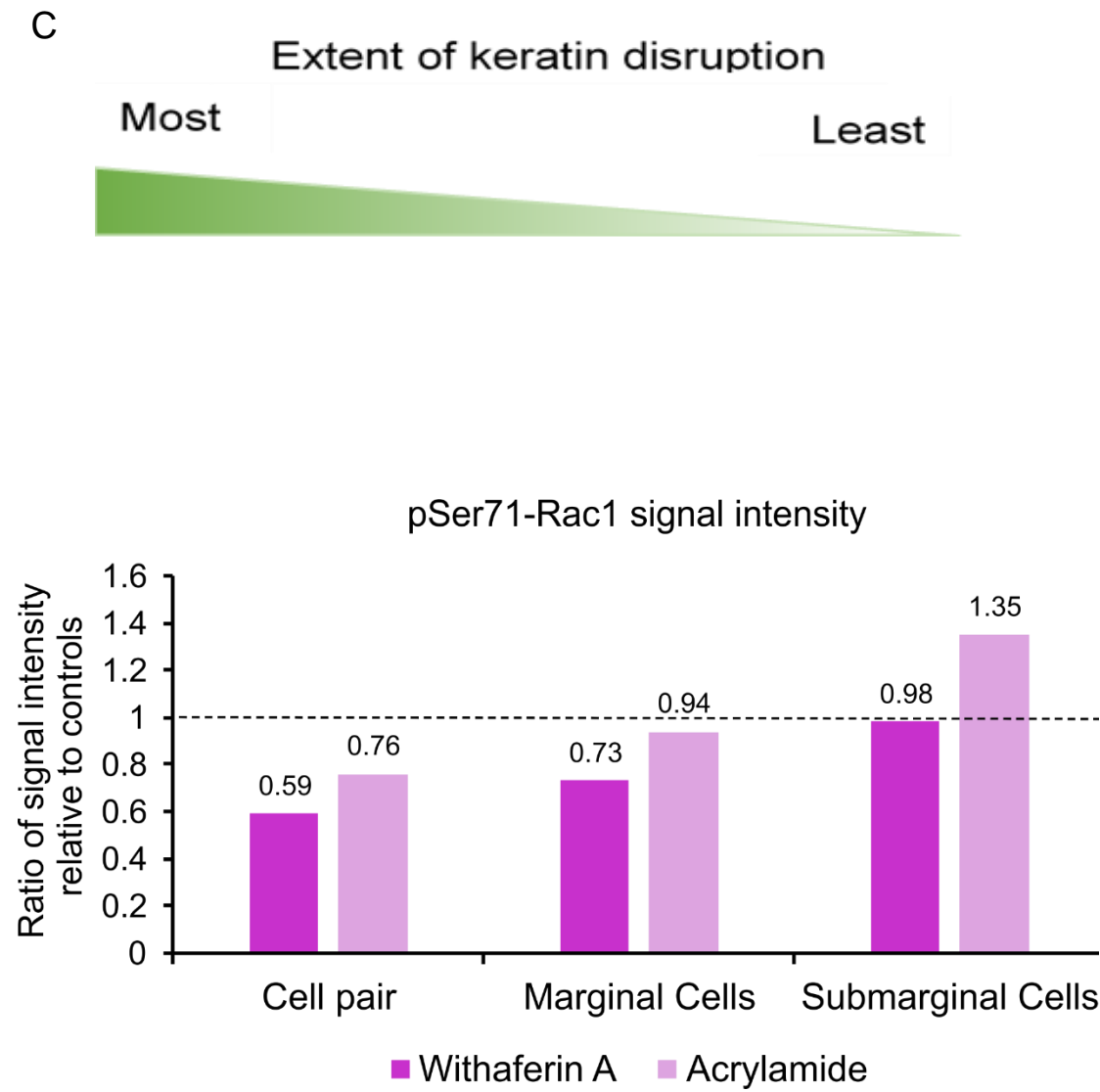


Figure 8.2: Acute disruption of keratin filaments alters pSer71-Rac1 localization at cell-cell contacts.

Immunofluorescence images of WT MDCK cells exposed to 6.0 μ M WFA (**A**) and 6.0 mM acrylamide (**B**). Methanol fixed cells post 1hr treatment were double stained with pan-keratin and pSer71-Rac1 antibodies and counterstained with Hoechst dye. Keratin network (green) organization, pSer71-Rac1 (violet) and nuclear (blue) morphology were examined using Zeiss Cell Observer spinning disk confocal microscope (63X/1.4 NA, 1.0X optovar). Confocal images (maximum intensity projections of 0.25-0.28 μ m thick optical sections) of control (untreated cells and DMSO treated) images show cell density dependent localization of pSer71-Rac1 at cell-cell contact sites, whereas, inhibitor induced disruption of keratin filaments (**arrowheads**) reduce pSer71-Rac1 signal intensity at cell-cell contacts (**arrows**). Quantitative representation of ratio of signal intensity of pSer71-Rac1 (inhibitor/control) (**C**). Panels show representative images of two independent experiments. (DMSO, n=116; WFA, n=220; untreated n=68; acrylamide, n=120). Bars, 10 μ m

Figure 8.3

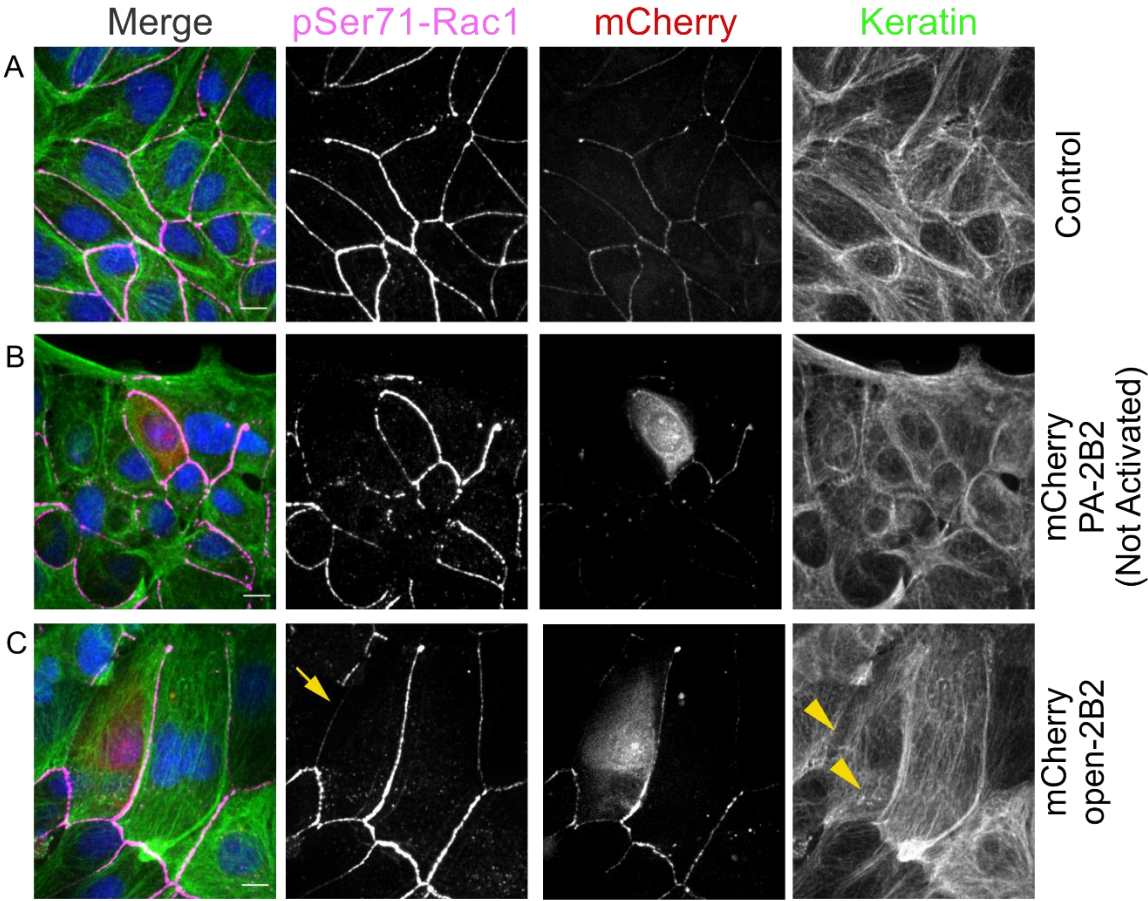


Figure 8.3

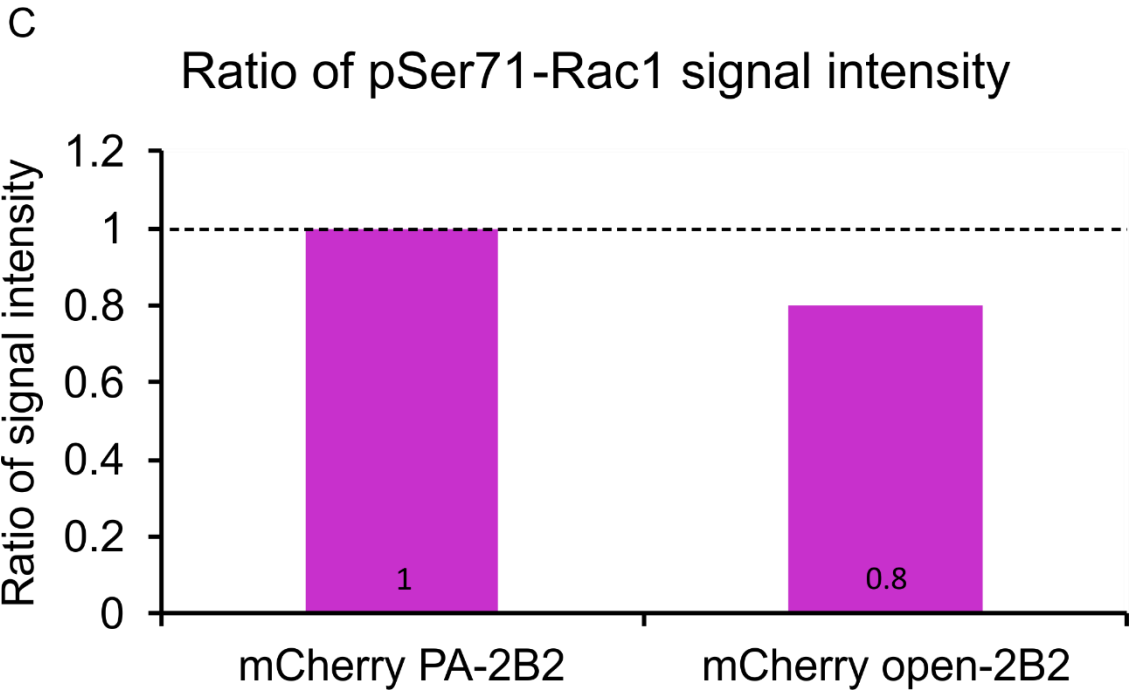


Figure 8.3: Specific disruption of keratin filaments reduces pSer71-Rac1 localization at cell-cell contacts.

pSer71-Rac1 localization at cell-cell contacts was observed in WT MDCK cells transfected with mCherry (control) (**A**); mCherry open-2B2 (**B**); mCherry PA-2B2 (**C**), 12 hrs post transfection. Confocal images (maximum intensity projections of 0.28 μm thick optical sections) of cells fixed and double stained with pan-keratin and pRac1(ser71) antibodies and counterstained with Hoechst dye show localization of pSer71-Rac1 at cell-cell contact sites in control cells. Whereas, 2B2 peptide induced disruption of keratin filaments (**arrowheads**) reduce pSer71-Rac1 signal intensity at cell-cell contacts (**arrows**). Keratin network (green) organization, p- Ser71-Rac1 (violet) and nuclear (blue) morphology were examined using Zeiss Cell Observer spinning disk confocal microscope (63X/1.4 NA, 1.0X optovar). Ratio of signal intensity of pSer71-Rac (mCherry positive/ mCherry negative) in cells expressing 2B2 modules (**E**). Panels show representative images of two independent experiments. Bars, 10 μm

Discussion

Disruption of the keratins either by inhibitor treatment or specifically by the open-2B2 reduces the localization of pSer71-Rac1 at cell-cell contacts. This observation is particularly interesting, since local activation of PA-Rac1 induces retraction and disruption of intermediate filaments into smaller subunits of IFs such as squiggles and precursors with subsequent lamellipodia formation (Helfand et al., 2011; Sonavane et al., 2017). Such a reciprocal relationship between keratin and Rac1 suggests that polymerized keratin filaments relocalized at the cell contacts most likely regulate Rac1. Understandably, phosphorylation of active Rac1 would be a convenient switch to temporarily inhibit PAK1 dependent protrusion formation (Schwarz et al., 2012) during migration. Taken together, a model emerges suggesting a mechanism for establishing migratory polarity. Keratin filaments at the rear establish non-protrusive region by regulating pSer71-Rac1 and thus inhibiting local Rac1, whereas keratin precursors in the front maintain the protrusion permissive region. Thus, the results presented here indicate the involvement of pSer71-Rac1 in maintaining the cells non-protrusive regions via keratin filaments.

3. To rationally improve the PA-2B2 photoswitch for applicability across other cell systems.

The photoactivatable tools are in an equilibrium between “on” and “off” and therefore, even in the dark state there is an equilibrium amount of activated peptide present inhibiting the keratin filaments. This “leakiness” requires careful titration of the protein expression levels. High expression levels of PA-2B2 was sufficient to cause disruption even in dark conditions, similar to open-2B2. It was apparent in all cell types that PA-2B2 did not disrupt keratin filaments in dark or under moderate expression levels. Lower and uniform expression levels could be achieved by adding the tetracycline inducible component in the plasmids. Using this approach expression levels can be regulated through titration of doxycycline. Both by suppressing the expression of PA-2B2 until the onset of the experiment and acquiring optimal expression levels the PA-2B2 activity in dark can be minimized. Additionally, the efficiency of PA-2B2 can be further improved upon by introducing appropriate mutations to enhance the caging in dark. Helix stabilizing mutations in the LOV domain should effectively decrease the undesirable low-level activity even in dark. For example, mutations (G528A and N538E) in the J α domain stabilized the docked LOV-J α , and thus improved the photoswitch LovTAP (Strickland et al., 2010). Similarly, mutation I532A have also shown to increase helix docking and improve dynamic photoswitching (Strickland et al., 2010). Mutations that stabilize the interactions between LOV β -sheet and J α -helix have also been utilized previously to improve the photoswitching dynamic range. Set of mutations (L514K and L531E) replace the hydrophobic residues, one in the J α helix and the other in the β -sheet and thus enhance

the caging of LOV-ipaA photoswitch (Lungu et al., 2012). Likewise, mutations T406A and T407A increased helix docking in the dark state and thus improving the caging of the photoswitch (Strickland et al., 2012). Alternative and/or combination of mutations described above should be further tested to stabilize the LOV-J α docking and thereby modulate the PA-2B2 effector activity in dark. Furthermore, additional analysis needs to be done in cell types with multiple intermediate filaments to ensure if PA-2B2 disrupts just keratin network or other networks such as vimentin too.

Table 8.1: List of mutations that improve caging of LOV-J α domain

Mutations	References
G528A	(Strickland et al., 2010)
N538E	(Strickland et al., 2010)
I532A	(Strickland et al., 2010)
T406A and T407A	(Strickland et al., 2012)
L514K and L531E	(Lungu et al., 2012)

4. *Keratin 8 mimetic 2B2 modules can potentially be employed to study lamin function*

Lamins are members of intermediate filament proteins that form a nuclear lamina at the nuclear periphery. Lamins are classified as type V intermediate filament proteins, which include A-type lamins (lamin A and C) and B-type lamins (lamin B1 and lamin B2). The major constituents of the lamina are A-type and B-type lamins. B type lamins are expressed in nearly all cells, while, the expression of A-type lamins is developmentally regulated. Similar to all IF proteins, lamins too have three domains, an N-terminal head domain, a central rod domain and a C-terminal tail domain. Some of the unique features of lamin proteins are, a nuclear localization signal (NLS), an immunoglobulin fold in the C-terminal and a carboxyl tail CaaX (C = cysteine, a = aliphatic amino acid, X = any amino acid) motif. Like cytoplasmic IF vimentin, lamins form distinct homodimers *in vivo* and the dimerization is driven by the helical rod domain. To form mature lamin filaments, the lamins also follow the similar assembly hierarchy as the cytoplasmic IFs. Lamins have multiple functions such as nuclear organization, chromatin organization, gene regulation, genome stability, mechanical stability and differentiation. To date many mutations have been found in nuclear lamins, especially lamin A, that cause a wide range of diseases, called ‘laminopathies’ (Dechat et al., 2010; Ho and Lammerding, 2012). Hence it would be highly advantageous to have specific disruptors to lamin filaments enabling the study of these IFs.

Preliminary results

Constitutively active open-2B2 can induce lamin disruption in cultured MDCK cells

The experiments carried out up until now with open-2B2 exhibited aberrant nuclear morphology hinting that these constructs along with keratin also disrupt lamin (Fig. 6.9). Furthermore, sequence comparison analysis also highlights that krt8 mimetic peptides 1A and 2B2 can be used to disrupt lamins (Fig. 6.1B & D). Hence to examine if 2B2 modules could disrupt lamin IFs, MDCK cells transfected with mCherry open-2B2 or mCherry PA-2B2 were methanol fixed and immunolabelled with anti-lamin antibody and counterstained with Hoechst. First of all, gross nuclear and lamin alterations were analyzed in control cells (**Fig. 8.4A**), mCherry open-2B2 (**Fig. 8.4B**) and mCherry PA-2B2 (not activated) (**Fig. 8.4C**). These morphologies were categorized as normal lamin, disrupted lamin and other abnormalities. Finally, cumulative analysis revealed the lamin and nuclear alterations that are caused by 2B2 modules. In comparison to 13% of controls cells (13%) and 7% of cells expressing mCherry PA-2B2 (dark) with disrupted lamins there were 36% of mCherry open-2B2 cells with disrupted lamin (**Fig. 8.4D**). Thus, open-2B2 along with keratin also seem to disrupt lamin IFs.

Constitutively active open-2B2 induces lamin disruption in cultured HEK293T cells

Since HEK293T cells transfected with open-2B2 constructs exhibited altered nuclear morphology (Fig. 6.10), lamin disruption pattern was detected in these cells. HEK293T

cells were transfected with mCherry open-2B2 or mCherry PA-2B2 and immunolabelled with anti-lamin antibody and counterstained with DAPI dye. Coincident with the abnormal morphology these cells also displayed disrupted lamin filaments (**Fig. 8.5**).

Figure 8.4

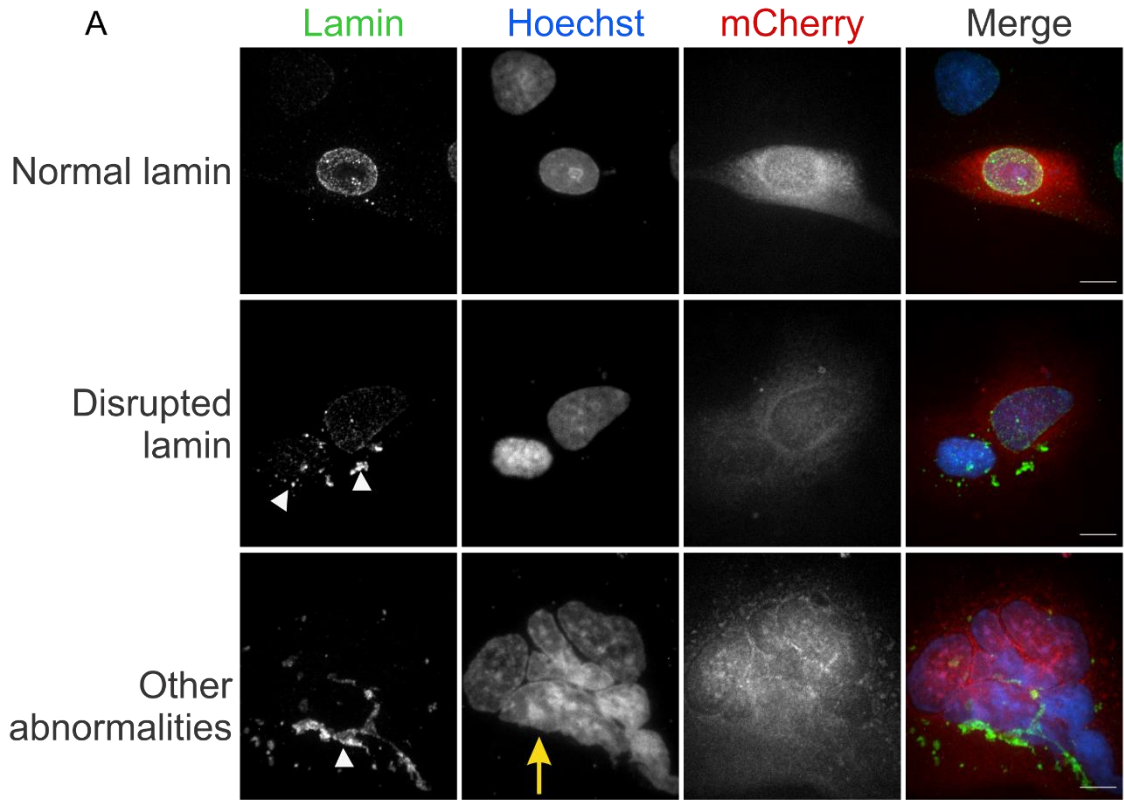


Figure 8.4

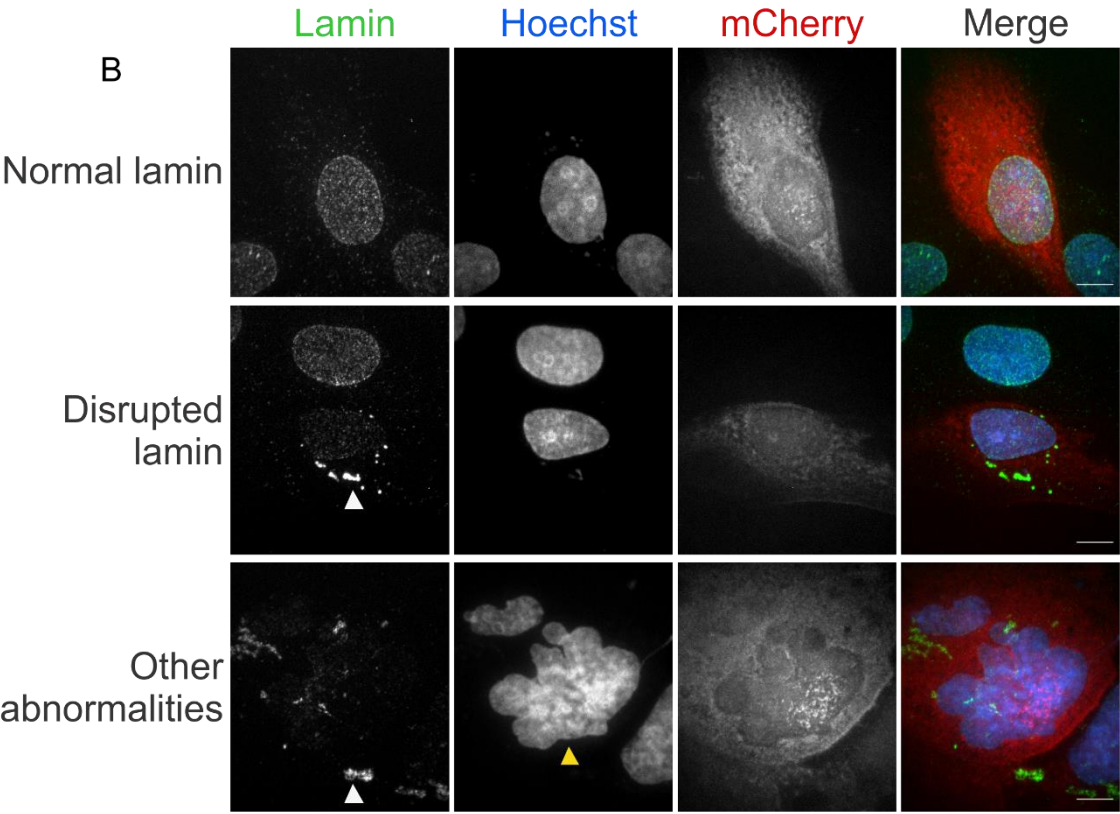


Figure 8.4

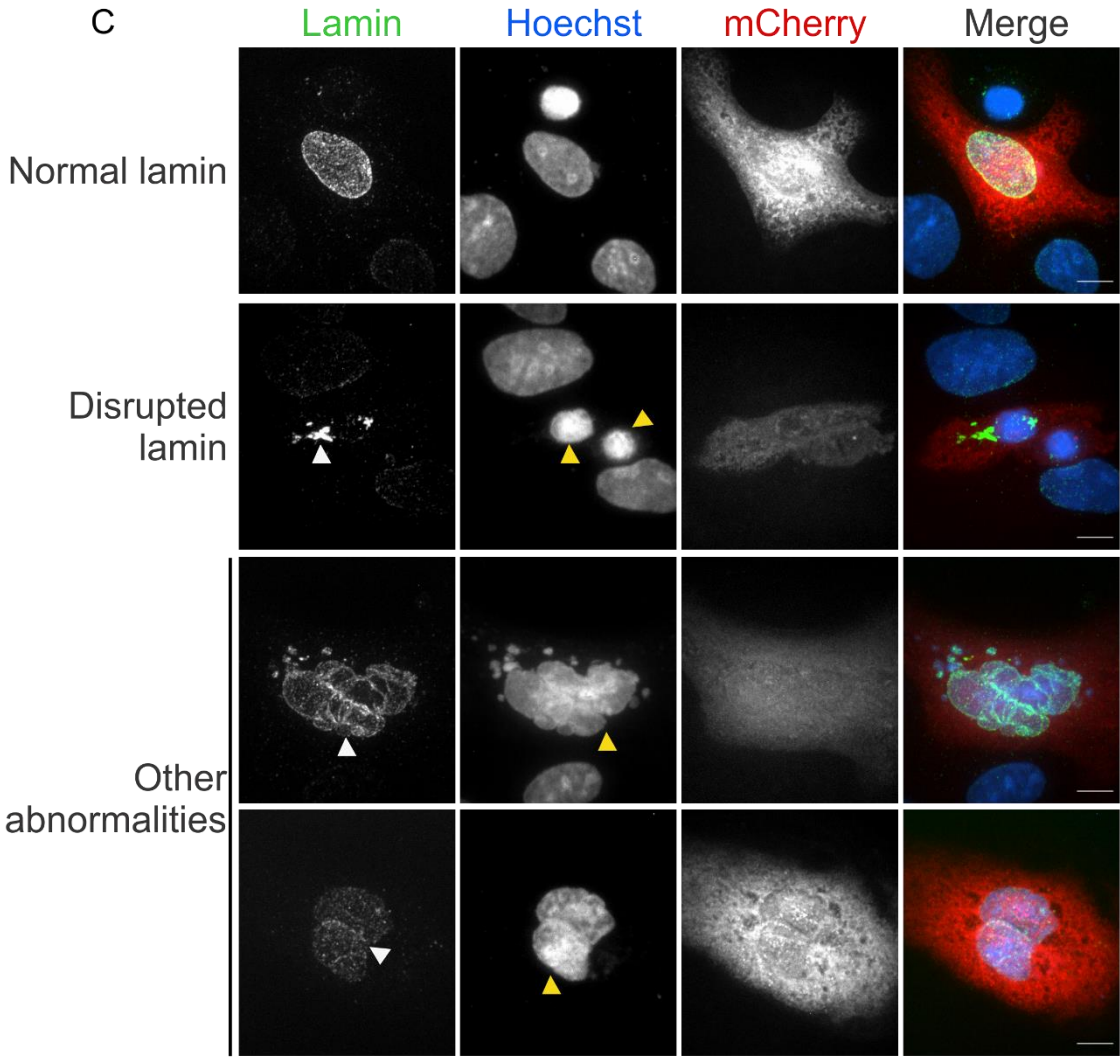


Figure 8.4

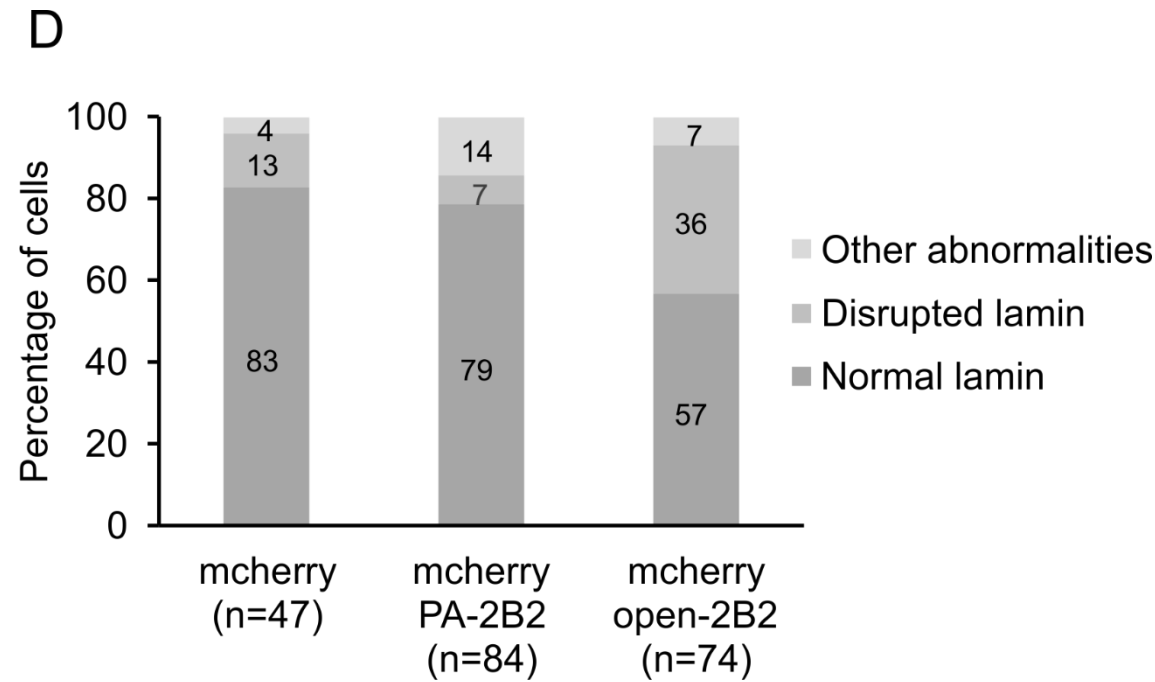


Figure 8.4: Constitutively active open-2B2 induces lamin disruption in cultured MDCK cells.

Lamin network was examined in WT MDCK cells transfected with either control construct (**A**); mCherry open-2B2 (**B**) or mCherry PA-2B2 (not activated) (**C**); 12 hrs post transfection and maintained in dark. Confocal images (maximum intensity projections of 0.23 μm thick optical sections) of cells immunostained with lamin-B antibody and counterstained with Hoechst dye, gauge the range of disruption of the lamin network and aberrant nuclei. Lamin network (green) organization and expression of 2B2 modules (red) was examined using Zeiss Cell Observer spinning disk confocal microscope (63X/1.4 NA, 1.6X optovar). (**D**) Graphical representation of percentage of cells with lamin disruption abnormalities. **Yellow arrowheads** show aberrant nuclear morphology and **white arrowheads** show altered lamin organization. Panels show representative images of two independent experiments. (Control, n= 47; mCherry open-2B2, n= 74; mCherry (C450A)2B2, n= 92; mCherry PA-2B2, n= 84). Bars, 10 μm .

Figure 8.5

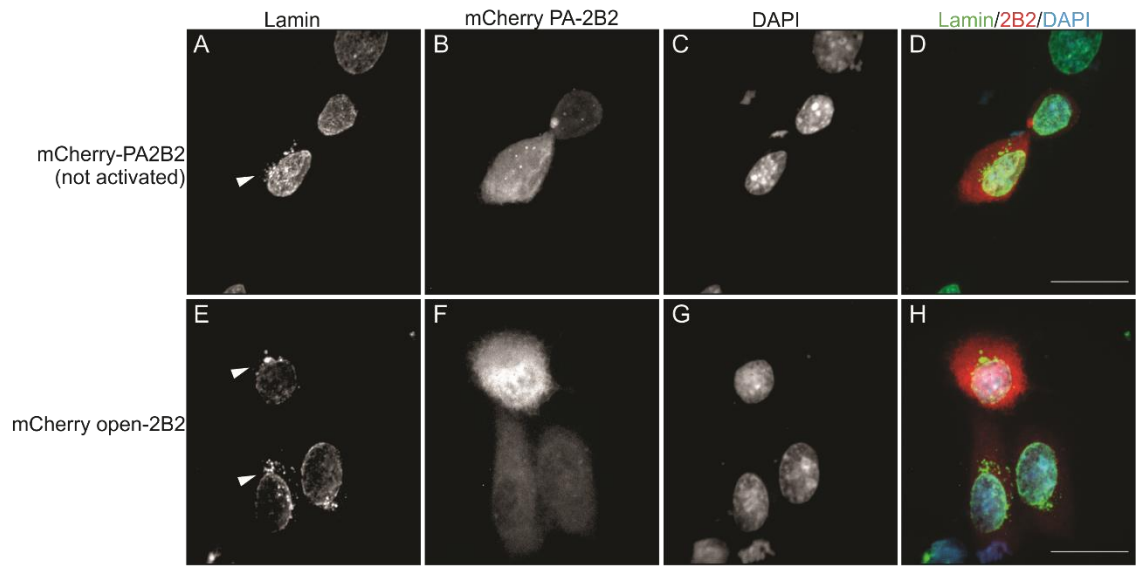


Figure 8.5: Constitutively active open-2B2 induces lamin disruption in cultured HEK293T cells.

Lamin network was examined in WT NIH3T3 cells transfected with either mCherry PA-2B2 (**A-D**) or mCherry open-2B2 (**E-L**), 12 hrs post transfection. Confocal images of cells immunostained with lamin-B antibody and counterstained with DAPI dye, depict the aberrant nuclei and disruption of the lamin network. Lamin network (green) organization and expression of 2B2 modules (red) was examined using Zeiss Cell Observer spinning disk confocal microscope. **White arrowheads** show altered lamin organization. Bars, 20 μ m.

Note: Figure prepared by Jiyeon Baek

Discussion

The preliminary results presented here show that mCherry open-2B2 disrupts lamins and therefore show a range of aberrant nuclear and lamin alterations. *In silico* analysis suggests that NLS sequence resides in the 2B region of the rod domain (Hobbs et al., 2016). The 2B2 sequence used here contains part of the NLS sequence and no NES sequence. Since lamins also show the sequence conservation of the 2B2 segment with the krt8 sequence (Fig. 6.1B), the developed open-2B2 may also be disrupting lamin filaments along with the keratin filaments. The most likely scenario is the passive transport of the krt8 2B2 inhibitory peptides due to their affinity for lamin filaments. This accumulation of the inhibitory peptides in the nucleus further causes disruption of lamin filaments and thus nuclear abnormalities. Another possibility could be that since keratins are known to bind to nucleus via plectin, distortion of keratin network leads to distortion of the nucleus and thus lamins. Thus, further experiments need to be performed to verify if the photoactivatable 2B2 could be used to disrupt lamin. The current tools can be further developed to specifically disrupt lamins, for example, by adding an NLS sequence.

Bibliography

- Ackbarow, T., Sen, D., Thaulow, C., and Buehler, M. J. (2009). Alpha-helical protein networks are self-protective and flaw-tolerant. *PLoS One* 4. doi:10.1371/journal.pone.0006015.
- Aggeler, J., and Seely, K. (1990). Cytoskeletal Dynamics in Rabbit Synovial Fibroblasts: I. Effects of Acrylamide on Intermediate Filaments and Microfilaments. *Cell Motil. Cytoskeleton* 16, 110–120. doi:10.1002/cm.970160205.
- Almeida, F. V., Walko, G., McMillan, J. R., McGrath, J. A., Wiche, G., Barber, A. H., et al. (2015). The cytolinker plectin regulates nuclear mechanotransduction in keratinocytes. *J. Cell Sci.* 128, 4475–86. doi:10.1242/jcs.173435.
- Arocena, M. (2006). Effect of acrylamide on the cytoskeleton and apoptosis of bovine lens epithelial cells. *Cell Biol. Int.* 30, 1007–1012. doi:10.1016/j.cellbi.2006.07.008.
- Babb, S. G., and Marrs, J. A. (2004). E-cadherin regulates cell movements and tissue formation in early zebrafish embryos. *Dev. Dyn.* 230, 263–277. doi:10.1002/dvdy.20057.
- Baneyx, G., Baugh, L., and Vogel, V. (2002). Fibronectin extension and unfolding within cell matrix fibrils controlled by cytoskeletal tension. *Proc. Natl. Acad. Sci. U. S. A.* doi:10.1073/pnas.072650799.
- Bär, J., Kumar, V., Roth, W., Schwarz, N., Richter, M., Leube, R. E., et al. (2014). Skin fragility and impaired desmosomal adhesion in mice lacking all keratins. *J. Invest. Dermatol.* 134, 1012–22. doi:10.1038/jid.2013.416.
- Bargagna-Mohan, P., Deokule, S. P., Thompson, K., Wizeman, J., Srinivasan, C., Vooturi, S., et al. (2013). Withaferin A effectively targets soluble vimentin in the glaucoma filtration surgical model of fibrosis. *PLoS One* 8, e63881. doi:10.1371/journal.pone.0063881.
- Bargagna-Mohan, P., Hamza, A., Kim, Y. E., Khuan (Abby) Ho, Y., Mor-Vaknin, N., Wendschlag, N., et al. (2007). The Tumor Inhibitor and Antiangiogenic Agent Withaferin A Targets the Intermediate Filament Protein Vimentin. *Chem. Biol.* 14, 623–634. doi:10.1016/j.chembiol.2007.04.010.

- Bargagna-mohan, P., Paranthan, R. R., Hamza, A., Dimova, N., Trucchi, B., Srinivasan, C., et al. (2010). Withaferin A Targets Intermediate Filaments Glial Fibrillary Acidic Protein and Vimentin in a Model of Retinal Gliosis. 285, 7657–7669. doi:10.1074/jbc.M109.093765.
- Bazellières, E., Conte, V., Elosegui-Artola, A., Serra-Picamal, X., Bintanel-Morcillo, M., Roca-Cusachs, P., et al. (2015). Control of cell-cell forces and collective cell dynamics by the intercellular adhesome. *Nat. Cell Biol.* 17, 409–420. doi:10.1038/ncb3135.
- Bear, M. D., Liu, T., Abualkhair, S., Ghamloush, M. A., Hill, N. S., Preston, I., et al. (2016). Alpha-Catulin Co-Localizes With Vimentin Intermediate Filaments and Functions in Pulmonary Vascular Endothelial Cell Migration via ROCK. *J. Cell. Physiol.* 231, 934–943. doi:10.1002/jcp.25185.
- Beil, M., Micoulet, A., von Wichert, G., Paschke, S., Walther, P., Omary, M. B., et al. (2003). Sphingosylphosphorylcholine regulates keratin network architecture and visco-elastic properties of human cancer cells. *Nat. Cell Biol.* 5, 803–811. doi:10.1038/ncb1037.
- Bhattacharya, R., Gonzalez, A. M., DeBiase, P. J., Trejo, H. E., Goldman, R. D., Flitney, F. W., et al. (2009). Recruitment of vimentin to the cell surface by $\beta 3$ integrin and plectin mediates adhesion strength. *J. Cell Sci.* 122, 1390–1400. doi:10.1242/jcs.043042.
- Bjerke, M. A., Dzamba, B., Wang, C., and DeSimone, D. W. (2014). FAK is required for tension-dependent organization of collective cell movements in *Xenopus* mesendoderm. *Dev. Biol.* 394, 1–17. doi:10.1016/j.ydbio.2014.07.023.
- Blikstad, I., and Lazarides, E. (1983). Vimentin filaments are assembled from a soluble precursor in avian erythroid cells. *J. Cell Biol.* 96, 1803–1808. doi:10.1083/jcb.96.6.1803.
- Bordeleau, F., Galarneau, L., Gilbert, S., Loranger, A., and Marceau, N. (2010). Keratin 8/18 Modulation of Protein Kinase C-mediated Integrin-dependent Adhesion and Migration of Liver Epithelial Cells. *Mol. Biol. Cell* 21, 1698–1713. doi:10.1091/mbc.E09.
- Bordeleau, F., Lapierre, M. E., Sheng, Y., and Marceau, N. (2012). Keratin 8/18 regulation of cell stiffness-extracellular matrix interplay through modulation of rho-mediated actin cytoskeleton dynamics. *PLoS One* 7, 1–10. doi:10.1371/journal.pone.0038780.

- Bouameur, J.-E., Favre, B., Fontao, L., Lingasamy, P., Begré, N., and Borradori, L. (2014). Interaction of plectin with keratins 5 and 14: dependence on several plectin domains and keratin quaternary structure. *J. Invest. Dermatol.* 134, 2776–83. doi:10.1038/jid.2014.255.
- Bouameur, J.-E., and Magin, T. M. (2017). “Lessons from Animal Models of Cytoplasmic Intermediate Filament Proteins,” in *Sub-cellular biochemistry*, 171–230. doi:10.1007/978-3-319-49674-0_7.
- Burgstaller, G., Gregor, M., Winter, L., and Wiche, G. (2010). Keeping the vimentin network under control: cell-matrix adhesion-associated plectin 1f affects cell shape and polarity of fibroblasts. *Mol. Biol. Cell* 21, 3362–75. doi:10.1091/mbc.E10-02-0094.
- Busch, T., Armacki, M., Eiseler, T., Joodi, G., Temme, C., Jansen, J., et al. (2012). Keratin 8 phosphorylation regulates keratin reorganization and migration of epithelial tumor cells. *J. Cell Sci.* 125, 2148–2159. doi:10.1242/jcs.080127.
- Cai, D., Chen, S. C., Prasad, M., He, L., Wang, X., Choesmel-Cadamuro, V., et al. (2014). Mechanical feedback through E-cadherin promotes direction sensing during collective cell migration. *Cell* 157, 1146–1159. doi:10.1016/j.cell.2014.03.045.
- Cary, R. B., Klymkowsky, M. W., Evans, R. M., Domingo, a, Dent, J. a, and Backhus, L. E. (1994). Vimentin’s tail interacts with actin-containing structures in vivo. *J. Cell Sci.* 107 (Pt 6, 1609–1622.
- Challa, A. A., and Stefanovic, B. (2011). A Novel Role of Vimentin Filaments: Binding and Stabilization of Collagen mRNAs. *Mol. Cell. Biol.* 31, 3773–3789. doi:10.1128/mcb.05263-11.
- Chang, I. A., Oh, M.-J., Kim, M. H., Park, S.-K., Kim, B. G., and Namgung, U. (2012). Vimentin phosphorylation by Cdc2 in Schwann cell controls axon growth via β 1-integrin activation. *FASEB J.* 26, 2401–2413. doi:10.1096/fj.11-199018.
- Chang, L., Barlan, K., Chou, Y.-H., Grin, B., Lakonishok, M., Serpinskaya, A. S., et al. (2009). The dynamic properties of intermediate filaments during organelle transport. *J. Cell Sci.* 122, 2914–2923. doi:10.1242/jcs.046789.
- Cheng, F., Shen, Y., Mohanasundaram, P., Lindström, M., Ivaska, J., Ny, T., et al. (2016). Vimentin coordinates fibroblast proliferation and keratinocyte differentiation in wound healing via TGF- β -Slug signaling. *Proc. Natl. Acad. Sci.* 113, E4320–E4327. doi:10.1073/pnas.1519197113.

- Chernyatina, A. A., Nicolet, S., Aebi, U., Herrmann, H., and Strelkov, S. V (2012). Atomic structure of the vimentin central alpha-helical domain and its implications for intermediate filament assembly. *Proc Natl Acad Sci U S A* 109, 13620–13625. doi:10.1073/pnas.1206836109.
- Cheung, K. J., Gabrielson, E., Werb, Z., and Ewald, A. J. (2013). Collective invasion in breast cancer requires a conserved basal epithelial program. *Cell* 155, 1639–1651. doi:10.1016/j.cell.2013.11.029.
- Cheung, K. J., Padmanaban, V., Silvestri, V., Schipper, K., Cohen, J. D., Fairchild, A. N., et al. (2016). Polyclonal breast cancer metastases arise from collective dissemination of keratin 14-expressing tumor cell clusters. *Proc. Natl. Acad. Sci.* 113, 201508541. doi:10.1073/pnas.1508541113.
- Cho, A., Kato, M., Whitwam, T., Kim, J. H., and Montell, D. J. (2016). An Atypical Tropomyosin in *Drosophila* with Intermediate Filament-like Properties. *Cell Rep.* 16, 928–938. doi:10.1016/j.celrep.2016.06.054.
- Choi, Y. S., and Gumbiner, B. (1989). Expression of cell adhesion molecule E-cadherin in *Xenopus* embryos begins at gastrulation and predominates in the ectoderm. *J. Cell Biol.* 108, 2449–2458. doi:10.1083/jcb.108.6.2449.
- Chou, Y., Ngai, K., and Goldman, R. (1991). The Regulation of Intermediate Filament Reorganization in Mitosis. *J Biol Chem.* 266, 7325–7328.
- Coleman, T. R., and Lazarides, E. (1992). Continuous growth of vimentin filaments in mouse fibroblasts. *J. Cell Sci.* 103 (Pt 3), 689–698.
- Conway, D. E., Breckenridge, M. T., Hinde, E., Gratton, E., Chen, C. S., and Schwartz, M. A. (2013). Fluid shear stress on endothelial cells modulates mechanical tension across VE-cadherin and PECAM-1. *Curr. Biol.* 23, 1024–1030. doi:10.1016/j.cub.2013.04.049.
- Correia, I., Chu, D., Chou, Y. H., Goldman, R. D., and Matsudaira, P. (1999). Integrating the actin and vimentin cytoskeletons: Adhesion-dependent formation of fimbrin-vimentin complexes in macrophages. *J. Cell Biol.* 146, 831–842. doi:10.1083/jcb.146.4.831.
- Crosson, S., and Moffat, K. (2001). Structure of a flavin-binding plant photoreceptor domain: Insights into light-mediated signal transduction. *Proc. Natl. Acad. Sci.* 98, 2995–3000. doi:10.1073/pnas.051520298.
- Das, T., Safferling, K., Rausch, S., Grabe, N., Boehm, H., and Spatz, J. P. (2015). A molecular mechanotransduction pathway regulates collective migration of epithelial cells. *Nat Cell Biol* 17, 276–287. doi:10.1038/ncb3115.

- Davidson, L. A., Hoffstrom, B. G., Keller, R., and DeSimone, D. W. (2002). Mesendoderm extension and mantle closure in *Xenopus laevis* gastrulation: Combined roles for integrin $\alpha 5 \beta 1$, fibronectin, and tissue geometry. *Dev. Biol.* 242, 109–129. doi:10.1006/dbio.2002.0537.
- Davidson, L. A., Marsden, M., Keller, R., and DeSimone, D. W. (2006). Integrin $\alpha 5 \beta 1$ and Fibronectin Regulate Polarized Cell Protrusions Required for *Xenopus* Convergence and Extension. *Curr. Biol.* doi:10.1016/j.cub.2006.03.038.
- Dechat, T., Adam, S. A., Taimen, P., Shimi, T., and Goldman, R. D. (2010). Nuclear lamins. *Cold Spring Harb. Perspect. Biol.* 2, 1–23. doi:10.1101/cshperspect.a000547.
- Deng, M., Zhang, W., Tang, H., Ye, Q., Liao, Q., Zhou, Y., et al. (2012). Lactotransferrin acts as a tumor suppressor in nasopharyngeal carcinoma by repressing AKT through multiple mechanisms. *Oncogene*, 4273–4283. doi:10.1038/onc.2012.434.
- Dmello, C., Sawant, S., Alam, H., Gangadaran, P., Tiwari, R., Dongre, H., et al. (2016). Vimentin-mediated regulation of cell motility through modulation of beta4 integrin protein levels in oral tumor derived cells. *Int. J. Biochem. Cell Biol.* 70, 161–172. doi:10.1016/j.biocel.2015.11.015.
- Dodemont, H., and Riemer, D. (1990). Structure of an invertebrate gene encoding cytoplasmic intermediate filament (IF) proteins : implications for the origin and the diversification of IF proteins. *EMBO J.* 9, 4083–4094. doi:10.1002/j.1460-2075.1990.tb07630.x.
- Döring, V., and Stick, R. (1990). Gene structure of nuclear lamin LIII of *Xenopus laevis*; a model for the evolution of IF proteins from a lamin-like ancestor. *EMBO J.* 9, 4073–4081. doi:10.1002/j.1460-2075.1990.tb07629.x.
- Dupin, I., Sakamoto, Y., and Etienne-Manneville, S. (2011). Cytoplasmic intermediate filaments mediate actin-driven positioning of the nucleus. *J. Cell Sci.* 124, 865–72. doi:10.1242/jcs.076356.
- Durham, H. D., Pena, S. D. J., and Carpenter, S. (1983). The neurotoxins 2,5-hexanedione and acrylamide promote aggregation of intermediate filaments in cultured fibroblasts. *Muscle Nerve* 6, 631–637. doi:10.1002/mus.880060903.
- Dzamba, B. J., Jakab, K. R., Marsden, M., Schwartz, M. A., and DeSimone, D. W. (2009). Cadherin Adhesion, Tissue Tension, and Noncanonical Wnt Signaling Regulate Fibronectin Matrix Organization. *Dev. Cell* 16, 421–432. doi:10.1016/j.devcel.2009.01.008.

- Eckert, B. (1985). Alteration of intermediate filament distribution in PtK1 cells by acrylamide. *Eur. J. Cell Biol.* 37, 169–174. doi:10.1002/cm.970060104.
- Eckes, B., Colucci-Guyon, E., Smola, H., Nodder, S., Babinet, C., Krieg, T., et al. (2000). Impaired wound healing in embryonic and adult mice lacking vimentin. *J. Cell Sci.* 113, 2455–2462.
- Eckes, B., Dogic, D., Colucci-Guyon, E., Wang, N., Maniotis, A., Ingber, D., et al. (1998). Impaired mechanical stability, migration and contractile capacity in vimentin-deficient fibroblasts. *J. Cell Sci.* 111, 1897–1907.
- Esue, O., Carson, A. A., Tseng, Y., and Wirtz, D. (2006). A direct interaction between actin and vimentin filaments mediated by the tail domain of vimentin. *J. Biol. Chem.* 281, 30393–30399. doi:10.1074/jbc.M605452200.
- Ewald, A. J., Brenot, A., Duong, M., Chan, B. S., and Werb, Z. (2008). Collective epithelial migration and cell rearrangements drive mammary branching morphogenesis. *Dev. Cell* 14, 570–581. doi:10.1016/j.devcel.2008.03.003.
- Farooqui, R., and Fenteany, G. (2005). Multiple rows of cells behind an epithelial wound edge extend cryptic lamellipodia to collectively drive cell- sheet movement. doi:10.1242/jcs.01577.
- Feng, L., Zhou, X., Liao, J., and Omary, M. B. (1999). Pervanadate-mediated tyrosine phosphorylation of keratins 8 and 19 via a p38 mitogen-activated protein kinase-dependent pathway. *J. Cell Sci.* 112 (Pt 1), 2081–90. Available at: <http://www.ncbi.nlm.nih.gov/pubmed/10362538>.
- Flitney, E. W., Kuczmarski, E. R., Adam, S. a, and Goldman, R. D. (2009). Insights into the mechanical properties of epithelial cells: the effects of shear stress on the assembly and remodeling of keratin intermediate filaments. *FASEB J.* 23, 2110–2119. doi:10.1096/fj.08-124453.
- Fogl, C., Mohammed, F., Al-Jassar, C., Jeeves, M., Knowles, T. J., Rodriguez-Zamora, P., et al. (2016). Mechanism of intermediate filament recognition by plakin repeat domains revealed by envoplakin targeting of vimentin. *Nat. Commun.* 7, 10827. doi:10.1038/ncomms10827.
- Fois, G., Weimer, M., Busch, T., Felder, E. T., Oswald, F., Wichert, G. Von, et al. (2013). Effects of keratin phosphorylation on the mechanical properties of keratin filaments in living cells. *FASEB J.* 27, 1322–1329. doi:10.1096/fj.12-215632.

- Fortier, A. M., Asselin, E., and Cadrin, M. (2013). Keratin 8 and 18 loss in epithelial cancer cells increases collective cell migration and cisplatin sensitivity through claudin1 up-regulation. *J. Biol. Chem.* 288, 11555–11571. doi:10.1074/jbc.M112.428920.
- Franke, W., Schiller, D., Schmid, R., and Engelbrecht, I. (1981). Diversity of cytokeratins. *J. Mol. Biol.* 153, 933–959. doi:10.1016/0022-2836(81)90460-5.
- Franke, W. W., Grund, C., Jackson, B. W., and Illmensee, K. (1980). Formation of cytoskeletal elements during mouse embryogenesis. Intermediate filaments of the cytokeratin type and desmosomes in preimplantation embryos. *Differentiation*. 17, 161–79. doi:10.1111/j.1432-0436.1984.tb01348.x.
- Franke, W. W., Schmid, E., Osborn, M., and Weber, K. (1978a). Different intermediate-sized filaments distinguished by immunofluorescence microscopy. *Proc. Natl. Acad. Sci.* 75, 5034–5038. doi:10.1073/pnas.75.10.5034.
- Franke, W. W., Weber, K., Osborn, M., Schmid, E., and Freudenstein, C. (1978b). Antibody to prekeratin. Decoration of tonofilament-like arrays in various cells of epithelial character. *Exp. Cell Res.* 116, 429–445. doi:10.1016/0014-4827(78)90466-4.
- Franz, J. K., and Franke, W. W. (1986). Cloning of cDNA and amino acid sequence of a cytokeratin expressed in oocytes of *Xenopus laevis*. *Proc. Natl. Acad. Sci. U. S. A.* 83, 6475–9. doi:10.1073/pnas.83.17.6475.
- Franz, J. K., Gall, L., Williams, M. A., Picheral, B., and Franke, W. W. (1983). Intermediate-size filaments in a germ cell: Expression of cytokeratins in oocytes and eggs of the frog *Xenopus*. *Proc. Natl. Acad. Sci. U. S. A.* 80, 6254–8. doi:10.1073/pnas.80.20.6254.
- Fudge, D., Russell, D., Beriault, D., Moore, W., Lane, E. B., and Vogl, A. W. (2008). The intermediate filament network in cultured human keratinocytes is remarkably extensible and resilient. *PLoS One* 3. doi:10.1371/journal.pone.0002327.
- Fujiwara, S., Ohashi, K., Mashiko, T., Kondo, H., and Mizuno, K. (2016). Interplay between Solo and keratin filaments is crucial for mechanical force-induced stress fiber reinforcement. *Mol. Biol. Cell* 58, 7250–7. doi:10.1091/mbc.E15-06-0417.
- Ganz, A., Lambert, M., Saez, A., Silberzan, P., Buguin, A., Mège, R. M., et al. (2006). Traction forces exerted through N-cadherin contacts. *Biol. Cell* 98, 721–730. doi:10.1042/BC20060039.

- Gao, Y. S., and Sztul, E. (2001). A novel interaction of the Golgi complex with the vimentin intermediate filament cytoskeleton. *J. Cell Biol.* 152, 877–893. doi:10.1083/jcb.152.5.877.
- Gautier, R., Douguet, D., Antonny, B., and Drin, G. (2008). HELIQUEST: a web server to screen sequences with specific α -helical properties. *Bioinformatics* 24, 2101–2102. doi:10.1093/bioinformatics/btn392.
- Geisler, N., and Weber, K. (1982). The amino acid sequence of chicken muscle desmin provides a common structural model for intermediate filament proteins. *EMBO J.* 1, 1649–1656. doi:10.1002/j.1460-2075.1982.tb01368.x.
- Gilles, C., Polette, M., Zahm, J. M., Tournier, J. M., Volders, L., Foidart, J. M., et al. (1999). Vimentin contributes to human mammary epithelial cell migration. *J. Cell Sci.* 112 (Pt 2, 4615–4625.
- Gittes, F., Mickey, B., Nettleton, J., and Howard, J. (1993). Flexural rigidity of microtubules and actin filaments measured from thermal fluctuations in shape. *J. Cell Biol.* 120, 923–934. doi:10.1083/jcb.120.4.923.
- Gladilin, E., Gonzalez, P., and Eils, R. (2014). Dissecting the contribution of actin and vimentin intermediate filaments to mechanical phenotype of suspended cells using high-throughput deformability measurements and computational modeling. *J. Biomech.* 47, 2598–2605. doi:10.1016/j.jbiomech.2014.05.020.
- Goldman, R. D., Goldman, A. E., Green, K. J., Jones, J. C., Jones, S. M., and Yang, H.-Y. (1986). Intermediate filament networks: organization and possible functions of a diverse group of cytoskeletal elements. *J. Cell Sci. Suppl.* 5, 69–97. doi:10.1242/jcs.1986.Supplement_5.5.
- Goldman, R. D., Khuon, S., Chou, Y. H., Opal, P., and Steinert, P. M. (1996). The function of intermediate filaments in cell shape and cytoskeletal integrity. *J. Cell Biol.* 134, 971–983. doi:10.1083/jcb.134.4.971.
- Goulielmos, G., Gounari, F., Remington, S., Müller, S., Häner, M., Aebi, U., et al. (1996). Filensin and phakinin form a novel type of beaded intermediate filaments and coassemble de novo in cultured cells. *J. Cell Biol.* 132, 643–655. doi:10.1083/jcb.132.4.643.
- Gregor, M., Osmanagic-Myers, S., Burgstaller, G., Wolfram, M., Fischer, I., Walko, G., et al. (2014). Mechanosensing through focal adhesion-anchored intermediate filaments. *FASEB J.* 28, 715–729. doi:10.1096/fj.13-231829.

- Grin, B., Mahammad, S., Wedig, T., Cleland, M. M., Tsai, L., Herrmann, H., et al. (2012). Withaferin A alters intermediate filament organization, cell shape and behavior. *PLoS One* 7, 1–13. doi:10.1371/journal.pone.0039065.
- Guo, M., Ehrlicher, A. J., Mahammad, S., Fabich, H., Jensen, M. H., Moore, J. R., et al. (2013). The role of vimentin intermediate filaments in cortical and cytoplasmic mechanics. *Biophys. J.* 105, 1562–1568. doi:10.1016/j.bpj.2013.08.037.
- Harada, N., Tamai, Y., Ishikawa, T. O., Sauer, B., Takaku, K., Oshima, M., et al. (1999). Intestinal polyposis in mice with a dominant stable mutation of the β -catenin gene. *EMBO J.* 18, 5931–5942. doi:10.1093/emboj/18.21.5931.
- Harper, S. M., Neil, L. C., Day, I. J., Hore, P. J., and Gardner, K. H. (2004). Conformational Changes in a Photosensory LOV Domain Monitored by Time-Resolved NMR Spectroscopy. *J. Am. Chem. Soc.* 126, 3390–3391. doi:10.1021/ja038224f.
- Harper, S. M., Neil, L. C., and Gardner, K. H. (2003). Structural basis of a phototropin light switch. *Science* (80-.). 301, 1541–1544. doi:10.1126/science.1086810.
- Harris, A. R., Daeden, A., and Charras, G. T. (2014). Formation of adherens junctions leads to the emergence of a tissue-level tension in epithelial monolayers. *J. Cell Sci.* 127, 2507–2517. doi:10.1242/jcs.142349.
- Hartley, C. L., Anderson, V. E. R., Anderson, B. H., and Robertson, J. (1997). Acrylamide and 2,5-hexanedione induce collapse of neurofilaments in SH-SY5Y human neuroblastoma cells to form perikaryal inclusion bodies. *Neuropathol. Appl. Neurobiol.* 23, 364–372. doi:10.1111/j.1365-2990.1997.tb01310.x.
- Hatzfeld, M., and Franke, W. W. (1985). Pair formation and promiscuity of cytokeratins: Formation in vitro of heterotypic complexes and intermediate-sized filaments by homologous and heterologous recombinations of purified polypeptides. *J. Cell Biol.* 101, 1826–1841. doi:10.1083/jcb.101.5.1826.
- Hatzfeld, M., and Weber, K. (1992). A synthetic peptide representing the consensus sequence motif at the carboxy-terminal end of the rod domain inhibits intermediate filament assembly and disassembles preformed filaments. *J. Cell Biol.* 116, 157–166.
- Havel, L. S., Kline, E. R., Salgueiro, A. M., and Marcus, A. I. (2015). Vimentin regulates lung cancer cell adhesion through a VAV2-Rac1 pathway to control focal adhesion kinase activity. *Oncogene* 34, 1979–1990. doi:10.1038/onc.2014.123.

- He, T., Stepulak, A., Holmström, T. H., Bishr Omary, M., and Eriksson, J. E. (2002). The intermediate filament protein keratin 8 is a novel cytoplasmic substrate for c-Jun N-terminal kinase. *J. Biol. Chem.* 277, 10767–10774. doi:10.1074/jbc.M111436200.
- Heasman, J., Torpey, N., and Wylie, C. (1992). The role of intermediate filaments in early *Xenopus* development studied by antisense depletion of maternal mRNA. *Dev. Suppl.* 125, 119–125.
- Helfand, B. T., Mendez, M. G., Murthy, S. N. P., Shumaker, D. K., Grin, B., Mahammad, S., et al. (2011). Vimentin organization modulates the formation of lamellipodia. *Mol. Biol. Cell* 22, 1274–1289. doi:10.1091/mbc.E10-08-0699.
- Helfand, B. T., Mikami, A., Vallee, R. B., and Goldman, R. D. (2002). A requirement for cytoplasmic dynein and dynactin in intermediate filament network assembly and organization. *J. Cell Biol.* 157, 795–806. doi:10.1083/jcb.200202027.
- Helmke, B. P., Goldman, R. D., and Davies, P. F. (2000). Rapid displacement of vimentin intermediate filaments in living endothelial cells exposed to flow. *Circ. Res.* 86, 745–752. doi:10.1161/01.RES.86.7.745.
- Helmke, B. P., Thakker, D. B., Goldman, R. D., and Davies, P. F. (2001). Spatiotemporal analysis of flow-induced intermediate filament displacement in living endothelial cells. *Biophys. J.* 80, 184–94. doi:10.1016/S0006-3495(01)76006-7.
- Hering, L., Bouameur, J. E., Reichelt, J., Magin, T. M., and Mayer, G. (2016). Novel origin of lamin-derived cytoplasmic intermediate filaments in tardigrades. *Elife* 5, e11117. doi:10.7554/eLife.11117.
- Herrmann, H., Häner, M., Brettel, M., Ku, N. O., and Aebi, U. (1999). Characterization of distinct early assembly units of different intermediate filament proteins. *J. Mol. Biol.* 286, 1403–1420. doi:10.1006/jmbi.1999.2528.
- Herrmann, H., Häner, M., Brettel, M., Müller, S. a, Goldie, K. N., Fedtke, B., et al. (1996). Structure and assembly properties of the intermediate filament protein vimentin: the role of its head, rod and tail domains. *J. Mol. Biol.* 264, 933–53. doi:10.1006/jmbi.1996.0688.
- Herrmann, H., Kreplak, L., and Aebi, U. (2004). Isolation, characterization, and in vitro assembly of intermediate filaments. *Methods Cell Biol.* 78, 3–24. doi:10.1016/S0091-679X(04)78001-2.
- Herrmann, H., and Strelkov, S. V (2011). History and phylogeny of intermediate filaments: now in insects. *BMC Biol.* 9, 16. doi:10.1186/1741-7007-9-16.

- Herrmann, H., Wedig, T., Porter, R. M., Lane, B., and Aebi, U. (2002). Characterization of early assembly intermediates of recombinant human keratins. *J. Struct. Biol.* 137, 82–96. doi:10.1006/jsbi.2002.4466.
- Hesse, M., Franz, T., Tamai, Y., Taketo, M. M., and Magin, T. M. (2000). Targeted deletion of keratins 18 and 19 leads to trophoblast fragility and early embryonic lethality. *Embo J* 19, 5060–5070. doi:10.1093/emboj/19.19.5060.
- Hesse, M., Magin, T. M., and Weber, K. (2001). Genes for intermediate filament proteins and the draft sequence of the human genome: novel keratin genes and a surprisingly high number of pseudogenes related to keratin genes 8 and 18. *J. Cell Sci.* 114, 2569–75.
- Hirsh, G., Dzamba, B. J., Sonavane, P. R., Shook, D. R., Allen, C., and DeSimone, D. W. (2018). Multiple functions for the catenin family member plakoglobin in cadherin-dependent adhesion, fibronectin matrix assembly and *Xenopus* gastrulation movements. 1–45. doi:https://doi.org/10.1101/318774.
- Ho, C. L., Martys, J. L., Mikhailov, A., Gundersen, G. G., and Liem, R. K. (1998). Novel features of intermediate filament dynamics revealed by green fluorescent protein chimeras. *J. Cell Sci.* 111 (Pt 1, 1767–78.
- Ho, C. Y., and Lammerding, J. (2012). Lamins at a glance. *J. Cell Sci.* 125, 2087–2093. doi:10.1242/jcs.087288.
- Hobbs, R. P., Jacob, J. T., and Coulombe, P. A. (2016). Keratins Are Going Nuclear. *Dev. Cell* 38, 227–233. doi:10.1016/j.devcel.2016.07.022.
- Homberg, M., Ramms, L., Schwarz, N., Dreissen, G., Leube, R. E., Merkel, R., et al. (2015). Distinct Impact of two Keratin Mutations Causing Epidermolysis Bullosa Simplex on Keratinocyte Adhesion and Stiffness. *J. Invest. Dermatol.* 135, 1–29. doi:10.1038/jid.2015.184.
- Hookway, C., Ding, L., Davidson, M. W., Rappoport, J. Z., Danuser, G., and Gelfand, V. I. (2015). Microtubule-dependent transport and dynamics of vimentin intermediate filaments. *Mol. Biol. Cell* 26. doi:10.1091/mbc.E14-09-1398.
- Huala, E. (1997). Arabidopsis NPH1: A Protein Kinase with a Putative Redox-Sensing Domain. *Science* (80-.). 278, 2120–2123. doi:10.1126/science.278.5346.2120.
- Hyder, C. L., Kemppainen, K., Isoniemi, K. O., Imanishi, S. Y., Goto, H., Inagaki, M., et al. (2015). Sphingolipids inhibit vimentin-dependent cell migration. *J. Cell Sci.* 128, 2057–69. doi:10.1242/jcs.160341.

- Ibrahim, H., and Winklbauer, R. (2001). Mechanisms of mesendoderm internalization in the *Xenopus* gastrula: Lessons from the ventral side. *Dev. Biol.* 240, 108–122. doi:10.1006/dbio.2001.0459.
- Ivaska, J., Vuoriluoto, K., Huovinen, T., Izawa, I., Inagaki, M., and Parker, P. J. (2005). PKC ϵ -mediated phosphorylation of vimentin controls integrin recycling and motility. *EMBO J.* 24, 3834–3845. doi:10.1038/sj.emboj.7600847.
- Janmey, P. A., Euteneuer, U., Traub, P., and Schliwa, M. (1991). Viscoelastic properties of vimentin compared with other filamentous biopolymer networks. *J. Cell Biol.* 113, 155–160. doi:10.1083/jcb.113.1.155.
- Janosch, P., Kieser, A., Eulitz, M., Lovric, J., Sauer, G., Reichert, M., et al. (2000). The Raf-1 kinase associates with vimentin kinases and regulates the structure of vimentin filaments. *FASEB J.* 14, 2008–2021. doi:10.1096/fj.99-0883com.
- Jiu, Y., Peränen, J., Schaible, N., Cheng, F., and Eriksson, J. E. (2017). Vimentin intermediate filaments control actin stress fiber assembly through GEF-H1 and RhoA. *J. Cell Sci.* 130, 892–902. doi:10.1242/jcs.196881.
- Johnson, C. P., Tang, H.-Y., Carag, C., Speicher, D. W., and Discher, D. E. (2007). Forced unfolding of proteins within cells. *Science* 317, 663–6. doi:10.1126/science.1139857.
- Ju, J.-H., Oh, S., Lee, K.-M., Yang, W., Nam, K. S., Moon, H.-G., et al. (2015). Cytokeratin19 induced by HER2/ERK binds and stabilizes HER2 on cell membranes. *Cell Death Differ.* 22, 665–676. doi:10.1038/cdd.2014.155.
- Kane, D. A. (2005). Mutations in half baked/E-cadherin block cell behaviors that are necessary for teleost epiboly. *Development* 132, 1105–1116. doi:10.1242/dev.01668.
- Karabinos, A., Zimek, A., and Weber, K. (2004). The genome of the early chordate *Ciona intestinalis* encodes only five cytoplasmic intermediate filament proteins including a single type I and type II keratin and a unique IF-annexin fusion protein. *Gene* 326, 123–9.
- Kayser, J., Haslbeck, M., Dempfle, L., Krause, M., Grashoff, C., Buchner, J., et al. (2013). The small heat shock protein Hsp27 affects assembly dynamics and structure of keratin intermediate filament networks. *Biophys. J.* 105, 1778–1785. doi:10.1016/j.bpj.2013.09.007.
- Keller, R., Davidson, L. A., and Shook, D. R. (2003). How we are shaped: The biomechanics of gastrulation. *Differentiation* 71, 171–205. doi:10.1046/j.1432-0436.2003.710301.x.

- Keller, R. E. (1975). Vital Dye Mapping of the Gastrula *Xenopus laevis* and Neurula of *Xenopus laevis*. *Dev. Biol.* 42, 42, 222–241.
- Keller, R. E. (1978). Time-lapse cinemicrographic analysis of superficial cell behavior during and prior to gastrulation in *Xenopus laevis*. *J. Morphol.* 157, 223–247. doi:10.1002/jmor.1051570209.
- Keller, R. E. (1980). The cellular basis of epiboly: an SEM study of deep-cell rearrangement during gastrulation in *Xenopus laevis*. *J. Embryol. Exp. Morphol.* 60, 201–234.
- Kelley, L. A., Mezulis, S., Yates, C. M., Wass, M. N., and Sternberg, M. J. E. (2015). The Pyre2 web portal for protein modeling, prediction and analysis. *Nat. Protoc.* 10, 845–858. doi:10.1038/nprot.2015.053.
- Ketema, M., Wilhelmsen, K., Kuikman, I., Janssen, H., Hodzic, D., and Sonnenberg, A. (2007). Requirements for the localization of nesprin-3 at the nuclear envelope and its interaction with plectin. *J. Cell Sci.* 120, 3384–94. doi:10.1242/jcs.014191.
- Kim, H., Nakamura, F., Lee, W., Shifrin, Y., Arora, P., McCulloch, C. A., et al. (2010). Filamin A is required for vimentin-mediated cell adhesion and spreading. *Am J Physiol Cell Physiol* 298, 221–236. doi:10.1152/ajpcell.00323.2009.
- Kim, J. S., Lee, C. H., Su, B. Y., and Coulombe, P. A. (2012). Mathematical modeling of the impact of actin and keratin filaments on keratinocyte cell spreading. *Biophys. J.* 103, 1828–1838. doi:10.1016/j.bpj.2012.09.016.
- Kim, J., Yang, C., Kim, E. J., Jang, J., Kim, S.-J., Kang, S. M., et al. (2016). Vimentin filaments regulate integrin-ligand interactions by binding to the cytoplasmic tail of integrin $\beta 3$. *J. Cell Sci.* 129, 2030–2042. doi:10.1242/jcs.180315.
- Kim, S., Wong, P., and Coulombe, P. a (2006). A keratin cytoskeletal protein regulates protein synthesis and epithelial cell growth. *Nature* 441, 362–365. doi:10.1038/nature04659.
- Kim, Y. J., Sauer, C., Testa, K., Wahl, J. K., Svoboda, R. A., Johnson, K. R., et al. (2005). Modulating the strength of cadherin adhesion: evidence for a novel adhesion complex. *J Cell Sci* 118, 3883–3894. doi:10.1242/jcs.02508.
- Kirmse, R., Portet, S., Mücke, N., Aebi, U., Herrmann, H., and Langowski, J. (2007). A quantitative kinetic model for the in vitro assembly of intermediate filaments from tetrameric vimentin. *J. Biol. Chem.* 282, 18563–18572. doi:10.1074/jbc.M701063200.

- Kitt, K. N., and Nelson, W. J. (2011). Rapid suppression of activated rac1 by cadherins and nectins during De Novo cell-cell adhesion. *PLoS One* 6. doi:10.1371/journal.pone.0017841.
- Klymkowsky, M. W. (1988). Metabolic inhibitors and intermediate filament organization in human fibroblasts. *Exp. Cell Res.* 174, 282–290. doi:10.1016/0014-4827(88)90162-0.
- Klymkowsky, M. W., Miller, R. H., and Lane, E. B. (1983). Morphology , Behavior , and Interaction of Cultured Epithelial Cells after the Antibody-induced Disruption of Keratin Filament Organization. 96. doi:10.1083/jcb.96.2.494.
- Klymkowsky, M. W., Shook, D. R., and Maynell, L. a (1992). Evidence that the deep keratin filament systems of the *Xenopus* embryo act to ensure normal gastrulation. *Proc. Natl. Acad. Sci. U. S. A.* 89, 8736–8740. doi:10.1073/pnas.89.18.8736.
- Knapp, L. W., O’Guin, W. M., and Sawyer, R. H. (1983). Rearrangement of the keratin cytoskeleton after combined treatment with microtubule and microfilament inhibitors. *J. Cell Biol.* 97, 1788–1794. doi:10.1083/jcb.97.6.1788.
- Kolega, J. (1986). Effects of mechanical tension on protrusive activity and microfilament and intermediate filament organization in an epidermal epithelium moving in culture. *J. Cell Biol.* 102, 1400–1411. doi:10.1083/jcb.102.4.1400.
- Kölsch, A., Windoffer, R., and Leube, R. E. (2009). Actin-dependent dynamics of keratin filament precursors. *Cell Motil. Cytoskeleton* 66, 976–985. doi:10.1002/cm.20395.
- Kolsch, A., Windoffer, R., Wurflinger, T., Aach, T., and Leube, R. E. (2010). The keratin-filament cycle of assembly and disassembly. *J. Cell Sci.* 123, 2266–2272. doi:10.1242/jcs.068080.
- Kouklis, P. D., Traub, P., and Georgatos, S. D. (1992). Involvement of the consensus sequence motif at coil 2b in the assembly and stability of vimentin filaments. *J. Cell Sci.* 102 (Pt 1, 31–41.
- Kreitzer, G., Liao, G., and Gundersen, G. G. (1999). Detyrosination of tubulin regulates the interaction of intermediate filaments with microtubules in vivo via a kinesin-dependent mechanism. *Mol. Biol. Cell* 10, 1105–1118. doi:PMC25238.
- Kreplak, L., Bär, H., Leterrier, J. F., Herrmann, H., and Aebi, U. (2005). Exploring the mechanical behavior of single intermediate filaments. *J. Mol. Biol.* 354, 569–577. doi:10.1016/j.jmb.2005.09.092.

- Kröger, C., Loschke, F., Schwarz, N., Windoffer, R., Leube, R. E., and Magin, T. M. (2013). Keratins control intercellular adhesion involving PKC- α -mediated desmoplakin phosphorylation. *J. Cell Biol.* 201, 681–692. doi:10.1083/jcb.201208162.
- Ku, N.-O., Toivola, D. M., Strnad, P., and Omary, M. B. (2010). Cytoskeletal keratin glycosylation protects epithelial tissue from injury. *Nat. Cell Biol.* 12, 876–885. doi:10.1038/ncb2091.
- Ku, N., Michie, S., Resurreccion, E. Z., Broome, R. L., and Omary, M. B. (2002). Keratin binding to 14-3-3 proteins modulates keratin filaments and hepatocyte mitotic progression. *Proc. Natl. Acad. Sci. U. S. A.* 99, 4373–4378. doi:10.1073/pnas.072624299.
- Ku, N. O., Fu, H., and Omary, M. B. (2004). Raf-1 activation disrupts its binding to keratins during cell stress. *J. Cell Biol.* 166, 479–485. doi:10.1083/jcb.200402051.
- Ku, N. O., Liao, J., and Omary, M. B. (1998). Phosphorylation of human keratin 18 serine 33 regulates binding to 14-3-3 proteins. *EMBO J.* 17, 1892–1906. doi:10.1093/emboj/17.7.1892.
- Ku, N. O., Michie, S. A., Soetikno, R. M., Resurreccion, E. Z., Broome, R. L., Oshima, R. G., et al. (1996). Susceptibility to hepatotoxicity in transgenic mice that express a dominant-negative human keratin 18 mutant. *J. Clin. Invest.* 98, 1034–1046. doi:10.1172/JCI118864.
- Ku, N. O., and Omary, M. B. (2000). Keratins turn over by ubiquitination in a phosphorylation-modulated fashion. *J. Cell Biol.* 149, 547–552. doi:10.1083/jcb.149.3.547.
- Ku, N. O., and Omary, M. B. (2006). A disease- and phosphorylation-related nonmechanical function for keratin 8. *J. Cell Biol.* 174, 115–125. doi:10.1083/jcb.200602146.
- Kumar, N., Robidoux, J., Daniel, K. W., Guzman, G., Floering, L. M., and Collins, S. (2007). Requirement of vimentin filament assembly for beta3-adrenergic receptor activation of ERK MAP kinase and lipolysis. *J. Biol. Chem.* 282, 9244–9250. doi:10.1074/jbc.M605571200.
- Kumar, V., Bouameur, J. E., Bär, J., Rice, R. H., Hornig-Do, H. T., Roop, D. R., et al. (2015). A keratin scaffold regulates epidermal barrier formation, mitochondrial lipid composition, and activity. *J. Cell Biol.* 211, 1057–1075. doi:10.1083/jcb.201404147.

- Labouesse, C., Gabella, C., Meister, J.-J., Vianay, B., and Verkhovsky, A. B. (2016). Microsurgery-aided in-situ force probing reveals extensibility and viscoelastic properties of individual stress fibers. *Sci. Rep.* 6, 23722. doi:10.1038/srep23722.
- Lai, Y. K., Lee, W. C., and Chen, K. D. (1993). Vimentin serves as a phosphate sink during the apparent activation of protein kinases by okadaic acid in mammalian cells. *J. Cell. Biochem.* 53, 161–8. doi:10.1002/jcb.240530209.
- LeBert, D., Squirrell, J. M., Freisinger, C., Rindy, J., Golenberg, N., Frecentese, G., et al. (2018). Damage-induced reactive oxygen species regulate vimentin and dynamic collagen- based projections to mediate wound repair. *Elife* 7, 1–26. doi:10.7554/eLife.30703.
- Lee, G., Hynes, R., and Kirschner, M. (1984). Temporal and spatial regulation of fibronectin in early *Xenopus* development. *Cell* 36, 729–740. doi:10.1016/0092-8674(84)90353-2.
- Lehtonen, E., Lehto, V. P., Vartio, T., Badley, R. A., and Virtanen, I. (1983). Expression of cytokeratin polypeptides in mouse oocytes and preimplantation embryos. *Dev. Biol.* 100, 158–165. doi:10.1016/0012-1606(83)90206-3.
- Leonard, M., Chan, Y., and Menko, A. S. (2008). Identification of a novel intermediate filament-linked N-cadherin/ γ -catenin complex involved in the establishment of the cytoarchitecture of differentiated lens fiber cells. *Dev. Biol.* 319, 298–308. doi:10.1016/j.ydbio.2008.04.036.
- Leterrier, J. F., Rusakov, D. A., Nelson, B. D., and Linden, M. (1994). Interactions between brain mitochondria and cytoskeleton: Evidence for specialized outer membrane domains involved in the association of cytoskeleton-associated proteins to mitochondria in situ and in vitro. *Microsc. Res. Tech.* doi:10.1002/jemt.1070270305.
- Lichtenstern, T., Mücke, N., Aebi, U., Mauermann, M., and Herrmann, H. (2012). Complex formation and kinetics of filament assembly exhibited by the simple epithelial keratins K8 and K18. *J. Struct. Biol.* 177, 54–62. doi:10.1016/j.jsb.2011.11.003.
- Lin, Y. C., Yao, N. Y., Broedersz, C. P., Herrmann, H., MacKintosh, F. C., and Weitz, D. A. (2010). Origins of elasticity in intermediate filament networks. *Phys. Rev. Lett.* 104, 1–4. doi:10.1103/PhysRevLett.104.058101.
- Liovic, M., Mogensen, M. M., Prescott, A. R., and Lane, E. B. (2003). Observation of keratin particles showing fast bidirectional movement colocalized with microtubules. *J. Cell Sci.* 116, 1417–27. doi:10.1242/jcs.00363.

- Liu, C., Lin, H., Tang, M., and Wang, Y. (2015). Vimentin contributes to epithelial-mesenchymal transition cancer cell mechanics by mediating cytoskeletal organization and focal adhesion maturation. *Oncotarget* 6, 15966–15983. doi:10.18632/oncotarget.3862.
- Liu, Z., Tan, J. L., Cohen, D. M., Yang, M. T., Sniadecki, N. J., Ruiz, S. A., et al. (2010). Mechanical tugging force regulates the size of cell-cell junctions. *Proc. Natl. Acad. Sci.* 107, 9944–9949. doi:10.1073/pnas.0914547107.
- Lombardi, M. L., Jaalouk, D. E., Shanahan, C. M., Burke, B., Roux, K. J., and Lammerding, J. (2011). The interaction between nesprins and sun proteins at the nuclear envelope is critical for force transmission between the nucleus and cytoskeleton. *J. Biol. Chem.* 286, 26743–26753. doi:10.1074/jbc.M111.233700.
- Long, H. a, Boczonadi, V., McInroy, L., Goldberg, M., and Määttä, A. (2006). Periplakin-dependent re-organisation of keratin cytoskeleton and loss of collective migration in keratin-8-downregulated epithelial sheets. *J. Cell Sci.* 119, 5147–5159. doi:10.1242/10.1242/jcs.03304.
- Loschke, F., Homberg, M., and Magin, T. M. (2016). Keratin Isotypes Control Desmosome Stability and Dynamics through PKC α . *J. Invest. Dermatol.* 136, 202–213. doi:10.1038/JID.2015.403.
- Lund, N., Henrion, D., Tiede, P., Ziche, M., Schunkert, H., and Ito, W. D. (2010). Vimentin expression influences flow dependent VASP phosphorylation and regulates cell migration and proliferation. *Biochem. Biophys. Res. Commun.* 395, 401–406. doi:10.1016/j.bbrc.2010.04.033.
- Lungu, O. I., Hallett, R. a., Choi, E. J., Aiken, M. J., Hahn, K. M., and Kuhlman, B. (2012). Designing Photoswitchable Peptides Using the AsLOV2 Domain. *Chem. Biol.* 19, 507–517. doi:10.1016/j.chembiol.2012.02.006.
- Lynch, C. D., Lazar, A. M., Iskratsch, T., Zhang, X., and Sheetz, M. P. (2013). Endoplasmic spreading requires coalescence of vimentin intermediate filaments at force-bearing adhesions. *Mol. Biol. Cell* 24, 21–30. doi:10.1091/mbc.E12-05-0377.
- Ma, L., Xu, J., Coulombe, P. A., and Wirtz, D. (1999). Keratin filament suspensions show unique micromechanical properties. *J. Biol. Chem.* 274, 19145–19151. doi:10.1074/jbc.274.27.19145.
- Ma, L., Yamada, S., Wirtz, D., and Coulombe, P. a (2001). A “hot-spot” mutation alters the mechanical properties of keratin filament networks. *Nat. Cell Biol.* 3, 503–506. doi:10.1038/35074576.

- Machacek, M., Hodgson, L., Welch, C., Elliott, H., Pertz, O., Nalbant, P., et al. (2009). Coordination of Rho GTPase activities during cell protrusion. *Nature* 461, 99–103. doi:10.1038/nature08242.
- Magin, T. M., Schröder, R., Leitgeb, S., Wanninger, F., Zatloukal, K., Grund, C., et al. (1998). Lessons from keratin 18 knockout mice: Formation of novel keratin filaments, secondary loss of keratin 7 and accumulation of liver-specific keratin 8-positive aggregates. *J. Cell Biol.* 140, 1441–1451. doi:10.1083/jcb.140.6.1441.
- Margolis, S. S., Perry, J. A., Forester, C. M., Nutt, L. K., Guo, Y., Jardim, M. J., et al. (2006). Role for the PP2A/B56 δ Phosphatase in Regulating 14-3-3 Release from Cdc25 to Control Mitosis. *Cell* 127, 759–773. doi:10.1016/j.cell.2006.10.035.
- Marsden, M., and DeSimone, D. W. (2001). Regulation of cell polarity, radial intercalation and epiboly in *Xenopus*: novel roles for integrin and fibronectin. *Development* 128, 3635–3647.
- Marsden, M., and DeSimone, D. W. (2003). Integrin-ECM interactions regulate cadherin-dependent cell adhesion and are required for convergent extension in *Xenopus*. *Curr. Biol.* doi:10.1016/S0960-9822(03)00433-0.
- Maruthamuthu, V., Sabass, B., Schwarz, U. S., and Gardel, M. L. (2011). Cell-ECM traction force modulates endogenous tension at cell-cell contacts. *Proc. Natl. Acad. Sci. U. S. A.* 108, 4708–13. doi:10.1073/pnas.1011123108.
- Matveeva, E. A., Venkova, L. S., Chernoiivanenko, I. S., and Minin, A. A. (2015). Vimentin is involved in regulation of mitochondrial motility and membrane potential by Rac1. *Biol. Open* 4, 1290–7. doi:10.1242/bio.011874.
- Mendez, M. G., Kojima, S.-I., and Goldman, R. D. (2010). Vimentin induces changes in cell shape, motility, and adhesion during the epithelial to mesenchymal transition. *FASEB J.* 24, 1838–51. doi:10.1096/fj.09-151639.
- Mendez, M. G., Restle, D., and Janmey, P. A. (2014). Vimentin enhances cell elastic behavior and protects against compressive stress. *Biophys. J.* 107, 314–323. doi:10.1016/j.bpj.2014.04.050.
- Menko, A. S., Bleaken, B. M., Libowitz, A. A., Zhang, L., Stepp, M. A., and Walker, J. L. (2014). A central role for vimentin in regulating repair function during healing of the lens epithelium. *Mol. Biol. Cell* 25, 776–790. doi:10.1091/mbc.E12-12-0900.
- Miller, R. K., Vikstrom, K., and Goldman, R. D. (1991). Keratin incorporation into intermediate filament networks is a rapid process. *J. Cell Biol.* 113, 843–855. doi:10.1083/jcb.113.4.843.

- Möglich, A., Ayers, R. A., and Moffat, K. (2009). Design and Signaling Mechanism of Light-Regulated Histidine Kinases. *J. Mol. Biol.* 385, 1433–1444. doi:10.1016/j.jmb.2008.12.017.
- Mohan, R., Hammers, H., Bargagna-Mohan, P., Zhan, X., Herbstritt, C., Ruiz, A., et al. (2004). Withaferin A is a potent inhibitor of angiogenesis. *Angiogenesis* 7, 115–122. doi:10.1007/s10456-004-1026-3.
- Morgan, J. T., Pfeiffer, E. R., Thirkill, T. L., Kumar, P., Peng, G., Fridolfsson, H. N., et al. (2011). Nesprin-3 regulates endothelial cell morphology, perinuclear cytoskeletal architecture, and flow-induced polarization. *Mol. Biol. Cell* 22, 4324–34. doi:10.1091/mbc.E11-04-0287.
- Morley, S. M., D'Alessandro, M., Sexton, C., Rugg, E. L., Navsaria, H., Shemanko, C. S., et al. (2003). Generation and characterization of epidermolysis bullosa simplex cell lines: Scratch assays show faster migration with disruptive keratin mutations. *Br. J. Dermatol.* 149, 46–58. doi:10.1046/j.1365-2133.2003.05493.x.
- Mücke, N., Kreplak, L., Kirmse, R., Wedig, T., Herrmann, H., Aebi, U., et al. (2004). Assessing the Flexibility of Intermediate Filaments by Atomic Force Microscopy. *J. Mol. Biol.* 335, 1241–1250. doi:10.1016/j.jmb.2003.11.038.
- Murray, M. E., Mendez, M. G., and Janmey, P. A. (2014). Substrate stiffness regulates solubility of cellular vimentin. *Mol Biol Cell* 25, 87–94. doi:10.1091/mbc.E13-06-0326.
- Nafeey, S., Martin, I., Felder, T., Walther, P., and Felder, E. (2016). Branching of keratin intermediate filaments. *J. Struct. Biol.* 194, 415–422. doi:10.1016/j.jsb.2016.03.023.
- Nakatsuji, N., and Johnson, K. E. (1983). Comparative study of extracellular fibrils on the ectodermal layer in gastrulae of five amphibian species. *J Cell Sci* 59, 61–70.
- Nakatsuji, N., Smolira, M. A., and Wylie, C. C. (1985). Fibronectin visualized by scanning electron microscopy immunocytochemistry on the substratum for cell migration in *Xenopus laevis* gastrulae. *Dev. Biol.* 107, 264–268. doi:10.1016/0012-1606(85)90395-1.
- Nekrasova, O. E., Mendez, M. G., Chernoivanenko, I. S., Tyurin-Kuzmin, P. A., Kuczmarski, E. R., Gelfand, V. I., et al. (2011). Vimentin intermediate filaments modulate the motility of mitochondria. *Mol. Biol. Cell* 22, 2282–9. doi:10.1091/mbc.E10-09-0766.
- Ngai, J., Coleman, T. R., and Lazarides, E. (1990). Localization of newly synthesized vimentin subunits reveals a novel mechanism of intermediate filament assembly. *Cell* 60, 415–27. doi:10.1016/0092-8674(90)90593-4.

- Nicolet, S., Herrmann, H., Aepli, U., and Strelkov, S. V. (2010). Atomic structure of vimentin coil 2. *J. Struct. Biol.* 170, 369–376. doi:10.1016/j.jsb.2010.02.012.
- Nieset, J. E., Redfield, A. R., Jin, F., Knudsen, K. A., Johnson, K. R., and Wheelock, M. J. (1997). Characterization of the interactions of alpha-catenin with alpha-actinin and beta-catenin/plakoglobin. *J. Cell Sci.*
- Nieuwkoop, P. D., and Faber, J. (1994). *Normal table of Xenopus laevis (Daudin) : a systematical and chronological survey of the development from the fertilized egg till the end of metamorphosis*. Garland Pub.
- Nöding, B., Herrmann, H., and Köster, S. (2014). Direct observation of subunit exchange along mature vimentin intermediate filaments. *Biophys. J.* 107, 2923–31. doi:10.1016/j.bpj.2014.09.050.
- Nolting, J. F., and Koster, S. (2013). Influence of microfluidic shear on keratin networks in living cells. *New J. Phys.* 15, 13pp. doi:10.1088/1367-2630/15/4/045025.
- Nolting, J. F., Mobius, W., and Koster, S. (2015). Mechanics of individual keratin bundles in living cells. *Biophys. J.* 107, 2693–2699. doi:10.1016/j.bpj.2014.10.039.
- Ohtsuka, T., Sakaguchi, M., Yamamoto, H., Tomida, S., Takata, K., Shien, K., et al. (2016). Interaction of cytokeratin 19 head domain and HER2 in the cytoplasm leads to activation of HER2-Erk pathway. *Sci. Rep.* 6, 39557. doi:10.1038/srep39557.
- Omary, M. B., Ku, N. O., Liao, J., and Price, D. (1998). Keratin modifications and solubility properties in epithelial cells and in vitro. *Subcell. Biochem.* 31, 105–140.
- Omary, M. B., Ku, N. O., Tao, G. Z., Toivola, D. M., and Liao, J. (2006). “Heads and tails” of intermediate filament phosphorylation: multiple sites and functional insights. *Trends Biochem. Sci.* 31, 383–394. doi:10.1016/j.tibs.2006.05.008.
- Osborn, M., Franke, W., and Weber, K. (1980). Direct demonstration of the presence of two immunologically distinct intermediate-sized filament systems in the same cell by double immunofluorescence microscopy. *Exp. Cell Res.* 125, 37–46. doi:10.1016/0014-4827(80)90186-X.
- Osmanagic-Myers, S., Gregor, M., Walko, G., Burgstaller, G., Reipert, S., and Wiche, G. (2006). Plectin-controlled keratin cytoarchitecture affects MAP kinases involved in cellular stress response and migration. *J. Cell Biol.* 174, 557–568. doi:10.1083/jcb.200605172.

- Osmanagic-Myers, S., Rus, S., Wolfram, M., Brunner, D., Goldmann, W. H., Bonakdar, N., et al. (2015). Plectin reinforces vascular integrity by mediating crosstalk between the vimentin and the actin networks. *J. Cell Sci.* 128, 4138–4150. doi:10.1242/jcs.172056.
- Osmanagic-Myers, S., and Wiche, G. (2004). Plectin-RACK1 (receptor for activated C kinase 1) scaffolding: A novel mechanism to regulate protein kinase C activity. *J. Biol. Chem.* 279, 18701–18710. doi:10.1074/jbc.M312382200.
- Pankov, R., Cukierman, E., Katz, B. Z., Matsumoto, K., Lin, D. C., Lin, S., et al. (2000). Integrin dynamics and matrix assembly: Tensin-dependent translocation of $\alpha 5 \beta 1$ integrins promotes early fibronectin fibrillogenesis. *J. Cell Biol.* doi:10.1083/jcb.148.5.1075.
- Pankov, R., Endo, Y., Even-Ram, S., Araki, M., Clark, K., Cukierman, E., et al. (2005). A Rac switch regulates random versus directionally persistent cell migration. *J. Cell Biol.* 170, 793–802. doi:10.1083/jcb.200503152.
- Paramio, J. M., Segrelles, C., and Ruiz, S. (2001). Inhibition of Protein Kinase B (PKB) and PKC ζ Mediates Keratin K10-Induced Cell Cycle Arrest. *Mol. Cell. Biol.* 21, 7449–7459. doi:10.1128/MCB.21.21.7449.
- Park, B., Nguyen, N. T., Dutt, P., Merdek, K. D., Bashar, M., Sterpetti, P., et al. (2002). Association of Lbc Rho guanine nucleotide exchange factor with alpha-catenin-related protein, alpha-catulin/CTNNAL1, supports serum response factor activation. *J. Biol. Chem.* 277, 45361–45370. doi:10.1074/jbc.M202447200.
- Pawelzyk, P., Mücke, N., Herrmann, H., and Willenbacher, N. (2014). Attractive interactions among intermediate filaments determine network mechanics in vitro. *PLoS One* 9. doi:10.1371/journal.pone.0093194.
- Pérez-Sala, D., Oeste, C. L., Martínez, A. E., Carrasco, M. J., Garzón, B., and Cañada, F. J. (2015). Vimentin filament organization and stress sensing depend on its single cysteine residue and zinc binding. *Nat. Commun.* 6, 7287. doi:10.1038/ncomms8287.
- Perlson, E., Hanz, S., Ben-Yaakov, K., Segal-Ruder, Y., Seger, R., and Fainzilber, M. (2005). Vimentin-dependent spatial translocation of an activated MAP kinase in injured nerve. *Neuron* 45, 715–726. doi:10.1016/j.neuron.2005.01.023.
- Perlson, E., Michaelievski, I., Kowalsman, N., Ben-Yaakov, K., Shaked, M., Seger, R., et al. (2006). Vimentin Binding to Phosphorylated Erk Sterically Hinders Enzymatic Dephosphorylation of the Kinase. *J. Mol. Biol.* 364, 938–944. doi:10.1016/j.jmb.2006.09.056.

- Peter, A., and Stick, R. (2015). Evolutionary aspects in intermediate filament proteins. *Curr. Opin. Cell Biol.* 32, 48–55. doi:10.1016/j.ceb.2014.12.009.
- Peuhu, E., Virtakoivu, R., Mai, A., Wärri, A., and Ivaska, J. (2017). Epithelial vimentin plays a functional role in mammary gland development. *Development* 144, 4103–4113. doi:10.1242/dev.154229.
- Plutoni, C., Bazellieres, E., Le Borgne-Rochet, M., Comunale, F., Brugues, A., Séveno, M., et al. (2016). P-cadherin promotes collective cell migration via a Cdc42-mediated increase in mechanical forces. *J. Cell Biol.* 212, 199–217. doi:10.1083/jcb.201505105.
- Pollack, V., Scheiber, K., Pfaller, W., and Schramek, H. (1997). Loss of cytokeratin expression and formation of actin stress fibers in dedifferentiated MDCK-C7 cell lines. *Biochem. Biophys. Res. Commun.* 241, 541–547. doi:10.1006/bbrc.1997.7837.
- Postel, R., Ketema, M., Kuikman, I., de Pereda, J. M., and Sonnenberg, A. (2011). Nesprin-3 augments peripheral nuclear localization of intermediate filaments in zebrafish. *J. Cell Sci.* 124, 755–764. doi:10.1242/jcs.081174.
- Prahlad, V., Yoon, M., Moir, R. D., Vale, R. D., and Goldman, R. D. (1998). Rapid movements of vimentin on microtubule tracks: Kinesin-dependent assembly of intermediate filament networks. *J. Cell Biol.* 143, 159–170. doi:10.1083/jcb.143.1.159.
- Qin, Z., Kreplak, L., and Buehler, M. J. (2009). Hierarchical structure controls nanomechanical properties of vimentin intermediate filaments. *PLoS One* 4. doi:10.1371/journal.pone.0007294.
- Quinlan, R. A., Hatzfeld, M., Franke, W. W., Lustig, A., Schulthess, T., and Engel, J. (1986). Characterization of dimer subunits of intermediate filament proteins. *J. Mol. Biol.* 192, 337–349. doi:10.1016/0022-2836(86)90369-4.
- Ramms, L., Fabris, G., Windoffer, R., Schwarz, N., Springer, R., Zhou, C., et al. (2013). Keratins as the main component for the mechanical integrity of keratinocytes. *Proc. Natl. Acad. Sci. U. S. A.* 110, 18513–8. doi:10.1073/pnas.1313491110.
- Ramos, J. W. (1996). Xenopus embryonic cell adhesion to fibronectin: position-specific activation of RGD/synergy site-dependent migratory behavior at gastrulation. *J. Cell Biol.* 134, 227–240. doi:10.1083/jcb.134.1.227.
- Reichelt, J., Büssow, H., Grund, C., and Magin, T. M. (2001). Formation of a normal epidermis supported by increased stability of keratins 5 and 14 in keratin 10 null mice. *Mol. Biol. Cell* 12, 1557–68. doi:10.1091/mbc.12.6.1557.

- Reichelt, J., and Magin, T. M. (2002). Hyperproliferation, induction of c-Myc and 14-3-3 σ , but no cell fragility in keratin-10-null mice. *J. Cell Sci.* 115, 2639–2650.
- Ren, R., Nagel, M., Tahinci, E., Winklbauer, R., and Symes, K. (2006). Migrating Anterior Mesoderm Cells and Intercalating Trunk Mesoderm Cells Have Distinct Responses to Rho and Rac During *Xenopus* Gastrulation. 1090–1099. doi:10.1002/dvdy.20711.
- Ridge, K. M., Linz, L., Flitney, F. W., Kuczmarski, E. R., Chou, Y. H., Omary, M. B., et al. (2005). Keratin 8 Phosphorylation by Protein Kinase C δ Regulates Shear Stress-mediated Disassembly of Keratin Intermediate Filaments in Alveolar Epithelial Cells. *J. Biol. Chem.* 280, 30400–30405. doi:10.1074/jbc.M504239200.
- Riveline, D., Zamir, E., Balaban, N. Q., Schwarz, U. S., Ishizaki, T., Narumiya, S., et al. (2001). Focal contacts as mechanosensors: Externally applied local mechanical force induces growth of focal contacts by an mDia1-dependent and ROCK-independent mechanism. *J. Cell Biol.* 153, 1175–1185. doi:10.1083/jcb.153.6.1175.
- Robert, A., Herrmann, H., Davidson, M. W., and Gelfand, V. I. (2014). Microtubule-dependent transport of vimentin filament precursors is regulated by actin and by the concerted action of Rho- and p21-activated kinases. *FASEB J.* 28, 2879–2890. doi:10.1096/fj.14-250019.
- Rogel, M. R., Soni, P. N., Troken, J. R., Sitikov, A., Trejo, H. E., and Ridge, K. M. (2011). Vimentin is sufficient and required for wound repair and remodeling in alveolar epithelial cells. *FASEB J.* 25, 3873–83. doi:10.1096/fj.10-170795.
- Rotty, J. D., and Coulombe, P. A. (2012). A wound-induced keratin inhibits Src activity during keratinocyte migration and tissue repair. *J. Cell Biol.* 197, 381–389. doi:10.1083/jcb.201107078.
- Rozario, T., Dzamba, B., Weber, G. F., Davidson, L. A., and DeSimone, D. W. (2009). The physical state of fibronectin matrix differentially regulates morphogenetic movements in vivo. *Dev. Biol.* 327, 386–398. doi:10.1016/j.ydbio.2008.12.025.
- Russell, D., Andrews, P. D., James, J., and Lane, E. B. (2004). Mechanical stress induces profound remodelling of keratin filaments and cell junctions in epidermolysis bullosa simplex keratinocytes. *J. Cell Sci.* 117, 5233–5243. doi:10.1242/jcs.01407.
- Sager, P. R. (1989). Cytoskeletal effects of acrylamide and 2,5-hexanedione: Selective aggregation of vimentin filaments. *Toxicol. Appl. Pharmacol.* 97, 141–155. doi:10.1016/0041-008X(89)90063-X.

- Saha, S. K., Choi, H. Y., Kim, B. W., Dayem, A. A., Yang, G.-M., Kim, K. S., et al. (2017). KRT19 directly interacts with β -catenin/RAC1 complex to regulate NUMB-dependent NOTCH signaling pathway and breast cancer properties. *Oncogene* 36, 332–349. doi:10.1038/onc.2016.221.
- Sakamoto, Y., Boëda, B., and Etienne-Manneville, S. (2013). APC binds intermediate filaments and is required for their reorganization during cell migration. *J. Cell Biol.* 200, 249–258. doi:10.1083/jcb.201206010.
- Sankar, S., Tanner, J. M., Bell, R., Chaturvedi, A., Randall, R. L., Beckerle, M. C., et al. (2013). A novel role for keratin 17 in coordinating oncogenic transformation and cellular adhesion in Ewing sarcoma. *Mol. Cell. Biol.* 33, 4448–4460. doi:10.1128/MCB.00241-13.
- Schopferer, M., Bär, H., Hochstein, B., Sharma, S., Mücke, N., Herrmann, H., et al. (2009). Desmin and Vimentin Intermediate Filament Networks: Their Viscoelastic Properties Investigated by Mechanical Rheometry. *J. Mol. Biol.* 388, 133–143. doi:10.1016/j.jmb.2009.03.005.
- Schwarz, J., Proff, J., Hävemeier, A., Ladwein, M., Rottner, K., Barlag, B., et al. (2012). Serine-71 phosphorylation of Rac1 modulates downstream signaling. *PLoS One* 7. doi:10.1371/journal.pone.0044358.
- Schwarz, N., Windoffer, R., Magin, T. M., and Leube, R. E. (2015). Dissection of keratin network formation, turnover and reorganization in living murine embryos. *Sci. Rep.* 5, 9007. doi:10.1038/srep09007.
- Seltmann, K., Cheng, F., Wiche, G., Eriksson, J. E., and Magin, T. M. (2015). Keratins Stabilize Hemidesmosomes through Regulation of β 4-Integrin Turnover. *J. Invest. Dermatol.* 135, 1609–1620. doi:10.1038/jid.2015.46.
- Seltmann, K., Fritsch, A. W., Käs, J. a, and Magin, T. M. (2013a). Keratins significantly contribute to cell stiffness and impact invasive behavior. *Proc. Natl. Acad. Sci. U. S. A.* 110, 18507–12. doi:10.1073/pnas.1310493110.
- Seltmann, K., Roth, W., Kröger, C., Loschke, F., Lederer, M., Hüttelmaier, S., et al. (2013b). Keratins Mediate Localization of Hemidesmosomes and Repress Cell Motility. *J. Invest. Dermatol.* 133, 181–190. doi:10.1038/jid.2012.256.
- Shabana, A. H. M., Oboeuf, M., and Forest, N. (1994). Cytoplasmic desmosomes and intermediate filament disturbance following acrylamide treatment in cultured rat keratinocytes. *Tissue Cell* 26, 43–55. doi:10.1016/0040-8166(94)90082-5.

- Shabbir, S. H., Cleland, M. M., Goldman, R. D., and Mrksich, M. (2014). Geometric control of vimentin intermediate filaments. *Biomaterials* 35, 1359–1366. doi:10.1016/j.biomaterials.2013.10.008.
- Sharma, P., Bolten, Z. T., Wagner, D. R., and Hsieh, A. H. (2017). Deformability of Human Mesenchymal Stem Cells Is Dependent on Vimentin Intermediate Filaments. *Ann Biomed Eng* 45, 1365–1374. doi:10.1007/s10439-016-1787-z.
- Sin, W. C., Chen, X. Q., Leung, T., and Lim, L. (1998). RhoA-binding kinase α translocation is facilitated by the collapse of the vimentin intermediate filament network. *Mol. Cell. Biol.* 18, 6325–39. doi:10.1128/MCB.18.11.6325.
- Sivaramakrishnan, S., DeGiulio, J. V., Lorand, L., Goldman, R. D., and Ridge, K. M. (2008). Micromechanical properties of keratin intermediate filament networks. *Proc. Natl. Acad. Sci. U. S. A.* 105, 889–894. doi:10.1073/pnas.0710728105.
- Sivaramakrishnan, S., Schneider, J. L., Sitikov, A., Goldman, R. D., and Ridge, K. M. (2009). Shear stress induced reorganization of the keratin intermediate filament network requires phosphorylation by protein kinase C ζ . *Mol. Biol. Cell* 20, 2755–2765. doi:10.1091/mbc.E08-10-1028.
- Snider, N. T., Leonard, J. M., Kwan, R., Griggs, N. W., Rui, L., and Bishr Omary, M. (2013a). Glucose and SIRT2 reciprocally mediate the regulation of keratin 8 by lysine acetylation. *J. Cell Biol.* 200, 241–247. doi:10.1083/jcb.201209028.
- Snider, N. T., and Omary, M. B. (2014). Post-translational modifications of intermediate filament proteins: mechanisms and functions. *Nat. Rev. Mol. Cell Biol.* 15, 163–77. doi:10.1038/nrm3753.
- Snider, N. T., Park, H., and Bishr Omary, M. (2013b). A conserved rod domain phosphotyrosine that is targeted by the phosphatase PTP1B promotes keratin 8 protein insolubility and filament organization. *J. Biol. Chem.* 288, 31329–31337. doi:10.1074/jbc.M113.502724.
- Snider, N. T., Weerasinghe, S. V. W., Iñiguez-Lluhí, J. A., Herrmann, H., and Omary, M. B. (2011). Keratin hypersumoylation alters filament dynamics and is a marker for human liver disease and keratin mutation. *J. Biol. Chem.* 286, 2273–2284. doi:10.1074/jbc.M110.171314.
- Soellner, P., Quinlan, R. A., and Franke, W. W. (1985). Identification of a distinct soluble subunit of an intermediate filament protein: tetrameric vimentin from living cells. *Proc. Natl. Acad. Sci. U. S. A.* 82, 7929–33. doi:10.1073/pnas.82.23.7929.

- Sokolova, A. V., Kreplak, L., Wedig, T., Mücke, N., Svergun, D. I., Herrmann, H., et al. (2006). Monitoring intermediate filament assembly by small-angle x-ray scattering reveals the molecular architecture of assembly intermediates. *Proc. Natl. Acad. Sci.* 103, 16206–16211. doi:10.1073/pnas.0603629103.
- Sonavane, P. R., Wang, C., Dzamba, B., Weber, G. F., Periasamy, A., and DeSimone, D. W. (2017). Mechanical and signaling roles for keratin intermediate filaments in the assembly and morphogenesis of mesendoderm tissue at gastrulation. *Development*, dev.155200. doi:10.1242/dev.155200.
- Spazierer, D., Raberger, J., Gross, K., Fuchs, P., and Wiche, G. (2008). Stress-induced recruitment of epiplakin to keratin networks increases their resistance to hyperphosphorylation-induced disruption. *J. Cell Sci.* 121, 825–33. doi:10.1242/jcs.013755.
- Steinert, P. M., Cantieri, J. S., Teller, D. C., Lonsdale-Eccles, J. D., and Dale, B. A. (1981a). Characterization of a class of cationic proteins that specifically interact with intermediate filaments. *Proc. Natl. Acad. Sci. U. S. A.* 78, 4097–101. doi:10.1073/pnas.78.7.4097.
- Steinert, P. M., Idler, W. W., Cabral, F., Gottesman, M. M., and Goldman, R. D. (1981b). In vitro assembly of homopolymer and copolymer filaments from intermediate filament subunits of muscle and fibroblastic cells. *Proc. Natl. Acad. Sci. U. S. A.* 78, 3692–6. doi:10.1073/pnas.78.6.3692.
- Steinert, P. M., Idler, W. W., and Zimmerman, S. B. (1976). Self-assembly of bovine epidermal keratin filaments in vitro. *J. Mol. Biol.* 108, 547–567. doi:10.1016/S0022-2836(76)80136-2.
- Steinert, P. M., Marekov, L. N., Fraser, R. D. B., and Parry, D. A. D. (1993a). Keratin intermediate filament structure. Crosslinking studies yield quantitative information on molecular dimensions and mechanism of assembly. *J. Mol. Biol.* 230, 436–452. doi:10.1006/jmbi.1993.1161.
- Steinert, P. M., Yang, J. M., Bale, S. J., and Compton, J. G. (1993b). Concurrence between the molecular overlap regions in keratin intermediate filaments and the locations of keratin mutations in genodermatoses. *Biochem. Biophys. Res. Commun.* 197, 840–848. doi:10.1006/bbrc.1993.2555.
- Strelkov, S. V., Herrmann, H., Geisler, N., Wedig, T., Zimbelmann, R., Aebi, U., et al. (2002). Conserved segments 1A and 2B of the intermediate filament dimer: Their atomic structures and role in filament assembly. *EMBO J.* 21, 1255–1266. doi:10.1093/emboj/21.6.1255.

- Strickland, D., Lin, Y., Wagner, E., Hope, C. M., Zayner, J., Antoniou, C., et al. (2012). TULIPs: Tunable, light-controlled interacting protein tags for cell biology. *Nat. Methods*. doi:10.1038/nmeth.1904.
- Strickland, D., Yao, X., Gawlak, G., Rosen, M. K., Gardner, K. H., and Sosnick, T. R. (2010). Rationally improving LOV-domain based photoswitches. *Nat. Methods* 7, 623–626. doi:10.1038/nmeth.1473.
- Strnad, P., Windoffer, R., and Leube, R. E. (2001). In vivo detection of cytokeratin filament network breakdown in cells treated with the phosphatase inhibitor okadaic acid. *Cell Tissue Res.* 306, 277–93. doi:10.1007/s004410100455.
- Strnad, P., Windoffer, R., and Leube, R. E. (2002). Induction of rapid and reversible cytokeratin filament network remodeling by inhibition of tyrosine phosphatases. *J. Cell Sci.* 115, 4133–4148. doi:10.1242/jcs.00096.
- Sun, P., Yuan, Y., Li, A., Li, B., and Dai, X. (2010). Cytokeratin expression during mouse embryonic and early postnatal mammary gland development. *Histochem. Cell Biol.* 133, 213–221. doi:10.1007/s00418-009-0662-5.
- Svitkina, T. M., Verkhovsky, A. B., and Borisy, G. G. (1996). Plectin sidearms mediate interaction of intermediate filaments with microtubules and other components of the cytoskeleton. *J. Cell Biol.* 135, 991–1007. doi:10.1083/jcb.135.4.991.
- Swartz, T. E., Corchnoy, S. B., Christie, J. M., Lewis, J. W., Szundi, I., Briggs, W. R., et al. (2001). The Photocycle of a Flavin-binding Domain of the Blue Light Photoreceptor Phototropin. *J. Biol. Chem.* 276, 36493–36500. doi:10.1074/jbc.M103114200.
- Terriac, E., Coceano, G., Mavajian, Z., Hageman, T., Christ, A., Testa, I., et al. (2017). Vimentin Levels and Serine 71 Phosphorylation in the Control of Cell-Matrix Adhesions, Migration Speed, and Shape of Transformed Human Fibroblasts. *Cells* 6, 2. doi:10.3390/cells6010002.
- Thaiparambil, J. T., Bender, L., Ganesh, T., Kline, E., Patel, P., Liu, Y., et al. (2011). Withaferin A inhibits breast cancer invasion and metastasis at sub-cytotoxic doses by inducing vimentin disassembly and serine 56 phosphorylation. *Int. J. Cancer* 129, 2744–2755. doi:10.1002/ijc.25938.
- Theveneau, E., Marchant, L., Kuriyama, S., Gull, M., Moepps, B., Parsons, M., et al. (2010). Collective Chemotaxis Requires Contact-Dependent Cell Polarity. *Dev. Cell* 19, 39–53. doi:10.1016/j.devcel.2010.06.012.

- Todorović, V., Desai, B. V, Patterson, M. J. S., Amargo, E. V, Dubash, A. D., Yin, T., et al. (2010). Plakoglobin regulates cell motility through Rho- and fibronectin-dependent Src signaling. *J. Cell Sci.* 123, 3576–3586. doi:10.1242/jcs.070391.
- Toivola, D. M., Goldman, R. D., Garrod, D. R., and Eriksson, J. E. (1997). Protein phosphatases maintain the organization and structural interactions of hepatic keratin intermediate filaments. 33, 23–33.
- Toivola, D. M., Zhou, Q., English, L. S., and Omary, M. B. (2002). Type II keratins are phosphorylated on a unique motif during stress and mitosis in tissues and cultured cells. *Mol. Biol. Cell* 13, 1857–70. doi:10.1091/mbc.01-12-0591.
- Torpey, N., Wylie, C. C., and Heasman, J. (1992). Function of maternal cytokeratin in *Xenopus* development. *Nature* 357, 413–5. doi:10.1038/357413a0.
- Toyoizumi, R., and Takeuchi, S. (1995). The behavior of chick gastrula mesodermal cells under the unidirectional tractive force parallel to the substrata. *J. Cell Sci.* 108 (Pt 2), 557–67. doi:10.1002/jez.1402600309.
- Tsuruta, D., and Jones, J. C. (2003). The vimentin cytoskeleton regulates focal contact size and adhesion of endothelial cells subjected to shear stress. *J. Cell Sci.* 116, 4977–4984. doi:10.1242/jcs.00823.
- Tzivion, G., Luo, Z. J., and Avruch, J. (2000). Calyculin A-induced vimentin phosphorylation sequesters 14-3-3 and displaces other 14-3-3 partners in vivo. *J. Biol. Chem.* 275, 29772–29778. doi:10.1074/jbc.M001207200.
- Velez-delValle, C., Marsch-Moreno, M., Castro-Muñozledo, F., Galván-Mendoza, I. J., and Kuri-Harcuch, W. (2016). Epithelial cell migration requires the interaction between the vimentin and keratin intermediate filaments. *Sci. Rep.* 6, 24389. doi:10.1038/srep24389.
- Vijayaraj, P., Kröger, C., Reuter, U., Windoffer, R., Leube, R. E., and Magin, T. M. (2009). Keratins regulate protein biosynthesis through localization of GLUT1 and -3 upstream of AMP kinase and Raptor. *J. Cell Biol.* 187, 175–184. doi:10.1083/jcb.200906094.
- Vikstrom, K. L., Borisy, G. G., and Goldman, R. D. (1989). Dynamic aspects of intermediate filament networks in BHK-21 cells. *Proc. Natl. Acad. Sci. U. S. A.* 86, 549–53. doi:10.1073/pnas.86.2.549.
- Vikstrom, K. L., Lim, S. S., Goldman, R. D., and Borisy, G. G. (1992). Steady state dynamics of intermediate filament networks. *J Cell Biol* 118, 121–129. doi:10.1083/jcb.118.1.121.

- Vuoriluoto, K., Haugen, H., Kiviluoto, S., Mpindi, J.-P., Nevo, J., Gjerdrum, C., et al. (2011). Vimentin regulates EMT induction by Slug and oncogenic H-Ras and migration by governing Axl expression in breast cancer. *Oncogene* 30, 1436–48. doi:10.1038/onc.2010.509.
- Wang, N., and Stamenović, D. (2000). Contribution of intermediate filaments to cell stiffness, stiffening, and growth. *Am. J. Physiol. Cell Physiol.* 279, C188–C194. doi:10.1109/IEMBS.1999.802102.
- Wang, X., He, L., Wu, Y. I., Hahn, K. M., and Montell, D. J. (2010). Light-mediated activation reveals a key role for Rac in collective guidance of cell movement in vivo. *Nat. Cell Biol.* 12, 591–597. doi:10.1038/ncb2061.
- Weber, G. F., Bjerke, M. A., and DeSimone, D. W. (2012). A Mechanoresponsive Cadherin-Keratin Complex Directs Polarized Protrusive Behavior and Collective Cell Migration. *Dev. Cell* 22, 104–115. doi:10.1016/j.devcel.2011.10.013.
- Wen, J. W., and Winklbauer, R. (2017). Ingression-type cell migration drives vegetal endoderm internalisation in the *Xenopus* gastrula. *Elife* 6, 1–35. doi:10.7554/elife.27190.
- Wilhelmsen, K., Litjens, S. H. M., Kuikman, I., Tshimbalanga, N., Janssen, H., Van Bout, I. Den, et al. (2005). Nesprin-3, a novel outer nuclear membrane protein, associates with the cytoskeletal linker protein plectin. *J. Cell Biol.* 171, 799–810. doi:10.1083/jcb.200506083.
- Wilson, P., and Keller, R. (1991). Cell rearrangement during gastrulation of *Xenopus*: direct observation of cultured explants. *Development* 112, 289–300.
- Windoffer, R., Beil, M., Magin, T. M., and Leube, R. E. (2011). Cytoskeleton in motion: The dynamics of keratin intermediate filaments in epithelia. *J. Cell Biol.* 194, 669–678. doi:10.1083/jcb.201008095.
- Windoffer, R., Kölsch, A., Wöll, S., and Leube, R. E. (2006). Focal adhesions are hotspots for keratin filament precursor formation. *J. Cell Biol.* 173, 341–348. doi:10.1083/jcb.200511124.
- Windoffer, R., and Leube, R. E. (1999). Detection of cytokeratin dynamics by time-lapse fluorescence microscopy in living cells. *J. Cell Sci.* 112, 4521–34.
- Windoffer, R., Wöll, S., Strnad, P., and Leube, R. E. (2004). Identification of novel principles of keratin filament network turnover in living cells. *Mol. Biol. Cell* 15, 2436–48. doi:10.1091/mbc.E03-09-0707.

- Winheim, S., Hieb, A. R., Silbermann, M., Surmann, E. M., Wedig, T., Herrmann, H., et al. (2011). Deconstructing the late phase of vimentin assembly by total internal reflection fluorescence microscopy (TIRFM). *PLoS One* 6, 2–8. doi:10.1371/journal.pone.0019202.
- Winklbauer, R. (1998). Conditions for fibronectin fibril formation in the early *Xenopus* embryo. *Dev. Dyn.* doi:10.1002/(SICI)1097-0177(199807)212:3<335::AID-AJA1>3.0.CO;2-I.
- Winklbauer, R., Nagel, M., Selchow, A., and Wacker, S. (1996). Mesoderm migration in the *Xenopus* gastrula. *Int. J. Dev. Biol.* 40, 305–311. doi:10.1016/0012-1606(91)90275-8.
- Winklbauer, R., and Schürfeld, M. (1999). Vegetal rotation, a new gastrulation movement involved in the internalization of the mesoderm and endoderm in *Xenopus*. *Development* 126, 3703–3713.
- Wöll, S., Windoffer, R., and Leube, R. E. (2005). Dissection of keratin dynamics: different contributions of the actin and microtubule systems. *Eur. J. Cell Biol.* 84, 311–28. doi:10.1016/j.ejcb.2004.12.004.
- Woo, W. M., Goncharov, A., Jin, Y., and Chisholm, A. D. (2004). Intermediate filaments are required for *C. elegans* epidermal elongation. *Dev. Biol.* 267, 216–229. doi:10.1016/j.ydbio.2003.11.007.
- Wu, C., Keivenst, V. M., O'Toole, T. E., McDonald, J. A., and Ginsberg, M. H. (1995). Integrin activation and cytoskeletal interaction are essential for the assembly of a fibronectin matrix. *Cell*. doi:10.1016/0092-8674(95)90184-1.
- Wu, Y. I., Frey, D., Lungu, O. I., Jaehrig, A., Schlichting, I., Kuhlman, B., et al. (2009). A genetically encoded photoactivatable Rac controls the motility of living cells. *Nature* 461, 104–108. doi:10.1038/nature08241.
- Yamada, S., and Nelson, W. J. (2007). Localized zones of Rho and Rac activities drive initiation and expansion of epithelial cell–cell adhesion. 178, 517–527. doi:10.1083/jcb.200701058.
- Yamaguchi, N., Mizutani, T., Kawabata, K., and Haga, H. (2015). Leader cells regulate collective cell migration via Rac activation in the downstream signaling of integrin $\beta 1$ and PI3K. *Sci. Rep.* 5, 7656. doi:10.1038/srep07656.
- Yoo, S. K., Deng, Q., Cavnar, P. J., Wu, Y. I., Hahn, K. M., and Huttenlocher, A. (2010). Differential Regulation of Protrusion and Polarity by PI(3)K during Neutrophil Motility in Live Zebrafish. *Dev. Cell* 18, 226–236. doi:10.1016/j.devcel.2009.11.015.

- Yoon, K. H., Yoon, M., Moir, R. D., Khuon, S., Flitney, F. W., and Goldman, R. D. (2001). Insights into the dynamic properties of keratin intermediate filaments in living epithelial cells. *J. Cell Biol.* 152, 503–516. doi:10.1083/jcb.152.3.503.
- Yoon, M., Moir, R. D., Prahlad, V., and Goldman, R. D. (1998). Motile properties of vimentin intermediate filament networks in living cells. *J. Cell Biol.* 143, 147–157. doi:10.1083/jcb.143.1.147.
- Zhang, H., Landmann, F., Zahreddine, H., Rodriguez, D., Koch, M., and Labouesse, M. (2011). A tension-induced mechanotransduction pathway promotes epithelial morphogenesis. *Nature* 471, 99–103. doi:10.1038/nature09765.
- Zhong, C., Chrzanowska-Wodnicka, M., Brown, J., Shaub, A., Belkin, A. M., and Burridge, K. (1998). Rho-mediated contractility exposes a cryptic site in fibronectin and induces fibronectin matrix assembly. *J. Cell Biol.* doi:10.1083/jcb.141.2.539.
- Zhou, Q., Cadrin, M., Herrmann, H., Chen, C. H., Chalkley, R. J., Burlingame, A. L., et al. (2006). Keratin 20 serine 13 phosphorylation is a stress and intestinal goblet cell marker. *J. Biol. Chem.* 281, 16453–16461. doi:10.1074/jbc.M512284200.
- Zimmerman, S. P., Kuhlman, B., and Yumerefendi, H. (2016). “Engineering and Application of LOV2-Based Photoswitches,” in *Methods in Enzymology* doi:10.1016/bs.mie.2016.05.058.